



**Design of Hybrid Photo-Voltaic/Thermal Solar Systems and Performance
Analysis for Residential Building Case Studies.**

A Thesis submitted in partial fulfilment of the requirements for the award of
Doctor of Philosophy at Newcastle University

by

Anu Antony

Newcastle University

December 2019



Sir Joseph
Swan Centre
for energy research

Table of Contents

Table of Contents	2
Abstract	5
Publications	6
Acknowledgements	7
List of Figures	8
List of Tables	11
Nomenclature	12
Chapter 1. Introduction	20
1.1 Research Background	20
1.2 Research Gaps.....	24
1.3 Research Questions.....	25
1.4 Limitations	26
1.5 Aim and Objectives	26
1.5.1 Aim:	26
1.5.2 Objectives:.....	26
1.6 Research Novelty –A Summary	27
1.7 Structure of Thesis	29
Chapter 2. Literature Review	30
2.1 Introduction.....	30
2.2 Concept, Theory and Classification.....	30
2.2.1 Air PV/T	40
2.2.2 Liquid PV/T.....	41
2.2.3 Glazed PV/T Collectors.....	48
2.2.4 Unglazed PV/T Collectors.....	49
2.2.5 PV/T Norm Classification	52
2.3 Existing Standards	59
2.4 Performance Indicators	61
2.5 Limitations of PV/T	63
2.6 Current Research in PV/T.....	63
2.7 Concept Design of the PV/T System	65
2.7.1 Solar Angel DG-01	65
2.7.2 Glazing Cover.....	66
2.7.3 Poly-Crystalline PV Cells.....	66
2.7.4 EVA Layers	67
2.7.5 Absorber	67

2.7.6	Flat-Plate Heat Exchanger	68
2.7.7	Insulation	71
2.7.8	Electrical Storage Unit.....	71
2.7.9	Thermal Storage Unit	72
2.8	Chapter Summary	74
Chapter 3. Real-Time System Performance Analysis.....		76
3.1	Lisbon PV and Solar Collector and PV/T.....	76
3.1.1	Experimental Rig Portugal and System Description	76
3.1.2	Data Collection and Analysis	78
3.2	Newcastle PV/T System	82
3.2.1	Experimental Rig (USB, Newcastle).....	83
3.2.2	Detailed Description of PV/T and Parameters	87
3.2.3	Data Collection and Analysis	89
3.3	Lab System:	90
3.3.1	Laboratory Rig (Newcastle)	90
3.3.2	System Description.....	92
3.3.3	Data Collection and Analysis	94
3.4	Domestic Case for Newcastle	94
3.5	Domestic Case for Cochin	96
3.6	Summary	98
Chapter 4. PV/T Modelling and Validation		99
4.1	Introduction.....	99
4.2	Analytical Model and Theory for Radiation.....	99
4.2.1	Sky Radiation Modelling.....	99
4.2.2	PV Model.....	112
4.2.3	Solar Collector Model	118
4.2.4	PV/T Collectors	119
4.3	Steady State Modelling for PV/T.....	123
4.4	Dynamic Modelling Method.....	133
4.5	Validation Methods and Resources	137
4.6	Impact of Factors	140
4.7	Chapter Summary	143
Chapter 5. Results and Discussion		145
5.1	Introduction.....	145
5.2	Dynamic Model Simulation and Evaluation.....	145
5.2.1	Simulation and Real-Time Results for Portugal.....	146

5.2.2	Simulation and Real-Time Laboratory Results for Newcastle.....	150
5.2.3	Efficiency.....	153
5.3	Further Discussion	154
5.3.1	Design and Application in Residential Systems.....	156
5.4	Chapter Summary	163
Chapter 6.	Exergy and Economic Analysis	165
6.1	Introduction.....	165
6.2	Annual Operational Performance	165
6.3	Economic Analysis of the Lab Prototype	167
6.4	Exergy Analysis.....	167
6.5	Mean Absolute Error	173
6.6	Sensitivity and Uncertainty.....	174
Chapter 7.	Conclusion and Future Work.....	176
7.1	Conclusion	176
7.2	Advantages.....	177
7.3	Errors and Challenges	177
7.4	Future Work and Opportunities	177
7.4.1	The Module Design	178
7.4.2	Long-Term Reliability	179
7.4.3	Replicability	179
7.4.4	Policy Support	179
7.4.5	Present and Future Market for PV/T	180
References.....		181
Appendices.....		190
I. Sunpath Diagram		190
II. Diffuse Hourly Diffuse Radiation vs Clearness Index.....		190
III. Hourly Diffuse Radiation Models.....		191
IV. Correcting Factor Equations.....		191
V. Radiation generated for Newcastle		192
V. Pump Controls for Manual Operation		192
VI. Data From All Microinverters 8th to 15th April		192
VII. Solar Angel Data Sheet and Manufacturer Parameters From Polysun.....		195
VIII. TRNSYS Model of PV/T.....		195
IX. Main Code of PV/T (without functions).....		196

Abstract

PV/T systems (Photovoltaic/Thermal Systems) is a hybrid assembly of PV and solar thermal collector technology and generates both electric and heat energy. Over the past three decades, various numerical analysis was conducted on PV/T systems under steady-state, quasi-dynamic state and dynamic state. It was realised that a set of factors affected the performance of the PV/T. However, a lack of standard for the PV/T, combined with limited experimental data to assess the variation in operating performance with respect to all the affecting factors is low.

The aim of this research is to study and model the dynamic behaviour of PV/T systems while identifying all the contributing factors responsible for its performance at any location. These factors are then investigated further to enable an accurate working model for application in residential buildings. The dynamic model that can identify the performance, efficiency, and impact of various factors for the given PV/T system was proposed and validated based on the experimental data and three different case studies were chosen based at three different locations(Newcastle, Lisbon and Cochin).

The main methodology chosen here was by solving the energy balance equations using the RK4 method in MATLAB which is supported by experimental results at real-time conditions in Newcastle with error of 4.2%. It was found that there is a significant improvement in the efficiency of at least 3% when compared to a real-time PV and solar collector unit in Portugal. The model was designed to supply load-demand for two residential cases (4-bed domestic house in Newcastle and Cochin). An exergy analysis was conducted to find the feasibility of these simulated models. The life-cycle cost efficiency for the case study in Newcastle was found to be 10.6% while in Cochin the life cycle cost efficiency was found to be at 23.2% with respect to exergy. The simulated model thus indicates that the exergy from Cochin is more feasible than from the system in Newcastle for the case studies considered in their respective locations.

Employing this model, the performance effect of various parameters can be established, an improved system can be designed and applied for residential buildings. This model can also be used as an indicator to comprehend PV/T performance based on location and thus, can act as a rudimentary support for PV/T standardisation.

Publications

- Antony, A., Y.D. Wang, and A.P. Roskilly, A Detailed Optimisation of Solar Photovoltaic/Thermal Systems and its Application. Energy Procedia, 2019. **158**: p. 1141-1148.
- Royapoor, M., A. Antony, and T. Roskilly, A review of building climate and plant controls, and a survey of industry perspectives. Energy and Buildings, 2018. 158:p.453-465.
(Contribution: Emerging Trends with renewable energy integration into buildings using an appropriate optimising algorithm)
- Under preparation: Designing a PV/T domestic system with storage—(Step by step considerations based on location and other parameters)—using an optimised tool
- Under preparation: Parametric dependence of PV/T with respect to location.

Acknowledgements

I thank God Almighty for all the blessings He has given to me throughout this venture.

I would like to express my sincere and heartfelt gratitude to my supervisors Professor Tony Roskilly and Dr. Yao Dong Wang for their continued support and guidance as well as for their enthusiasm, motivation, patience and their influence during the whole course of my research. I am also indebted for their immense support with lab systems and installation which helped with the validation of my research.

I would also like to express my gratitude to Dr. Mohammad Royapoor and Dr. Wan Iman Wan Mohd Nazi for their support during the initial stages of my research. I also wish to thank Newcastle University for their continual support throughout out the whole process. I also acknowledge the lab technicians for their assistance during the construction and installation of the research prototype.

Finally, I would also like to express my gratefulness to my wonderful husband, my parents and my brother for their endless support.

List of Figures

Figure 1: Global final energy consumption from all fuel resources (REN21, 2018).....	20
Figure 2: Global Final Energy Consumption from Renewables(REN21, 2018)	21
Figure 3:Final energy consumption for the EU	21
Figure 4: Renewable energy capacity growth (Masson and Kaizuka, 2018)	22
Figure 5: Classification of PV/T	32
Figure 6: Simple layout of PV/T(Chow, 2010).....	33
Figure 7:Equivalent circuit of simplified battery (Dubey, 2010).....	36
Figure 8:Natural circulation mode.	38
Figure 9: Forced circulation mode.	39
Figure 10:Types of PV/T air collectors (Chow, 2010).....	40
Figure 11:Types of PV/T liquid collectors (Chow, 2010)	42
Figure 12: Thermal efficiency of PV/T without electrical output production(Zondag, 2008)	44
Figure 13: Electrical efficiency of PV and PV/T(Zondag, 2008).....	44
Figure 14:Classification of PV/T liquid collectors (Daghigh et al., 2011).....	45
Figure 15:Glazed collector(Kim and Kim, 2012)	49
Figure 16:Unglazed collector(Kim and Kim, 2012)	50
Figure 17: PV/T layer efficiency(Zondag, 2008)	51
Figure 18:Type 1A collector(Department of Buisness, 2016).....	53
Figure 19:Type 1B collector assembly and configuration(Department of Buisness, 2016) ...	53
Figure 20:Type 2 Solar-Angel collector(Department of Buisness, 2016).....	54
Figure 21: Application in a domestic hot water system using type 2 collector(Solarangel, 2016).....	55
Figure 22:Type 3 collector (Nakedenergy, 2018)	56
Figure 23: Type 3 solar ventilation system collector(Department of Buisness, 2016).....	56
Figure 24:Application of Type 3 as a solar ventilation system(Solarventi-International, 2019)	56
Figure 25: Standard integrated roof tile as Type 4(Department of Buisness, 2016).....	57
Figure 26:Cross-section of Type4 from example used in Figure 25(Department of Buisness, 2016).....	57
Figure 27: Type 5 Solarus concentrator collector (Solarus, 2018).....	58
Figure 28:Active indoor pool heating(Kalogirou, 2009b, Kalogirou, 2009e, Kalogirou, 2009c, Kalogirou, 2009d).....	59
Figure 29:Type of sheet and tube configuration(Wu et al., 2017).	69
Figure 30:Flow in different heat-pipes (Parallel/harp, extruded heat pipe, fin tube and a coil/serpentine design) (Wu et al., 2017).....	69
Figure 31:(a) Direct flow design/harp, (b) Serpentine flow design, (c) Parallel–serpentine flow design, (d) Modified serpentine–parallel flow design, (e) Oscillatory flow design, (f) Spiral flow design/heat mat, (g) Web flow design(Ibrahim et al., 2009).	70
Figure 32: Standard principle for electrical storage of PV output.....	71
Figure 33:Hot and cold storage tank	72
Figure 34:Case study locations.....	73
Figure 35: PV and Solar Collector system in Lisbon.....	76
Figure 36: Layout of PV system in Lisbon.	77
Figure 37:Data sheet values of the Portugal collector	78
Figure 38:PV power generated during the winter months.....	79
Figure 39:PV power generated in summer months.....	79

Figure 40: Average energy over the year.....	80
Figure 41: Current reduction at the PV due to dust accumulation.....	80
Figure 42:Improved current at PV.....	81
Figure 43:Average temperature at Solar collector output.....	81
Figure 44:Summer months temperature.....	82
Figure 45: Winter months temperature.....	82
Figure 46:Layout of PV/T on USB.....	83
Figure 47:PVe output.....	84
Figure 48:PV/T layout with data logger.....	85
Figure 49:Weather sensors.....	86
Figure 50: Sensors and pump system installed on USB.....	86
Figure 51:Isometric view of PV/T.....	87
Figure 52:Annual USB electric energy data from Meteorology.....	89
Figure 53: Temperature sensors at the USB.....	90
Figure 54:LAB demonstration unit.....	91
Figure 55:Lab unit setup in snow and sunny conditions.....	92
Figure 56:Electrical energy generated in the rig during the test week.....	92
Figure 57:PV/T connection assembly (using RESOL).....	93
Figure 58:Piping systems.....	94
Figure 59:Data logger.....	94
Figure 60:Domestic residential case for Newcastle.....	95
Figure 61: Average of Electricity Consumption for 4bed domestic house in Newcastle.....	95
Figure 62:Load heat demand in Newcastle.....	96
Figure 63: Domestic case study.....	97
Figure 64:Solar Irradiation in Cochin.....	97
Figure 65:Load Demand for the 4 bed house.....	98
Figure 66:Angles describing beam radiation on a tilted surface.....	102
Figure 67: An example validating the incidence angle for UK (period of 48 hours).....	105
Figure 68: (a) Reflectance at various interactions of layers(Martin and Ruiz, 2001) (b) Code generated reflectance.....	109
Figure 69:Radiation at tilted surface of the PV/T(Simón-Martín et al., 2016).....	111
Figure 70: Beam and Diffuse Radiation from Sky modelling using the new method for Newcastle, UK.....	111
Figure 71:Single diode equivalent of PV cell.....	113
Figure 72:IV curve at STC and NOCT radiations.....	117
Figure 73: Series connection for modelling in steady state (Kalogirou, 2009b, Kalogirou, 2009d).....	124
Figure 74: Analogous resistance circuit for PV/T (hr and hc are the heat transfer coefficients of radiation and conduction components of each layer).....	128
Figure 75:Flow chart of steady state model.....	131
Figure 76:Lisbon thermal yield.....	132
Figure 77:Newcastle annual thermal yield.....	132
Figure 78:Cochin annual thermal yield.....	133
Figure 79: Ray-trace method (The resistance values changes with respect to the input conditions).....	134
Figure 80:Side cross section of PV/T.....	134
Figure 81:Flow chart of dynamic modelling.....	137

<i>Figure 82: (a)Variability of measured and simulated total energy (b)Simulated vs actual electrical energy over a period of six months with a measured sampling rate of 30 min/interval (c) Simulated vs actual heat energy over a period of six months with a measured sampling rate of 5 min/interval.....</i>	<i>139</i>
<i>Figure 83: Shadow formation for multi-array collectors(Duffie and Beckman, 2013)</i>	<i>142</i>
<i>Figure 84: Performance curve for collector at different radiations at 0.025kg/s (simulated output).....</i>	<i>146</i>
<i>Figure 85: Simulated PV/T output vs measured PV.....</i>	<i>146</i>
<i>Figure 86:PV only PV/T system</i>	<i>147</i>
<i>Figure 87:Two cover PV/T thermal only system.....</i>	<i>147</i>
<i>Figure 88:Efficiency at different locations.....</i>	<i>148</i>
<i>Figure 89:Thermal heat gain</i>	<i>149</i>
<i>Figure 90:Cell Vs ambient temperature (UK).....</i>	<i>149</i>
<i>Figure 91:Cell temperature values for Portugal.....</i>	<i>150</i>
<i>Figure 92: Power generated by the PV of PV/T (collected from one of the microinverters) 151</i>	
<i>Figure 93: Real-time IV characteristics</i>	<i>152</i>
<i>Figure 94:Temperature distribution of components</i>	<i>153</i>
<i>Figure 95:Effect of Tilt angles on electric output in a day</i>	<i>155</i>
<i>Figure 96:Variation of FR with respect to mass flow rate and NOCT at 45 °C,47 °C and 48 °C.</i>	<i>155</i>
<i>Figure 97:Thermal gain in KWh</i>	<i>159</i>
<i>Figure 98:Schematic for PV/T in UK case study</i>	<i>160</i>
<i>Figure 99:Predicted design for Cochin.....</i>	<i>161</i>
<i>Figure 100:Schematic of Cochin.....</i>	<i>163</i>
<i>Figure 101: Location based (a) monthly radiation (b) temperature (c) wind speed for all three cases</i>	<i>166</i>
<i>Figure 102: PV cell temperature variation in three cases</i>	<i>167</i>
<i>Figure 103: Embodied energy of PV/T.....</i>	<i>172</i>
<i>Figure 104: Component prices.....</i>	<i>168</i>
<i>Figure 105: Cost breakdown of installation</i>	<i>169</i>
<i>Figure 106: Block diagram of PV/T model</i>	<i>178</i>

List of Tables

Table 1: Comparison of different PV/T types (Y. Tripanagnostopoulos, H. Schranzhofer, 2005, Daghigh et al., 2011) 45

Table 2: Efficiency of unglazed and glazed PV/T 50

Table 3: Case studies selected 73

Table 4: Absorptance of black paint (Kalogirou, 2009a) 104

Table 5: Incidence Angle comparison 105

Table 6: Comparison of various software that include PV/T modelling 108

Table 7: Empirical values for the coefficients of Back surface module (King et. al., 2004) 116

Table 8: Design Parameters of the steady state system 124

Table 9: Array current for Newcastle case study 157

Table 10: Solar Angel parameters 157

Table 11: Array current for Cochin case study 161

Table 12: Cost breakdown of LAB system installed (from the Newcastle University cost directory) 168

Nomenclature

A	Area of collector (m^2)	Dext	Diameter of the external tube (m)
S	Absorbed radiation (W/m^2)	Di	Diameter of inner tube (m)
b	Absorber node	ID	Diffuse radiation at tilted angle
Abg	Absorber gross area (m^2)	mCe	Effective heat capacity (J/K.m)
Ta	Ambient temperature (celsius)	F'	Efficiency factor
Ag	Area of radiation incident on glass (m^2)	Ep	Electric power generated by PV (W)
Ab	Area of the absorber (m^2)	Ep	Electricity generated at PV (W)
Ac	Area of the solar cell (m^2)	eg	emissivity of glass
Apv	Area of the solar module (m^2)	ep	emissivity of PV
Ibatt	Battery current (amperes)	E	Equation of time (minutes)
V_{batt}	Battery voltage (volts)	Exeff	Exergy efficiency (%)
IB	Beam radiation at tilted angle (degrees)	Exin	Exergy input (Wh)
Tcell	Cell temperature ($^{\circ}C$)	Exsun	Exergy of the sun (Wh)
Kt	Clearness Index	Exout	Exergy output (Wh)
c	Convection transfer	G₀	Extra-terrestrial radiation (W/m^2)
N	Day of the year	f	Fluid node

<i>g</i>	<i>Glass node</i>	<i>mf</i>	<i>Mass density of the fluid (Kg.m⁻³)</i>
<i>IG</i>	<i>Ground reflection radiation at tilted angle (W/m²)</i>	<i>mg</i>	<i>Mass density of the glass (Kg.m⁻³)</i>
<i>qb</i>	<i>Heat absorbed (W)</i>	<i>mins</i>	<i>Mass density of the insulation layer (Kg.m⁻³)</i>
<i>C</i>	<i>Heat capacity (J/kg.K)</i>	<i>mp</i>	<i>Mass density of the PV(Kg.m⁻³)</i>
<i>UL</i>	<i>Heat loss transfer coefficient</i>	<i>mu</i>	<i>Mass density of the tubing layer (Kg.m⁻³)</i>
<i>Fr</i>	<i>Heat removal factor</i>	<i>ṁ</i>	<i>Mass flow rate (kg/sec)</i>
<i>FR</i>	<i>Heat removal factor</i>	<i>M</i>	<i>Mass of the object (kg)</i>
<i>h(wa)</i>	<i>Heat transfer coefficient along the tube. (W/m² °C)</i>	<i>Tm</i>	<i>Mean plate temperature (°C)</i>
<i>H</i>	<i>Heat-transfer coefficient (W/m²K)</i>	<i>Np</i>	<i>Number of cells in parallel</i>
<i>Kθ</i>	<i>Incidence angle modifier</i>	<i>Ns</i>	<i>Number of cells in series</i>
<i>Tfin</i>	<i>Inlet fluid temperature (°C)</i>	<i>Nu</i>	<i>Nusslet number</i>
<i>Tin</i>	<i>Inlet temperature (°C)</i>	<i>V₀</i>	<i>Open circuit voltage (volts)</i>
<i>Di</i>	<i>Inner diameter of the tube (m)</i>	<i>Tfoutlet</i>	<i>Outlet fluid temperature (°C)</i>
<i>i</i>	<i>Insulation node</i>	<i>Tout</i>	<i>Outlet temperature (°C)</i>
<i>x</i>	<i>Length of the tube (m)</i>	<i>POC</i>	<i>Point of contact</i>
<i>ltube</i>	<i>length of tube m</i>	<i>K</i>	<i>Polarization constant</i>
<i>LST</i>	<i>Local standard time</i>	<i>P_{pump}</i>	<i>Power consumed by the pump (W)</i>
<i>L_{loc}</i>	<i>Location longitude (degrees)</i>	<i>Pr</i>	<i>Prandtl number</i>
<i>mb</i>	<i>Mass density of the absorber layer (Kg.m⁻³)</i>	<i>pf</i>	<i>Profile angle</i>
<i>meva</i>	<i>Mass density of the eva layer (Kg.m⁻³)</i>	<i>p</i>	<i>PV node</i>

<i>r</i>	<i>Radiation transfer</i>	<i>Cu</i>	<i>Specific heat capacity of the tubing and bond (J/Kg.K)</i>
<i>Ra</i>	<i>Raleigh number</i>	<i>T</i>	<i>Temperature of respective node (°C)</i>
<i>p</i>	<i>reflectance</i>	<i>Rb</i>	<i>Terminal resistance independent of soc</i>
<i>krf</i>	<i>Reindal 2 fit</i>	<i>E</i>	<i>Terminal voltage</i>
<i>Re</i>	<i>Reynolds number</i>	λb	<i>Thermal conductivity of the absorber layer (1/K.m)</i>
<i>Rs</i>	<i>Series resistance</i>	λeva	<i>Thermal conductivity of the eva layer (1/K.m)</i>
<i>Isc</i>	<i>Short-circuit current (amperes)</i>	λg	<i>Thermal conductivity of the glass (1/K.m)</i>
<i>Rsh</i>	<i>Shunt resistance</i>	λins	<i>Thermal conductivity of the insulation layer (1/K.m)</i>
<i>az</i>	<i>Solar azimuth angle (degrees)</i>	λp	<i>Thermal conductivity of the PV (1/K.m)</i>
G_{sc}	<i>Solar constant (W/m²)</i>	λu	<i>Thermal conductivity of the tubing layer (1/K.m)</i>
<i>Ws</i>	<i>Spacing distance between tubes (m)</i>	<i>thickb</i>	<i>Thickness of absorber layer (m)</i>
<i>Cbo</i>	<i>Specific capacity of the weld bond (J/Kg.K)</i>	<i>thickeva</i>	<i>Thickness of EVA layer (m)</i>
<i>Cb</i>	<i>Specific heat capacity of the absorber (J/Kg.K)</i>	<i>thickg</i>	<i>Thickness of glass layer (m)</i>
<i>Ceva</i>	<i>Specific heat capacity of the eva layer (J/Kg.K)</i>	<i>thickins</i>	<i>Thickness of insulation (m)</i>
<i>Cf</i>	<i>Specific heat capacity of the fluid (J/Kg.K)</i>	<i>thickp</i>	<i>Thickness of PV layer (m)</i>
<i>Cg</i>	<i>Specific heat capacity of the glass (J/Kg.K)</i>	<i>thickt</i>	<i>Thickness of the tube (m)</i>

Cp	<i>Specific heat capacity of the PV (J/Kg.K)</i>	Mu	<i>Total mass of the tube (Kg)</i>
t	<i>Time</i>	Quele	<i>Useful electrical energy (W)</i>
Ul	<i>Total heat loss coefficient (W/m²k)</i>	Qu	<i>Useful heat gain (w)</i>
Mb	<i>Total mass of absorber (Kg)</i>	Mu	<i>Total mass of the tube (Kg)</i>
Meva	<i>Total mass of EVA layer (Kg)</i>	Quth	<i>Useful thermal energy (W)</i>
Mf	<i>Total mass of the fluid (Kg)</i>	u	<i>Weld bond node</i>
Mg	<i>Total mass of the glass (Kg)</i>	Cu_bond	<i>Weld bond specific heat capacity (J/Kg.K)</i>
M ins	<i>Total mass of the insulation (Kg)</i>	hw	<i>wind heat transfer coefficient (W/m² °C)</i>
M ins	<i>Total mass of the insulation (Kg)</i>	W	<i>Wind velocity (m/s)</i>
Mp	<i>Total mass of the PV unit (Kg)</i>	z	<i>Zenith angle</i>

GREEK LETTERS

α	<i>absorptance</i>	η_e	<i>Electrical Efficiency (%)</i>
β	<i>Slope of the surface (degrees)</i>	α_s	<i>Solar altitude angle (degrees)</i>
γ	<i>Surface azimuth angle (degrees)</i>	ϕ	<i>Latitude angle(degrees)</i>
θ	<i>Incidence Angle (degrees)</i>	δ	<i>Declination angle(degrees)</i>
ρ	<i>reflectivity</i>	ε	<i>emissivity</i>
$\tau/\tau\alpha$	<i>Transmittance/transmittance-absorptance product</i>	η_{th}	<i>Thermal Efficiency (%)</i>

ω	<i>Hour angle (degrees)</i>	σ	<i>Boltzmann constant</i>
<u>ABBREVIATIONS</u>			
<i>ASA</i>	<i>Adjoint Sensitivity Analysis</i>		
<i>AC</i>	<i>Alternating Current</i>		
<i>Al</i>	<i>Aluminium</i>		
<i>ASHRAE</i>	<i>American Society of Heating, Refrigerating and Air-Conditioning Engineers</i>		
<i>A-Si</i>	<i>Amorphous-Crystalline Silicon</i>		
<i>BIPVT</i>	<i>Building Integrated Photovoltaic/Thermal</i>		
<i>BR</i>	<i>Beam Radiation</i>		
<i>CdTe</i>	<i>Cadmium Telluride</i>		
<i>CIS</i>	<i>Copper Indium Selenide/Sulphide</i>		
<i>c-Si</i>	<i>Multi-Crystalline Silicon</i>		
<i>CSP</i>	<i>Concentrated Solar Power</i>		
<i>DC</i>	<i>Direct Current</i>		
<i>DHW</i>	<i>Domestic Hot Water</i>		
<i>DR</i>	<i>Diffuse Radiation</i>		
<i>DST</i>	<i>Daylight Savings Time</i>		

<i>EPBT</i>	<i>Energy Payback Time</i>
<i>EPF</i>	<i>Energy Production Factor</i>
<i>EU</i>	<i>European Union</i>
<i>EVA</i>	<i>Ethylene-Vinyl Acetate</i>
<i>FEM</i>	<i>Finite Element Method</i>
<i>FPC</i>	<i>Flat Plate Collector</i>
<i>FSA</i>	<i>Forward Sensitivity Analysis</i>
<i>GHG</i>	<i>Green House Gases</i>
<i>GHR</i>	<i>Global Horizontal Radiation</i>
<i>GRR</i>	<i>Ground Reflection Radiation</i>
<i>GTG</i>	<i>Glass to Glass</i>
<i>GTT</i>	<i>Glass to Tedlar</i>
<i>HDKR</i>	<i>Hay, Davies, Klucher, Reindl</i>
<i>HTF</i>	<i>Heat Transfer Fluid</i>
<i>HVAC</i>	<i>Heating, Ventilation and Air Conditioning</i>
<i>IA</i>	<i>Incidence Angle</i>
<i>IAM</i>	<i>Incidence Angle Modifier</i>

<i>IEA</i>	<i>International Energy Agency</i>
<i>IM</i>	<i>Iterative Method</i>
<i>IPV/T</i>	<i>Integrated Photovoltaic/Thermal System</i>
<i>IRENA</i>	<i>International Renewable Energy Agency</i>
<i>LCCE</i>	<i>Life Cycle Cost Efficiency</i>
<i>LPG</i>	<i>Liquid Petroleum Gas</i>
<i>MFR</i>	<i>Mass Flow Rate</i>
<i>MPP</i>	<i>Maximum Power Point</i>
<i>NOAA</i>	<i>National Oceanic and Atmospheric Administration</i>
<i>NOCT</i>	<i>Nominal Operating Cell Temperature</i>
<i>NREAP</i>	<i>National Renewable Energy Action Plans</i>
<i>ODE</i>	<i>Ordinary Differential Equation</i>
<i>PCM</i>	<i>Phase Change Material</i>
<i>pc-Si</i>	<i>Poly-Crystalline Silicon</i>
<i>PDE</i>	<i>Partial Differential Equation</i>
<i>POC</i>	<i>Point of Contact</i>
<i>PV</i>	<i>Photovoltaic</i>

<i>PV/FPHP</i>	<i>Photovoltaic/Flat-Plate Heat Pipe</i>
<i>PV/T</i>	<i>Photovoltaic/Thermal</i>
<i>QD</i>	<i>Quasi Dynamic</i>
<i>RES</i>	<i>Renewable Energy Share</i>
<i>RES-E</i>	<i>Renewable Energy Share-Electricity</i>
<i>RES-T</i>	<i>Renewable Energy Share-Thermal</i>
<i>RHI</i>	<i>Renewable Heat Incentive</i>
<i>RK4</i>	<i>4th Order Runge-Kutta</i>
<i>RMSE</i>	<i>Root Mean Square Error</i>
<i>SOC</i>	<i>State of Charge</i>
<i>SS</i>	<i>Steady State</i>
<i>STC</i>	<i>Standard Testing Conditions</i>
<i>TES</i>	<i>Thermal Storage System</i>
<i>USB</i>	<i>Urban Science Building</i>

CHAPTER 1. INTRODUCTION

1.1 Research Background

The 1970's energy crisis was the first reality check for the world regarding its energy supply security. The twenty first century has seen more environmental problems, fluctuating fuel prices and lesser security in availability of energy than the past few decades. These problems are expected to double or triple as the population growth rises and third world countries expand their economic development in the following years. When renewable energy provided a solution for stabilising the energy security instability, governments all over the world began working towards more sustainable sources of energy, reducing fossil fuel usage and creating better environmental policies. This has been further fuelled by the ever-increasing interest in the electrification and digitalisation of every sector. In light of these developments, over 179 countries have initiated renewable energy targets in their policies by 2017 (REN21, 2018, Sawin et al., 2018).

According to the Renewables Global status (RGS) report 2018, an estimate on a global scale shows that 10.4 % of the final energy consumed was from renewables, while 79.5% was still provided by fossil fuels as shown in Figure 1.

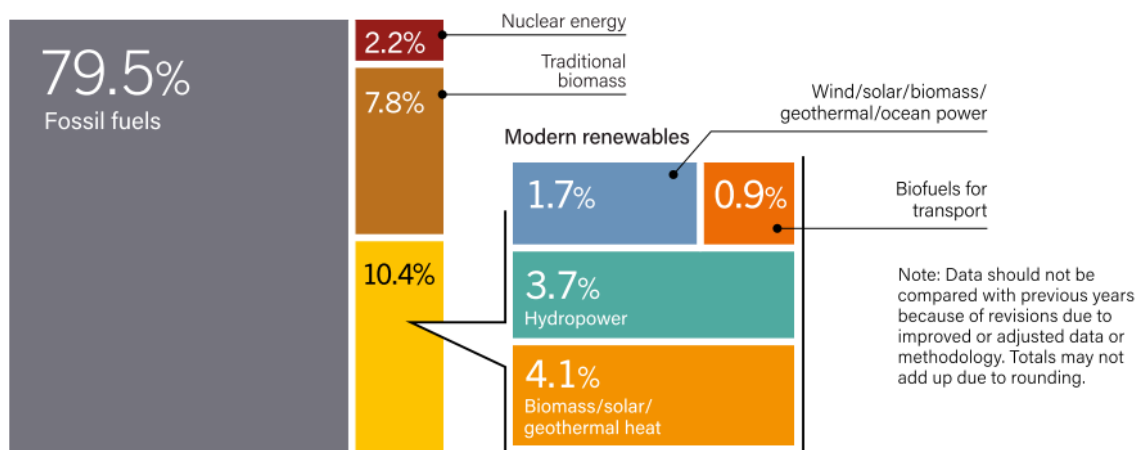


Figure 1: Global final energy consumption from all fuel resources (REN21, 2018)

The heating and cooling sector infers to thermal applications involving space heating, cooking, agricultural products, and domestic water heating. The power sector is mainly related to electric generation and consumption from renewable and non-renewable sources. Finally, the transport sector is directed to applications that consume fuels like biofuels, electricity and other fossil fuels. The energy consumption is influenced by all the above three sectors, of which, the renewable energy consumption from these sectors is attributed to the

contribution of around 27% for heat generation, 25% for total electricity generation and 3% or transport fuels as shown in Figure 2.

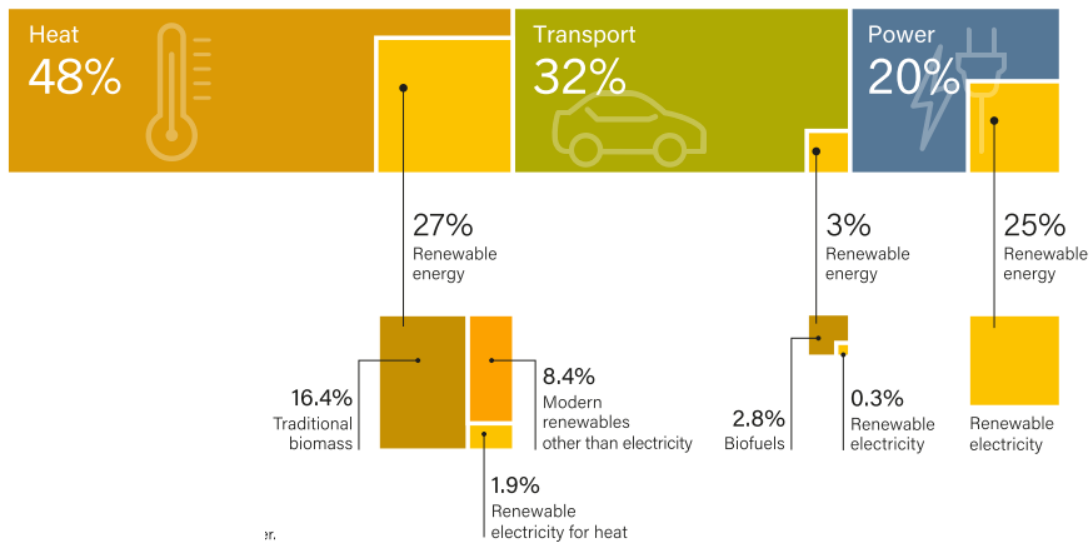


Figure 2: Global Final Energy Consumption from Renewables(REN21, 2018)

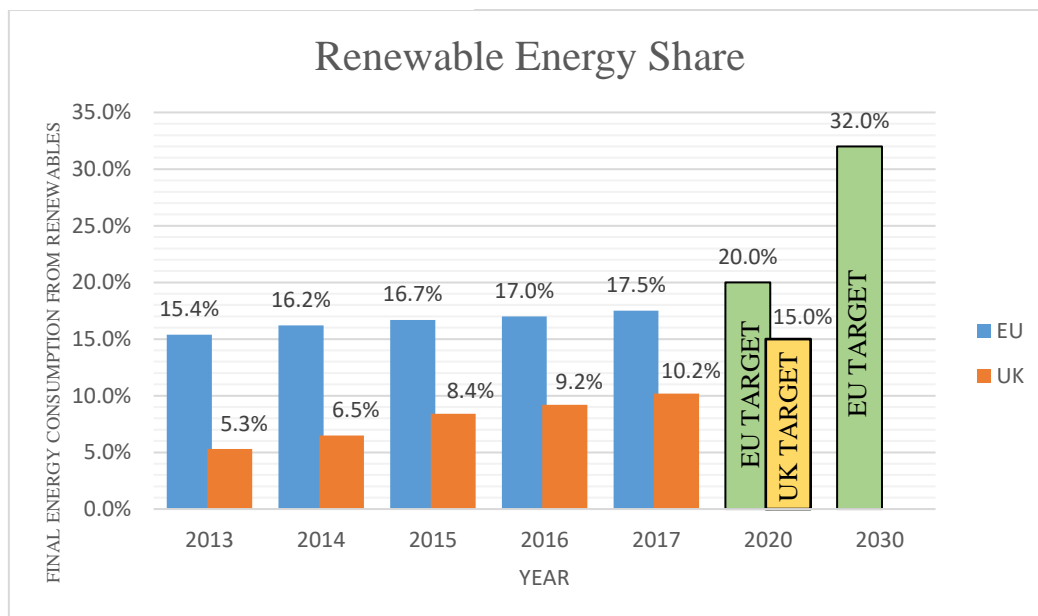


Figure 3:Final energy consumption for the EU

The European Union (EU) renewable energy share (RES) for consumption has reached to 16.7% by 2015 and aims to reach 20% of RES by 2020. The original target (decided in 2018) was 27% for the EU by 2030, with the introduction of newer encouraging policies(Sawin et al., 2015, Sawin et al., 2016, Sawin et al., 2017, Sawin et al., 2018). However, as of 2019, the binding renewable energy target has risen to 32%

(Europeancommission, 2019) as shown in **Figure 3**. Major efforts are underway to either reduce the primary energy consumed from non-renewable sources or increase the energy efficiency and consumption from renewables, as the Paris agreement aims to achieve full decarbonisation by 2060(IRENA, 2017).

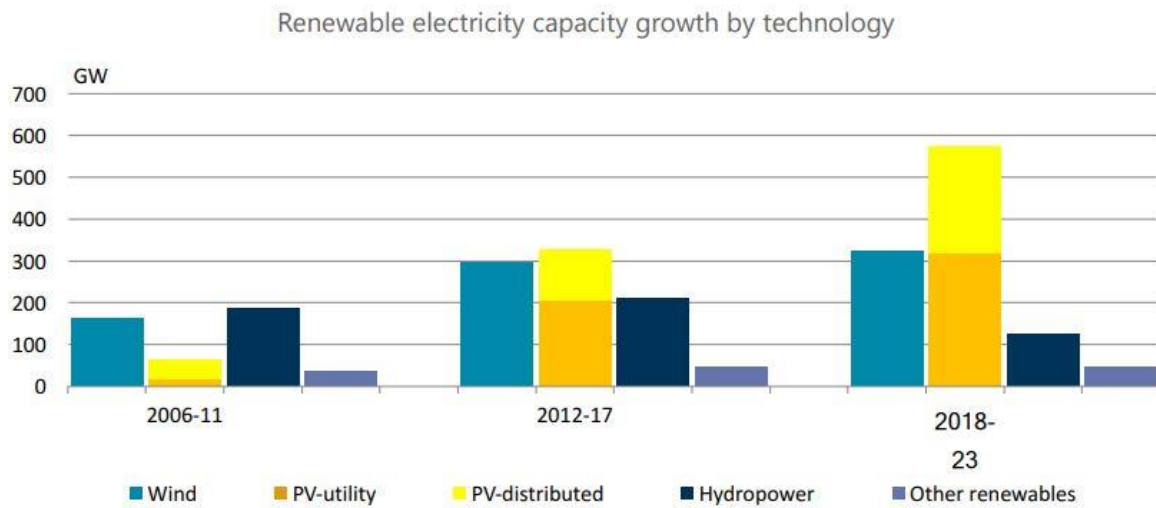


Figure 4: Renewable energy capacity growth (Masson and Kaizuka, 2018)

Solar PV and wind remains the major contributor in renewable electricity as seen in Figure 4 (Masson and Kaizuka, 2018). The growth of photo-voltaic (PV) installations has been quite notable since it surpassed wind and other technologies especially during 2016-17, while renewable heating and cooling had a slower evolution(REN21, 2018). In 2018, electric generation global solar PV energy contributed to around 25% of the electricity generation and 8.4% of solar heat generation. It has been estimated that the carbon emissions can be reduced from 1000g CO₂/KWh to 90g CO₂/KWh while using Solar PV panels instead of traditional fossil fuels like coal. However, a concerning report from the International Energy Agency (IEA) in 2018 stated that the global CO₂ emissions have been increasing rather than reducing(Masson and Kaizuka, 2018).

The renewable energy share of electricity (RES-E) for the EU has been way ahead of its directive while renewable energy share of thermal (RES-T) in heating and cooling needs to be improved drastically. The growth of RES-T has been slower than RES-E even though the deployment of heating and cooling sector is larger (Europeancommission, 2017c). Solar thermal technologies have been unable to keep up with the projections of the National Renewable Energy Action Plans (NREAP). This is mainly due to warmer winters, higher competition from lower priced fossil fuels and heat pumps. Another observation was the lack of energy efficient systems that can compete with other systems

in the market. If the switch to renewable heating systems is not made, then there is a risk of depending on only fossil fuels and thus using efficient heating and cooling technologies remain a major challenge. Low grade heat will always be a requirement for domestic consumers (eg. an indoor swimming pool or space heating). If primary electricity is used to generate low grade heat for domestic purposes, it would be very uneconomical and it can be used effectively in other sectors, where there is an imminent need to reduce fossil fuels. Hence, combining solar thermal systems with efficiency can be the best outcome for developers, investors and end consumers especially in the case of domestic hot water or space heating. The efficiency increment must also reflect the quality of the energy produced. This can be achieved using solar thermal production from renewable sources. Renewable energy policies integrating heating and cooling with other sectors is still evolving and has tremendous potential for improvement.

However, like every technology, PV has its disadvantages, one of which constitutes the initial cost. PV electricity production costs 3 times more than wind and geothermal energy and 6 times more than coal and other fossil fuels. Another disadvantage being the dependency of efficiency on weather conditions of the location. According to IRENA (International Renewable Energy Agency) in the years between 2010 and 2016, the average global cost of electricity generated from PV cell dropped down by a whopping 69% indicated in cost as a reduction from 0.36 USD/KWh to 0.11 USD/KWh (IRENA, 2017). So, it becomes an even more stressing requirement for ways to improve the efficiency of PV cells. In order to increase the efficiency of the PV panels, various methods have been proposed, one of which is PV cooling. These cooling methods can either be active or passive, where active method needs an external energy to drive the system (For example: A circulating pump with a fluid to remove the heat generated at the PV) or passive cooling (For example: Phase-change material (PCM) system) which works simply on the principle of endothermic and exothermic reactions without the need for an external driver.

There is an increasing rise in attention for using energy from solar PV to generate heat. Indeed, solar energy is currently playing a crucial role in the energy supply field for buildings using different conversion methods. Applications of solar energy in terms of solar thermal collectors and PV devices (called hybrid photo-voltaic and thermal collectors (PV/T)) have been emerging on the market for years and still have space for growth, which would be driven by continuous technical advances and increased concerns regarding energy saving and environmental protection.

The hybrid collector thus has a marketing potential for its complementary characteristics, as well as for its reduced space and cost for useful energy production.

The domestic sector in the UK utilises over 64% in space heating (European Commission, 2017b). One of the most popular means of utilising and collecting solar thermal energy is by solar water heaters as they are a very feasible technological solution and are economically attractive when compared with the other kinds of solar energy (which is electrical). Thermal energy can also be used for space heating, produce hot water or air, for heating pools and drying agricultural products. Today more than 30 million square metres of solar collectors have been installed around the globe, and the commercial markets of solar collectors have already become an established industry. Thus, a PV/T (Photo-Voltaic Thermal) system uses the familiar design of collectors and PV cells and combines the two systems to its advantage. Four case studies using passive PCM system added as an external heat sink for the PV cells was studied by Atkin et. al. (Atkin and Farid, 2015). The paper concluded that the PV cells perform at their maximum efficiency when the PCM and aluminium heat sink acts as a thermal regulator with infused graphite PCM. Therefore, a PV/T system should be able to increase the efficiency of the PV cells while removing the excess heat and utilise this heat for other domestic purposes. The PV/T systems conserves two times the area needed for installation when compared with the installation of a separate PV and conventional collector system and help generate hot water during periods of high demand.

Thus, from above it is summarised that the PV/T module is a hybrid unit with PV generating electricity and solar thermal collector generating thermal energy concurrently. It is then evident that the designing and installation of such a system will be complicated than its counterpart of individual units (separate PV and collector units). This technology is not as simple as pasting a PV on solar collectors, as it will become more coherent in the following chapters. Their behaviour is quite complex and needs to be understood in detail for utilising the system to its full potential. Therefore, the principles and technology that is applied to individual units may not be suitable for the entire unit and it is investigated in the following chapters.

1.2 Research Gaps

There has been various experimental analysis conducted on various types of PV/T and results suggest that the output is controlled by a variety of factors. According to the report from the department of Business, energy and Industrial strategy, hardly any of the studies

address the accountability of all factors together with respect to one another and their percentage effect on performance with experimental validation. The study here aims to accumulate those factors responsible and analyse them in various case studies for a comparative analysis of the effect of the parameters on the PV/T system with the help of validation from a real-time experiment of the same. This will be foot forward in standardising the performance of the PV/T system. Even though the solar key mark certificate in the Annex J of the SKN decision list was agreed in 2015 and updated in the meeting for Solar Keymark Scheme in 2018, for the PV/T and other products, due to the variations in definitions of the PV/T systems, there is still a few gaps and issues that needs to be addressed and still prevail in the performance and testing of the PV/T system based on the variable parameters(Cencertificationcommitte, 2018). This study can also help in designing and diagnosing PV/T systems with ease by finding the optimised long-term real-time behaviour in each location with all parameters defined.

Testing of commercial PV/T can either be done at indoor or outdoor conditions. Generally, the outdoor conditions are done at steady state conditions of clear weather and noon. However, the northern parts of Europe needs data for at least 6 months due to irresolution values at noon in wintertime, hence, needs a larger sample size. Indoor tests can be done faster and easier results to comprehend, but these results hardly reflect actual data. This type of testing is done for more of a base level evaluation. But outdoor testing methods have yet not been standardised fully. In order to avail the PV/T system to the commercial and research market, an international standard need to be established. The outdoor conditions are not usually done on dynamic testing. This research also aims to link variable factors with dynamic results in outdoor conditions. This allows for a generalised model to be aimed at standardising PV/T testing process. It can also be extended for use in residential applications.

1.3 Research Questions

There are quite a few studies in place to evaluate the PV/T unit under dynamic conditions, however, there are not enough parametric studies to have conclusive results to understand the effects of various parameters in real-time. The focus of this thesis ventures to understand solutions for the subsequent research questions.

Are there any existing methods to investigate the efficiency, performance and operation of the PV/T systems under any conditions and if so, are there any limitations? Are these methods as efficient as in the simulation as real-time conditions? Can this be improved

through a new method that includes all the parameters (even under no existing standards) and provide an inexhaustible tool to evaluate and design the PV/T system under dynamic conditions. The research question also investigates to realise whether the new model can be used to identify multiple parameters that affect performance. In this understanding, can this be designed to a real-time application like a residential building and does the parametric identification and control be influenced for a higher efficiency system?

This thesis investigates the various parameters with experimental data to assess the PV/T system performance for long term efficiency.

1.4 Limitations

The heating and cooling sector occupies more than half of the energy demand, but falls behind the renewable power sector when it comes to policies that support technology development and deployment (IRENA, 2017). Due to this, the slower deployment of solar thermal systems has held back its market in Europe and China (Feldman and Margolis, 2018).

The input data required for renewable energy sector has improved; however, there are significant limitations. With increased data, improved modelling techniques, higher accessibility and defined standards, the quality of delivered results will be higher. This will significantly improve the market share for PV/T systems. PV/T systems can be limited by niche markets investors. But this can be improved with higher marketability and higher quality than its counterparts and education on the market potential that can be utilised to drive more policies in favour of such a system.

1.5 Aim and Objectives

1.5.1 Aim:

The aim of this research is to validate and predict the dynamic behaviour of PV/T systems while accurately describing the factor responsible for the loss of efficiency at any point in time under various weather constraints.

1.5.2 Objectives:

- Investigate the long-term dynamic operation and develop a sustainable and general PV/T system data with storage under real climatic conditions from data acquired to predict the performance. (See chapter 3 section 3.1, 3.2 and 3.3)

- Experimentally track actual dynamic data for the PV/T to validate the dynamically simulated model from the data sheet and realise various factors needed to optimise the system while depending on certain limiting factors as well as analyse the behaviour of the system. (See chapter 3 section 3.2 and chapter 4 section 4.5)
- Predict the performance and performance factors at any conditions for any type of PV/T system installed and obtaining data on performance issues at each layer of the PV/T system. (See chapter 4 section 4.4)
- Establish basis for a standard and testing protocol for assessing PV/T performance (See chapter 4 section 4.4)
- Assess long-term dynamic performance of PV/T technology (See chapter 4 section 4.6)
- Provide evidential data analysis for determining all performance parameters (solar irradiance, heat and electricity, ambient temperature, operational temperatures, flow rates and thermal storage capacity) (See chapter 5 section 5.2)
- Assess accurate PV/T behaviour with respect to an equivalent PV under different weather conditions. (See chapter 5 section 5.3)
- Generate a feasible exergy and economic analysis of the system defined. (See chapter 6 section 6.3 and 6.4)

1.6 Research Novelty –A Summary

Concept- There is an absence of collective studies with valid evidence that investigate the performance in real-time and validate for all parameters with experimental systems. The concept design of the system was implemented by selecting a commercial product (Solar Angel DG-01) that is already available on the market as a real-time system. This was commissioned for validation with modified modelling techniques. The system can also help to find which parameters effect the system the most and can be modified to optimise the output. The practical knowledge and application of PV/T systems in real-time is not as effective as its counterparts.

System Structure and Case studies-As the system is a commercial product, optimising an existing system and improving the efficiency and standardising the testing performance is going to be promising for any future stakeholders. For the purpose of comparing variation

of the behaviour of PV/T systems, we have chosen three different case studies with different climates.

Methodology and simulation –A fully functional code in MATLAB has been developed from scratch and compared with other existing software(Riffat and Cuce, 2011). This ensures higher flexibility and reusability. The system has been validated with experimental system for two different locations and designed for a third location with full dynamic simulation models for any point in time in a year. The PV/T system is inherently dynamic as its input is not steady and steady state analysis will not be enough for a rigorous study of thermal behaviour and for controlling the system according to the parameters. Although a steady state analysis is also done, we also consider a dynamic modelling using explicit analysis/implicit analysis of the entire system with the corresponding energy and exergy analysis. Explicit analysis of the system maybe unstable if the stability condition is not met. Implicit analysis gives a more accurate representation the system but is slightly complex than explicit analysis. Thus, an implicit analysis and fourth order Runge-Kutta (RK-4) method is used to solve the system to compare the solution for a more accurate measure. A mathematical model describing the flat-plate solar collector system considering the transient properties of its different zones is constructed. In the proposed model, the analysed control volume of the flat-plate solar collector contains one tube that is divided into six nodes. We consider six nodes/six layers of the cross section and obtain energy balance equations at each node. The energy balance caused by the mass transfer during the circulating of the fluid within the solar collector is included by the definition that the collector's temperature depends on the coordinate in the direction of the fluid flow. Taking N nodes in the flow direction means that the model describes (6 x N) nodes. The governing ordinary differential equations (ODE's) were derived by applying the general energy balance for each zone in the analysed control volume of the solar collector. For one-dimensional heat transfer, the general energy balance principle is given by the change in internal energy is equivalent to the heat generated and the difference of heat transfer rates in the system.

Validation –Real-time data behaviour, laboratory testing and validation with existing published studies is proposed for validation for each different case study.

Contribution to research –The performance effect of various parameters on location can be compared cost effectively; a design for an optimised system applicable to that location can

be generated and it can be used as a reusable indicator for standardisation. The designed model can also be modified to any solar cell characteristic to predict the right output.

1.7 Structure of Thesis

Chapter 1: Introduction: This chapter briefly describes the research background, gaps, aims and objectives, the need for such a research and its novelty.

Chapter 2: Literature Review: This chapter covers fundamentals of PV/T system and existing studies revolving around PV/T studies, the potential barriers that need to be overcome and the case studies selected in this study. In this chapter, the technology that was used is analysed in detail. The pros and cons of this system are also discussed. This chapter also has a description of each system components design and changes of performance of different types studied over the years.

Chapter 3: An in-depth analysis of the real-time data is investigated. This is supported by appropriate data and references from the case study site. Three different case studies are analysed, and data is collected, and preliminary observations are made.

Chapter 4: The analytical theory behind steady state and dynamic state modelling is explained while recounting the studies done in the past and, the advantages and their drawbacks. A modified modelling of the system has been proposed and an extensive modelling section also describes the different ways of validation with real-time system. The impact of factors is also investigated.

Chapter 5: The simulation results and discussions of the steady state and dynamic state have been described in detail for all the case studies. As the validation is completed in the previous chapter, this model is put to test and used for designing a complete residential system for two locations with 100% sizing. The major impacting factors are also observed for their significance.

Chapter 6: An exergy and a brief economic analysis were done for in depth analysis. The major contributing factors can be isolated and used for application in several residential case studies. An optimisation can be completed through further feedback and validation.

Chapter 7: The conclusion addresses the challenges faced, real time results and the contribution to research. This chapter also describes the nature of future opportunities attainable through this area of research.

CHAPTER 2. LITERATURE REVIEW

2.1 Introduction

Human beings have relied on fossil fuels for a long time and the concern for the environment and its resources was only recognised during the 1970's oil crisis. Hence reinvestigating renewable resources of energy that is sustainable and abundant is urgent and necessary. One of the benefits of solar energy when paralleled with other modes of energy is that solar energy is readily available and environment friendly and generates energy without causing any pollution (Tyagi et al., 2012). Solar energy can be harnessed in two forms, electrical or thermal energy and this is acquired by Photo-voltaic (PV) cells and solar collectors (SC). These systems are usually used as two different components and generate efficiencies up to 15% (PV) and 60% (collector). PV systems convert incoming radiation into electric energy and heat (Araneo et al., 2014). The efficiency of PV cells suffers as this heat rises due to ambient temperature or configuration of the PV system. Hence in order to operate the system in optimum conditions, it is imperative to reduce the temperature of the PV cells. This is achieved with a PV/T system. The integration of PV and thermal system is re-named as a hybrid PV/T system (Balcombe et al., 2015). There are numerous types and configurations of PV and collectors and so combining these systems generate new types of configurations for which their behaviour needs to be analysed. This type of system generates both electricity and heat. Conventional solar collectors needs an external electric system for heat pumps, there have been models proposed to utilise the electric energy from PV/T to operate the heat pump systems and thus making them self-sufficient (Daghigh et al., 2011). The main advantage of PV/T lies in the ability to generate electric and heat output utilising 40% lesser area (Danilo Yu et al.). Research have also found that when optimised for electrical output of the PV/T system, it can meet up to 51% of the total electrical demand and around 36% of the total heat demand for a domestic property of 15m² collector area which is an improvement from a PV only system by minimum 2% (Herrando et al., 2014).

2.2 Concept, Theory and Classification

Within renewable sources of energy, the solar resource is contemplated to be the most feasible as it is eco-friendly with no emission, easier integration and faster payback due to the abundance of energy that is available. (Akhtar and Mullick, 1999). Solar energy is mainly captured by two methods. Photo-Voltaic (PV) energy is the energy generated when solar radiation is converted from the shortwave radiation and thermal energy is the energy generated from long-wave radiation. Even though PV cells are highly efficient in their

working, they can only convert 10-20% of the incident radiation, as a lot of energy is wasted as heat or dispersed into the atmosphere (Al Tarabsheh et al., 2016). If the heat generated is not removed, PV cells are affected by this temperature rise, thus affecting their performance. If the wasted heat can be captured as usable energy and the potential for improving the PV cell performance can be made higher, it is a successful investment in terms of energy, cost, performance and cost. The concept of PV/T systems was brought about in the 1970's. However the modelling was combined from already known models like the flat plate collector and the PV modelling methods (Duffie and Beckman, 2013). There have since been various methods in dynamic steady state and quasi steady state to numerically analyse the performance of the PV/T system with a reasonable level of accuracy. Several researches have studied singular effects of parameters on the output, but the level of combined experimental parametric studies is lower than the simulated studies.

PV/T system has enticed researchers for several years due to their higher stability of performance and efficiency when compared with separate units since 1970. The primary objective was to increase the efficiency of PV cells, as they reject 85% of the incoming radiation as heat and on prolonged exposure to such conditions, the behaviour of the PV cells starts to deteriorate (Charalambous et al., 2007). Hence there is a necessity to remove such excess heat. There are various ways in which PV/T systems are classified depending on their configuration, type of fluid used or design components. This classification can be summarised in the Figure 5 below which is quite self-explanatory.

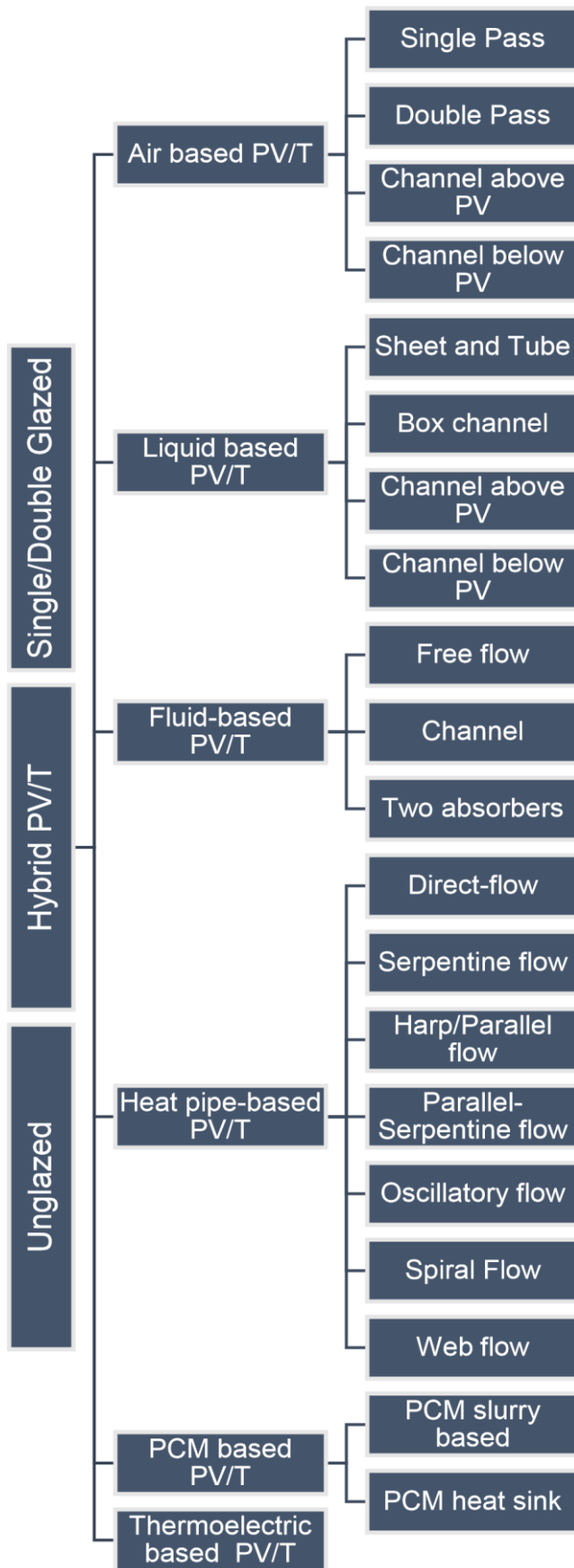


Figure 5: Classification of PV/T

The PV/T air systems are said to have lower heat conductivity, lower heat capacity and lower density than PV/T liquid systems resulting in a lower heat transfer. However liquid systems have slightly higher maintenance cost on account of regular checking for the insulated connections of the tubes and any corrosive problems. To remove heat from the PV, there might be channels below or above the cells and this can be achieved by natural or forced circulation. The generation cost of PV electrical energy is still slightly higher than conventional sources, this disadvantage can be overcome by using a PV/T system which in turn curtails the payback period due to more energy production (Abedi et al., 2012).

There are many components that make up a PV/T system. A typical PV/T system is shown in Figure 6

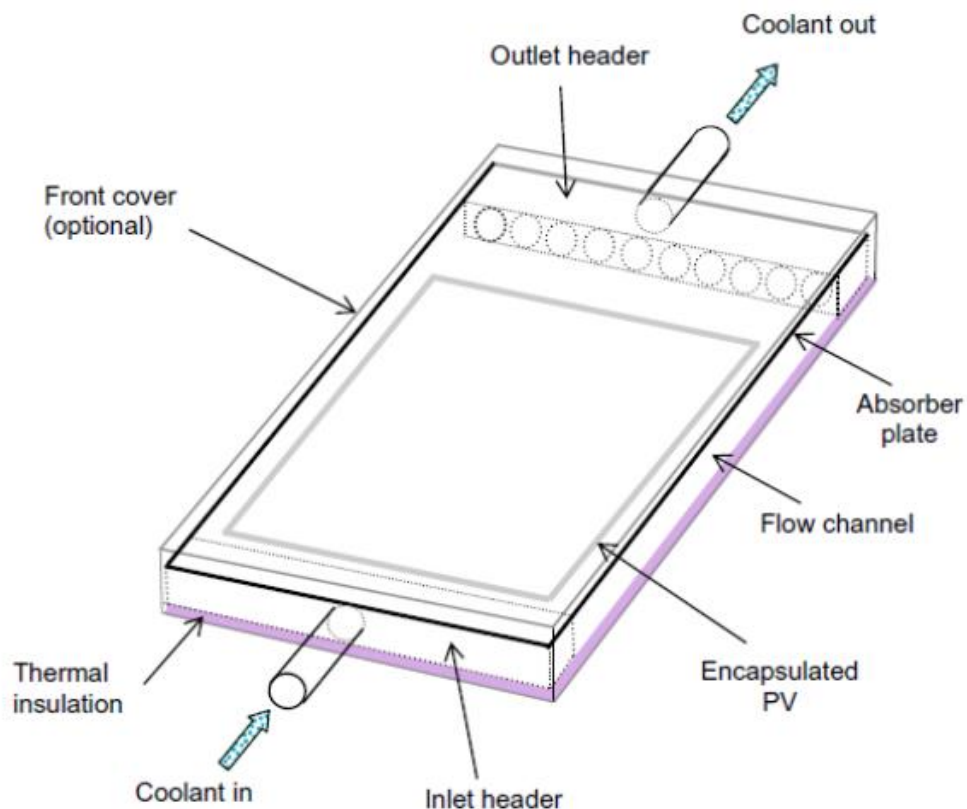


Figure 6: Simple layout of PV/T (Chow, 2010)

The main components in a typical PV/T are low-iron glass (to reduce emissivity). The presence of glass indicates that it is a glazed type of PV/T and unglazed layer has no air layer. The glazed layer is the first section where it is a layer of glass that protects the underlying layer from dust and external conditions, however this reduces the irradiation reaching the PV layer and hence lower electrical output, but a higher thermal output is obtained. The unglazed configurations have no glass layer and are considered when higher electrical output is needed

and lower thermal output. The glazed and unglazed layers are added to increase the heat energy obtained over the electric energy obtained or vice versa. The unglazed layer can encounter overheating issues on account of no protection from external factors. Thus glazed PV/T provide higher heat energy and unglazed provide better electric energy (Diab et al., 2017).

EVA encapsulate helps bond the cells together thermally and has very good transmission-absorption value, which reduces transmission losses for radiation. PV cells which can be either multi-crystalline (c-Si) or Poly-Crystalline (pc-Si) or Amorphous Silicon (a-Si). Each of these silicon cells vary in their impurity during manufacture and determines the efficiency of the PV generation. pc-Si (12% efficient) is the cheapest technology available and performs better than a-Si (6% efficient). c-Si (15% efficient) is the purest form of silicon and hence shows maximum efficiency relatively. Thin film PV cells use materials like cadmium telluride (CdTe), and copper indium selenide/sulphide (CIS) due to their inexpensive manufacturing nature when compared with amorphous silicon and can reach efficiencies up to 8-9% and 10-13% respectively. Recent researches have suggested that gallium arsenide cells reach efficiencies of up to 28.8% (Battersby, 2019). However due to their toxicity levels and slightly carcinogenic properties, their applications are limited to satellites or demonstration of solar powered cars. Organic-based PV solutions are still under research. Researchers have recently found a new novel solar cell material called the lead halide perovskites and predicts that the performance and efficiency of PV cells will be higher than gallium-arsenide cells (Kumar and Mullick, 2012). Solar collectors or the heat exchanger section of the PV/T are classified into various types like flat-plate, evacuated tube, concentrator type collector, parabolic and grooved. The flat plate and evacuated collectors are more commonly used than other types. Insulation may or may not be present in the system and is generally a co-polymer foam for retaining the heat without losses. The type of heat extraction mechanism can be by using air, liquid, via a heat pipe or heat exchanger to remove the heat generated or through a more passive method of using a PCM system and even using a PCM based slurry to extract heat which has proven better than just water (Felix Regin et al., 2009). The liquid used in PV/T liquid-based collectors encounters problems in climates with below freezing temperature and to avoid this a mixture of ethylene glycol and water can be added. A usual standard practices 30-40% ethylene glycol mixture, any more might unfavourably affect the heat transfer rate of the system. Thermo-electric based materials work similar to the principle of PCM, but has lower energy density and is able to store more energy. However, they tend to be more expensive.

PV/T systems can also be divided on the type of integrating mechanism like PV/T standalone roof-top systems or grid systems or Building integrated PV/T (BIPV/T) systems(Dutil et al., 2011).The design decisions are made according to the collector type, solar fraction and thermal to electric yield ratios which in turn affect the operation, performance and system mode of the PV/T.

PV/T cells have an overall efficiency of 70-80%, while PV cells and solar collectors have an efficiency of about 15% and 60% respectively. The design of the PV/T can be controlled to obtain either more heat energy or electric energy according to the requirement of the system by adding a glazed layer on the PV cells (glass layer) for capturing more heat, thus obtaining more heat energy and this layer can be removed if higher electrical energy is desired. Adding two layers of glass can increase the thermal energy output further. However, a third glazed layer will significantly decrease the electricity generated and this is not desired(Avezov et al., 2011).

The electric storage used in photo-voltaic applications is influenced by small variations in the state of charge (SOC) which is either a charge or discharge state depending on the weather conditions. This indicates the need for such a storage to be robust and flexible enough to accommodate sudden variations in load. Thereby the stand-alone PV unit storage is required to compensate for the deficient energy on cloudy days and in the evenings. This determines the sizing of the battery and needs to be designed appropriately.

PV/T cells have an electrical output and thermal output indicating a need to consider both types of storage types(Danilo Yu et al.). This project considers design for small-scale or a domestic plan; hence a Li-ion battery/super-capacitor that has a high specific energy and efficiency is considered and researched. A nickel metal hydride can also be scrutinised for storage which is common for PV storage however it has overheating issues if ambient temperature rises. The Lithium-ion battery is a very efficient system in terms of cost and efficiency as it is cheap and has a high energy density. It is difficult to simulate the precise behaviour of the battery due to its internal reactions (Schweiger et al., 2010). However, it has been simplified to equivalent circuits where its output is determined by equations describing its state of charge, current output and time for charging and recharging. The equivalent circuit is as shown in Figure 7

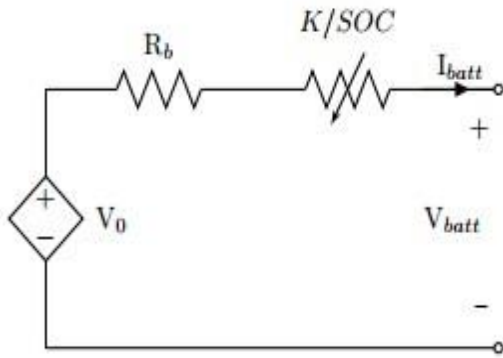


Figure 7:Equivalent circuit of simplified battery (Dubey, 2010)

The equations that describe the above system are as follows:

$$V_{batt} = V_0 - I_{batt} (R_b + K / SOC) \quad (2-1)$$

Where V_{batt} - Battery Voltage, V_0 -Open circuit Voltage, R_b -Terminal resistance independent of SOC, K -Polarization constant, I_{batt} -Battery current. The K/SOC factor shows a sharp reduction if the value of charge voltage is low. However, as the SOC approaches 1 (fully charged), there is no rise in voltage. The advantage of using this model is that the results can be corroborated with SOC of the manufacturer (Dubey, 2010, Schweiger et al., 2010, Madani et al., 2019).

Thermal storage can be of different types such as sensible heat which is the most common form of thermal storage however its low energy density is overcompensated by its size and Latent heat that uses phase change material (PCM) technology including a heat enhancing technique on account of its defective heat transfers although it has a higher storage capacity. The lesser developed thermo-chemical sorption storage has a very high energy density and storage capacity. The commercially developed products are the sensible and PCM whereas sorption technology is still under development. Latent and sorption uses lesser volume to store heat and has higher energy density, hence energy research should be driven in this direction (Danilo Yu et al.). However the materials needed are expensive, but it is predicted that since the fossil fuel prices increase because of shortage, this system will be viable replacement and hence will remunerate its initial cost in the future. Calcium chloride hexahydrate is the common form of material considered for PCM and zeolites/silica gel for thermo-physical sorption storage or Ammonia/ $MnCl_2$ salts for chemi-sorption (Günter Gartler, 2004, Pal et al., 2014, Qu et al., 2014).

The thermal and electrical efficiency and heat transfer coefficients of PV/T with storage systems can then be analysed and studied under the parameters considered, in depth, to find out the irregularities according to varying solar radiations, temperatures, storage capacity and time in terms with experimental and simulated models. This can be utilised to find out the effective variables that can be regulated to attain the optimised model of the system(Buonomano et al., 2016).

The thermal storage system (TES) has been the pivotal topic for the last two decades because it provides a secure match during delay of supply or demand and a continuous supply can be achieved while having thermal protection and inertia(Bhattarai et al., 2012).

TES systems with PCMs can thus eliminate the problems of fossil fuels usage and improve the environmental effects of global warming. The usage of TES with PCM either as a storage system or as in buildings to increase thermal comfort provides a promising sustainable solution for future developments with the same technology(Gaur et al., 2017).

Phase change process occurs due to large differences in enthalpy or sometimes a constant temperature. PCM systems store energy at higher energy density than latent heat systems and hence have greater storage capability over a smaller temperature span.

A portion of the benefits of PCM are:

- No requirement for additional thermal energy as it can store at the actual temperature of process application
- PCM stores energy in latent heat and hence the same amount of energy can be extracted without much losses.
- It is easier to switch from electrical energy to thermal energy when required.
- Carbon footprint will be reduced
- PCM systems are flexible enough to store at off peak hours and easily switched on during high demand peak hours, which can help to stabilise the grid.

The PCM type of storage system has a faster response time than the latent thermal storage. PCM has also an added advantage of switching from cooling and heating that can help reduce peak time stress. This also reduces maintenance costs and is more economically feasible.

In this project, sensible heat storage will be a main part of the laboratory systems due to its simplicity and cost limitations and PCM can be investigated into in future simulations.

The next system that needs to be reviewed is the solar water heating system. It consists of the collector and the storage. The collector or the absorber collects the solar irradiation on the FPC. The heat transfer fluid (HTF) flows through the thermal system of pipes and pumping unit for the heat to be removed to be transferred to the storage. The storage is insulated well to avoid any losses.

(i) Natural circulation: No pump is required for this system; gravity is the main contender for this type of installation. The schematic diagram of a solar water heater in natural circulation mode is shown in Figure 8. The heated water from the collector rises to the storage tank and cold water is circulated using gravity.

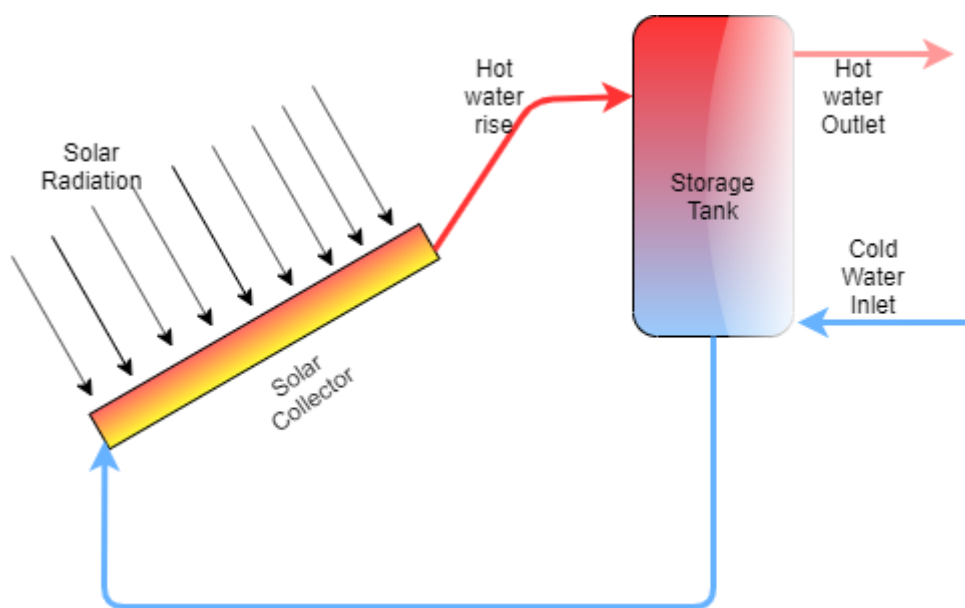


Figure 8: Natural circulation mode.

(ii) Forced circulation mode: A small pump is needed to extract hot water and pump the cold water through the piping and to the storage tank. This is usually the type of system used in most settings like in Figure 9.

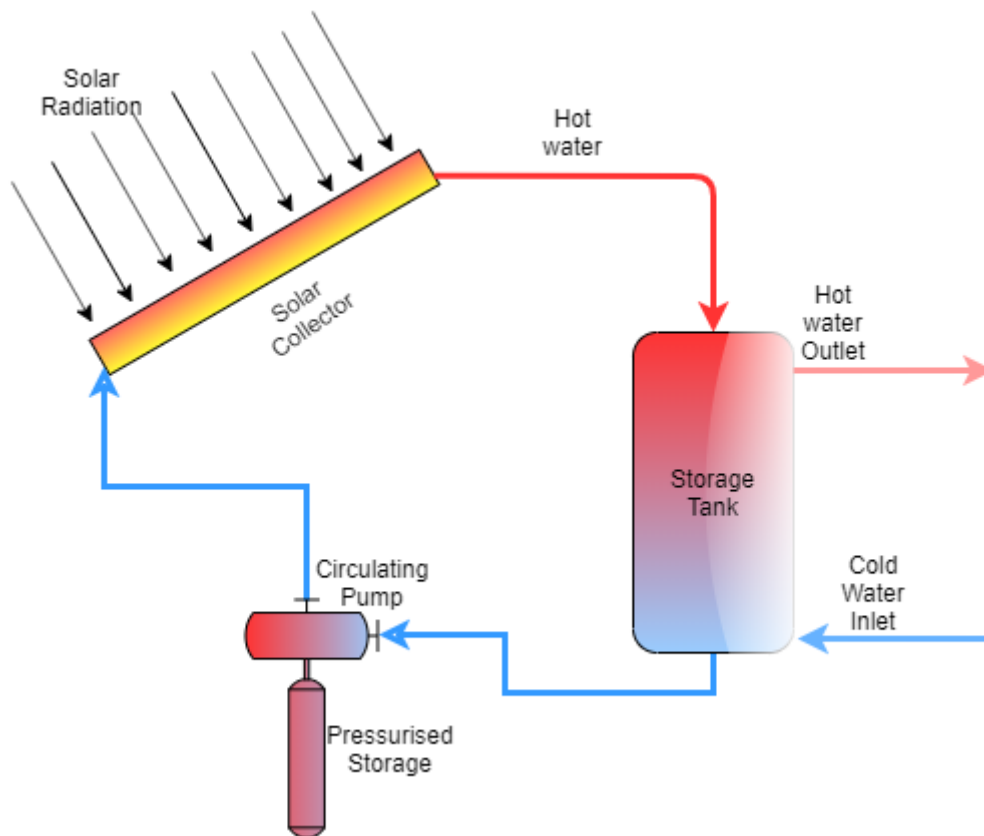


Figure 9: Forced circulation mode.

The storage system has usually two inlets, one is for hot water and the other is for cold water. There are also two outlets to extract hot water and the other one allows cold water into the piping system of the collector. This also for them to not mix at the bottom. If a higher temperature is needed connecting the system in series helps to provide a higher thermal energy. The PV/T system used here uses a pump system for the HTF. The energy balance of the system can be written as follows:

$$Q_{useful} = O_t \frac{dT_m}{dt} + U_T A_C (T_m - T_a) + M(t) C_w (T_m - T_a) \quad (2-2)$$

Where Q_{useful} is the useful thermal gain, O_t is the overall thermal loss coefficient, U_T is the heat transfer loss coefficient of collector unit and A_C is the area of the collector. $M(t)$ is the variable mass flow rate with respect to time period t and C_w is the specific heat capacity of the fluid used. T_m and T_a are the mean plate temperature of the collector and ambient temperature respectively.

2.2.1 Air PV/T

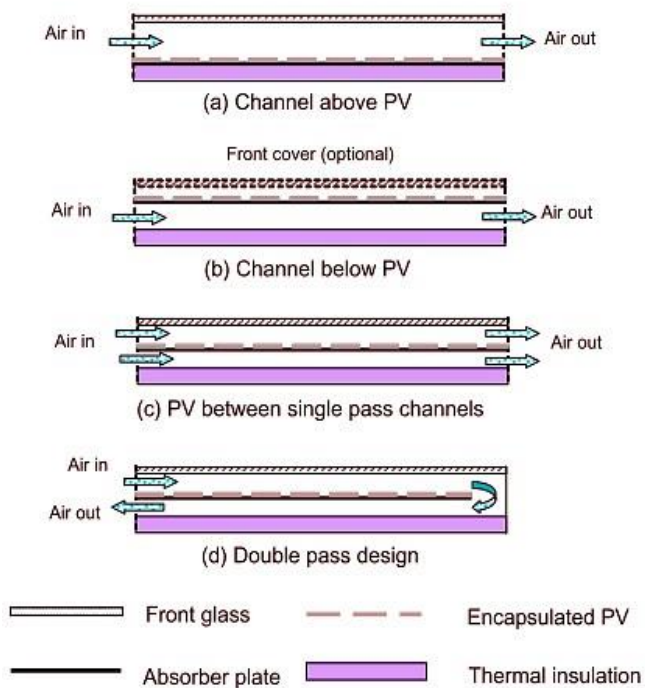


Figure 10: Types of PV/T air collectors (Chow, 2010).

PV/T air collector is an extremely simple and easy solution to cool PV modules as the air that is heated can be removed either by free or forced flow by ventilation systems. Perceptibly forced flow is more efficient since the convective and conductive heat transfer is faster and better. However, this can adversely affect the electric gain due to the extra output required for the fan. An expansive investigation was performed by Chow on four different types of air PV/T collectors shown in Figure 10 (Chow, 2010). The analysis of a numerical nature revealed results as that the first type of mode (a) to be of the lowest performance, while mode 3 (c) consumes the least fan power. A higher value of output was obtained when reflectors were added. Chow analysed a PV/T model in explicit method which allows for a multi-node dynamic analysis and was validated by sensitivity analysis (Chow, 2003). Zakharchenko et al., also noted that commercial PV is not very efficient to be used with a PV/T system and that PV and the absorber needs to have a significant thermal contact for better heat removal and overall system performance (Zakharchenko et al., 2004). This can be done by an EVA (ethyl vinyl acetate) film layer as a substrate and it has better thermal conductive properties than other materials intended to be used (Mcintosh et al., 2009b). The aluminium absorber plate used here was 2mm and a thinner insulating film of lower thermal conductivity and the observation was also drawn to point that the area of absorber should be larger than solar cells and should be located where the coolant enters the system. Using various authenticated

theoretical models a study was conducted by Tonui & Tripanagnostopoulos to find the amount of improvement when adding a metal sheet in the air channel (J.K. Tonui and Y. Tripanagnostopoulos, 2007). It was shown that this is quite an effective method especially when replicated with building integrated PV/T (BIPV/T) air integrations but depth of channel, mass flow rate (MFR), length of system or power consumed by fan had relatively less effect on the system performance. A bi-fluid collector was presented improving from previous research. The best mode of heat extraction from the PV panels is by putting the heat exchanger behind the PV module for a combined air and fluid system (European Commission, 2017a). The integrated PV/T system can reduce cost payback period by 10 years when used as a low grade heat system in conjunction with electrical output generation. Another study used a bi-fluid combined system for preheating and for DHW (domestic hot water) generation (Matuska, 2014). Higher fluid temperature devices allow for coupling with cooling devices during summer and can also provide DHW system without using an auxiliary system. Zondag et al., developed 1D, 2D and 3D steady-state and dynamic models of PV/T that uses a serpentine design and was validated using experiments and an error tolerance of 5% was obtained (H. A. Zondag et al., 2002, Zondag, 2008). The 2D and 3D models generate a detailed model of the PV/T. Through simulations a set of nine different liquid PV/T configurations was defined. It was found that that thermal efficiency of unglazed and glazed was found to be 52% and 58% respectively and a configuration where the channel is above the PV obtained an efficiency of 65%. The channel below PV configuration has the best efficiency among all four models and glazed, sheet and tube design were the most cost efficient.

2.2.2 Liquid PV/T

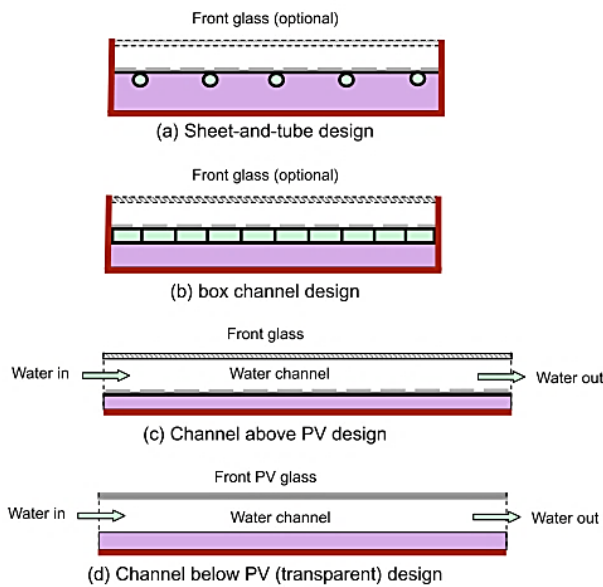


Figure 11:Types of PV/T liquid collectors (Chow, 2010)

When the fluid used for heat extraction is either water or a refrigerant or other fluid like brine/PCM slurry, such a system is called a liquid PV/T collector. Water is usually the commonly used fluid due to its easy accessibility, availability, usability for reducing heat generated.

The single glazed sheet and tube is the most commercially available product in the market and easily accessible especially for domestic hot water (DHW) and low-grade heating applications. The uncovered PV/T liquid collectors are recommended as the reflection losses and heat losses are small due to lower operating temperatures. In reference to Figure 11, it was noted from various studies that (a) and (b) were the uncovered types of PV/T design (when the glass layer is optional) and generated efficiencies from 52-58%, while (c) which shows the channel above PV had an efficiency potential of 65%, however (d) that shows the channel below PV design is recommended as the better configuration if efficiency is of utmost importance. However, the sheet and tube design provide a cheaper solution with the disadvantage of an efficiency reduction of 2%. This type is usually utilised in domestic hot water systems. Low grade heat is obtained when uncovered PV/T is used as there is no reduction in the transmittance absorptance product which is due to the absence of the glass layer (Chow, 2010).

The performance of liquid PV/T collectors with c-Si solar cells along with the polymer and thermal absorber was investigated. Box type absorber channels when filled with ceramic drill were found to improve heat transfer of the fluid (Rajput et al., 2018). The study also showed a

10% decrease in heat absorption of solar cells due to incident radiation the glass cover can also reduce the optical efficiency by around 5% (Saini et al., 2018). There are problems that can be solved and were lower PV efficiency, architectural uniformity and limited space and roof that influenced the combination of PV/T. The only problem that was discovered was the high cost and low efficiency which can be reduced by appropriate heat removal from the PV modules.

There are various types of PV/T that can be either grid-connected, standalone systems or building integrated PV/T (Y. Tripanagnostopoulos). Assimilation of a PV/T for domestic heating and Cooling was done in the island of Rhodes (Cremers et al., 2015). The simulation was done in comparison with the conventional solar collector and they concluded that the efficiency of conventional solar collector is about 9% higher than a PV/T system. However, despite this reduction it can provide the domestic heating and cooling demands for that region. Using different kind of solar cell materials have also been investigated in various studies and have been concluded that crystalline silicon and amorphous silicon and CuInSe₂ and it was concluded that to increase the heat demand for heat extraction mechanism that needs to be performed, the operation has to be optimised.

It was mentioned that the design of sheet and tube was the most simplest and easy to manufacture but only providing a efficiency of 2% less than its counterparts (Rekstad, 2002, Strutt, 2002, Kader et al., 2006, Aste et al., 2012). Different models of hybrid PV/T systems have been investigated by using different algorithms for quantitative predictions on the system and the module produced that heat from the system and can be predicted exactly. The predicted efficiency was in the range of 60-80% and an evaluation was also conducted on the PV/T system in Tokyo and a specified designed and constructed hybrid collector of non-selective aluminium with around tube absorber was conducted with a single cover system, the PV/T consists of glass wool as the insulating material, the performance study was done to compare conventional systems with the PV/T system that is also known as integrated photovoltaic/thermal system (IPV/TS) (Nualboonrueng et al., 2011). It showed that polycrystalline has been integrated with the coordinated polycarbonate sheet and tube system and produced extremely good thermal efficiency. Further improvement was recommended based on the insulation; low-cost amorphous silicon thin film solar cell was also suggested as one of the future works.

A comparative study from Netherlands by Keizer (De Keizer et al., 2016) estimates that the concepts of sheeting tube channel PV/T free flow to absorber PV/T liquid collectors that were

also effective than conventional sources. The liquid type has higher efficiency and better economic feasibility and fewer leakages as the heat transfer coefficient of liquids is more than air.

A typical thermal collector with no electrical output is shown in Figure 12 with effect of the number of covers. The type of absorber used here is the most common sheet and tube collector. Thermal efficiencies of solar collector are investigated in terms of $(T_{in}-T_a)/G$ where T_{in} is the inlet temperature, T_a is the ambient temperature and G is the incident radiation on the surface.

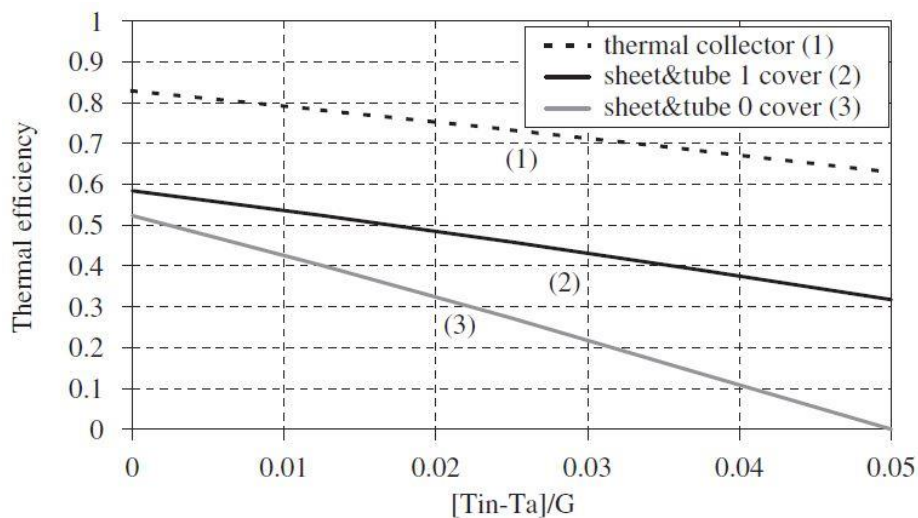


Figure 12: Thermal efficiency of PV/T without electrical output production(Zondag, 2008)

Figure 13 shows the electrical efficiency of the PV and PV/T systems and that of sheet and tube electrical efficiency with respect to a secondary axis. It is to be noted that the electrical efficiency is lower than conventional values.

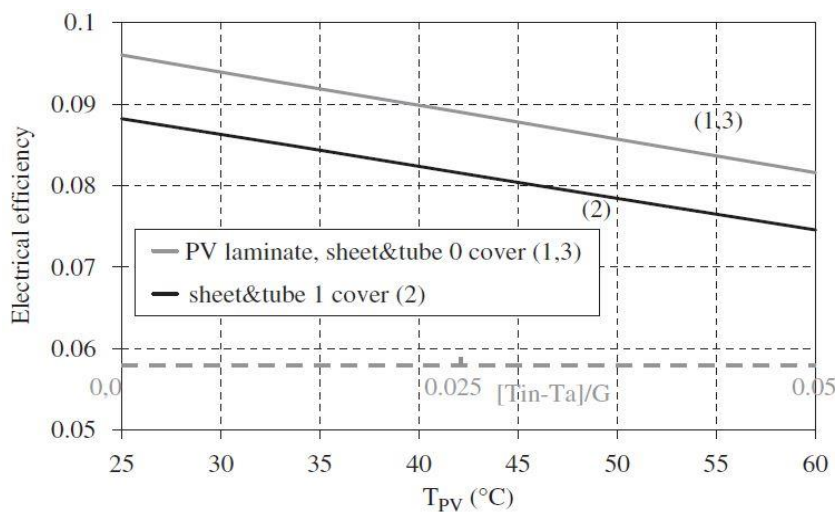


Figure 13: Electrical efficiency of PV and PV/T(Zondag, 2008)

The PV cells materials can contribute to the overall efficiency as mentioned previously. Mono-crystalline cells make up 80% of the PV cell production in the present PV cell market. The main factors that affect the efficiency of these cells are the incident radiation, maximum operating temperatures and different types of materials used as semiconductors in the PV cells. (Dupeyrat et al., 2014).As it is not possible to regulate every type of application and configuration of PV/T structures used by the manufactures, the practical and general way of controlling the system is by manipulating the temperatures at the PV cell which is perceptibly by controlling the factors at the heat extraction mechanism like the mass flow rate, outlet/inlet temperatures(De Soto et al., 2006).

According to Ibrahim et. al., different types of collector tube configurations were studied and found that spiral flow design provides better heat extraction and overall efficiency with low surface temperature than a single pass rectangular collector(Ibrahim et al., 2011).

PV/T liquid collectors are classified according to the type of liquid that is used and is clearly shown in Figure 14. The four types of liquid PV/T applications are also mentioned in the Table 1.

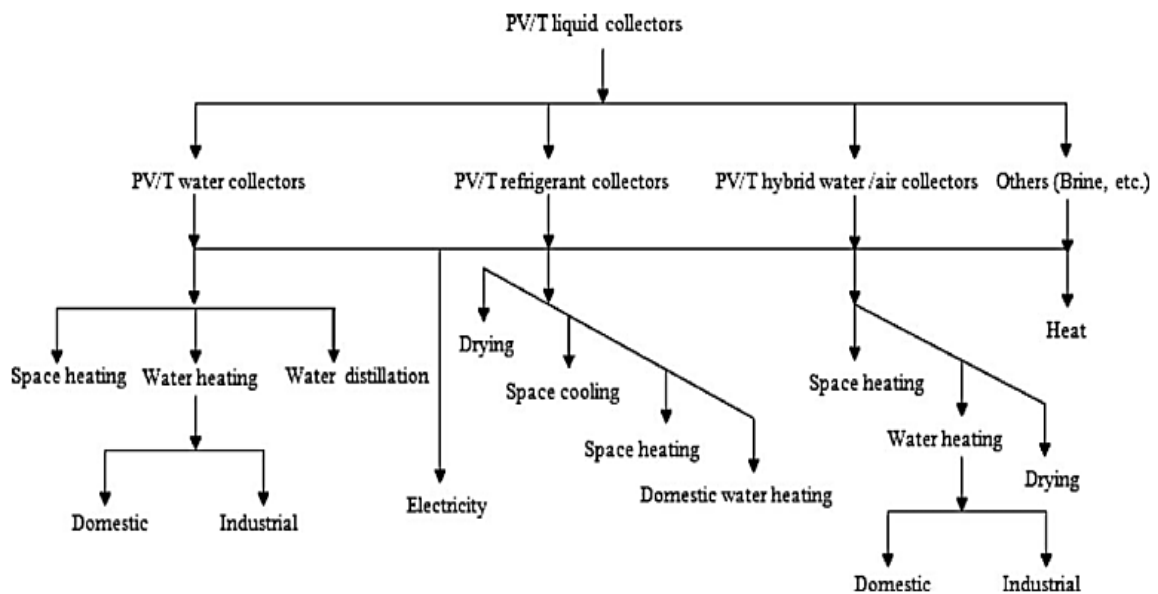


Figure 14:Classification of PV/T liquid collectors (Daghigh et al., 2011)

Table 1: Comparison of different PV/T types (Y. Tripanagnostopoulos, H. Schranzhofer, 2005, Daghigh et al., 2011)

PV/T models	Efficiency	Advantage	Disadvantages
-------------	------------	-----------	---------------

Air- based PV/T type	24%–47%	<ul style="list-style-type: none"> - Low cost - Simple structure 	<ul style="list-style-type: none"> - Low thermal mass - Large air volume - Low heat removal - High heat loss
Water-based PV/T type	33%–59%	<ul style="list-style-type: none"> - Low cost - Direct contribution - High thermal mass - Low flow volume 	<ul style="list-style-type: none"> - Lower grade heat removal temperature - Varying heat removal - Complex structure - Risk of fluid freezing in pipe
Refrigerant- based PV/T type	56%–74%	<ul style="list-style-type: none"> - Low PV temperature - Stable performance - High efficiency - Effective heat removal -No risk of freezing 	<ul style="list-style-type: none"> - Risk of leakage - Unequal liquid distribution - Higher cost - Difficult to operate
Brine/ PCM slurry based PV/T type	42%–68%	<ul style="list-style-type: none"> - Low PV temperature - Stable performance - High solar efficiency - Effective heat removal - Reduced power input 	<ul style="list-style-type: none"> - High Maintenance cost - Risk of damage - Complex structure -Still in development -Low grade heat (60-80°C)

According to Table 1, the most efficient system of the liquid collectors is the refrigerant based PV/T. In colder countries, due to the risk of freezing, a refrigerant based PV/T is used where a percentage of ethyl glycol (around 20-30%) is mixed with water to form a refrigerant based fluid. An experimental simulation was performed by Tripanagnostopoulos et. al.. on air and liquid collectors with various configurations and found that the production costs for air collector and liquid were 5% and 8% with p-Si cells(Tripanagnostopoulos et al., 2000). Some of the recommendations to reduce this cost was to provide a distance between collectors to avoid shading and diffuse reflectors to increase the radiation. The results stated the thermal

efficiency to be 38-50% for air collectors and 55-80% for liquid collectors, during steady state analysis at noon for Patra, Greece.

Kalogirou investigated unglazed PV/T collector system under the operating conditions of India geothermal energy efficiency were said to be around 40 to 45% and is said to be underperforming even under the presence of strong radiation. The lifecycle analysis showed that it's about 2 years a colder climate climatic condition was also analysed by Josh and Tiwari (Kalogirou, 2000, Tiwari et al., 2006, Joshi et al., 2009).

An experiment in Saudi Arabia by Saini, V., et. al. was done to evaluate the performance of the PV/T system under harsh conditions it was finally concluded that even though it has produced high thermal efficiency the PV cells were not able to perform optimally during summer due to extreme conditions and was not adaptable to that kind of weather(Saini et al., 2018).

For a simulation study of 12 cases with two different types of PV systems using polycrystalline silicon and amorphous silicon in three cities Athens, USA and Cyprus the major results showed that polycrystalline silicon have higher thermal contributions than amorphous silicon even though the amorphous silicon is cost efficient, the economic advantage of using poly-crystalline silicon is higher in the long run (Kambezidis and Psiloglou, 1997, Kalogirou, 2001, Usama Siddiqui et al., 2012). Similar conclusions were reached when studies were conducted on an industrial scale(Herrero López et al., 2015). A study by Saito in Japan was conducted to find out the performance of a single glazed sheet and tube PV/T collectors with brine solution as the coolant had improved the efficiency of the cell by 10-13% and the Collector efficiency by 40-50%(Cho et al., 2009, Nualboonrueng et al., 2012).

The main objective in this research is to enrich the electric efficiency while removing and utilising the waste heat. Vokas et. al. conducted a PV/T theoretical analysis at steady state in three sites for various tilt angles. The main conclusion was that heating and cooling of the PV/T is significantly affected by the location(Vokas et al., 2014). Dubey et. al., studied four diverse case studies of layouts of glass and PV, where glass to glass (GTG) PV modules was found to generate more electric efficiency and higher air temperature(Dubey et al., 2009). In a study by Guarracino et. al., the highest electric efficiency was generated by an unglazed collector while higher thermal efficiency was observed to be from the double-glazed collector. However, it was also noted that higher emissivity can unfavourably affect the thermal efficiency by 10%(Guarracino et al., 2016). In an expansive study by Sun et. al., the effects of

tilt angle and the type of different connection modes of collectors were investigated. The main conclusions from the study was that optimal tilt angle is quite closer to the actual latitude especially in lower latitude locations while tilt angle needs to be higher to improve the forecast. It was also observed that the parallel connection generate 2% higher electric efficiency and series combination improve thermal heat gain by 11.4%(Sun et al., 2016). Saini proposed the use of monocrystalline silicon by considering find different cases of PV/T concentrated collector and observed that monocrystalline silicon provided a better place than others when investigated in New Delhi(Saini et al., 2018). An experimental and theoretical performance of an asymmetric photovoltaic thermal system by Koronaki studying different asymmetric collectors and found that the collectors were able to produce 2.2 kilowatt useful energy in summer 2.8 kilowatt in spring and 2.6 kilowatt in autumn(Koronaki and Nitsas, 2018). A steady state analysis was conducted with the PV/T collector with a triangular groove and for a radiation of 385 to 820 W/m² and mass flow rate between 0.007 kg/s and .07 kg/s per second, an improvement was observed(Fudholi et al., 2018). Zohri shows that v groove has a higher thermal efficiency than other collectors(Zohri et al., 2017). Yandri observed the behaviour of dual heating on hybrid PV/T and obtain that there is a potential to improve the efficiency up to 13% through internal heating(Yandri, 2017). Lu et. al. investigated three different PV/T systems that have different configurations and concluded that PV/T 3 has a higher electric efficiency than the rest and PV/T 1 has a higher thermal efficiency potential and that the gap increases thermal efficiency(Lu et al., 2017). The location of PV cells and air gap is a useful design tool when designing future PV/T systems. Ziapour looked into a passive photovoltaic thermal system as a combination of photovoltaic panel and a compact solar water heater this was numerically studied and losses was observed and found that the use of removable insulation reflectors can actually result in saving extra thermal energy(Ziapour et al., 2016). Tiwari et. al., found an increase in thermal efficiency from 65.7% to 89.44% increase of mass flow rate for forced and natural mode respectively(Tiwari and Tiwari, 2016).

2.2.3 Glazed PV/T Collectors

There have been many definitions of glazed and unglazed collectors which have quite been contradictory in various journals and literature as well as being intermixed with uncovered and covered PV/T. The definitions used in this research pertain to unglazed collector as a PV/T hybrid system that has no layer of air in between the glass and PV layer while the glazed has that fluid layer in between.

The significant market for PV/T systems are for the most part connected with combinations of combi systems. These days the European market utilizes customary solar systems in private applications while 4/fifth of those applications is utilizing residential boiling water systems and 1/tenth is by utilizing the solar collectors for space warming and the remainder of the 1/tenth is utilized in different applications. Space heating and pool heating has a very niche market space (mainly at colder countries). PV/T can bolster this application alongside the local DHW. Be that as it may, in the present market the applications for coated PV/T have issues with higher stagnation temperatures and thermal losses. Notwithstanding this, there is additionally no standard of this kind of PV/T, which can make the market less engaging. An example of glazed collector is shown as in Figure 15.

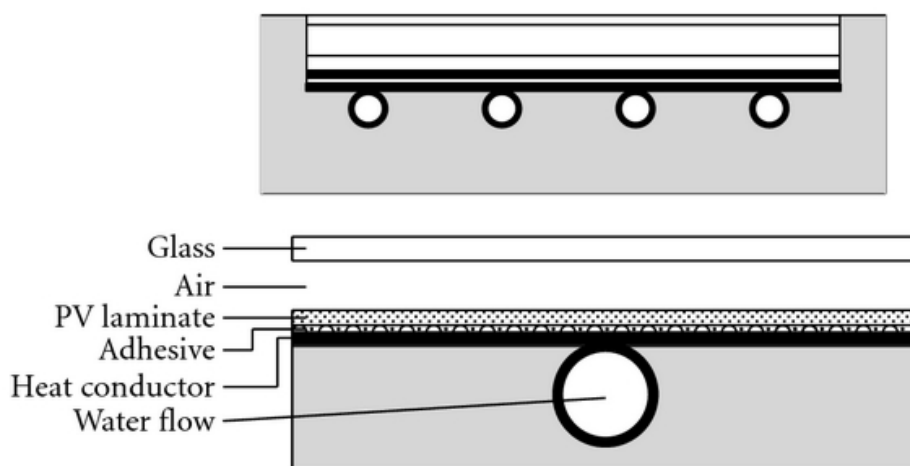


Figure 15: Glazed collector (Kim and Kim, 2012)

2.2.4 Unglazed PV/T Collectors

Unglazed fluid PV/T systems are utilized primarily for space warming or pool heating. In colder nations, pool heating has high potential. Be that as it may, in hotter nations or nations like the USA and Australia, pool warming has an undiscovered potential market and can be grown further. They have been PV/T frameworks that have been joined with heat pumps to create higher thermal yield. However, the present market for PV/T frameworks still needs assistance to advance the development of its capability to different sorts of strategies before wandering into different kinds of markets. The PV/T utilized in the design explored here is revealed in Figure 16.

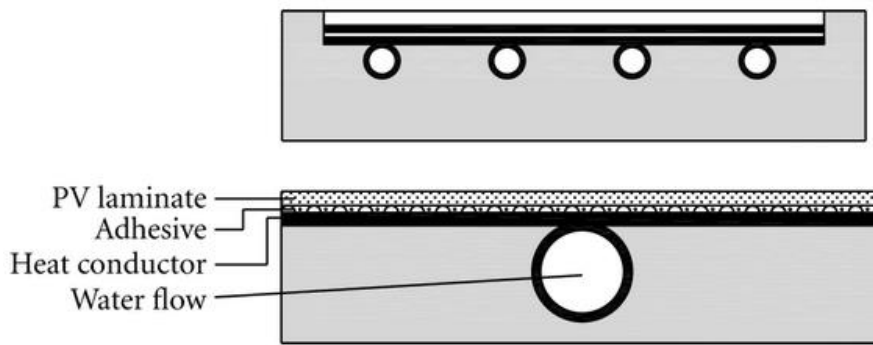


Figure 16: Unglazed collector (Kim and Kim, 2012)

According to Sandnes and Rekstad, the hybrid PV/T polymer collector investigated in their study showed that the thermal losses are reduced by using a glazed collector however this led to an increase in reflective losses. However unglazed collectors are mainly used for low temperature applications as they generate lower heat than glazed collectors (Rekstad, 2002). There are various parameters that affect the output of the PV/T. To name a few that have been popularly investigated are MFR, configuration of the system, and unglazed or glazed, design components of the systems, packing factor, stagnation temperature and HTF. It was also noted that MFR increases the heat transfer coefficient and in turn reduces the PV panel temperature.

In this research a commercially unglazed PV/T system is used to understand and obtain a higher efficient output through detailed research in order to expand the present available commercial products to motivate newer methods to improve PV/T systems. Unglazed PV/T systems used effectively have been shown to improve the electric efficiency by 4.1% when used in domestic heating setting with a lower solar fraction (Rekstad, 2002). Unglazed PV/T also generates higher exergetic energy and this is more advantageous than its conventional counterparts. It was also observed that there is a no standard of comparison between various PV/T systems, but a study in 2001 by the US data introduced a value of 4.24 flat plate PV and Solar collectors that did not depend on time or location. Table 2 summarises the features in glazed and unglazed PV/T liquid collectors.

Table 2: Efficiency of unglazed and glazed PV/T

Type of Collector	Thermal Efficiency	Electrical efficiency	Application	Disadvantages
-------------------	--------------------	-----------------------	-------------	---------------

Unglazed	38-60%	10-15%	<ul style="list-style-type: none"> • Used for higher electrical output • Used in low pressure applications • Space heating 	<ul style="list-style-type: none"> • Lower thermal losses
Glazed	60-80%	7.2-11%	<ul style="list-style-type: none"> • Used for higher thermal output • Pool heating 	<ul style="list-style-type: none"> • Higher reflective losses • Stagnation temperature issues

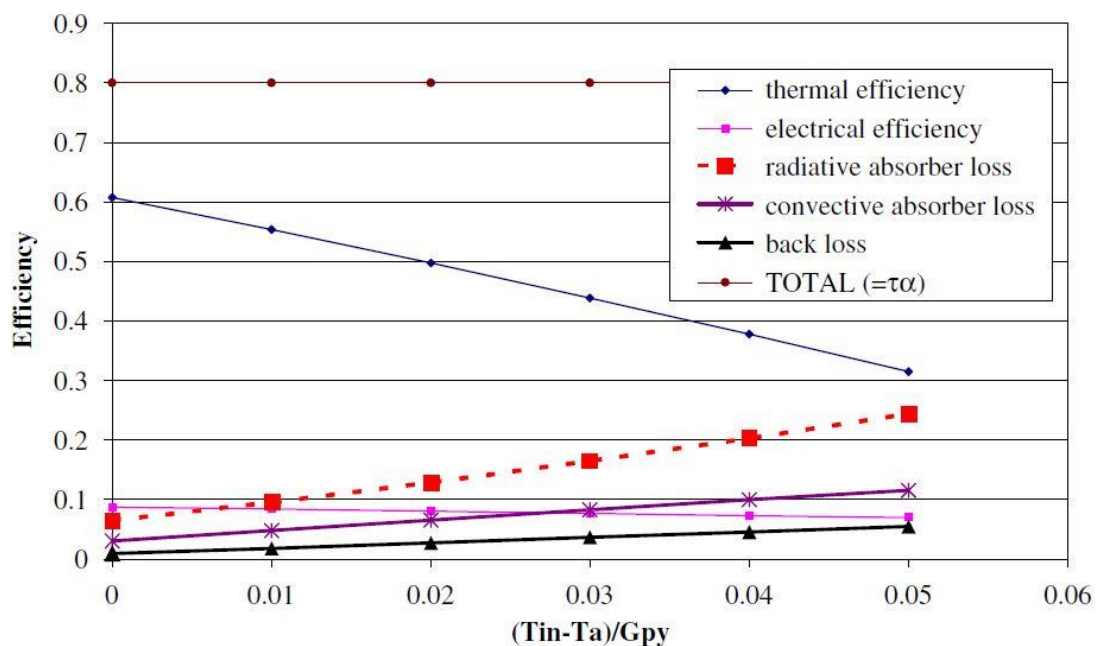


Figure 17: PV/T layer efficiency(Zondag, 2008)

Figure 17 shows the efficiency of the typical PV/T system at each different layer. It is quite evident that the efficiency of PV/T is somewhat lower than its conventional counterpart and this electrical efficiency is mainly because of higher reflection in solar radiation that is caused because of the glass layer over the PV laminate in the PV/T. A solution to this problem can be eliminated by using a low iron glass that reduces the efficiency by 8% however, if a higher transmission glasses used it reduces by 4%. The PV in the PV/T system is also affected by the additional heat generated in the system which reduces the cell efficiency.

The electrical efficiency is also affected by the type of PV cells used in the PV laminate which can be c-Si, a-Si and pc-Si. Although c-Si has a higher electrical efficiency, it drops as the temperature increases. In this case, pc-Si is chosen for the PV laminate as it is cost effective and has high heat tolerance and better efficiency than a-Si(Rajput et al., 2018).

The electrical efficiency is also affected by shading from the surrounding obstacles as well as the solar irradiation; ambient temperature and wind velocity as this disrupt the uniform temperature across the PV module.

2.2.5 PV/T Norm Classification

According to the PV/T Norm project of 2014, the PV/T have been classified as the following based on unglazed and glazed PV/T systems.

- I. Type 1A which is an unglazed layer without any installation
- II. Type 1B an unglazed layer without any thermal insulation along with a heat exchanger that is a separate unit from the PV
- III. Type 2 unglazed layer with thermal insulation
- IV. Type 3 which has glazed PV cells on the thermal absorber
- V. Type 4 which has glazed PV cells that are placed under a glass plane
- VI. Type 5 which is simply a PV/T collector with concentrators

Type 1A has no insulation under the collector and during higher temperature situations a condensation layer is formed under the Collector layer and provides a way of natural cooling for the solar PV cells. This system is quite easily integrated into roof systems. The major disadvantage of this system is the heat losses and the reduction of efficiency on the thermal performance. An example of type 1A (CGA technologies) is shown in Figure 18.

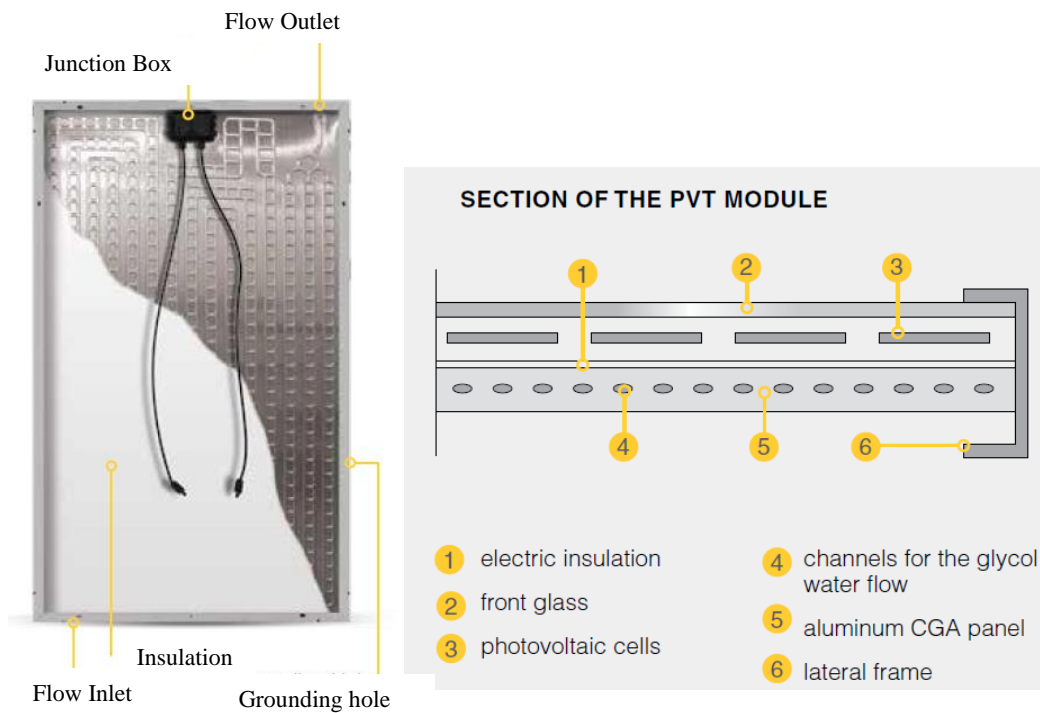


Figure 18: Type 1A collector (Department of Business, 2016)

Type 1B normally has an unglazed layer with a separate collector and PV unit. This can be either a ventilated PV system with the heat recovery unit. The major advantages of this type of system are that it can be easily integrated into roof systems and retrofitted into existing systems. As they are separate units, the PV system and the absorber can be selectively used to increase efficiency of the output. The major disadvantage of this system is that the heat transfer between the two elements can be quite tricky as the heat transfer coefficient is lower because of higher heat resistance. Figure 19 shows a product from GSE Air' System and C. Bösch Solator PV/T systems.

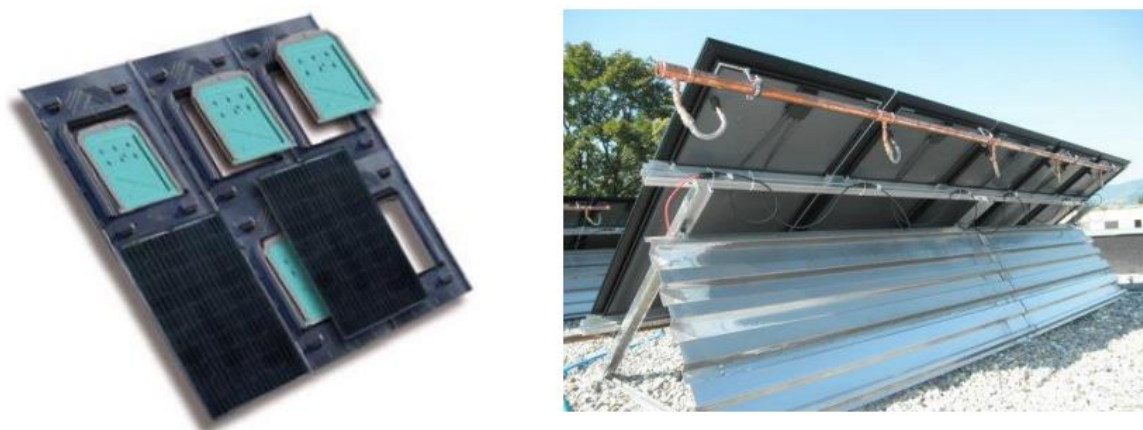


Figure 19: Type 1B collector assembly and configuration (Department of Business, 2016)

Type 2 systems have a key advantage over the type 1 systems as the heat generation is insulated and higher rate of transfer rate is ensured. This type of PV/T also generates a better

heat gain especially during cloudy days or when irradiation is low but the ambient temperature is high. The collector Solar Angel DG-01 is used in this project and its configuration is shown in Figure 20. An example of application of Solar Angel in a domestic setting is indicated in Figure 21.

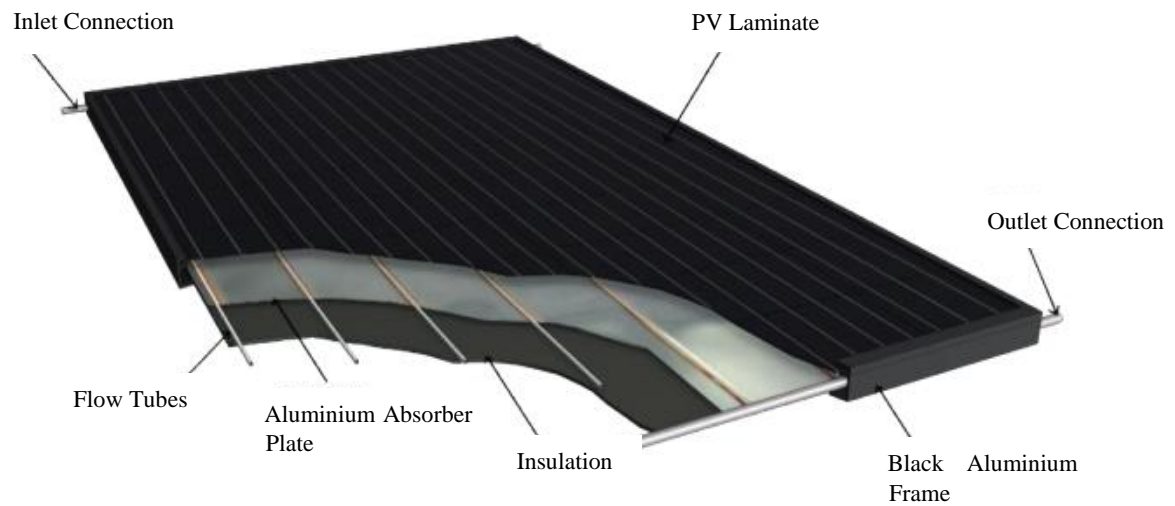


Figure 20: Type 2 Solar-Angel collector (Department of Business, 2016)

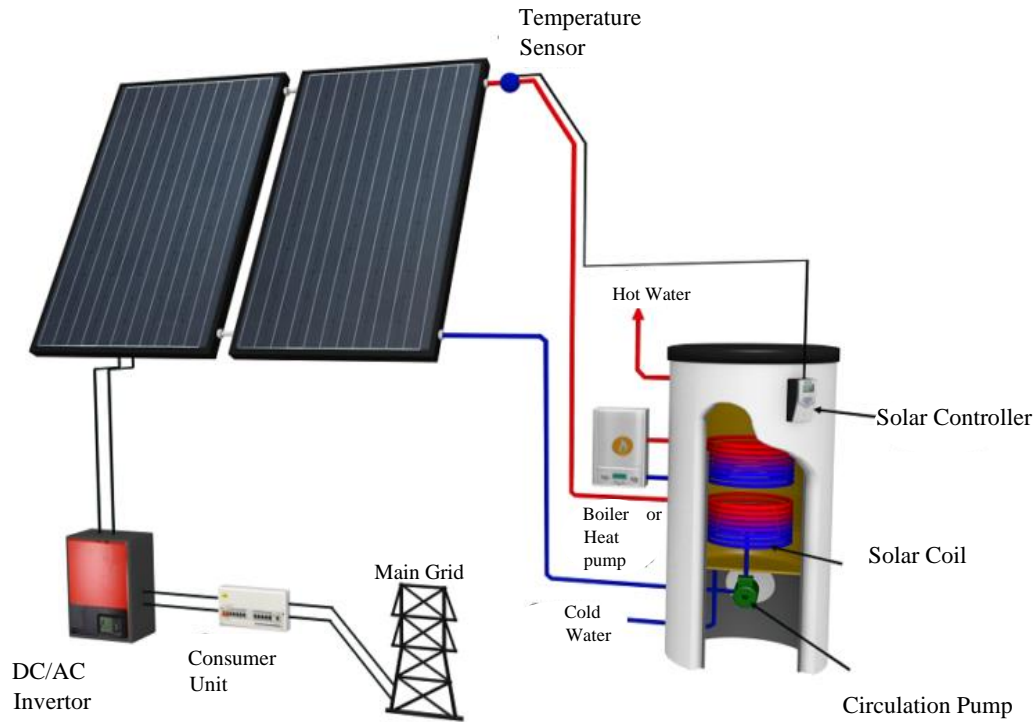


Figure 21: Application in a domestic hot water system using type 2 collector(Solarangel, 2016)

Type 3 is relatively new technology that is commercially available and the major advantage of this type of system is that it's useful for domestic hot water applications as well as higher temperature applications. However, there is the potential for material stress and lifetime expectancy. Figure 22 is a type 3 solar concentrator product that boasts to reduce at least 30% of area used by conventional systems and well as to reduce 80% of carbon emissions. Another example of type 3 system is a solar powered ventilation system which provides ventilation due humidification and space heating as shown in Figure 23 and the PV cells are solely used to power the fans and a control system is used for the operation of the unit. The working of the solar air ventilation system is summarised in

Figure 24.

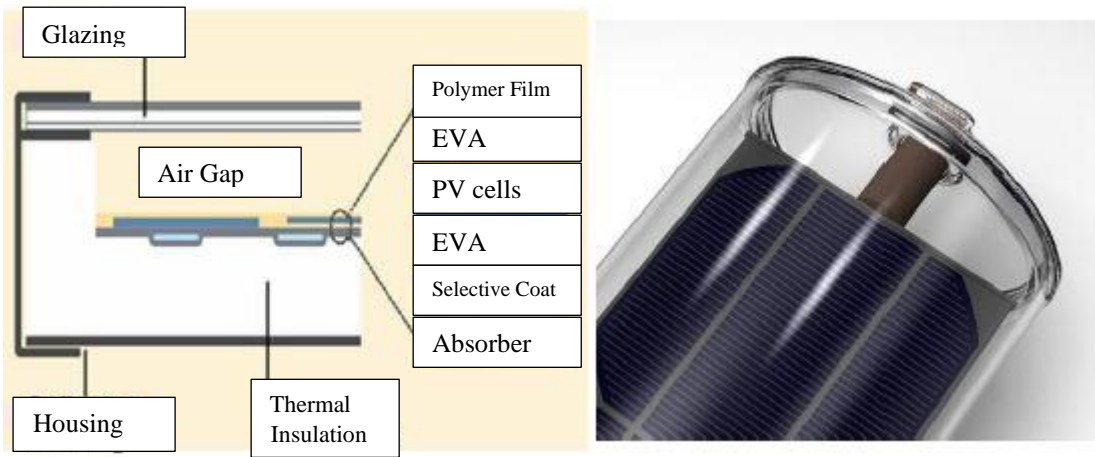


Figure 22: Type 3 collector (Nakedenergy, 2018)

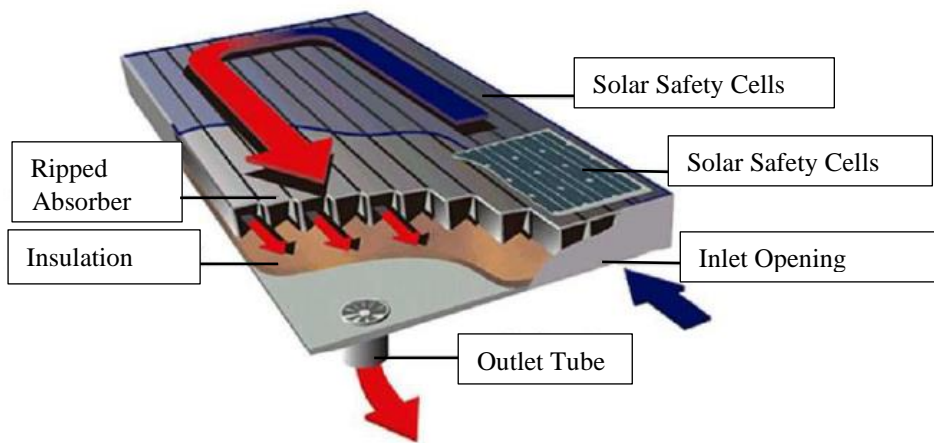


Figure 23: Type 3 solar ventilation system collector (Department of Buisness, 2016)

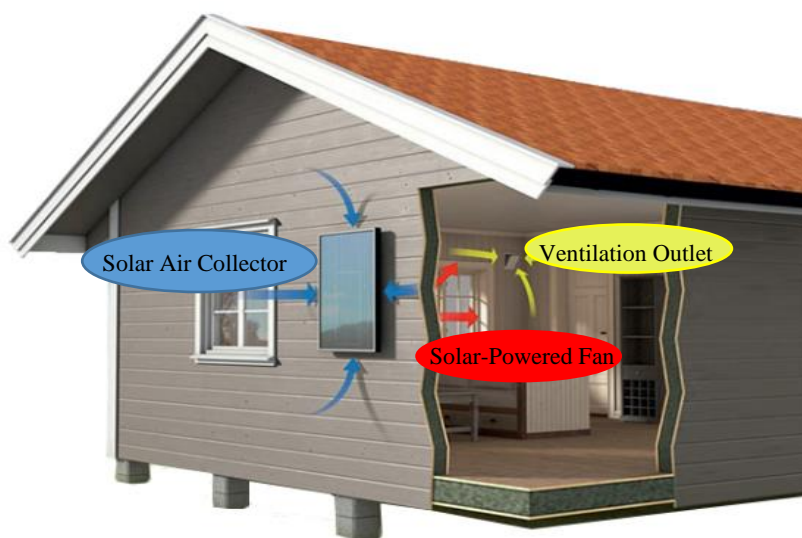


Figure 24: Application of Type 3 as a solar ventilation system (Solarventi-International, 2019)

The type 4 system is used in roofing products and integrated into the roofing tile. This is used when the temperature of the roof is not expected to be too high as the system does not have a

cooling unit. An example version of this type of configuration and principle is shown in Figure 25 and Figure 26 respectively.

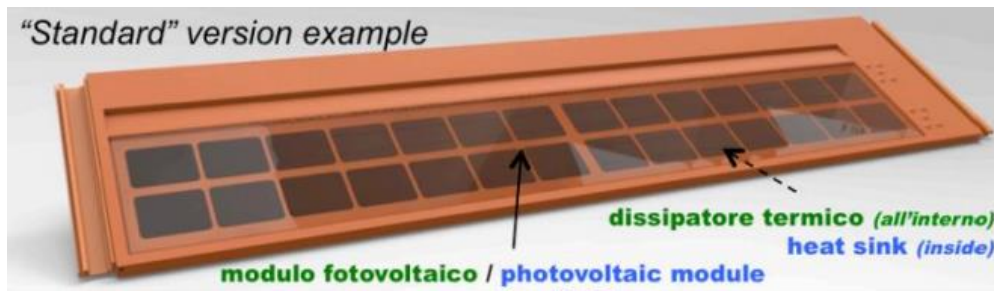


Figure 25: Standard integrated roof tile as Type 4(Department of Buisness, 2016)

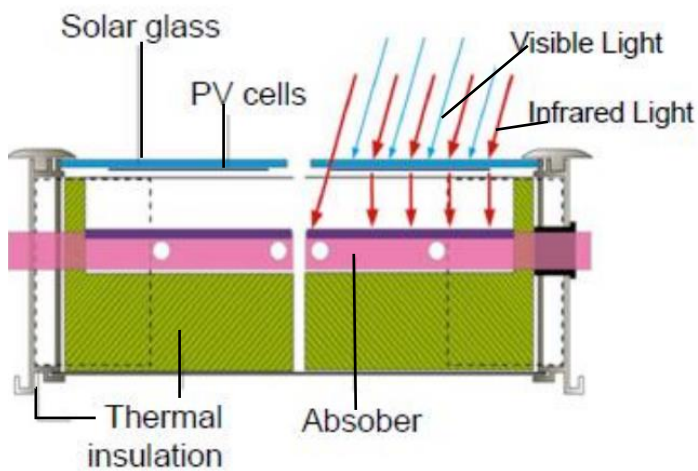


Figure 26:Cross-section of Type4 from example used in Figure 25(Department of Buisness, 2016)

Type 5 systems are generally considered the least applicable to colder countries as the heating loads are extremely high. An example of Solarus solar module is shown in Figure 27 below. This can be used for high heating demand in a domestic hot water distribution network.

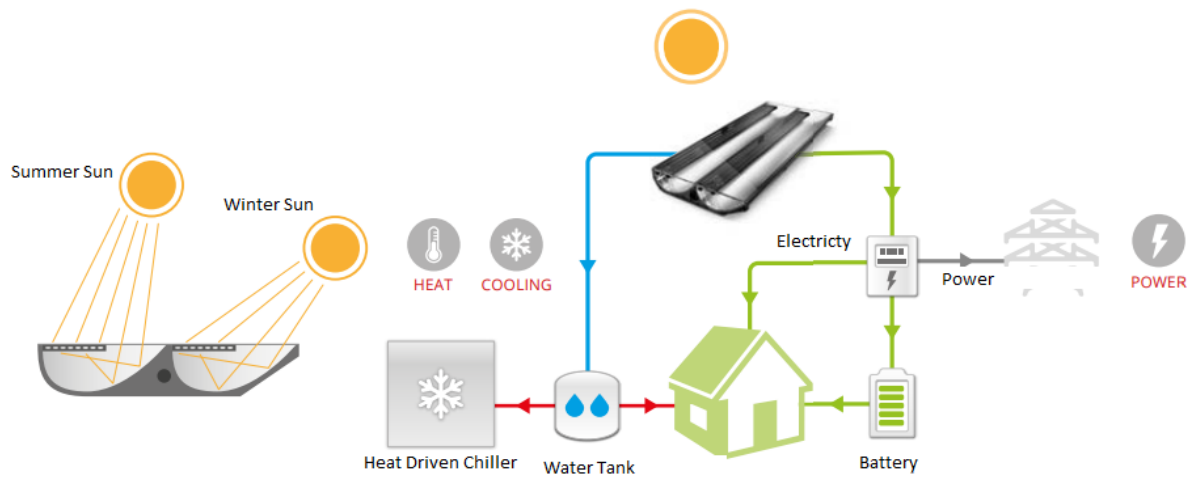


Figure 27: Type 5 Solarus concentrator collector (Solarus, 2018)

Solar energy of heat can be used for the low temperature heating of fluids. It can be done either by direct or by indirect method. The direct method is generally referred to as a passive system while the indirect method is known as an active system.

(a) Passive Heating of Swimming Pools:

A straightforward floatable plastic spread is utilized over the outside of the water in the pool during daylight hours. The base and side inward surface of the pool is ideally darkened to retain sun-based radiation. The sun-based radiation is transmitted through the straightforward plastic spread. It arrives at the base of the pool and is at last consumed by the darkened surface.

(b) Active Heating of Swimming Pool:

As clarified over, the temperature of pool water can be expanded barely by utilization of a passive heating system. In any case, under extraordinary cold climatic conditions, passive warming isn't adequate.

One of the applications of solar energy is in heating swimming pools. Outdoor swimming pools can be heated by both passive and active systems, while indoor swimming pools can only be heated by an active system shown in Figure 28.

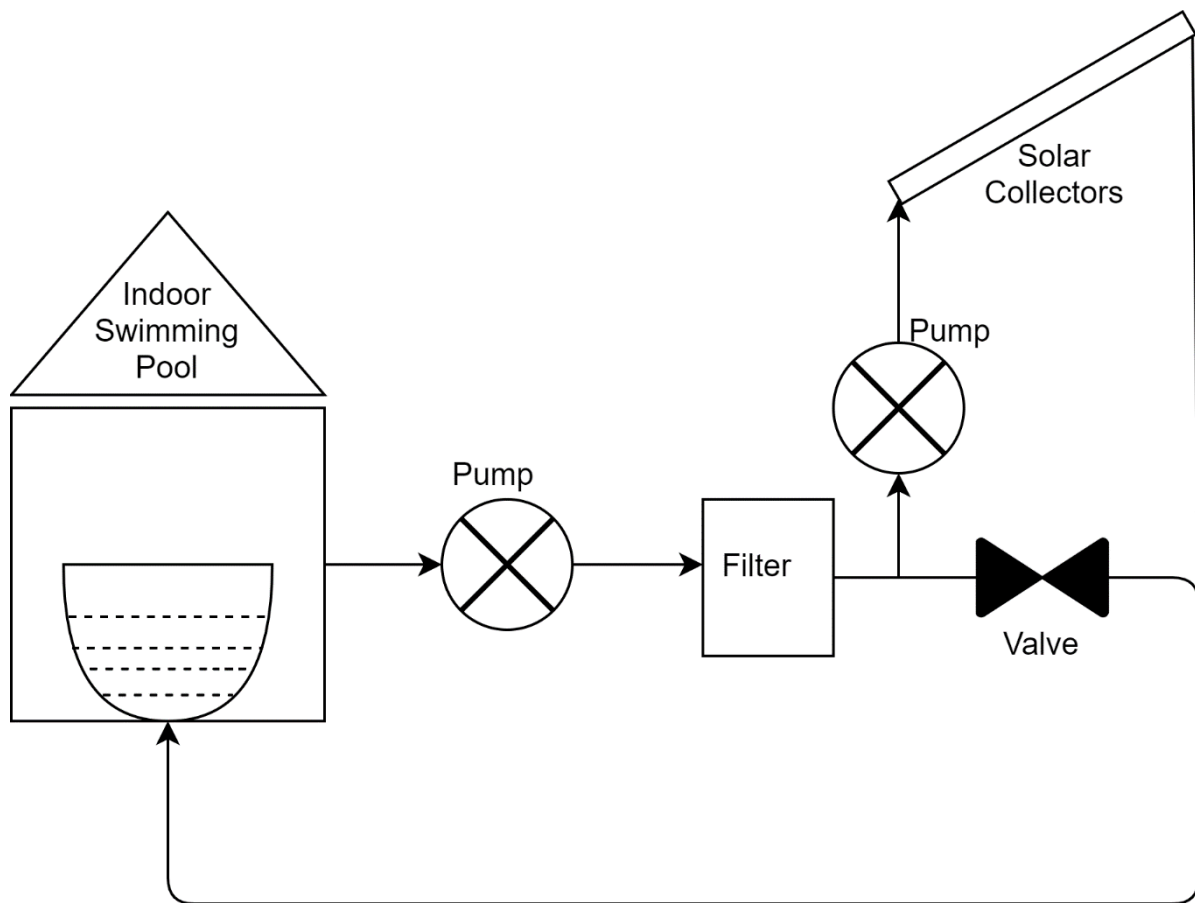


Figure 28:Active indoor pool heating(Kalogirou, 2009b, Kalogirou, 2009e, Kalogirou, 2009c, Kalogirou, 2009d)

Unglazed PV/T's are more financially feasible than any traditional flat plate collectors (FPC's). Since unglazed collectors have smaller temperature range, there are the most suitable for indoor/outdoor pool heating. If a higher temperature span is required, glazed collectors can be utilised. Unglazed collectors are more cost effective than any conventional FPCs.

2.3 Existing Standards

Standard testing conditions for a Solar cell and solar collectors have already been defined under American Society of Heating, Refrigerating and Air-Conditioning Engineers, Inc. (ASHRAE). There is no standard testing method for testing PV/T as a whole module yet. However the methods used are a combination of EN 12975 and IEC 61215 (collector and PV standard testing methods respectively)(Cencertificationcommitte, 2018, Iso9806, 2018, Network, 2018). Since then various research methods have been proposed to model a PV/T unit as a standardized method was not summarized for the same, as of yet, because of its unfamiliar concept. Fraunhofer institute for solar energy has also been involved in standardising the tests for PV/T. The major standard testing is generally based in the open circuit mode, the short circuit mode and the maximum power point.

The thermal efficiency curves that determine the thermal performance is observed under indoor solar simulations. However, the real time variations do not parallel indoor simulations. In order to understand the thermal performance with respect to the electric output, the tested temperature in maximum power point conditions are investigated for each different radiation. The radiations are varied, and output is recorded. Through this, a generalisation of the performance of the PV/T can be achieved. A notable observation by Fraunhofer institute for solar energy was that the PV/T system acted as a separate thermal collector when the electric output was not connected.

It was decided that Solar Key mark certification (which is a voluntary third-party certification for solar collectors) of PV/T collectors as a solar thermal product is possible, provided the measurements of the thermal performance are performed with electrical production under MPP (maximum power point) conditions. In addition, an optional thermal performance determination without electrical production (open circuit for PV-Module) is possible. For the electrical load applied for the electrical production an appropriate solution for the MPP tracking shall be used (Alam and Alouani, 2010). The system is tested to simulate solar irradiance, temperature control, mass flow rate control and performance monitoring with IAM (Incidence angle modifier) as a correction factor depending on the product requirement. The performance monitoring of the system mainly includes finding out the thermal and electrical efficiencies of the system when working together and then compared with thermal and electrical efficiencies of conventional PV and collector system.

Thermal efficiency curve is measured in two circuit conditions: One in open circuit mode pure collector and the other in MPP mode along with the collector in hybrid mode. The electrical testing methods work to find the temperature coefficients under lower irradiances and flasher tests working as a whole PV/T unit under IEC61215 (Cencertificationcommitte, 2018). There are two different methods under which the tests can be done to obtain the solar key mark certificate. They are the Steady State method (“SS”) and the Quasi Dynamic (“QD”) test method. According to the new updated list, the thermal part of PV/T is tested according to SKN decision list D7.M10 added in the EN 12975 (Ossenbrink et al., 2012). The steady state testing standards defined in the EN12795 has provided a comprehensive method for solar collectors however under various weather conditions around the globe, outdoor testing is not quite advanced.

As the performance analysis is done to predict the performance of the PV/T, it should be observed that the heat flows in PV/T systems are controlled by the fundamentals of fluid

mechanics. Since the input environmental conditions are dynamic, the performance also varies with time and these transient behaviours have been addressed in this research.

There have been various numerical methods to find the performance of PV/T. The most commonly used is analysing the PV/T using energy balance method either at steady state or at dynamic conditions. The steady state method is the simplest method to analyse PV/T, however, this does not predict the real time output. Dynamic conditions are evaluated with respect to time. There are implicit and explicit analysis. Explicit analysis is unstable when the step size is too large, an unstable condition can be encountered, but it is a simple method. Implicit analysis is complex but highly accurate. Zondag et. al. developed a PV/T system based on steady state and dynamic simulation, which included one, two- and three-dimensional modelling of a serpentine type of collector(H. A. Zondag et al., 2002). Two- and three-dimensional models are very accurate as they provide a detailed analysis than 1D. It was found that unglazed systems and glazed systems modelled obtain an efficiency of 52% and 58% respectively. Unglazed systems are recommended for low temperature applications, reflection losses are eliminated(H. A. Zondag et al., 2002). Chow was able to successfully implement an explicit dynamic FP(Flat-plate) PV/T model using finite control volume approach which uses a seven-node analysis while Aste et.al completed a 5-node analysis using various parameters of the desired system. The energy balance equations obtained for energy analysis can be solved in a numerical matrix/equation form and radiative coefficient equations by iterative method(Chow, 2003, Aste et al., 2015). The literature that has been performed so far has identified simple models addressing the heat balance across different parts and layers of the PV/T system through heat transfer. One dimensional, two-dimensional and three-dimensional dynamic models have also been examined using various mathematical models. It can be concluded that various steady state and dynamic analysis gave been carried out extensively.

2.4 Performance Indicators

Zondag et. al.. as mentioned before, completed an analysis using 9 different types of collectors and their performances (H. A. Zondag et al., 2002). The major findings of the study suggest that sheet and tube configuration is the highest efficiency configuration. It was also found that uncovered collectors generate a lower temperature due to lower reflection losses at the over. It was also observed by Tiwari and Sodha that in under 4 different configurations the most efficient and effective system at lower temperature was the uncovered/unglazed water PV/T collector with tedlar(Tiwari et al., 2006). It was also noted that PV/T systems with a glass layer has an electrical efficiency of 6.8% while conventional

PV systems generate an efficiency of 9.4% annually. Chow et. al.. looked into glazed and unglazed systems and concluded that glazed systems are actually affected by an increase in PV cell efficiency packing factor and wind velocity however the increased irradiation and ambient temperature was an effective compliment to the glazed system output (Chow et al., 2009). The effect of MFR is significantly studied in PV/T literature across various studies and experiments. Another study conducted the performance of liquid based PV/T systems and concluded that as the mass flow rate increases from find 0.001 to .0075kg per second, thermal efficiency only increases by 10%. This was also suggested to be used in a domestic hot water system as it would be helpful in a DHW network. Another study by Sopian et. al.. investigated a double pass hybrid PV/T collector mainly used for drying operations indicated that a mass flow rate of 0.036 kg per second with the radiation level of 800 W/m² with an expected temperature rise of 188°C the efficiency was said to be around 60% (Sopian et al., 2000).

Another study by a group suggested that the optimal flow rate for the system is .007 kg per second for a collector area of 5.7 m² (Daghigh et al., 2011). The tube dimensions effect was also studied, and it was observed that the outlet fluid temperature decreases as the width to diameter ratio of the tube increases from 1 to 10 mm. The fin configuration also affects the output of the PV/T system. However, the electrical efficiency is not highly varied due to this fact. It is also noted that several mathematical models were developed for analysing the PV/T models. The different types of absorber plates but also analysed in various studies and it was concluded that serpentine absorber plate has 40% less mass and higher turbulence that affects the outlet temperature. In this case study a harp design with the sheet and tube absorber type is selected.

According to the literature review, the main factors that are responsible for performance of the PV/T system that are quantifiable are described as follows

- Mass flow rate
- Ambient temperature
- Wind speed
- Solar radiation
- Configuration of the system
- Number of covers
- Area of collector
- Packing density

- NOCT
- Tilt angle
- Incidence angle modifier
- Cloud cover
- Shading
- Dust
- Material properties

2.5 Limitations of PV/T

PV/T can have a higher turnover of energy than the single unit PV and collector when used correctly. The function of generating two outputs (heat and thermal in a single unit) has a very good market potential. However, in realising this, the initial cost is higher than the competition due to the thermal components, which reduces the attraction of the wider market and over the conventional solar units. Studies have shown economic analysis of PV/T to be viable if there is a direct correlation between cost and energy generated (Kalogirou, 2001). There are also issues with low density, varying specific heat capacity and data affected by a non-standard method to evaluate the performance. Air PV/T systems have a disadvantage of freezing in colder climatic conditions and is worsened when the system is a bi-fluid PV/T unit. The heat from the PV/T is low grade heat, hence this needs to be preheated using an additional electric heater. This can reduce the overall efficiency by introducing losses. The additional complex nature of the system can also affect the operational performance.

2.6 Current Research in PV/T

PV/T collectors often suffer from very basic issues such as heat resistance which reduces the heat transfer coefficient and the efficiency. The working principle of PV/T is not as easy as pasting a PV module in front of a solar heat collector. Their behaviour needs to be analysed and understood on a much-detailed level. The issue of heat resistance can quite easily be solved by applying a very thin adhesive layer between the different layers of PV/T system. Insulation of the entire module is also effective in increasing its performance. As of now, there are several types of coatings for the PV/T absorbers to increase its absorption called selective absorption coating. PV/T air collectors are more economically feasible than PV/T liquid collectors. However, PV/T liquid collectors are more efficient and give a higher thermal output. The PV/T air collectors have a lower heat transfer rate. The next step to improve these issues is to increase the efforts of research in this field. Stagnation temperatures will be an issue if higher absorption coating layer is applied. It is also important to understand the standards of PV/T testing which actually establishes the PV/T performance however a

guideline for PV/T testing has not yet been fully established and hence further research is required to keep understanding the performance of PV/T with respect to its counterpart.

The potential in the PV/T market has been investigated and reiterated various times. However, these studies were limited to finding the performance of the system under certain constraints. Several studies have addressed the dynamic range of operation through different experimental studies. The lack of standards to categorise each parameter and its weightage to performance and thus optimise the system has not fully been executed. This project will also address these gaps in research and establish a full understanding of the parameters on the performance of the system. This will be a foundation for further research where the design can be optimised and analysed according to the results.

A PV/T system has been proven to be 3-12% more electrically efficient than its individual counterparts. However, there will always be a trade-off with respect to electric and thermal efficiency in a PV/T system. Thereby the type of output needs to be selected according to the requirement of the design. A PV/T unit does not have the capacity to maintain the required heat throughout the year, especially during the winter months. Hence it is common to integrate an auxiliary heating source with the PV/T to generate a constant and reliable temperature from the storage. In order to understand and evaluate the performance of different PV/T systems there needs to be a standard. However, the EU/British /international standards for PV/T systems have not yet been fully established. This was attributed to the fact that there were a concreated lack of studies basing all factors and their effect on the operating performance. This research aims to provide a step forward in this process.

The typical flow temperatures reached by PV/T range between 40 – 50°C even though they are usually rated to a stagnation temperature of 80°C. In circumstances the thermal storage reached the stagnation limit, the PV/T system will start to shut down or stagnate. Continuous high temperatures can affect the electric output and the systems overall efficiency. An easier way to deal with such a problem is to increase the capacity of the thermal storage, but this can be adversely affected during states of low temperature. The ideal solution to a PV/T system is mostly affected by the spectral capability of the PV cell, its absorption rate, the internal transfer of heat from PV to absorber, the type of orientation and inclination angle of installed PV/T, the electric and thermal demand which is integrated through storage systems and its temperature as well as integration of the PV/T into the domestic hot water system(Tiwari et al., 2016).

In terms of methodology the research process can be classified as

- a. Analytical theory and modelling
- b. Experimental case study investigation
- c. An amalgamation of the analytical theory, experimental case study and validation through modelling
- d. Application of the validated model
- e. Exergy and economic analysis and
- f. Feasibility of the technology

Throughout the last three decades, PV/T research has progressed immensely. Yet, there are issues that needs addressing and further research needs to be conducted to ensure that the PV/T systems are working at its full capacity. The intentions of this research involve generating the temperature distribution across various PV/T layers, controlling the parameters of PV/T system through experimental analysis and predicting the optimum conditions required to maintain an optimal output.

In brief the established analytical and experimental analysis has given an in-depth view of the existing PV/T technology and its functions and the system requirements to operate it at optimal conditions. A further improvement to these methods can be in the dynamic category of long-term performance for various PV/T at different locations using performance indicators to understand the performance in detail(Tiwari and Mishra, 2012, Tiwari et al., 2016).

This effort to develop a novel method to analyse the PV/T system at various locations is motivated due to the inherent barrier still faced by PV/T systems due ineffective heat removal, thermal and reflective losses configuration of the system insulation losses and continuous increase of water temperature during the operational duration and any potential risk of freezing the HTF. There are also additional problems and the long-term reliability of these systems especially in real-time climate conditions needs to be addresses which will be done through this research, which aims at finding the effect of variation of different parameters on the PV/T performance through experimental and theoretical analysis while developing a novel method to do so.

2.7 Concept Design of the PV/T System

2.7.1 Solar Angel DG-01

The PV/T model considered here is a commercial unit called ‘Solar-angel DG-01’. It has a low iron content glass for absorbing maximum short-wave radiation and reducing heat losses through an EVA layer. The PV panel and the Al absorber plate are held together by an EVA (Ethyl vinyl acetate) layer. The tubing for the thermal collector part is made of Al and it is

welded by an aluminium bond onto the absorber for higher thermal contact and the final layer is a poly-urethane foam of insulation to prevent any heat losses. According to the PV/T Norm classification, the above PV/T is classified as type 2, which is one of the common commercial product configurations in the UK. However, the definition of unglazed and glazed cells varies for some cases.

2.7.2 Glazing Cover

A thermal analysis by Dubey et. al. reports the investigation of glass to glass (GTG) and Glass to tedlar (GTT) module with and without duct. glass to glass type with duct gives higher output due to the fact the solar radiation reached the absorber through the non-packing area of the PV module, but in the glass to tedlar, the radiation is absorbed by the tedlar and carried away by conduction. It was also observed that increasing mass flow rate for GTG and GTT with duct shows an increase in air temperature for GTG due to radiation being transmitted directly instead of through the opaque tedlar layer. In the PV/T used here the glass layer precedes a layer of EVA (ethyl vinyl acetate) which transmits 100% of incoming solar radiation due to its negligible absorption. The PV layer is sandwiched between two layers of EVA. The glass layer used here is of low-iron content which is of 0.0032m and has a thermal conductivity of 1.05 W/m.K with an extinction coefficient of 4m^{-1} . One of the assumptions taken here is that thermal conductivity does not vary with temperature as the variation is quite negligible for smaller ranges of temperature. Low-iron glass has higher transmittivity and lower absorption and emission values so that the incoming solar radiation is mostly transmitted to the absorber without lower losses. Lu et. al. suggest that Glass to PV cells sandwiched by EVA layers shows a higher electric conversion efficiency than its air gap before PV cell configuration counterpart. However, system without air-gap shows a lower thermal efficiency than the system with an air gap. The system used here has no air gap and is selected and expected to provide higher electric output which is one of the main aims of this project. The number of covers also affects the output of the system. Higher number of covers increases thermal output but increases losses and lower electrical output while having lower temperature at glass covers. Only one cover is used in this project which is correlated with glass layer over the PV cells. EVA layers transmit almost 100% of the radiation and thus are negligible to be included as a two-cover system.

2.7.3 Poly-Crystalline PV Cells

PV cells can effectively convert solar radiation into electricity with the efficiency ranging from 5-25% depending on the technology of the PV cells. Different types of PV cells

influence the efficiency of the same. The materials used in the PV cells can be monocrystalline silicon which is more expensive than polycrystalline or amorphous silicon as the manufacturing process is more intricate. The mono-crystalline silicon cells has little to no impurities increasing their efficiency (about 15% efficient), while polycrystalline (about 12% efficient) and amorphous (about 6% efficient) materials have certain impurities are easier and cheaper to manufacture.

The 25% efficiency (average) of the PV systems suggests that the rest of the solar radiation received is converted to thermal energy and losses that might increase the working cell temperature of the PV. It is said that these temperatures can rise up to 40°C above ambient and will trigger an intrinsic carrier concentration at the P-N junction of the silicon PV cells causing an increase in dark-saturation current which eventually reduces the capacity of producing electrical power and the efficiency of these crystalline cells can drop to 0.2-0.5% for every 1°C rise in module temperature. The system used here is poly-crystalline due to readily available characteristics in the market and the cost effectiveness of the system. A fill factor of 0.7 is observed for a standard PV module with a thickness of 0.001m. Thermal conductivity of silicon PV cells was taken as 148 W/mK.

2.7.4 EVA Layers

EVA or ethyl vinyl acetate is a co-polymer of ethylene. It has low tensile strength and low density but high ductility. The thermal conductivity of EVA layer ranges from 0.315.56 W/mK with respect to the content of percentage of EVA used (10%-30% EVA content has a thermal conductivity of 0.34 W/mK) while the thickness of EVA layer used here is 0.0005m. According to Wu et. al., EVA encapsulation techniques are efficient than other techniques using tedlar and reduce the resistance between PV and fluid. They also have higher elasticity and higher elongation property when connected as a buffer directly with PV and aluminium tubes(Wu et al., 2017). EVA also can eliminate risks of air bubbles or small air-gaps which increases losses. This application is mostly effective for systems with temperatures up to 140° and care should be taken while designing systems higher than 140°. This is also a cost-effective method to reduce losses and integrate PV with absorber. There has not been a lot of PV/T studies with an EVA layered cell and this project can further improve and establish the EVA layer method to be a better solution than other conventional methods. EVA layer integration was proven to be the best cost effective method for integration of PV and absorber(Lamnatou and Chemisana, 2017).

2.7.5 Absorber

Standard absorber used in solar collector is either made from copper or aluminium. A black coating is painted on the surface to increase absorption of the long wave radiation. It is desirable to have a higher absorptance for general FPC's than lower emittance. A relation between the ratio of solar absorptance and solar absorptance at normal incidence versus the incidence angle of radiation was described by Beckmann et. al. (1977). Grooved collectors have different absorption rates than FPC's where the final absorption rate depends on the absorptances of the inner cavities(Haro Velastegui et al., 2015). Thermal absorbers are responsible for the cooling PV cells and can influence the efficiency of the system. The heat collected by the PV cells needs to be transferred to the PV/T system and thus needs to have good thermal contact between those layers(Aleksiejuk et al., 2018). An EVA layer even though has a lower thermal conductivity provides resistance is lower than any other material used which can account for losses otherwise. Ilaria et. al. states that operating temperature of the module is affected by the design of the system. Stagnation temperature, nominal operating temperature determines the effective output from the system under constraints. The stagnation temperature of the defined system here was rated at 79°C. The thermal output of the thermal cell is quite limited by the absorption capacity and optical properties of the absorber system. Sometimes a selective surface can be coated to absorb certain desired wavelengths of the radiation specifically long wave radiation of which majority can be converted to useful heat. Solar fraction is the ratio of solar energy to the total energy used by the heating system. An aluminium absorber is used in the investigated model with a thermal conductivity of 401 W/mK and 0.002m thickness. (Mcintosh et al., 2009a)

2.7.6 Flat-Plate Heat Exchanger

The type of heat exchanger integrated with the absorber depends on the type of integration; description of demand and each of the systems vary on the working principle due to difference in configurations. There are also different types of heat pipe systems. The most common type is the sheet and tube system. It is further classified as follows in Figure 29 where the variation in the position of the metal sheet determines the type of system. Flat sheet tube where the tube is below the absorber is the configuration used in this project.

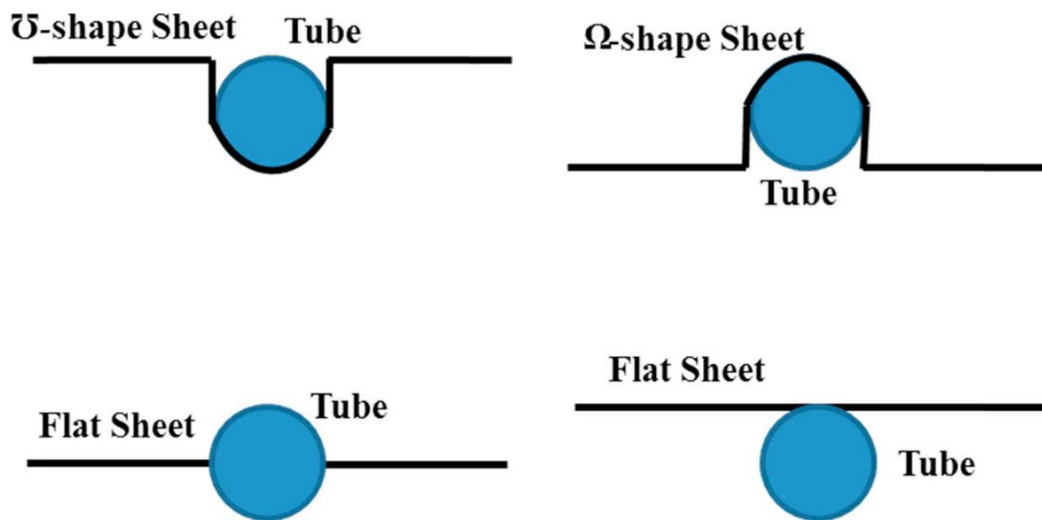


Figure 29: Type of sheet and tube configuration (Wu et al., 2017).

There are also quite several heat pipe configurations for the Heat transfer fluid to transport the heat from one end to the other. The one used here is referred to harp or parallel configuration (Li et al., 2019). Harp pipe can handle low and high mass flow rates without a higher effect of turbulence while serpentine designs can suffer losses due to turbulence at higher mass flow rates. Some of the heat-pipe designs have been shown in Figure 30 and a detailed version of the flow is shown in Figure 31. Studies comparing the harp and serpentine conclude that the harp configuration perform slightly better and the highest efficiency was obtained from the spiral flow design (Ibrahim et al., 2011).

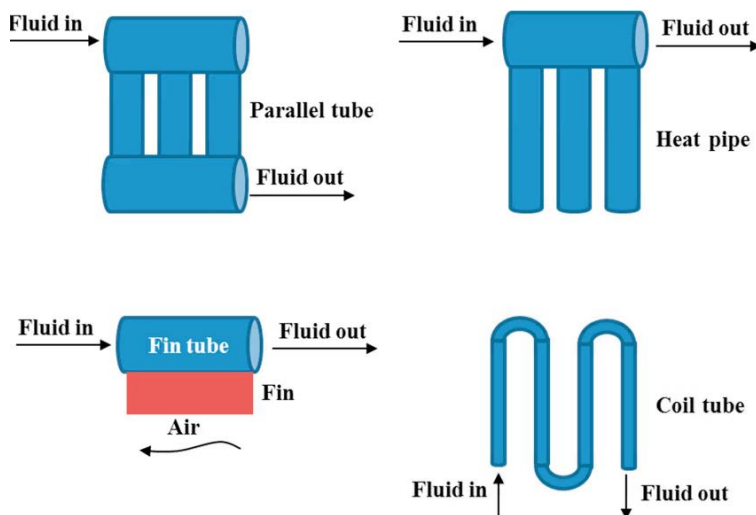


Figure 30: Flow in different heat-pipes (Parallel/harp, extruded heat pipe, fin tube and a coil/serpentine design) (Wu et al., 2017).

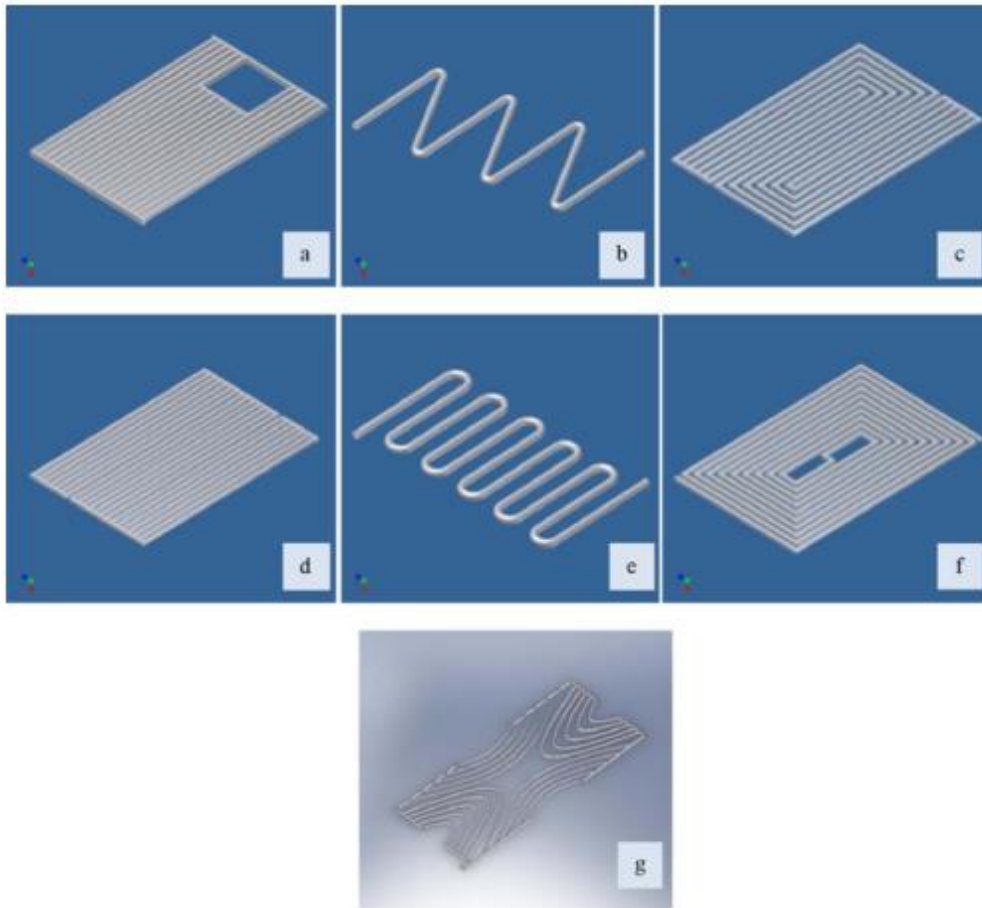


Figure 31:(a) Direct flow design/harp, (b) Serpentine flow design, (c) Parallel-serpentine flow design, (d) Modified serpentine-parallel flow design, (e) Oscillatory flow design, (f) Spiral flow design/heat mat, (g) Web flow design(Ibrahim et al., 2009).

Over the years, various endeavours were conducted to develop the hybrid PV-T system using either air, water or a solution mixed with water and ethylene glycol to prevent freezing in colder climates) that generates thermal and electrical output effectively at the same time (Spirkl, 1993). The percentage of ethylene glycol also varies from location to location which also affects the efficiency. The sheet and tube system is said to have a higher heat transfer efficiency and higher cost effectiveness than its counterparts. The tubes in the PV/T model are made from aluminium and have the same conductivity as the absorber. The Inner tube diameter is 0.007m and outer diameter is 0.008m. With a system of 8 parallel tubes each at a distance of 0.0001235m or 0.0001m with a length of 1.536m. Lisbon and Cochin have hardly any freezing temperature conditions and hence ethylene glycol is not required and thermal capacity of the fluid is 4.18 J/Kg °C and for Newcastle when freezing weather is encountered, ethylene glycol combination of 30% is added with water in a closed loop which reduces the capacity to 3.87 J/Kg °C

2.7.7 Insulation

Polymer foams can either be classified as thermoplastics or thermosets, which is further divided into flexible or rigid foams (Ziapour et al., 2016). The PV/T system insulation uses flexible polyurethane foam. These foams are the most commercially used foams due to their low density and low heat transfer which reduces losses. Polyurethane foams are often thermosets which also means they are very difficult to melt. Due to the nature of the system being renewable, it is recommended to use biodegradable foams for construction of an entirely sustainable system. The insulation layer is around 0.0188m with a thermal conductivity in the range of 0.022W/mK to 0.028 W/mK. (Beikircher et al., 2014, Lämmle et al., 2016)

2.7.8 Electrical Storage Unit

The basic principle for a PV system is defined in the Figure 32 below.

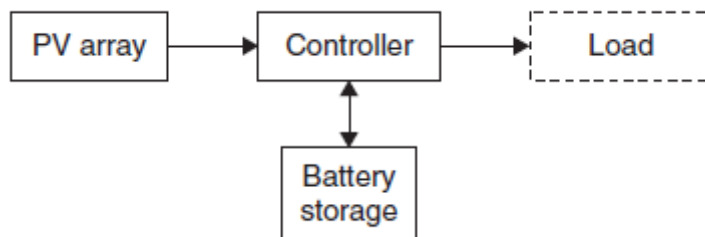


Figure 32: Standard principle for electrical storage of PV output

As can be seen, the PV array produces electricity, which can be conducted from the controller to either battery storage or a load. Whenever there is no sunshine, the battery can supply power to the load if it has a satisfactory capacity, otherwise an auxiliary supply needs to be provided. A standalone system is a self-sufficient system when access to electricity from the grid is limited. An inverter can also be added to convert DC (direct current) to AC (alternating current) for using AC appliances. In a grid-connected system, the grid becomes a storage or backup when the power generated from the PV is not quite enough. A battery system using super-capacitor and Li-Ion is also intended for simulation using LABVIEW/MATLAB as an extra component for further simulation used with the PV/T system (El-Shatter et al., 2006). As the PV system size is quite varied according to the demand. In a grid system, if there is not enough power from the PV, there are always other sources of power to compensate. But in a stand-alone system, if there is either no power or excess power without battery storage, the

losses will be quite incomprehensible. Hence it is sensible to install battery storage for a standalone system.

2.7.9 Thermal Storage Unit

Two sensible heat storage tanks of 400litres is considered for the Lab system of the project as cooling and heating tanks in the lab demonstration as shown in Figure 33 The installed lab layout has been explained below .Each of the hot and cold storage tanks have 2 inlets for hot water from collector and hot water from PV/T. This system also has two cold outputs for cooling the PV/T and collector systems. An auxiliary heating is also inserted in case of a generation shortage. The maintained temperature is at least 60°C.

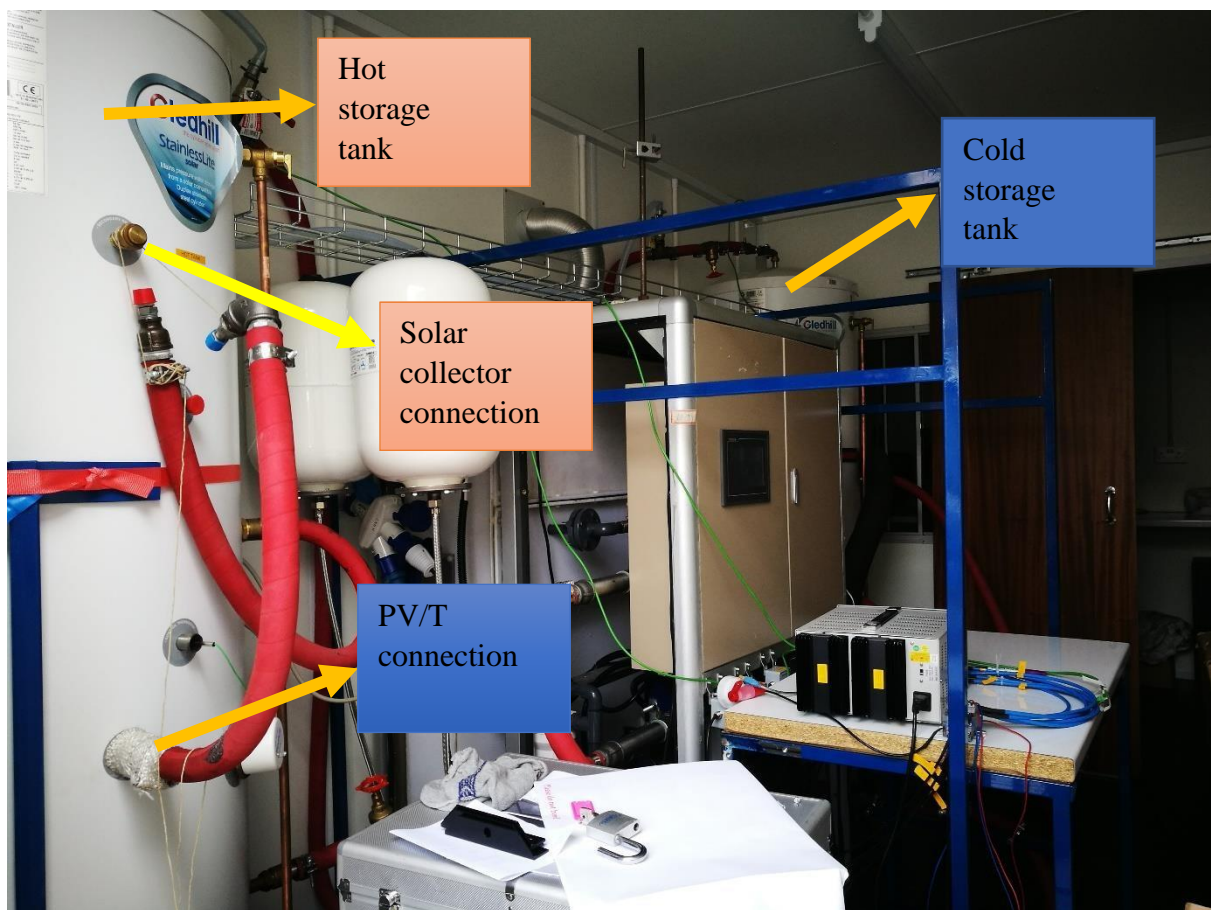


Figure 33: Hot and cold storage tank

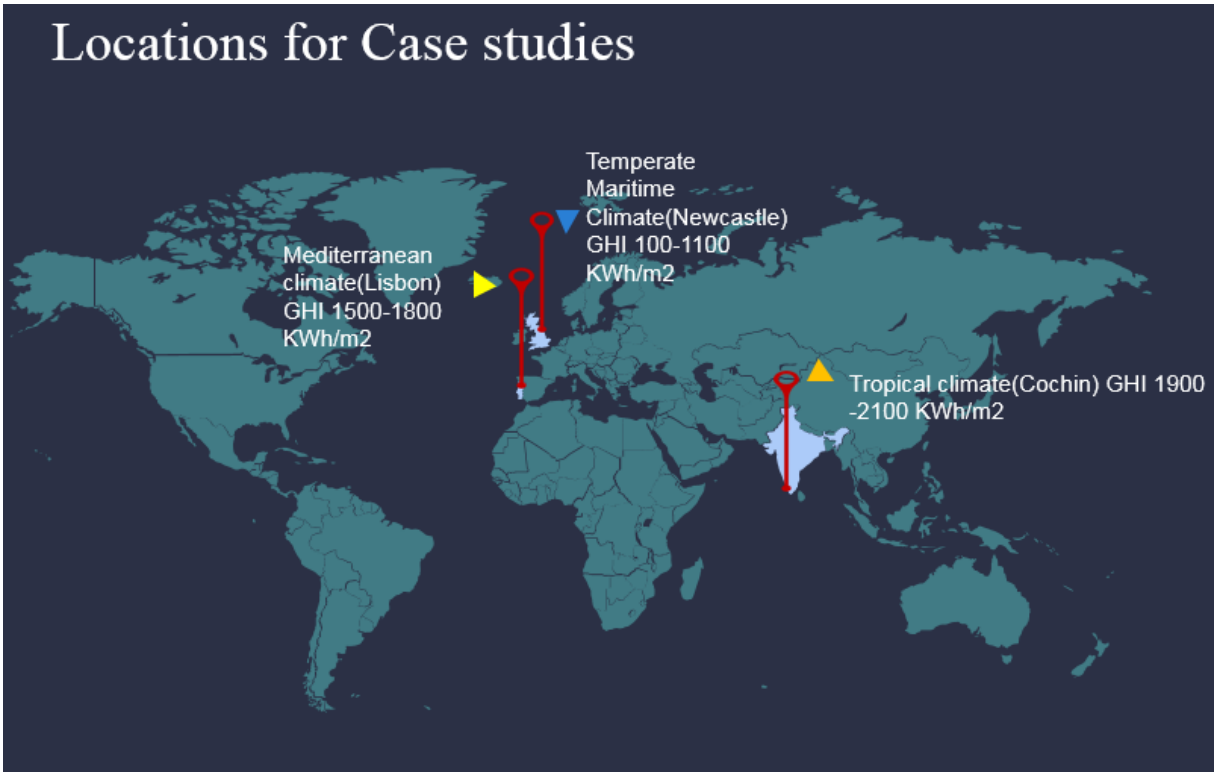


Figure 34:Case study locations

Table 3:Case studies selected

Location	<i>Newcastle-Upon-Tyne ,UK</i>	<i>Lisbon, Portugal</i>	<i>Cochin, Kerala, India</i>
Type of climate	<i>Temperate Maritime</i>	<i>Mediterranean</i>	<i>Tropical</i>
Global Horizontal Irradiation(GHI)in KWh/m ²	<i>100-1100</i>	<i>1500-1800</i>	<i>1900-2100</i>

Once the type of systems utilised, are defined, the location of the case studies is selected as shown in Figure 34. The data is studied in three locations and analysed for four different purposes. A summary in Table 3 is also given.

- In Lisbon, a PV and a separate solar collector unit plant were defined, and data is used for comparing the data from simulated PV/T at the same location.
- The data in Newcastle is used to validate the performance of the PV/T located at the USB.

- The Lab data at Newcastle is used for comparison of the PV/T model result with the experiment data.
- And finally, the data of load from a 4-bed house in Newcastle and Cochin is updated for application of the said model in design.

The performance of PV/T systems can indicatively be assessed using the performance indicators. These indicators are obtained from the collective studies from the results analysing the electricity generated, thermal energy generated, useful heat transfer, flow in and flow out temperatures, storage tank temperature and solar input irradiance obtained at the location. As mentioned previously the studies that include all parametric variations on the performance is relatively lower and thus results are inclusive to design an accurate performing model. But these studies do provide an understanding of output performance based on the fixed input variation. A collective of similar data can be used for conclusive results. Through this project, all the parameters were considered, and enough data was collected for an unbiased comparison and analysis.

2.8 Chapter Summary

A summary of current literature regarding PV/T has been investigated. Some patterns were observed as well as a lot of technological advancement was made over the last 30 years. Some of the major gaps were identified and this project addresses them through a simple methodology yet with an accurate understanding of the behaviour of the various parameters.

Several variables required for accurate interpretation of the system performance were summarised, including the design mainly consisting of the structure, geometry, material and external some variable factors. The chapter also presents the chosen design of the system and explains the motivations for selection of such a system including the technological advantages and limitations of each layer. A comprehensive literature of the design and various numerical methods of analysing the layers of PV/T like the glazing cover, PV layer, absorber layer, heat exchanger layer, the insulation layer and the type of electric and thermal storage was reviewed. A lack of standardisation for the testing of PV/T was also signified, contributing to a lack a standard model for evaluating the PV/T. Three different locations Lisbon, Newcastle upon Tyne and Cochin were considered for a comparison of different extreme, moderate and low temperature conditions. A PV/T of capacity 2.5KW at 20° tilt angle and a fixed flow rate system was considered for validation with an real-time PV/T system installed at Newcastle University. A practical system that was installed in Lisbon with separate PV and Solar collector was installed and effect of installation of a PV/T with respect

to its individual counterparts has been investigated through comparison and simulations as explained in detail in the following chapter. The main purpose of this chapter was to investigate various PV/T types by their system components and its effect on the output as well as comprehend the design of the PV/T in detail. This chapter has established the motivation for the case studies selected and examine the sizing for the selected case studies This information is used to develop the modelling methods for further analysis and validation in the next chapter.

CHAPTER 3. REAL-TIME SYTEM PERFORMANCE ANALYSIS

3.1 Lisbon PV and Solar Collector and PV/T

The system in Portugal has PV and collector system as individual units. The system is monitored for a period of one year and the same is simulated using the developed model for PV and collector system as individual units for further validating the model even for PV and Solar collector use. This system is carefully chosen to evaluate the feasibility in the same location in reference to a separate PV and solar collector unit.

3.1.1 Experimental Rig Portugal and System Description

A practical system in Lisbon, Portugal at 38.38° N, 9.13° W of a separate conventional PV and solar collector were installed (Tecnoveritas) and online data can be accessed that can be useful for comparison of the output of water temperatures and PV output. A picture of the installed system is shown in Figure 35.



Figure 35: PV and Solar Collector system in Lisbon.

Specifications and data about the PV and solar collector were obtained from the owner of the system is available in the Appendix. The layout of the PV cell modules that were used in this installation was GSS-180A-E1 with a maximum power output of 180Wp and 13.97% efficiency. The GSS5-180AE Gloria model PV panel has an open circuit voltage of 45.16 V and short-circuit current of 5.31 amps. The PV/T panel of solar angel DG-01 used for this project is designed for a maximum power of 250W. The GSS5 is slighter thicker and lighter than the PV/T module due to a higher insulation thickness. The Portugal plant has a total of 24 PV modules hence the total power expected is 4320W at standard testing conditions (STC). The configuration of connecting the PV cells is shown in Figure 36. These PV modules are subjected to conditions at Lisbon. The PV/T system chosen for this project is modelled and compared with this model via their efficiencies and generated power, by changing the parameters of current and voltage with the extra component of heat removal to investigate any changes in the efficiency before and after.

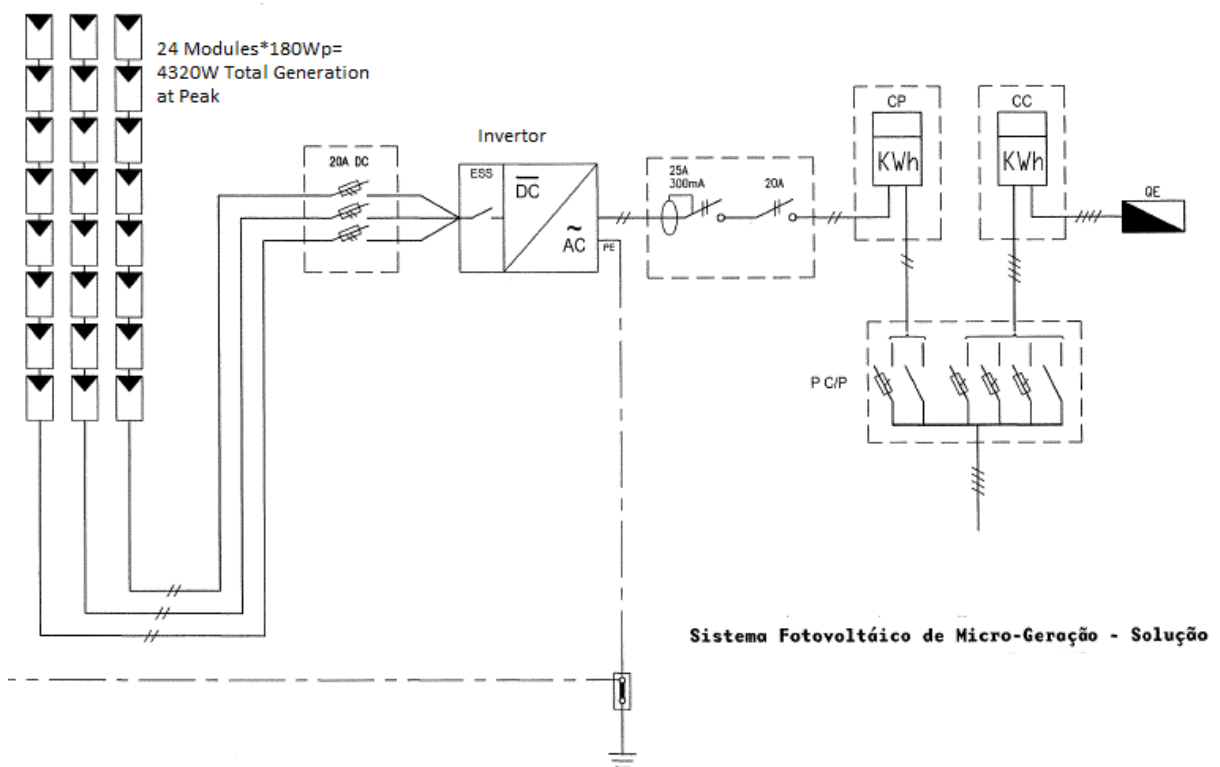


Figure 36: Layout of PV system in Lisbon.

Referência / Type reference	LEATE – PLANO COM COBERTURA SELECTIVA
Tipo / Type	Coletor plano / Flat plate collector
Área do absorvedor / Absorber area (m ²)	1,00
Área de abertura / Aperture area (m ²)	1,01
Área total / Gross area (m ²)	1,14
Dimensões / Dimensions (mm x mm x mm)	1068 x 1067 x 82
Peso / Weight (kg)	31
Fluido de transferência / Transference fluid	Água e glicol / Water and glycol
Pressão máxima de funcionamento Maximum operation pressure (kPa)	600 (6 bar)
Perda de Carga / Caudal (kPa - kg/h) Drop pressure / Mass flow rate	0 – 0 0,25 – 19 0,65 – 42 1,11 – 61 2,02 – 88 2,85 – 108
Temperatura de estagnação / Stagnation temperature (°C)	154
Constante de tempo / Time constant (s)	75
Capacidade térmica / Thermal capacity (kJ/(m ² K))	13,3
Modificador de ângulo (Ângulo de incidência) Incidence angle modifier (Incidence angle)	K _L (θ= 50°) = 0,83
Rendimento instantâneo / Instantaneous efficiency	
η_0	0,774
a_1 (W m ⁻² K ⁻¹)	4,8
a_2 (W m ⁻² K ⁻²)	0,005
Pico de potência / Peak power (W)	785

Figure 37: Data sheet values of the Portugal collector

The solar collector of the plant has the dimensions and data sheet as described in Figure 37, producing about 785W of peak thermal power while the DG-01 system is expected to produce 648W of power at peak operating conditions. Some of the preliminary results are discussed in chapter 4. Sizing of the system is modelled with respect to the plant in order to compare with PV/T of similar size to comprehend the differences in the operational performance and efficiency.

3.1.2 Data Collection and Analysis

BOEM Techno-veritas own the solar plant in Lisbon. The system has an online access to the data generated instantaneously. A period of six months data was used for analysis for pre-comparison before analysing performance with an actual PV system and solar collector units. Weather data was purchased from Whitebox technologies for the year 2013. The irradiation data from 2016 and 2017 is also available. An example of the system is shown below. A layout of the structure of this data is given in the appendix. The values are mainly collected from 2016-2017. In order to meet the demand of the load that has to be designed in Portugal, two days with the highest and lowest power generated at worst and best summer and winter months has been selected funnelling a series of 8 days of reference points where the power generated or not generated can be appropriately compensated by predicting an accurate

performance of the designed system. This has been summarized below using hourly values of power generated for each day. The data generated at the highest and lowest power in the winter months of January and December is shown in Figure 38. While the PV power during the peak summer months of June and July data is given in Figure 39. The data is collected every 30 minutes.

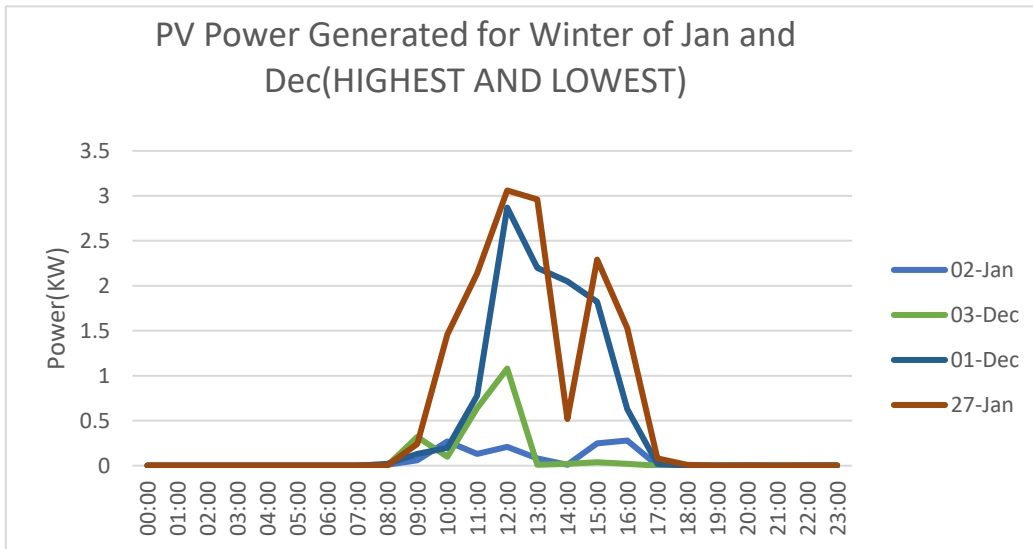


Figure 38: PV power generated during the winter months.

It can be observed from Figure 38 and Figure 39, that the highest power generated for both the winter and summer months on 27th January and 3rd June are quite close to each other, generating 3KW and 3.5KW respectively. This is since in Portugal the ambient conditions are warmer than in the UK.

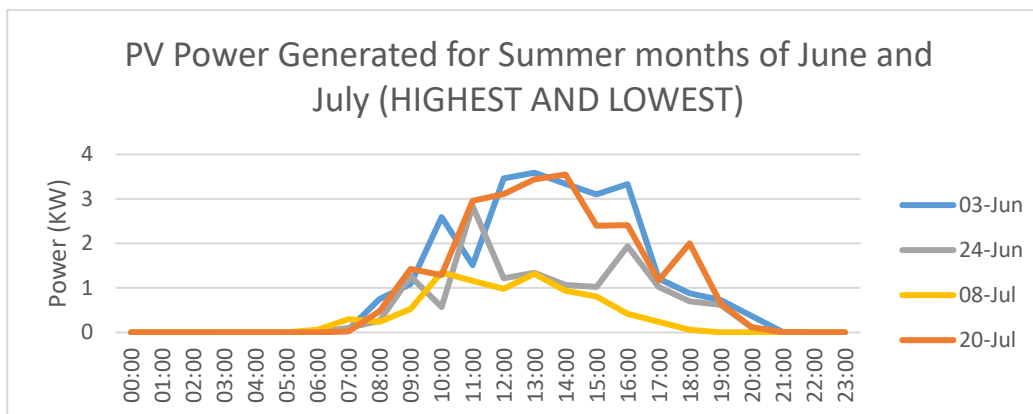


Figure 39: PV power generated in summer months.

The average annual generated energy from the 24 PV modules is shown in Figure 40 where an average of 300 KWh is maintained. This indicates a minimum supply of 300KWh throughout the year and this can be utilised for an efficient design.

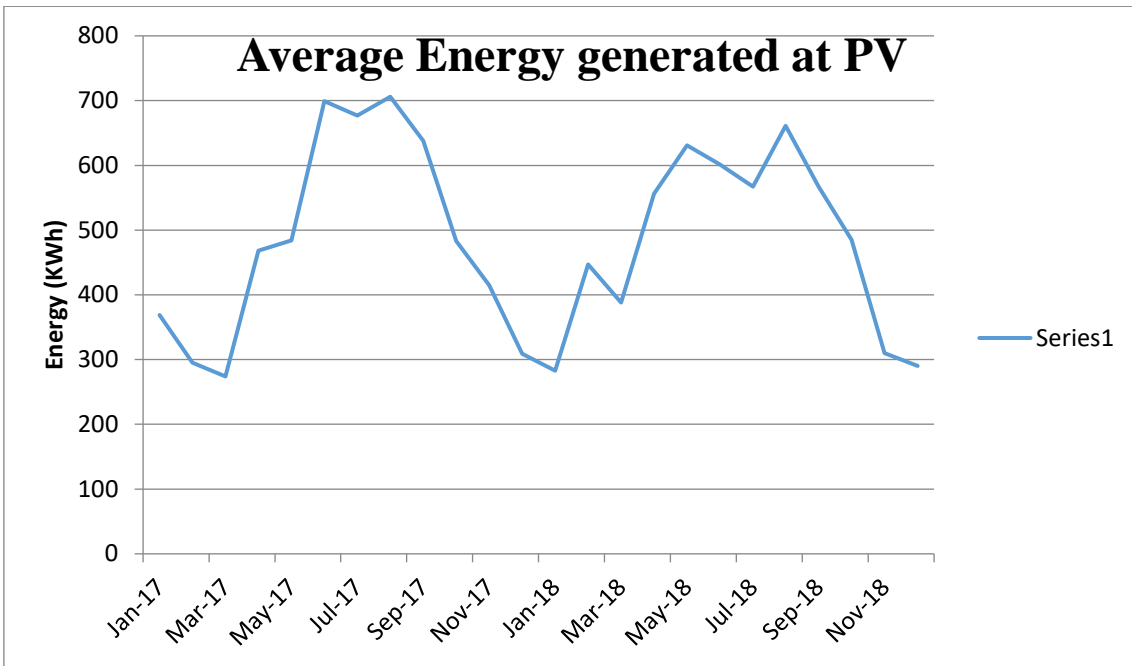


Figure 40: Average energy over the year.

The radiation and other weather data has been obtained from white-box weather technologies. The current recorded at the PV system shown in Figure 41, displays a drop which is due to dust accumulation. The accumulation of dust had decreased the current generation of PV drastically by 50%.

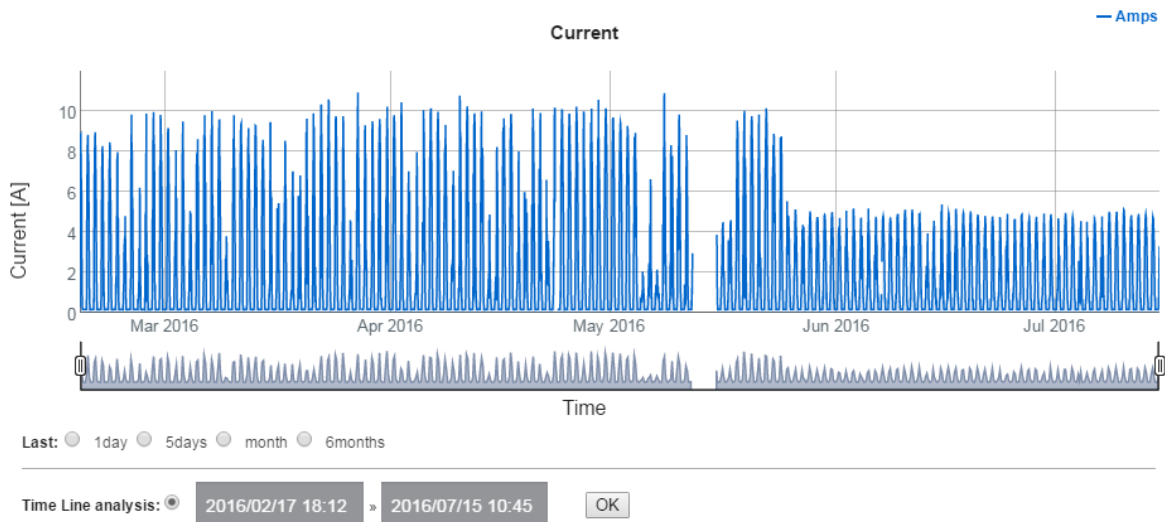


Figure 41: Current reduction at the PV due to dust accumulation.

When this was cleaned, and an improved output is observed as in Figure 42. This shows the effect of dust accumulation on the output of the PV and needs constant maintenance to ensure higher output.

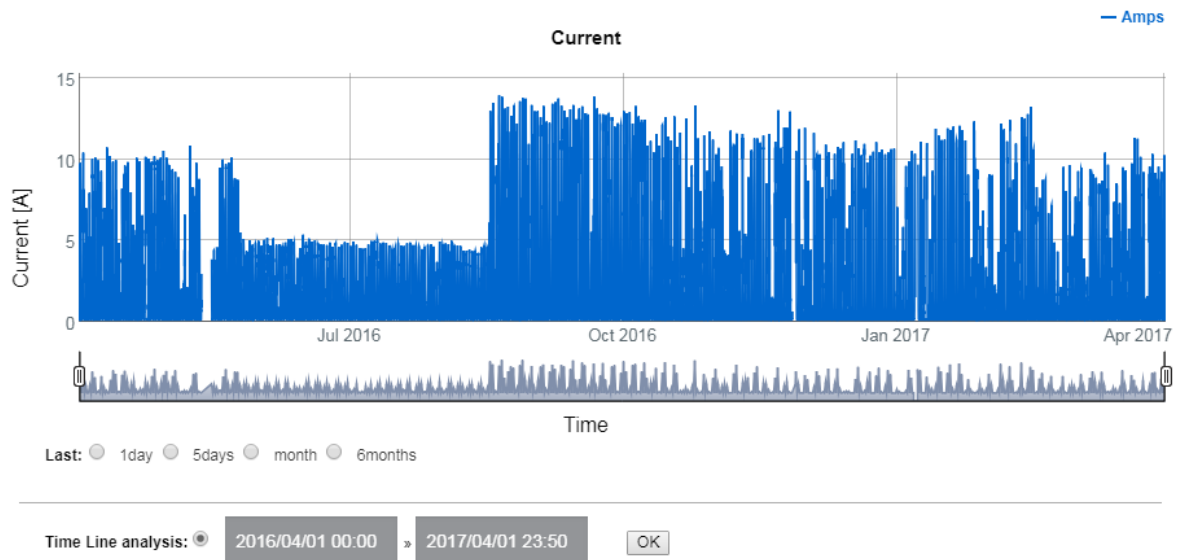


Figure 42: Improved current at PV

The solar collector output is generated for the same days as shown below in Figure 43. The average temperature generated during the year is observed to be maintained at 27°C.

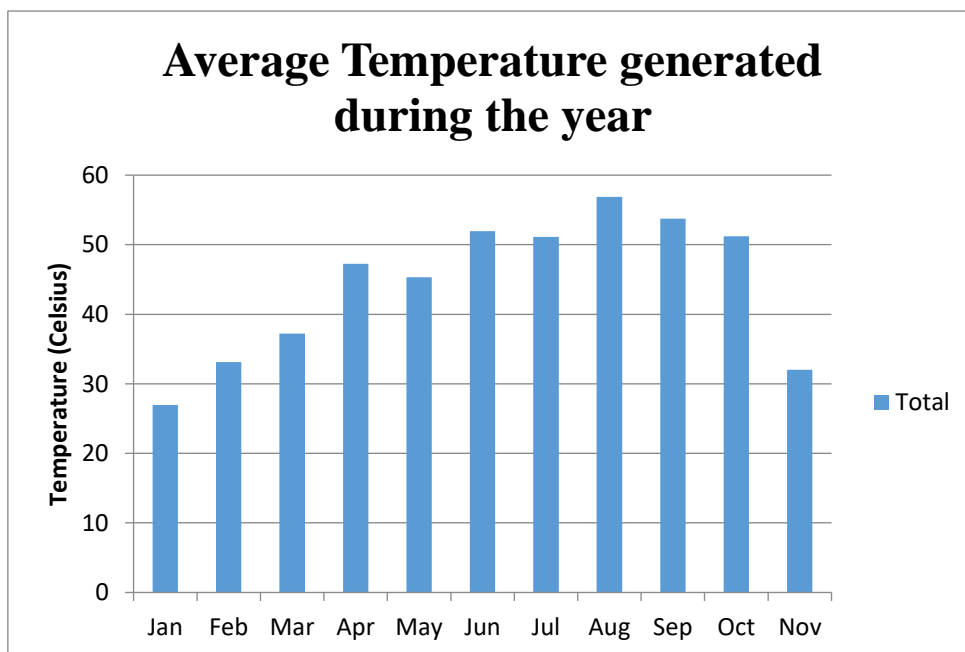


Figure 43: Average temperature at Solar collector output

The narrowed down eight day section is also applied to the collector output and this variation is observed in the data shown in Figure 44 and Figure 45.

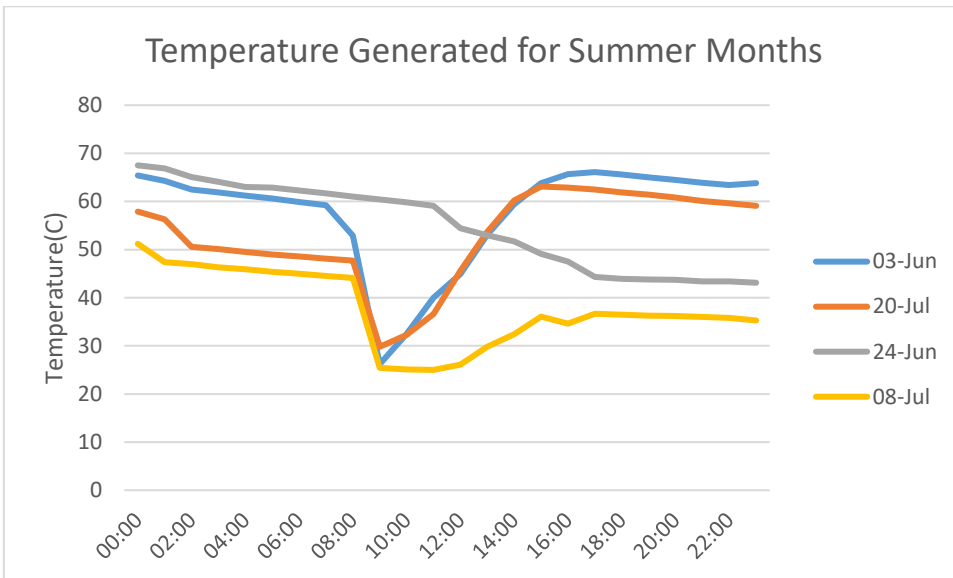


Figure 44: Summer months temperature

In Figure 44, it can be observed that 24th June data shows a lower drop in temperature while all the other three days have sharp drop of temperature in the morning.

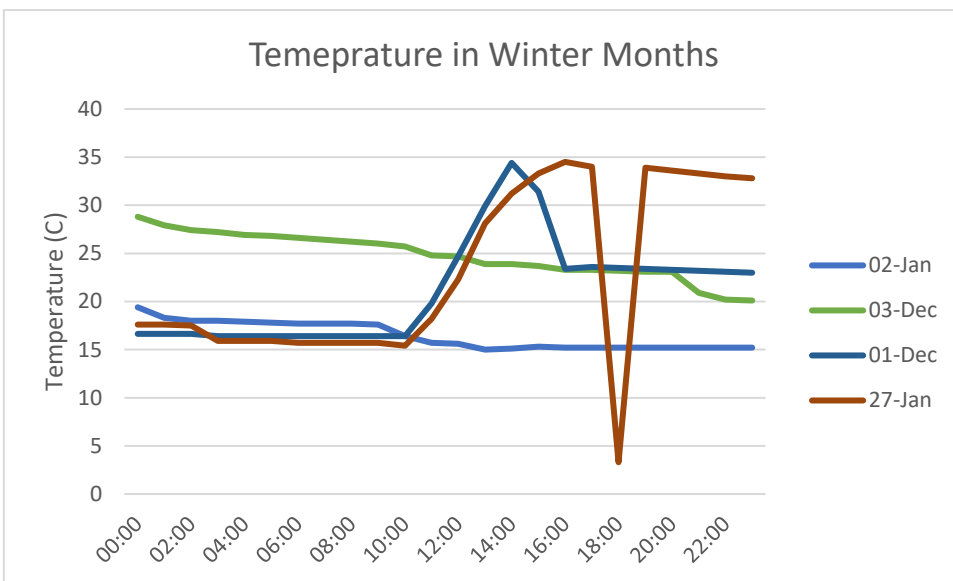


Figure 45: Winter months temperature

In Figure 45, again a step drop in temperature can be observed on 27th January and a PV/T simulation needs to be observed whether there is a similar drop in temperature or efficiency or a different performance of the system.

3.2 Newcastle PV/T System

The PV/T system installed in Newcastle has a series of 12 PV/T with two 6 series of panels in parallel. The data logger and the PQube takes in data to be viewed online. Any changes to the system can be tweaked manually using the temperature band for the pump operation.

3.2.1 Experimental Rig (USB, Newcastle)



Figure 46:Layout of PV/T on USB

The collector system consists of 12 PV/T's six of which are connected in parallel configuration. However, the system installed does not take in electricity output from all the panels in from six panel row. Only 4 panels have electric output from six panel row and six panels from the rear end six panel row. Hence in total all 12 panels have thermal output but only 10 panels have electric output due to a mismatch in installation process. The output from the collector is only significant when there is 6°C temperature difference between the inlet and the outlet flow and this controlled by the pump station control automatically. All the

panels are at an inclination of 20° due to high velocity wind issues at the rooftop shown in Figure 46. PV/T are connected to an inverter system for a direct connection to the DC output and it is also converted to AC for connection with distribution board as shown below in Figure 47. Hence the output for thermal system is expected to be 3.888KWp and for the PV system it is expected to be 2.5KWp at STC.

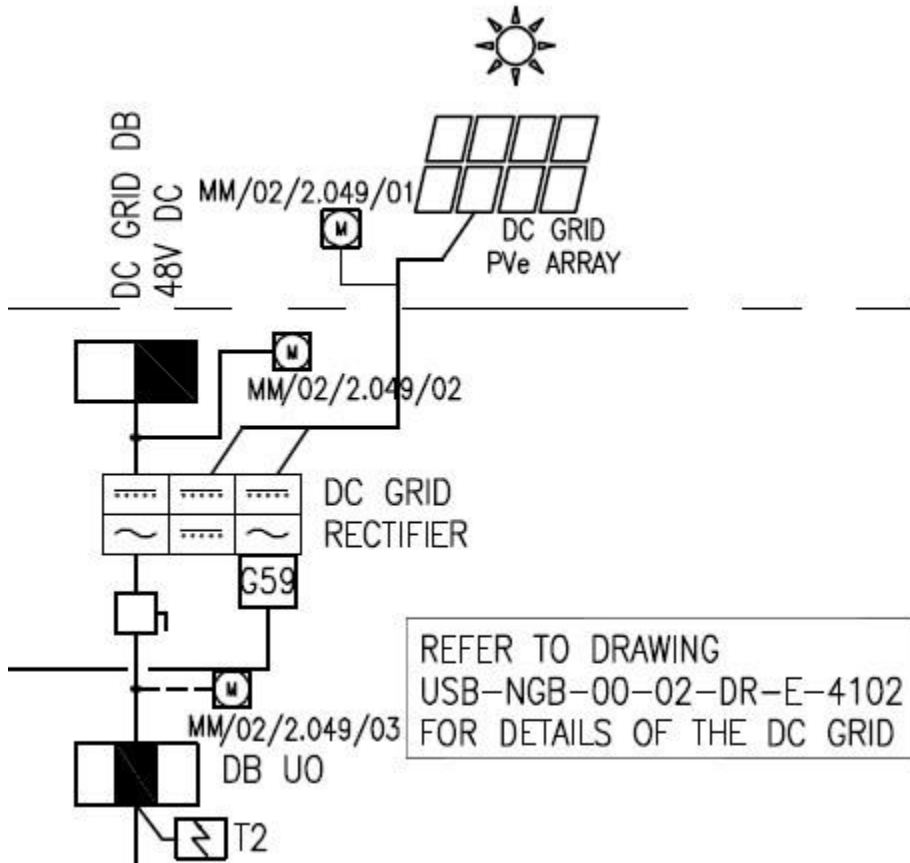


Figure 47:PVe output

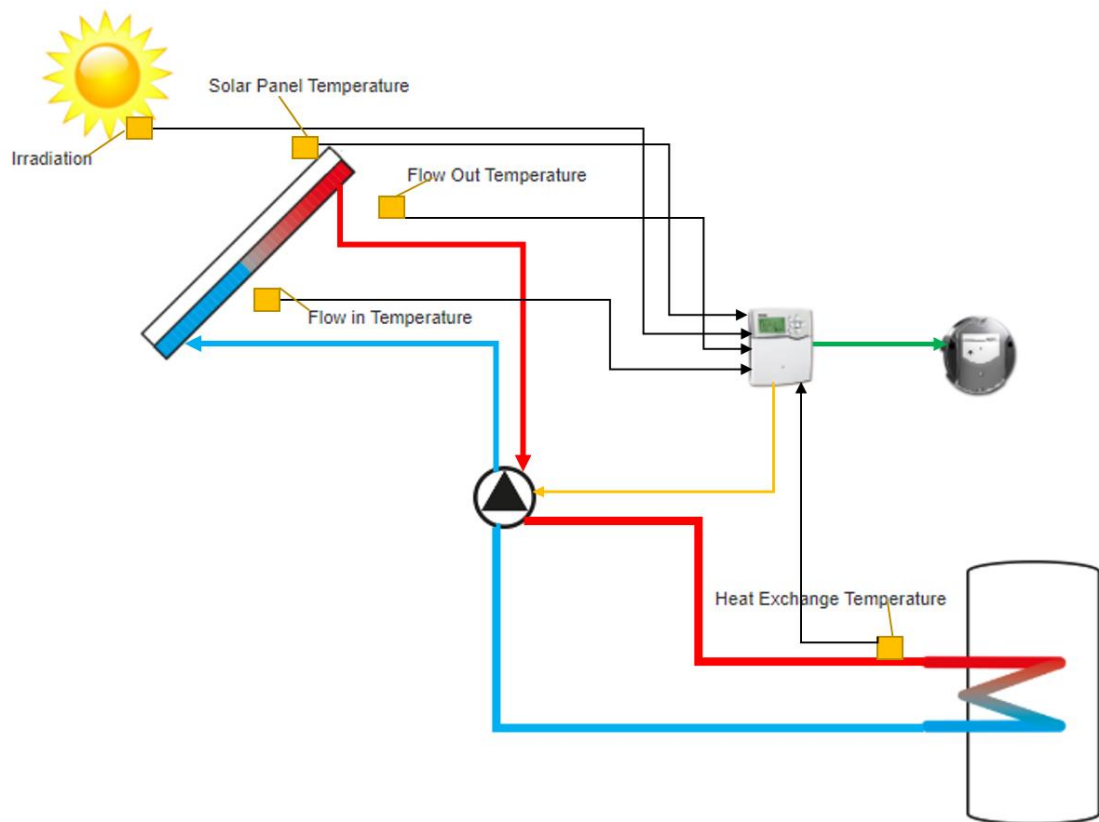


Figure 48:PV/T layout with data logger

The system has a series of sensors for wind, humidity, temperature, solar radiation and precipitation. This has been installed in 2018 and the data can be accessed online. The weather needed for the model has been obtained from the meteorology system installed at this location. The PV/T layout of the sensor location is described as in Figure 48.



Figure 49: Weather sensors



Figure 50: Sensors and pump system installed on USB

Through the urban observatory project at Newcastle university, the weather data is collected at 1min intervals each day with the use of sensors installed as seen in Figure 49. The PV/T pump system data is collected through the online RESOL data logger as seen in Figure 50 at 1 minute intervals or 1800 sec or 3600 sec, as this data can be selected to read at lower or higher sampling rates.

3.2.2 Detailed Description of PV/T and Parameters

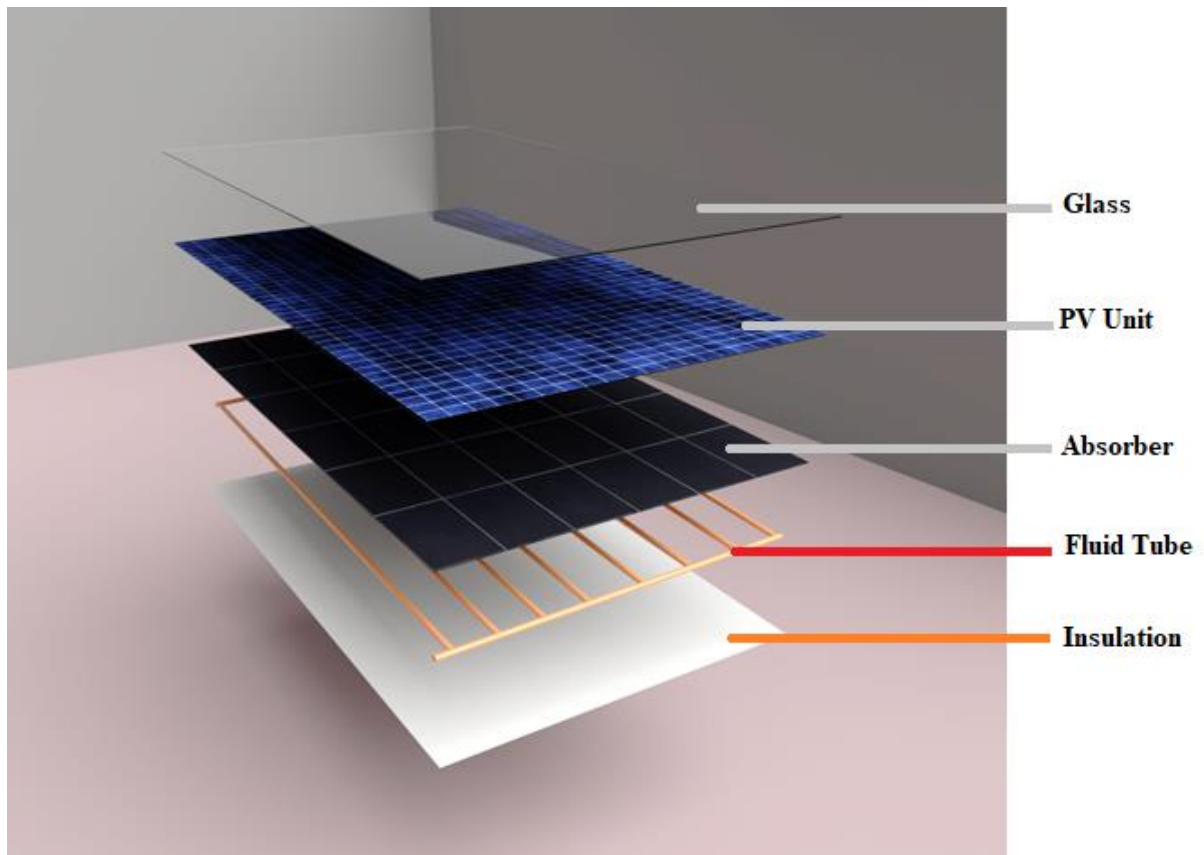


Figure 51: Isometric view of PV/T

In this study, the thermal circuit is solved for both resistances and capacitance consisting of 6 nodes perpendicular to the fluid flow. Each of these nodes represents each layer of the PV/T (glass cover, PV layer, absorber, tube bond, fluid, and insulation) shown in Figure 51. In the direction of the flow, the collector is divided into N nodes which essentially means that each section of the PV/T is considered as a finite element of ' N ' nodes. The higher the number of node value, the higher the accuracy, but this increases the computational speed and thus, the model is referred to a $6 \times N$ node model. The method is based on solving the energy balance equations for the glass cover, PV layer, absorber, tube bond, fluid, and insulation. The heat transfer coefficients for each of these layers vary according to time, incident radiation, wind speed, ambient temperatures, and location by latitude and incidence angle that changes as it passes at every layer. This model in fact considers real-time data from each location for comparison with its relevant field data for validation. The system parameters that can be varied to find significant changes are outlet/inlet temperatures and the flow rates for an entire annual year. As previously discussed, to reiterate, the PV/T system is intrinsically dynamic as its input is unstable and steady state analysis is inconclusive for a thorough study of thermal

behaviour with respect to its parameters. Therefore, dynamic modelling methods are explored using explicit analysis/implicit analysis of the entire system with the corresponding energy and exergy analysis. An implicit analysis is chosen, and the RK-4 method is used to solve the system to for a better solution.

In order to study the PV/T model (DG-01), the technical performance needs to be understood which can be studied over a range of analysis like energy analysis and exergy analysis. The energy analysis is based on energy balance equations and does not give the complete data needed to examine the PV/T model. The exergy analysis gives the user the grade of the quality of the electricity and thermal energy produced.

Large quantity of research work has been carried out to study the performance of various liquid types of PV/T configurations, optimize their geometrical sizes and suggest the favourite operational parameters related to the PV/T. As the result, many useful results and conclusive remarks have been obtained and these are selectively indicated as follows and this data can be used for comparison and addressing any gaps through the simulation and study of this project.

As the DG-01 model has a gap or space between the PV and the absorber, the output is expected to be improved. Hence the system is modelled for complete analysis removing any excess heat from the PV panels.

The model considered here is modelled in MATLAB solved by fourth order Runge-Kutta and implicit method for a more accurate result on a 6-node analysis. Some of the assumptions considered for the DG-01 model:

- All materials have isotropic properties
- For a single glass cover of low iron, ambient temperature is considered approximately equal to the sky temperature.
- Uniform flow distribution rate is assumed due to higher performance.
- All elements of the analysed control volume have dimensions identical to the elements of the real collector.
- The thermo-physical properties of the materials are constants.
- All heat transfer coefficients computed in real-time
- The PV layer is opaque.
- Dust and Shading effects are neglected and accounts for 1-2% of the losses calculated.
- Ambient temperature is considered equal to environment temperature because thermal and electricity gains increase only by less than 1% for every 15 °C.

- Fluid tube has a metallic bond for higher heat transfer to the fluid.

Temperature distribution in X-direction will not affect the temperature distribution in Y-direction.

The nodes are Glass, PV with EVA, Absorber with EVA, tubing with weld bond, fluid flow and insulation. The energy balance method is used here, accounts for the heat energy transferred removing any losses, thus calculating only the accurate measure of useful thermal gain from the PV/T unit. At each node this balance is calculated using ray trace method and six energy balanced equations are generated with the variable heat transfer coefficients. These equations can then be solved using RK-4 implicit method and the set of ODEs are solved repeatedly to find the temperature at each node. A separate PV analysis is also done to reveal the electric energy for comparison with an individual PV unit without the presence of an thermal absorber to remove the excess heat. The factors like mass flow rate, Nominal operating cell temperature (NOCT), solar radiation, wind velocity, ambient temperature, incidence angle (that changes over location) and tilt angles were varied, and preliminary observations are made. It should also be note that the heat removal factor is co-dependent on the geometry, the fluid capacity of the system, mass flow rate and the heat transfer coefficients and the useful heat gain is directly proportional to the heat removal factor. The stagnation temperature is decided from manufacturer testing and was found to be 79 °C. The packing factor for this PV/T unit was 0.7 which is a reasonably good value of PV without attracting too many losses.

3.2.3 Data Collection and Analysis

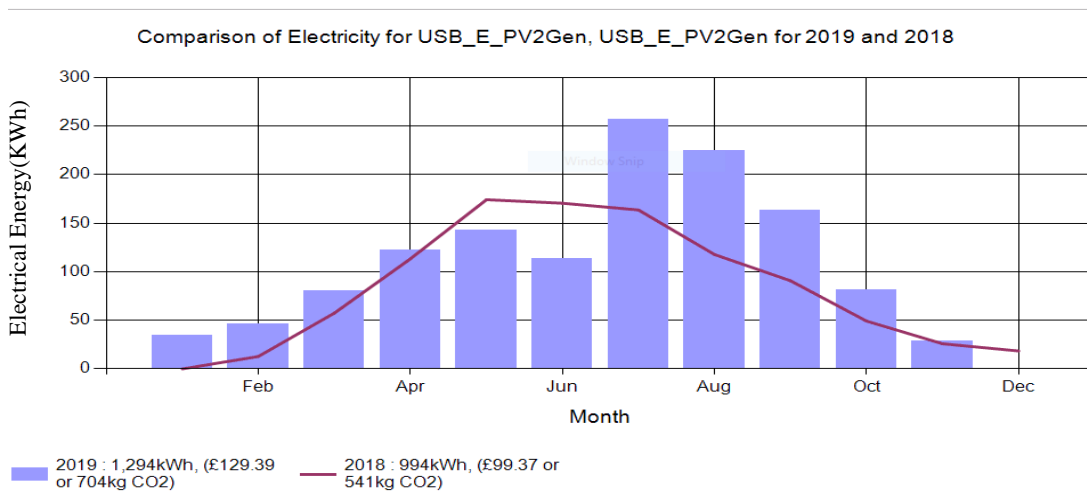


Figure 52: Annual USB electric energy data from Meteorology

Weather data was also collected from the MetOffice by special request. The electric data is collected at every 30 min interval. Very recent information was downloaded from the USB as

data was collected through PQubes and this has been under investigation with 80% completion. A less accurate PV data was also collected from METERology online database for present comparison shown in Figure 52. METERology provides a detailed description of energy and power generated. A PV panel system of 121 panels is also available as data. However, the PQube data did still have some inconsistency and this has been further rectified for 100% completion by narrowing down the number of months where output is available.

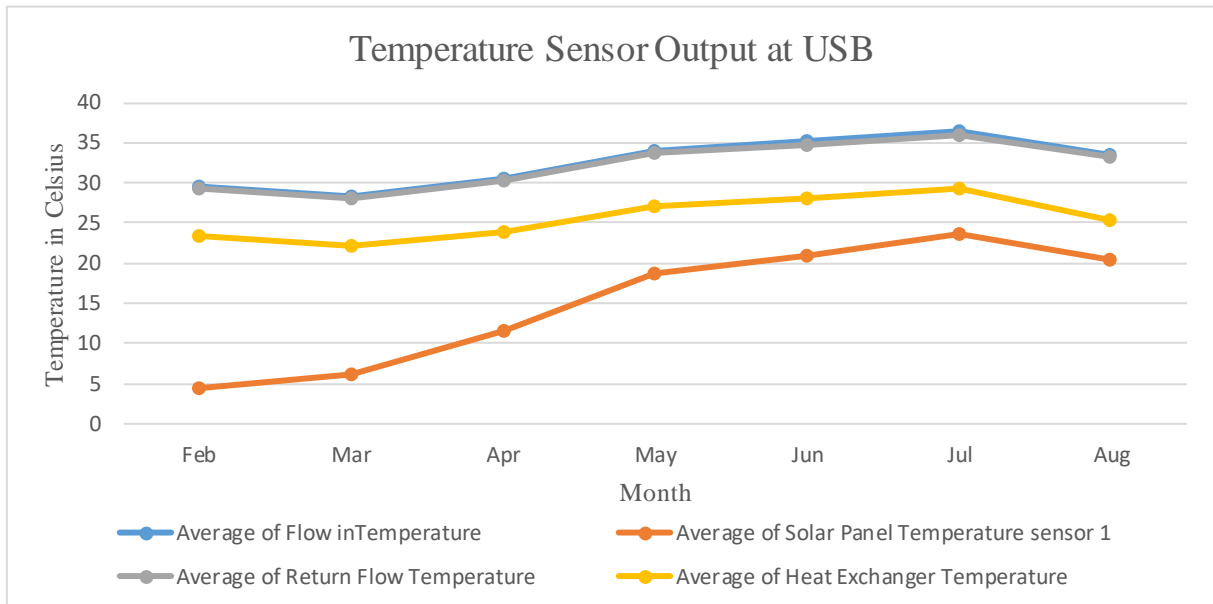


Figure 53: Temperature sensors at the USB

Data collection for the USB building is taken from RESOL data logger (online and from the SD for reconfirmation) for the PV/T thermal output which has 4 sensors that obtain the solar panel temperature, heat exchanger temperature and flow in and out temperature. Weather data was obtained from a previous Kings-Gate Newcastle university study and updated from USB publicly accessible data for irradiation, temperature and wind conditions. The flow in temperature of the fluid was at 30°C. The values of flow-out, flow-in, solar panel temperature sensor and heat exchanger sensors as connected in Figure 48 is shown in Figure 53. The inlet and outlet are quite close to each other as the temperature at the inlet is high and the pump turns on when the temperature difference is less than or equal to 6°C. The sampling rate of this data is recorded at 1 data point per minute. However, as this can cause huge increments of data, it can also be set to collect at every 5 min interval.

3.3 Lab System:

3.3.1 Laboratory Rig (Newcastle)

The LAB demonstration unit was installed on MAY 14th 2018 for demonstration and run with 4 PV/T units and a solar collector unit for surplus energy. The system is typically controlled by the pump depending on the temperature bandwidth setting which is set at 1.5K difference. The maximum that can be set is 6K. A load demand has been drawn for Newcastle as shown below. A layout drawing of the installed LAB demonstration unit is shown in Figure 54.

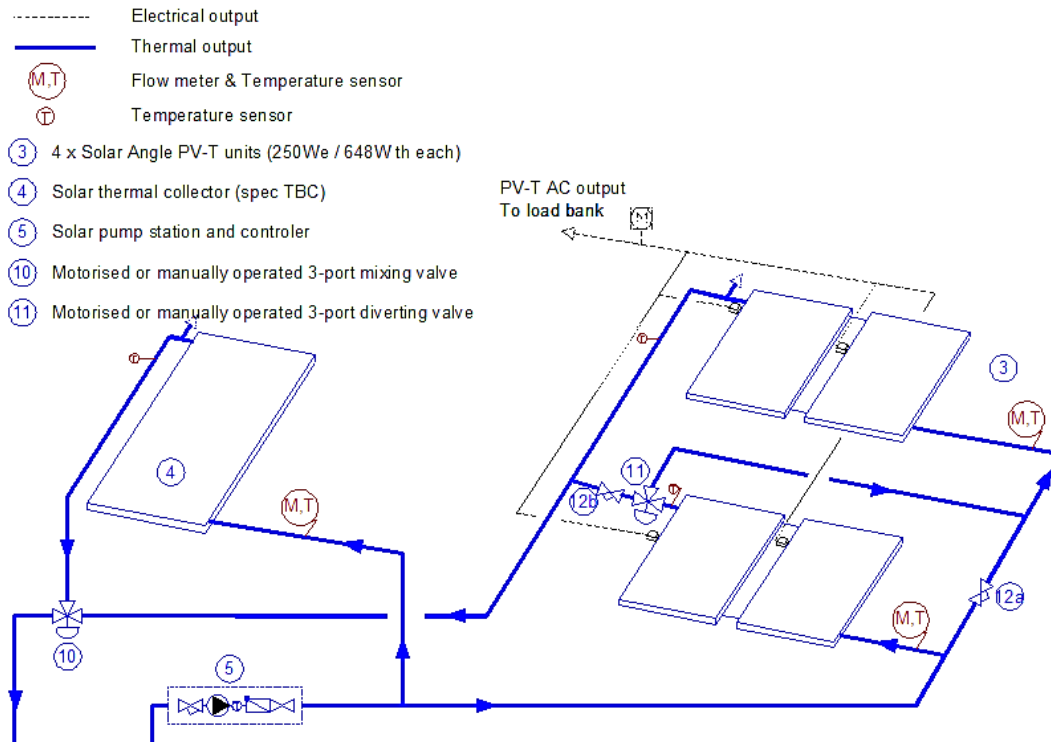


Figure 54:LAB demonstration unit

The system has also been tested and run at different weather conditions for comparability and reliability of the data collected. Data was collected under sunny and snowy conditions to test the legitimacy of the data which was found to be reliable as setup in Figure 55 .



Figure 55: Lab unit setup in snow and sunny conditions

3.3.2 System Description

The data generated at the lab system is collected for a week in April (8th to 15th) and the generation electricity versus consumption is shown below in Figure 56. The pump level at 43W was run from 8th to 11th and the switched to the third pump level at 49W from 11th to 15th. A maximum output power of 750W was observed on April 9th after the first pump was switched on at 43W. On the 11th April, the next level of pump at 49W was applied.

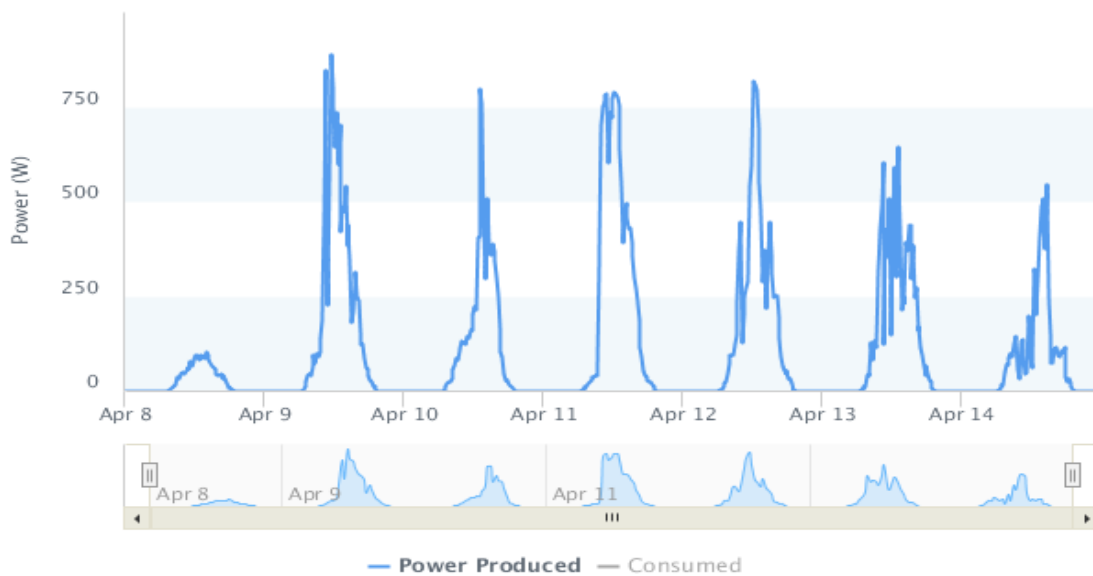


Figure 56: Electrical energy generated in the rig during the test week

The outdoor experimental rig for the whole system was continuously operated and recorded in sunny or cloudy weather conditions from April 8th to 15th 2019 in Newcastle (54.9783° N, 1.6178° W) throughout the day and night. The testing for the operating facility was run for twenty-four hours daily and all the instruments were fixed. The test data was recorded at 1-minute intervals using a data taker for the temperature values. The electric energy was recorded every 15 minutes by an online enphase system where each panel has a microinverter that records the DC voltage and current and temperature generated. These results have been given in the Appendix VI. The outdoor experimental rig is displayed as in the following figures

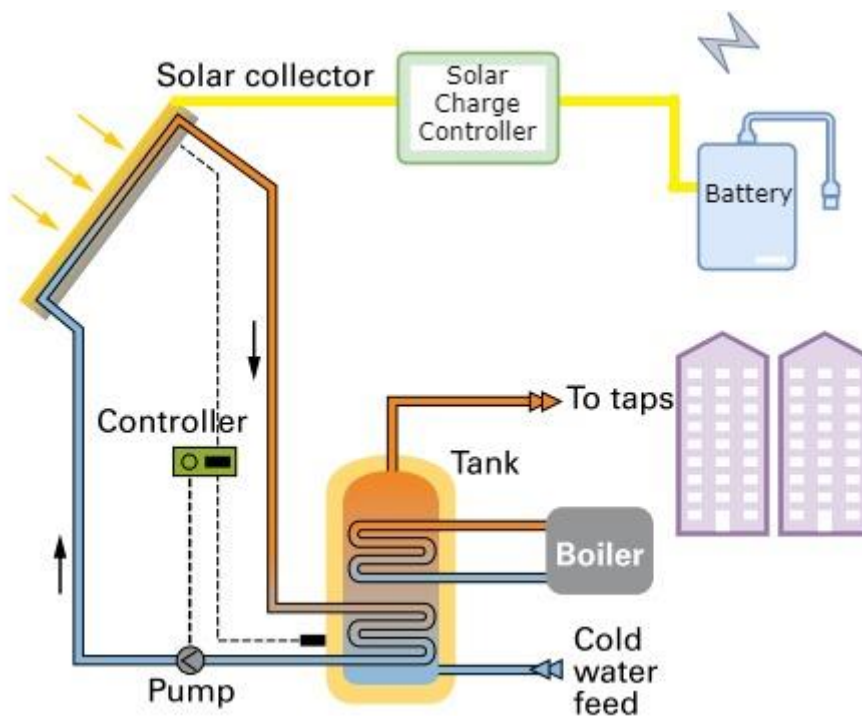


Figure 57:PV/T connection assembly (using RESOL)

The PV/T connection assembly is detailed in Figure 57, where the electric output is connected to the solar charge controller. This is either connected to a battery or a DC/DC converter for boosting the power usable for household DC appliances. A DC/AC converter is also used for AC appliance connections for domestic use or for the connection to the grid. The heating system runs through a heat exchanger and sometimes an auxiliary electric heater can also be used if the hot water is used for domestic hot water as the water temperature needs to be maintained at 60°C in order to prevent salmonella. The piping of the PV/T is such that the four PV/T can be connected in two series or two parallel PV/T using a two and three way valve which is shown in Figure 58.



Figure 58:Piping systems

3.3.3 Data Collection and Analysis

Electricity data collection for the LAB is taken from Enphase microinverters accessible through the online portal, where the data can be accessed at a sampling rate of 5 minutes. As the USB data logger RESOL is the same system used at the lab, the same portal can be used to access this data (both online and from the SD card for reconfirmation). The enphase microinverters also generate current, DC voltage ,temperature at each PV/T output which can be analysed further.

The lab data is also collected via a data logger (like in Figure 59) and micrometres. The PV output from the PV/T is obtained using micro-inverters unlike USB to optimise the output. The Lab PV/T's are also tilted at 30° for a complete and optimised output.



Figure 59:Data logger

3.4 Domestic Case for Newcastle

The case study chosen shows the ability of the model to predict for any demand at any point in time. This makes the design from model very flexible. A 4-bed residential house has been selected for application of the model shown as in Figure 60. The overall demand for the house has been drawn for an entire year using the average over a period of two years (2017-2018).



Figure 60: Domestic residential case for Newcastle

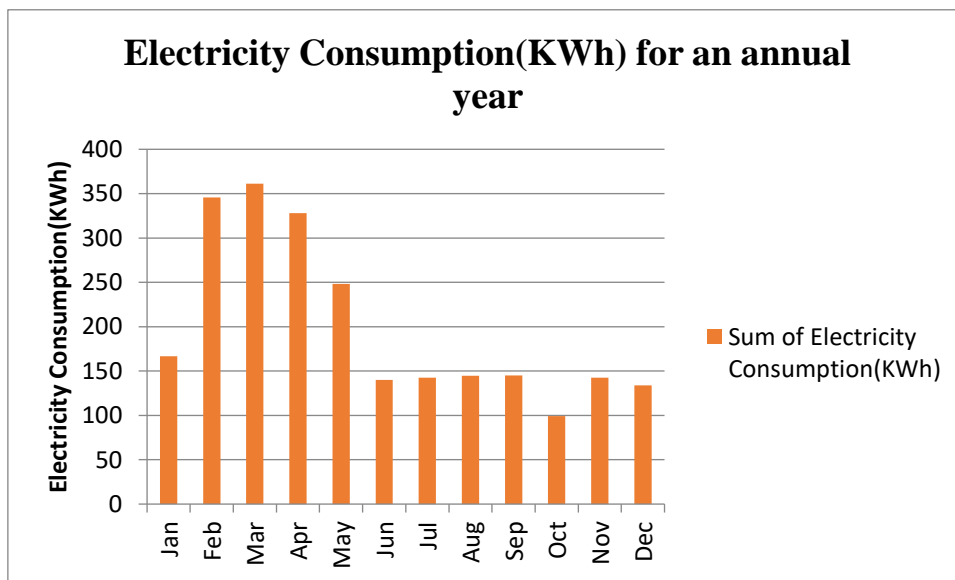


Figure 61: Average of Electricity Consumption for 4bed domestic house in Newcastle

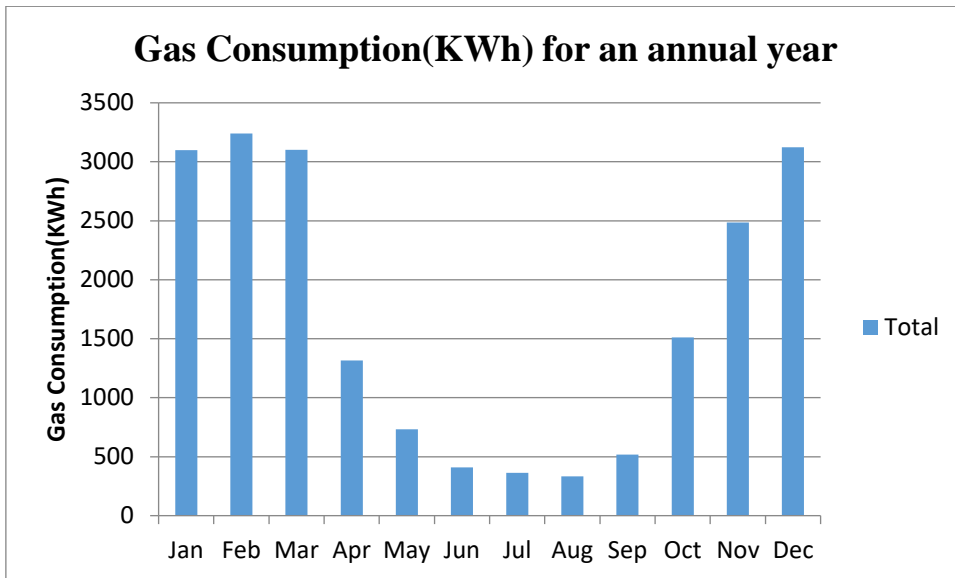


Figure 62: Load heat demand in Newcastle

This demand is used for the design calculations from the load output of the lab. The load demand and supply balance can then be readjusted to the demands. A 4-bedroom domestic house in Newcastle is considered for load demand and a system is sized to match the requirement when designing a practical system based on experimental results. The electric load is noted to be highest during the spring months (Figure 61) while the gas consumption is the highest during the colder months (Figure 62).

3.5 Domestic Case for Cochin

A 4-bed domestic house (Figure 63) load demand in Cochin is considered for sizing a system with recommendations of what parameters need to control for optimum output. Available Energy Demand for the case study house in Cochin is provided. There is lot of extra space on the roof and the second floor for external storage systems. The house has 4 open space balconies and available roof space with at least 400sq.m area. Load data is collected from the yearly consumption over a period of two years. The heat demand of the house is met by electric heater for hot water and domestic liquid petroleum gas (LPG) cylinders. Using the weather condition from Whitebox technologies, the diffuse and beam radiation at the optimal tilted angle of 22 is calculated and is generated as Figure 64.



Figure 63: Domestic case study

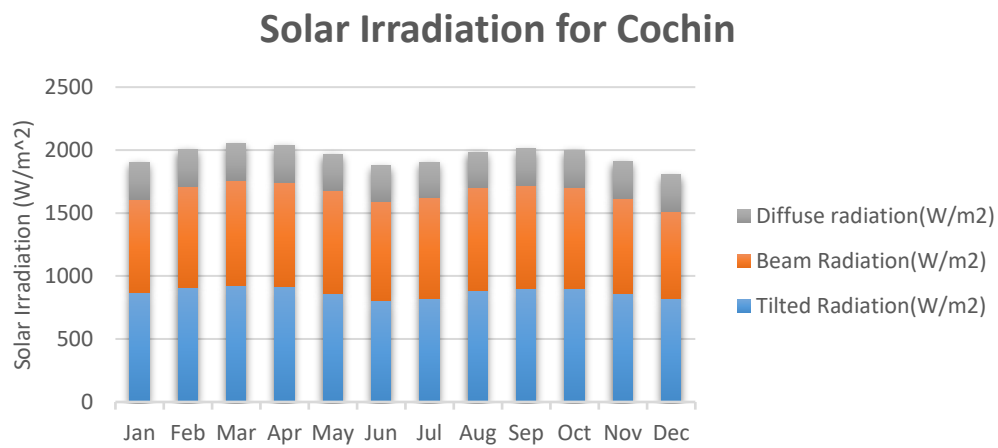


Figure 64: Solar Irradiation in Cochin

As mentioned, weather data is collected from White-box technologies. The load data is obtained from a 4-bed house in Cochin from a year of consumption.

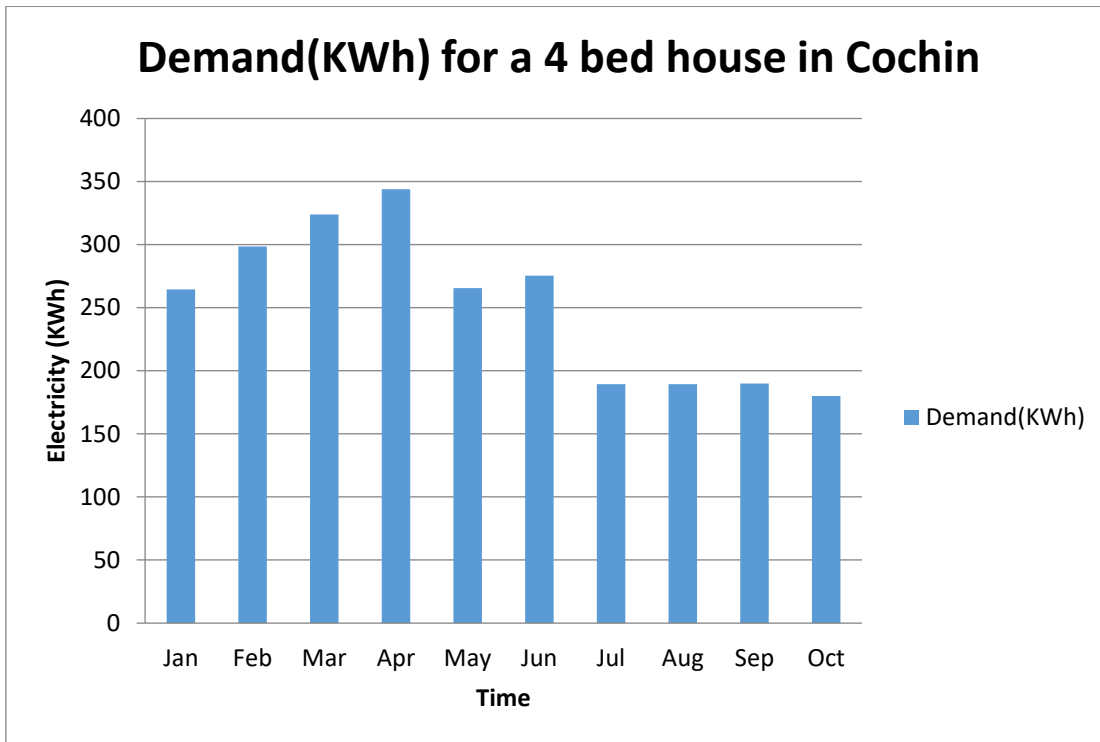


Figure 65: Load Demand for the 4 bed house

The higher electric demand can be met by adding a storage system (for off-grid) or increasing the number of PV/T panels (for on-grid) as there is ample space on the domestic house roof. A heat storage system can be used for hot water or a can be used on a liquid desiccant system for cooling. The load data indicated that the demand is the highest during the summer months as seen in Figure 65.

3.6 Summary

In order to comprehend and analyse the effect of variable factors on the output, MFR and temperature band difference of the pump was varied from 8th April 2019 to 11th April 2019 and not a significant effect was observed on the power output, however there was a small increase in power. The temperature effects however need to be investigated and analysed in the next chapter. The parameters concerning the other two case studies were also described, including the method and the quality of data collection and analysis. All the data input is analysed and narrowed to be finessed as input due to the immense data that is available. All the case studies and their description of data collection was analysed in this chapter.

CHAPTER 4. PV/T MODELLING AND VALIDATION

4.1 Introduction

As discussed in the previous chapter, the PV/T have PV cells and absorber units in their structure which vary according to the type of PV/T. Modelling PV and solar thermal collector units on their own can help to give an insight of how the PV/T units behave individually while observing any variations in factors affecting the performance, and this can be compared with the collective unit operation. Thus, a solution can be modelled and optimised in order to increase the PV/T performance. It should also be noted that over the years there have been various models, that were developed to improve the performance of the PV/T, which are affected by a number of factors like position of the sun, time of the year, location, wind speed, ambient temperature, irradiation, mass flow rate, configuration of the panels, temperature cut-off, heat transfer fluid, stagnation temperature, nominal operating temperature, difference in structure, packing density, fill factor, thickness of each layer and heat removal factor. However an investigation of PV/T performance with all these factors have not yet been presented to its full extent.(Department of Business, 2016)

This chapter is mainly focussed on developing computer simulation models that is based on theoretical and experimental analysis of PV/T. Thereby, two theoretical models were built for steady state and dynamic state performance. A combination of iterative method (IM), Runge-Kutta method (RK4) and finite element method (FEM) were applied in the development of mathematical models in MATLAB. These models are then tested with published data and experimental data to validate the results. And finally, a novel structure of PV/T model is also proposed based on the modified simulation output (Ascher, 2011, Barenghi, 2012, Lopez, 2014b, Lopez, 2014a).

In the following sections PV, Solar collectors and the designated PV/T system and their models in detail are explored along with the limitations while establish a fitting solution.

4.2 Analytical Model and Theory for Radiation

4.2.1 Sky Radiation Modelling

The radiation received at the surface of the earth is categorised as shortwave radiation with wavelengths between about 0.29 and 4 μm , and thermal longwave radiation with wavelengths between 4 and 100 μm . The shortwave solar radiation is converted to electrical output by the PV cells and the longwave radiation is responsible for heat emission that can be captured by thermal collectors(Cibse, 2015). The distinction between irradiance and irradiation is

important. Solar irradiance is defined as the instantaneous flux of solar radiation on any surface which is the flow of radiant energy per unit time falling on unit area (Wh/m^2). Solar radiation is the solar energy received per unit area over a time period which is also measured in W/m^2 . Insolation signifies the irradiation in the limits of the solar energy spectrum.

Energy per unit time radiated perpendicular to the transmission direction of radiation over a unit area outside the atmosphere between sun and earth is termed as Solar Constant (G_{sc}) and it usually has a value of 1367 W/m^2 . The extra-terrestrial radiation (G_o) is the radiation available outside the atmosphere of the earth and it varies with respect to different days in a year (n) and can be calculated as follows. B is defined as factor by equation 5.2 and θ_z is the angle of the zenith.

$$G_o = G_{sc}[1.000110 + 0.034221 \cos B + 0.00128 \sin B + 0.000719 \cos 2B + 0.000077 \sin 2B] \cos \theta_z \quad (4-1)$$

$$B = (n - 1) * \frac{360}{365} \quad (4-2)$$

It is imperative to understand different types of radiation to calculate their effect on the orientation, tilt angle and the maximum possible value of radiation available for the PV or PV/T panels to utilise. The short-wave radiation falls on the earth's surface in three different forms defined as beam, diffuse and reflected diffuse or ground radiation. Beam radiation (BR) is the direct radiation from the sun that is not scattered by the atmosphere (also called direct radiation) and diffuse radiation (DR) is the radiation received due to scattering from the atmosphere where the intensity depends on cloudy or clear skies. Ground reflection radiation (GRR) is from the reflected components of both BR and DR as well from the ground (depending on whether the ground is smoother or rough or if there is snow.) as well as any additional variables like human or natural obstacles. The total solar radiation received by the panel is the sum of beam and diffuse and ground reflection radiation, also known as global horizontal radiation (GHR). Total global horizontal radiation is required for every calculation in the model. Decomposition models extract the DR from GHR where GHR is the usual input from weather stations (Mousavi Maleki et al., 2017). Hence to examine the effect of radiation on the inclination and orientation of the panel, it is necessary to find the BR and DR from GHR. According to Soga et. al., among the 54 different combinations of 9 beam and diffuse irradiance decomposition models and 6 sky irradiance models that were investigated, the Perez model was said have the least RMSE (root mean square error) (Soga et al., 1999).

The next best model was found as the Reindl model by Soga et. al. (Soga et al., 1999) and Kamali et. al. (Kamali et al., 2005). It has also been found that hourly models perform much better than daily models (Kambezidis and Psiloglou, 1997).

The accuracy of any sky radiation model depends on the quality of the input data for GHR and the efficiency of the model used. This means that the model should be able to favourably simulate irradiance close to actual results. The uncertainty in the data provided should also be investigated and considered before assessing the performance of the simulation. The equipment that measure GHR, DR and BR (Horizontal component) determine the quality of the data. The uncertainty resulting from these systems can be used in uncertainty analysis to avoid erroneous values. GRR can be calculated if it is not available, however, this can contribute to the errors.

In this thesis, four different decomposition models (Erbs, Reindal 2, Perez and DSRG) along with 2 sky irradiance model (HDKR and Perez) were selected and investigated and a modified a new decomposition model method was developed based on experimental and theoretical results (Kharseh, Kambezidis and Psiloglou, 1997, Gueymard, 2000, Kamali et al., 2005, Katiyar and Pandey, 2010, Chandel and Aggarwal, 2011, Huld, 2011, Hussein, 2012, Dal Pai et al., 2014, Cibse, 2015, Li et al., 2015, Lee et al., 2017, Ayvazoğluüksel and Filik, 2018, Laiti et al., 2018). Maxwell model is also calculated and shown in the appendix.

Once the incoming irradiation value is obtained and the sunrise and sunset hours determine the time range of the incidence angles on the PV/T unit, the next step is to define and find the changes in hourly incidence angles of the sun on the PV/T in question For this the solar time is first defined which is dependent on the local standard time (L_{st}) and the location longitude (L_{loc}) and then the hour angle can be calculated according to Duffie and Beckman (Duffie and Beckman, 2013) as follows

$$E = 229.2[0.000075 + 0.001868 \cos B - 0.032077 \sin B - 0.014615 \cos 2B - 0.04089 \sin 2B] \quad (4-3)$$

$$\text{Solar Time} = \text{Standard Time} + 4(L_{st} - L_{loc}) + E \quad (4-4)$$

Solar time is calculated and considered in all energy calculations as a location can be sometimes 1.5 hours (or 90 minutes) away from solar time and it can affect tracking, energy incident and shading factor that can have more than 2% effect on the output. As described previously in Chapter 3 and 4, three case studies will be investigated in this project and a

glimpse of the solar time variation in a year for the three case studies is shown below. It is to be noted that the case studies have taken into account of the daylight savings time (DST) in Lisbon and Newcastle during 2017-2018 from March to October (GMT+1hr) while there is no DST change in Cochin (GMT+5.5hrs)('A Comparison of Methods to Estimate Hourly Total Irradiation on Tilted Surfaces from Hourly Global Irradiation on a Horizontal Surface,' , Reifsnnyder, 1966, V.Badescu, 1991, Soga et al., 1999, Shukla et al., 2015, Yao et al., 2015, Shyam et al., 2016, Wang et al., 2018).

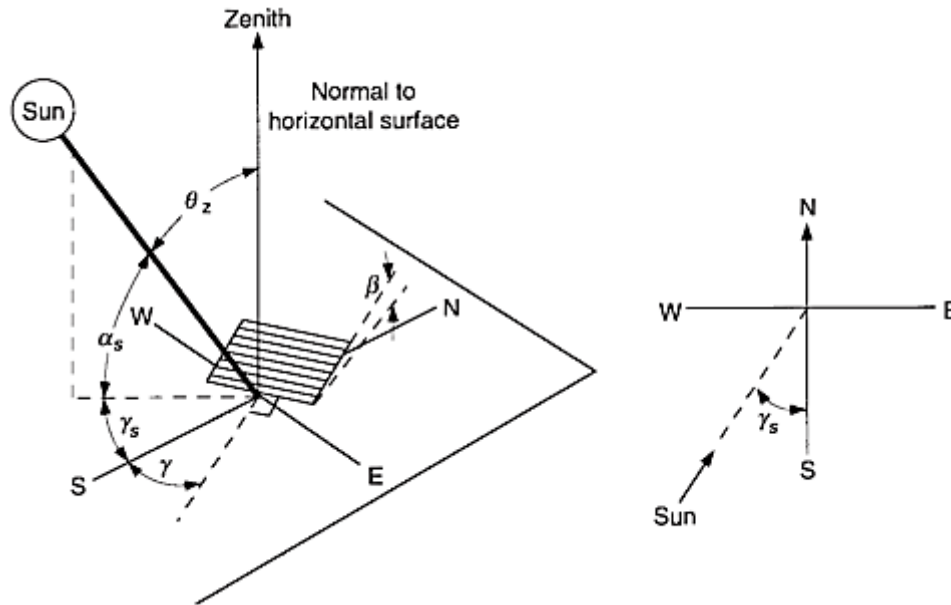


Figure 66:Angles describing beam radiation on a tilted surface

The orientation of beam radiation is described on a surface by various angles described as in Figure 66. The surface azimuth angle (γ) that ranges between $-180^\circ < \gamma < 180^\circ$ is the angle between the projection of the normal on a horizontal plane to the local meridian surface with east being negative and west being positive while south is zero, while hour angle (ω) is the displacement of the angle respective to the sun's west or east with morning being negative and afternoon as positive and angle of incidence (θ) is the angle between the beam and the normal to that surface. Zenith angle (z) is the angle between the line to sun and the vertical. Declination angle (δ ($-23.45^\circ < \delta < 23.5^\circ$)) describes the angular position of the sun at solar noon and tilt angle (β , when $\beta > 90$, the surface faces downward and ranges from $0^\circ - 180^\circ$) of a surface is the angle between the plane of the surface in question and the horizontal. α_s and α_z are the solar altitude (which is compliment of zenith) and Solar azimuth angle (angular displacement from south projection) respectively. To find the angle of incidence there is a need to obtain declination angle, tilt angle, hour angles and the latitude (ϕ) of the location in question and the surface azimuth angle (which can be taken as zero if the panel surface was

projected towards south)(Cibse, 2015). The surface azimuth angle at the USB is constructed such that it is at 20° away from due south and it is positioned at 20° tilt angle and this is considered in the model while validation. The PV/T on the LAB system is maintained at 35° and due south. For the case study in Portugal and for the design purpose in Kerala, the tilt angle is maintained at an optimal inclination angle which varies in summer and winter months depending on the location ($\beta = \varphi \pm 15^\circ$) and the panels are assumed to be due south (surface azimuth angle =0°) for maximum incident radiation. To favour the summer months, $\beta = \varphi - 15^\circ$ and for winter months, $\beta = \varphi + 15^\circ$. To support for an overall annual performance, $\beta = \varphi * 0.9$. For Cochin optimal tilt angle, $\beta = 8^\circ$ and for Lisbon, $\beta = 35^\circ$ (Mishra, 2012).

Angle of incidence of beam radiation θ

$$\begin{aligned} \cos\theta = & \sin(\delta)\sin(\varphi)\cos(\beta) - \sin(\delta)\cos(\varphi)\sin(\beta)\cos(\gamma) + \cos(\delta)\cos(\varphi)\cos(\beta)\cos(\omega) \\ & + \cos(\delta)\sin(\varphi)\sin(\beta)\cos(\gamma)\cos(\omega) + \cos(\delta)\sin(\beta)\sin(\gamma)\sin(\omega) \end{aligned} \quad (4-5)$$

When $\theta > 90^\circ$ the sun is behind the surface in question. And using Snell's law, angle of refraction can be found.

National Oceanic and Atmospheric Administration (NOAA) have modelled a solar angle calculator in accordance with Julian's charts and predicts the angles, sunset hour and sunrise hour within a latitude range of $\pm 72^\circ$ from 1901 to 2099. SPECTRAL2 (which is macro excel sheet) models the angles within a Macro code. In order to point the difference between the models, with other existing models, the generated incidence angles have been compared. This validates the angle of the location selected with the commercially available market models. One of the disadvantages of the existing models, is that the daylight savings time (DST) variation during the year needs to be inputted manually each time. The new model developed has eliminated this issue. Southern hemisphere declination has the opposite polarity to northern hemisphere regions. To determine shadows, solar profile angle is calculated, and this can be used to establish the exact position of the module.

$$\tan pf = \frac{\tan(90 - z)}{\cos(az - \gamma)} \quad (4-6)$$

Where pf is the profile angle, az is the solar azimuth angle, z is the zenith angle and γ is the azimuth angle.

The effect of shading can be investigated in conjunction with profile angle, profile of the obstacles and superficial dust if needed for further analysis. It has also been observed that the

absorptance of black paint or absorbing surfaces reduces with an increase in incidence angle. This means that the heat absorption slightly lowers during the morning and the evening as the incidence angle (IA) is found to be higher as seen from the Table 4 and Figure 67 .

Table 4: Absorptance of black paint (Kalogirou, 2009a)

Angle of Incidence	Absorptance for black paint
0-30	0.96
30-40	0.95
40-50	0.93
50-60	0.91
60-70	0.88
70-80	0.81
80-90	0.66

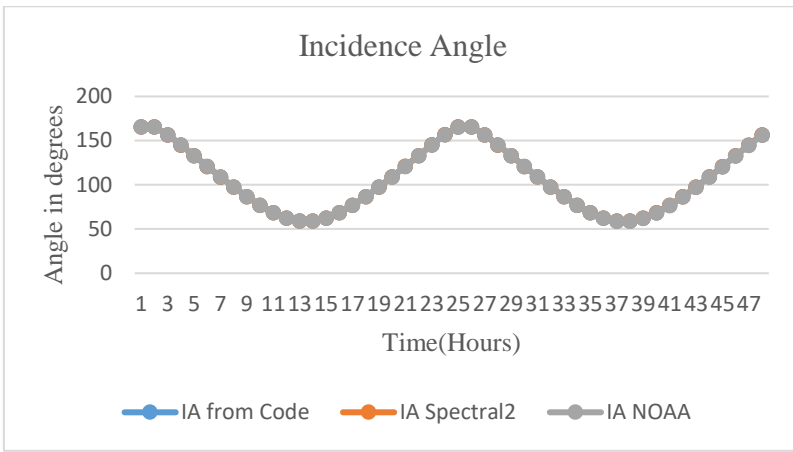


Figure 67: An example validating the incidence angle for UK (period of 48 hours)

In order to observe the differences in the results from the three methods used to generate the incidence angle is represented in the Table 5, as these differences are too small to show variation in a graph.

Table 5: Incidence Angle comparison

Time (hour)	IA from Code	IA Spectral2	IA NOAA
10:00	86.65	86.65	86.71
11:00	76.88	76.88	76.92
12:00	68.61	68.61	68.63
13:00	62.49	62.49	62.47
14:00	59.21	59.21	59.15
15:00	59.23	59.23	59.13
16:00	62.56	62.56	62.43
17:00	68.72	68.72	68.55
18:00	77.01	77.01	76.82

The incidence angle is limited to sunrise and sunset hours only (less than 90°), as incidence angles more than 90° indicate that the sun is behind the panel (Duffie and Beckman, 2013). This issue can be solved by limiting the hour angles at sunrise and sunset hours only which has been integrated into the model. Now the radiation is absorbed, transmitted and reflected as soon as it strikes the surface. Polarised and unpolarised radiation occurs on account of the

smoothness and material of the surface on which the radiation is incident. Given that the incidence angle is used to find the transmittance of the layers affecting the incoming radiation. The calculation of transmittance through a multiple layer node especially for a PV/T model is slightly complicated. In a steady/dynamic system the estimates consider the multiple reflection and radiations including transmission losses after the light ray falls through the layer of glass. Unpolarised radiation passes through from glass medium 1 and reaches PV medium 2 through EVA layer/air layer depending on the type of PV/T model. The low iron content glass used here is smooth and does not polarise radiation, but other partially transparent materials used in the PV/T unit can polarise due to uneven surface difference. The emissivity factor which is also taken as the correction factor determines the amount of infrared radiation that enters the module, of which glass is not a very good transmitter. Radiation energy is passed on to the PV plate through the glass which causes reflectance losses as well as absorptance losses. Now, this incident radiation is polarised and hence, the perpendicular and parallel components of reflectance, transmittance and absorptance are calculated as shown in the following equations. And finally, as the PV plate is partially transparent some radiation and reaches absorber through the EVA which is assumed to be negligible and not useful for thermal radiation estimation.

The first interaction which is at glass then at the PV and EVA layer, the transmittance-absorptance product of shortwave radiations is derived as follows (Duffie and Beckman, 2013). At the first interaction of the light ray at the glass medium, the following unpolarised equations are used. n_{air} and n_{gl} represents the refractive index of air and glass respectively. θ_1 and θ_2 are the incident and refracted angle. This is used to find the refracted angle at the glass-PV layer. The reflectance p , transmission t and absorptance α components in parallel and perpendicular are calculated to obtain the transmittance-absorptance ($\tau\alpha$) product that considers all the three components mentioned. The ' $\tau\alpha$ ' factor is the transmittance-absorptance product considering only absorption losses.

$$\theta_2 = \text{Refract} * \sin^{-1}(\sin(\theta_1) / \text{Refract}) \quad (4-7)$$

$$\tau u \alpha = (e^{-k * d / \cos(\theta_2)}) \quad (4-8)$$

$$r_{per} = (\sin(\theta_2 - \theta_1) / \sin(\theta_2 + \theta_1))^2 \quad (4-9)$$

$$t_{per} = (t_{ua} * (1 - r_{per})^2) / (1 - (r_{per} * \tau u \alpha)^2) \quad (4-10)$$

$$\rho_{per} = r_{per} * (1 + t_{per} * \tau u \alpha) \quad (4-11)$$

$$t = (t_{par} + t_{per}) / 2 \quad (4-12)$$

$$p = (\rho_{par} + \rho_{per}) / 2 \quad (4-13)$$

$$1 = \alpha + t + p \quad (4-14)$$

The transmittance, reflectance and absorptance for polarized calculation is required particularly when there are more than two types of different layers (Glass and PV) an extra layer of calculation is required. This is used for calculating the PV cell temperature that is generated at ambient conditions for the three case studies. (Skoplaki and Palyvos, 2009)

At the interaction at glass and PV layer, the polarized radiation values are derived as follows

$$t = 0.5 * [(t_{par1} * t_{par} / (1 - (\rho_{par1} * \rho_{par}))) + (t_{per1} * t_{per} / (1 - (\rho_{per1} * \rho_{per})))] \quad (4-15)$$

$$p = 0.5 * [(\rho_{par} + (t * \rho_{par1} * t_{par} / t_{par1})) + (\rho_{per} + (t * \rho_{per1} * t_{per} / t_{per1}))] \quad (4-16)$$

$$\tau \alpha = t * a / (1 - (1 - a) * p) \quad (4-17)$$

Various software like TRNSYS, Vela Solaris Polysun, PVsyst and Homer assumes that the transmittance-absorptance is unvarying and takes the value of 0.9 as this value is said to be having very little to no effect on the contribution to the temperature of the module. Since the model used here is of a completely different configuration from the general PV/T system, this factor has been modelled and integrated according to the weather factors at each location to reduce uncertainty errors. The input parameters (Irradiation, Temperature, Wind,

transmittance-absorptance product) are either fixed or simulated for monthly values (or default system that does not simulate PV/T). TRNSYS simulates for hourly basis, however not all parameters are continuously changing. A comparison of these differences is shown in the Table 6. RET SCREEN uses macro in excel inputs.

Table 6: Comparison of various software that include PV/T modelling

<i>Software</i>	<i>TRNSYS</i>	<i>Polysun</i>	<i>Code</i>	<i>Pvsyst</i>	<i>Homer(no pv/t)</i>
Cell temperature	NOCT initial and iterative	N/a	NOCT initial and then iterated	Faiman module temperature model.	NOCT
Diode circuit	5 parameter model	N/a	5 parameter model de soto model	5 parameter one diode model	5 parameter model
Diffuse model	Erbs	N/a	New diffuse model	Erbs	Erbs
Tilted radiation	HDKR/perez	N/a	HDKR and perez	HDKR	HDKR/perez
Version	Demo(limited to 5 components)	Design for application only (demo)	Full-version matlab (programmable to app)	Full-version	Demo(feasibility)
$\tau\alpha$	0.9	N/A	Variable with input	0.9	0.9

In a study by Martin and Ruiz (Martin and Ruiz, 2001), the transmittance, reflectance and absorptance is centred around the angular losses which can be calculated for varying layers on the module. This has also been validated along with the values generated using the simple new model proposed here(King et al., 2004). Angular losses reflect the influence by the

location, tilt angle and the amount of superficial dust on the panel. The short circuit current (I_{sc}) at various incidence angles can be corrected for the angular losses (correcting factors are F_B , F_D and F_G) as follows. ID , IB and IG are the DR, BR, and GGR at the appropriate tilted angle.

$$I_{sc} = \frac{\bar{I}_{sc}}{G} \left\{ \begin{array}{l} IB \cos \alpha [1 - F_B(\beta)] \\ + ID \left(\frac{1 + \cos \beta}{2} \right) [1 - F_D \beta] \\ + IG \left(\frac{1 - \cos \beta}{2} \right) [1 - F_G \beta] \end{array} \right\} \quad (4-18)$$

Using Martin's fit, angle of incidence versus reflectance in air/glass, air glass/Si and air/glass/EVA/Si are computed and validated as shown:

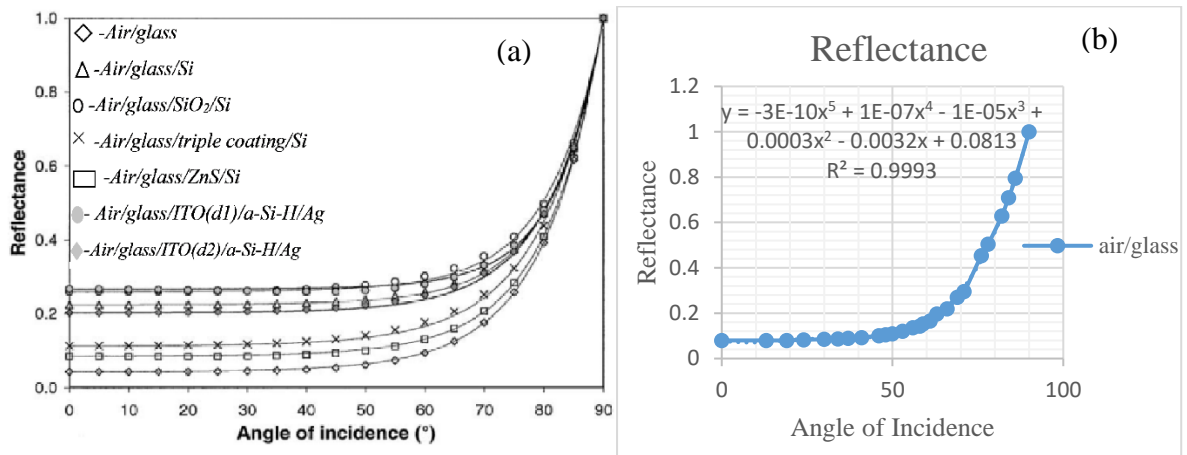


Figure 68: (a) Reflectance at various interactions of layers(Martin and Ruiz, 2001) (b) Code generated reflectance

The Zinc Sulphide coating has the lowest reflectance apart from the simple air/glass layer as seen in Figure 68.

It is to be mentioned that the above equations are only applicable to beam radiation. Diffuse radiations require more calculations as described in Duffie and Beckman. The correction factors are also applied to the irradiation for beam, diffuse and ground radiation for a tilted surface.

In order to understand the amount of radiation falling on the glass it is required to decompose the given radiation into beam, diffuse and ground radiation. On clear sky day, the calculation of clearness index K_t is calculated as

$$K_t = \frac{G}{G_o} \quad (4-19)$$

For a tilted surface, Erbs decomposition model is the easiest and basic model. There are various other models that generate the decomposed radiation. However, Erbs model can be tricky at lower radiations (Martín and Ruiz, 2002, Tsirakoglou, 2011, Mubarak et al., 2017). According to various studies, Reindal 2 model has the most accurate model. This is calculated as follows

$$\left. \begin{array}{l} K_t > 0 + K_t \leq 0.3 \\ k_{dr} = 0.020 - 0.254 * K_t + 0.0123 * \cos(z) \\ \text{When} \\ K_t > 0.3 + K_t \leq 0.78 \\ k_{dr} = 1.400 - 1.749 * K_t + 0.177 * \cos(z) \\ \text{When} \\ K_t > 0.78 + K_t \leq 1 \\ k_{dr} = 0.486 * K_t - 0.182 * \cos(z) \end{array} \right\} \quad (4-20)$$

However, the Reindal 2 fit (k_{rf}) is fitted by a modified method by the model to derive the following equation to fix the smoothness of curve, where a, b and c are coefficients calculated from correlation of the fit

$$k_{rf} = a * K_t^b + c \quad (4-21)$$

Utilising this fit, diffuse radiation can be calculated on horizontal surface of the PV. A transposition model like HDKR (Hay, Davies, Klucher, Reindl) model or Perez model is calculated the radiation on tilted surface of the PV/T module. The HDKR model is suggested when the surface is sloped toward the equator or when the azimuth angle is 0° and Perez model is used when the azimuth varies from 0° . This is automatically chosen and built into the code. However the only issue with Perez model is that an over estimation of radiation can be observed (Duffie and Beckman, 2013). The differences in beam and diffuse radiation is shown in Figure 69.

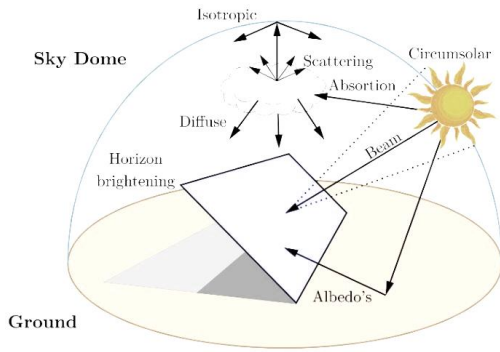


Figure 69: Radiation at tilted surface of the PV/T (Simón-Martín et al., 2016)

The beam diffuse and ground radiation can be calculated using the models described. Diffuse radiation can be obtained from incidence angle modifier ($K\theta$). The absorbed radiation (S) on the tilted surface for the Perez model is given as

$$S = IB * Rbr * \tau\alpha + ID * \tau\alpha_d * (1 + \cos(\beta)) / 2 + \rho_g * (IB + ID) * \tau\alpha_g * (1 - \cos(\beta)) / 2 \quad (4-22)$$

Where β is the slope of the collector and Rbr is the average ratio of the daily BR on the tilted surface to that on a horizontal surface in a time period of a month while $\tau\alpha_d$ and $\tau\alpha_g$ are the transmittance absorptance product of the IB and IG in W/m^2 . Equation 4-23 states that the sum of all the radiation generates the total radiation incident on the surface.

$$Beam + Diffuse + Ground = Total \quad (4-23)$$

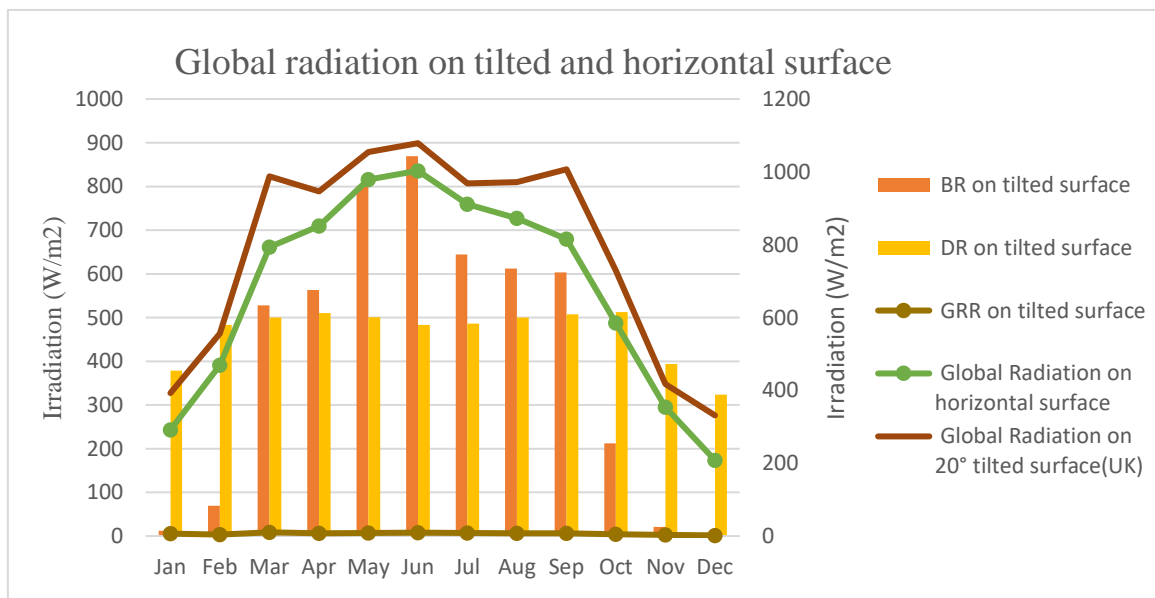


Figure 70: Beam and Diffuse Radiation from Sky modelling using the new method for Newcastle, UK. The total radiation on any surface installed in Newcastle University, in this case, at the Urban Science Building (USB) is calculated as in Figure 70, generating the highest irradiation at

900W/m². This is used for further calculations and deductions for the case study considered. This process can be repeated for other case studies as well with the basic weather conditions as input.

4.2.2 PV Model

The total radiation falling on the surface of the PV/T has been generated. This data is used to predict the output power generated at the PV module, which is used in designing and to assist in understanding the exergy of the system. In order to find the output for each location, PV and thermal output is modelled and calculated separately as PV and solar thermal collector and validated with the system in Lisbon that has discrete PV and Collector units. This method and concept are further extended to the steady state and dynamic modelling method for simulating the complete PV/T unit. It can also provide an insight into the operation of individual units at the locations of the case studies selected.

A single PV cell generates anywhere from 6Wh-10Wh of energy depending on the type of cell. The effective output of the solar cell is dependent on the manufacturer and the ratings defined at STC and thus that determines the design of the system. They can be summarised as

- a) Short-circuit Current (I_{SC})
- b) Open-circuit voltage (V_{OC})
- c) Maximum Power-point (P_M)
- d) Current at P_M (I_M)
- e) Voltage at P_M (V_M)
- f) Fill-factor (FF)
- g) Efficiency

The voltage from the PV module is determined by the number of solar cells and the current depends on the size of the cells and their conversion factor. Thus, the electricity generated is affected by the following parameters.

1. The conversion efficiency
2. Incoming radiation on the surface
3. Area of solar cell
4. Incidence angle of the radiation and
5. Operating temperature

The atmospheric air-mass is taken as the standard 1.5 and under $1000\text{W}/\text{m}^2$ at optimum tilt angles, for a commercial PV cell the current per unit area or current density is in the range of $30\text{ mA}/\text{cm}^2$ to $36\text{ mA}/\text{cm}^2$. The efficiency of PV cell and PV module are different and depends on the type of PV cell chosen. A p-Si cell is used in this research. PV modules output is affected by the packing density and fill factor of the cells. c-Si solar cells with area of 100cm^2 generates an electric current of around 3.5A from the module, while p-Si have generally a larger area of silicon PV cell and generated current of around 4A , but have a lower current density (Alam and Alouani, 2010). The output current from the PV is not affected by the temperature as much the voltage is, but the current quite largely depends on the tilt angle of the module ('Progress on Flat-Plate Water Based of Photovoltaic Thermal (Pv/T) System: A Review,' 2014).

Assuming that the PV cells have no dusting or shading effect and thus when working together in a module, it is said that the module IV characteristics resemble the individual solar cell and thus produces a multiple of the voltage and current depending on the number of cells (Calise et al., 2012). Taking a single diode equivalent for the solar cell as in Figure 71 the equation for the circuit becomes as follows where it is necessary to find the shunt and series resistance using an iterative method. Using Kirchoff's law to solve the equivalent circuit of a solar cell, the current-voltage relationship for a module or array can be extended from the single cell current and voltage relationship. The single cell area of the considered unit is 125 Sq.mm , consisting of 60 cells.

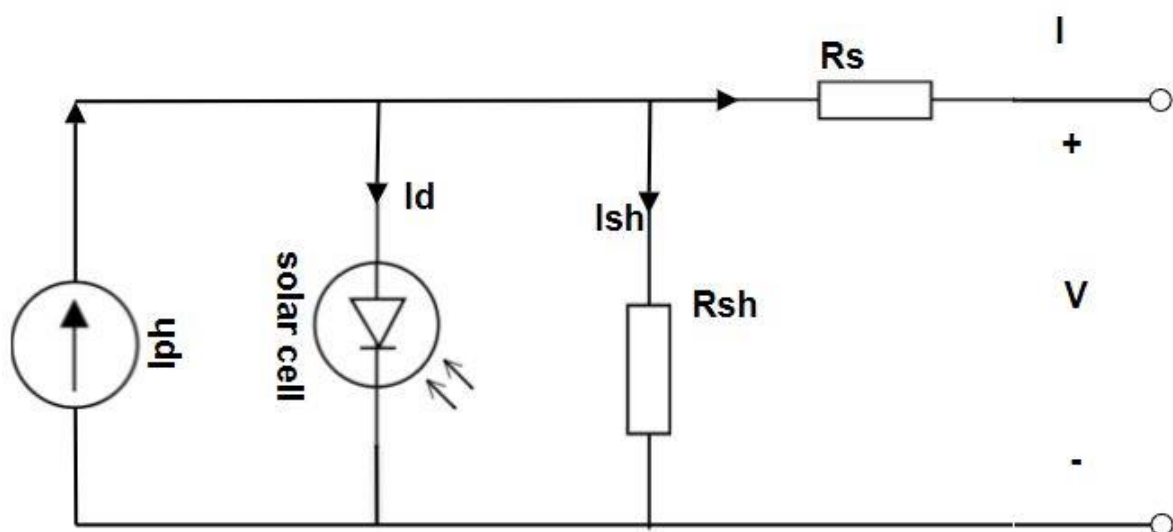


Figure 71: Single diode equivalent of PV cell

$$I = I_{ph} - I_d - I_{sh} \quad (4-24)$$

Where I_{ph} is the photo-current in amperes, which depends on the incoming radiation

I_d - is the diode saturation current (amperes)

I_{sh} -shunt current (amperes) and I is the total current generated by the PV cell in amperes.

When N_S is the number of cells in series in a module, the IV equation is expressed as

$$I_{mod} = I_{ph} - I_0 \left[e^{\left(\frac{q(V_{mod} + I_{mod} N_S R_s)}{N_S n k T_{cell}} \right)} - 1 \right] - \frac{V_{mod} + I_{mod} N_S R_s}{N_S R_{sh}} \quad (4-25)$$

Where R_s and R_{sh} is the series and shunt resistance of the circuit.

If there are N_m modules in series then $N_S = N_m * N_C$ (N_C is the number of series cells in a single module) and N_p is the number of modules in parallel. Hence for an array of PV/T modules. (n - ideality factor and k -Boltzmann's constant, T_{cell} -cell temperature and "ref" refers to parameters at the STC conditions)

$$I_A = N_p I_{ph} - N_p I_0 \left[\exp \left(\frac{q \left(V_A + I_A \frac{N_S}{N_p} R_s \right)}{N_S n k T_{cell}} \right) - 1 \right] - \frac{V_A + I_A \frac{N_S}{N_p} R_s}{\frac{N_S}{N_p} R_{sh}} \quad (4-26)$$

As

$$I_{ph} = I_{phref} \left(\frac{G}{G_{ref}} \right) [1 + \alpha_r^{sc} (T_{cell} - T_{ref})] \quad (4-27)$$

where α_r^{sc} is the relative temperature of short-circuit current. R_s is the same as R_{sref} ($R_s = R_{sref}$)

$$R_{sh} = R_{shref} * G / G_{ref}$$

(4-28)

$$I_0 = I_{0ref} \left[\frac{T_{cell}}{T_{ref}} \right]^3 e^{\left[\frac{E_{gref}}{kT_{ref}} - \frac{E_g}{kT_{cell}} \right]} \quad (4-29)$$

Length of PV panel=783.4mm, width of PV panel=1576.4mm, where E_{gref} is the bandgap energy in eV.

$$E_g = 1.16 - 7.02 \times 10^{-4} \left(\frac{T_{cell}^2}{T_{cell} - 1108} \right) \quad (4-30)$$

And T_{cell} is predicted by using the NOCT (Nominal operating cell temperature) which ranges from 45-48°C for a standard PV system (used in HOMER and PV syst).

$$T_{cell} = T_a + \left(\frac{NOCT - 20^\circ C}{0.8} \right) G \quad (4-31)$$

Homer calculates T_{cell} as equation 4-32.

$$\frac{\tau\alpha}{U_L} = \frac{T_{NOCT} - T_{a,NOCT}}{G_{NOCT}} \quad (4-32)$$

$$T_c = T_{NOCT} - T_{a,NOCT} \left[\frac{G}{G_{NOCT}} \right] \left[1 - \frac{\eta_e}{\tau\alpha} \right] + T_a \quad (4-33)$$

The T_{NOCT} cell temperature at NOCT and $T_{a,NOCT}$ is the ambient temperature at NOCT (800W/m² at 20°C and 45° tilt angle) the IAM model used here is from the Sandia report, T_{cell} is also calculated according to the Sandia Report (King et al., 2004) as

$$T_{cell} = T_m + \frac{IT}{G_{ref}} \Delta T \quad (4-34)$$

Where the T_m is back surface temperature of the module. IT is the irradiation received by the module, G_{ref} is the reference radiation at 1000W/m². ΔT is the difference of cell temperature and back surface temperature, which is generally 2-3°C for an open rack of glass/cell/Polymer type configuration which can be referenced from Table 7. T_m is calculated as in equation 4-35.

$$T_m = IT.(e^{a+Wb}) + Ta \quad (4-35)$$

Where a and b are coefficients described as below. And W is the wind velocity and Ta is the ambient temperature.

Table 7: Empirical values for the coefficients of Back surface module (King et. al., 2004)

Module Type	Mount	a	b	ΔT (°C)
Glass/cell/glass	Open rack	-3.47	-.0594	3
Glass/cell/glass	Close roof mount	-2.98	-.0471	1
Glass/cell/polymer sheet	Open rack	-3.56	-.0750	3
Glass/cell/polymer sheet	Insulated back	-2.81	-.0455	0
Polymer/thin-film/steel	Open rack	-3.58	-.113	3
22X Linear Concentrator	Tracker	-3.23	-.130	13

Using the five-parameter model and three conditions of the PV cell at open-circuit, short-circuit and maximum power point conditions, the IV curve at STC or any condition of the day can be solved for. It is to be noted that only ambient conditions and radiation is considered here. In dynamic state an additional input of the wind velocity, transmission-absorption product as well as incidence angles at a tilt angle is defined into consideration. An iterative solve method is used in MATLAB to solve and find the IV curve. It is also noted that for an ideal circuit, $R_s=0$ and $R_{sh}=+\infty$ and through iterative process or IM, R_s and R_{sh} was found as 0.4146Ω and 664.44226Ω respectively of the PV/T system at STC. Again, for the case study in Lisbon, Length of PV panel=783.4mm, width of PV panel=1576.4mm (removed 11.3 *2 from main dimensions)

Actual Area of PV panel=1.23495176 m² for one module.

The performance of the collector at 1000W/m² and 800W/m² at 25 °C is shown in the IV curve as in Figure 72.

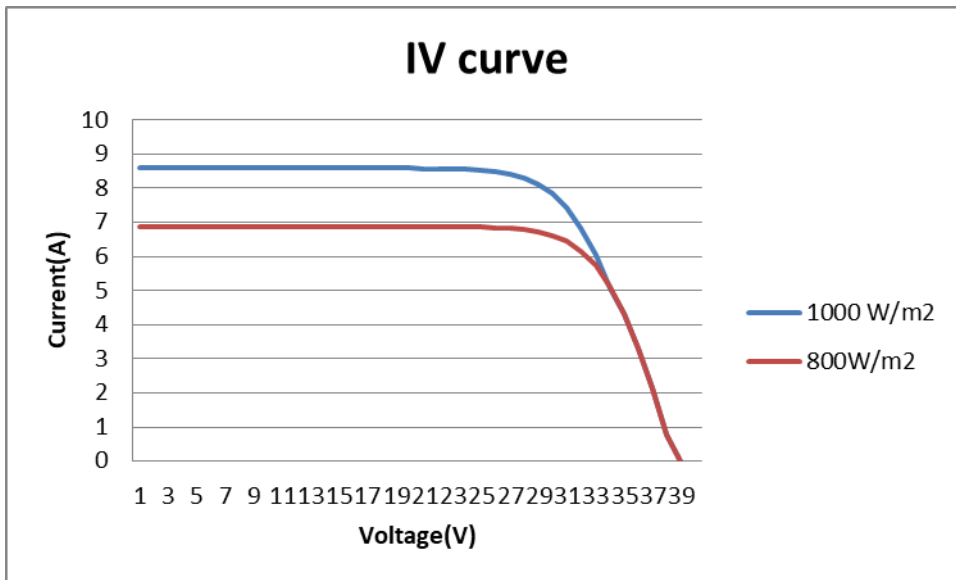


Figure 72: IV curve at STC and NOCT radiations

To differentiate between cell and module efficiency is done by a parameter called packing factor. (Tsai, 2010, Huld et al., 2011, Koch-Ciobotaru et al., 2012, Ossenbrink et al., 2012)

$$\text{Packing Factor } \beta_c = \frac{\text{area of all solar cells } A_{ac}}{\text{area of PV module } A_m} \quad (4-36)$$

$$\text{Cell Efficiency } \eta_c = \frac{\text{Module Efficiency } \eta_m}{\text{Packing Factor } \beta_c} \quad (4-37)$$

$$\text{Fillfactor}_{STC} = \frac{\eta_m * A_m * I_{P(STC)}}{100 * I_{sc} * V_{oc}} \quad (4-38)$$

Various parameters can be varied at STC to test the performance of the system. It can be noted that the variations are between ambient temperature and radiations or conditions at STC. In dynamic systems, the wind velocity, incidence angle and transmission-absorption product as affecting additional coefficients as well can be included (Koch-Ciobotaru et al., 2012, Ossenbrink et al., 2012, Pearsall and Gottschalg, 2012, Schwingshackl et al., 2013, Kirn et al., 2015, Burton et al., 2016, Kanyarusoke et al., 2016, Lave, 2016).

The actual electrical efficiency can be calculated with respect to the expected energy generated by observing the IV curve behaviour. This effective energy was without the presence of a collector. To obtain the thermal energy of a PV/T unit, the PV system in configuration in the modelling is taken as a two-cover system, where the transmittance-absorptance product changes due to the presence of two layers. This is modelled and modified

from an extended series from Duffie and Beckman(Duffie and Beckman, 2013) as explained in the following section.

4.2.3 Solar Collector Model

The most significant piece of the FPC is the plate comprised of either copper, aluminum or steel incorporated with the pipe or pipe. The fluid or air goes through the pipe/pipe that is in thermal contact with the plate for moving the heat from the absorber to the liquid/gas. The capacity of the plate is to assimilate the most extreme conceivable sunlight based radiation occurrence on it through the coating for reducing heat losses to the air from the top surface. It should be mentioned that the regions of the plate and glass spread are the equivalent on account of FPC (for example $A_c = A_g$). The covering of the plate ought to be with the end goal that it has high absorptivity and poor emissivity for the required temperature run. Specific surfaces are especially significant when the gatherer surface temperature is a lot higher than the surrounding air temperature. The base and sides of the gatherer are secured with protection to decrease the base/side conductive thermal losses. A distinction is drawn between the consumed sunlight-based radiation, Q_u , and the thermal losses. The instantaneous thermal efficiency is additionally determined from Q_u . U_L is the overall heat transfer coefficient and q_b is the heat energy absorbed..

It is given by,

$$Q_u = A_c \{q_b - U_L(T_b - T_a)\} \quad (4-39)$$

$$q_b = (\tau\alpha)IT \quad (4-40)$$

$$\eta = \frac{Q_u}{A_c.IT} \quad (4-41)$$

The overall efficiency of an FPC with respect to time given as

$$\eta_{overall} = \frac{\int Q_u.dt}{A_c \int IT(t).dt} \quad (4-42)$$

The FPC efficiency factor, F' , is defined as the ratio of actual rate of useful heat collection to the rate of useful heat collection rate when the collector absorbing plate (T_b) is placed at the local fluid temperature (T_f),

$$\left. \begin{aligned} F' &= \frac{Q_{useful}}{Q_u} \\ \text{when } (T_b = T_f) \\ Q_{useful} &= F' \cdot Q_u \end{aligned} \right] \quad (4-43)$$

The outlet fluid temperature in the direction of the flow at full length of the tube ($x = \text{Length of the tube}$) is described in terms of all the above calculated factors as

$$T_{f_{outlet}} = T_f(x=L) = \left[\left(\frac{qb}{UL} \right) + T_a \right] + [T_{fi} - T_a - \left(\frac{qb}{UL} \right)] e^{\left[\frac{-Ac \cdot UL \cdot F'}{m \cdot C_f} \right]} \quad (4-44)$$

The heat removal factor for forced circulation is shown as

$$FR = \frac{m \cdot C_f \cdot (T_{f_{outlet}} - T_{fi})}{Ac \cdot [qb - UL(T_{fi} - T_a)]} \quad (4-45)$$

It must be noted that since the PV/T collector system is generally connected as a system of modules connected in series or parallel. The PV/T modules are connected in series for increasing the thermal energy and connected in parallel to improve the electric efficiency. Now the outlet fluid temperature from a series connection can also be redefined as T_{fon} for a system of 'n' collectors. For a collector system T_{fon} is expressed as follows.

$$T_{fon} = \left(\frac{qb}{UL} + T_a \right) \left\{ 1 - e^{\left(\frac{-nAc \cdot UL \cdot F'}{m \cdot C_f} \right)} \right\} + T_{fi} \cdot e^{\left(\frac{-nAc \cdot UL \cdot F'}{m \cdot C_f} \right)} \quad (4-46)$$

$$Q_{un} = m \cdot C_f \cdot (T_{fon} - T_{fi}) \quad (4-47)$$

where Q_{un} is the useful energy of n collectors.

4.2.4 PV/T Collectors

A typical flat plate PV/T collector with a black absorber has an overall efficiency of 75% (Kumar and Mullick, 2010). However, the thermal losses increase when the operating temperature rises. The performance efficiency steps downwards from maximum efficiency where there is no relative temperature difference between adjacent layers. Stagnation temperature is the highest the PV/T fluid can reach when the generated heat is not removed through the closed loop. On reaching this temperature, the absorbed radiation is lost as thermal losses and the efficiency becomes zero as there is no useful thermal gain. Each stagnation temperature range is varied according to the type of manufacturer (Kumar and

Mullick, 2012, Tian and Zhao, 2013, Wojcicki, 2015, Hashim et al., 2016, Ramos et al., 2017, Yousef Nezhad and Hoseinzadeh, 2017, Aleksiejuk et al., 2018, Ampuño et al., 2018, Raj and Subudhi, 2018). The model used in this research has a stagnation temperature is rated at 79°C. Selective absorbers are shown to improve efficiency with maximum being 80% and display lower loss coefficients a_1 and a_2 , especially in central Europe, with stagnation that can reach up to 220°C. The two parameters that can determine such a change is collector area and the solar radiation. Temperature plays a significant role in the performance of the PV module and the initial cell temperature is calculated from the Sandia report where the coefficients are chosen depending on whether the PV/T module is integrated on the roof, on the ground or free standing or sloped(Nordmann and Clavadetscher, 2003, Sohel et al., 2014).

For the area of the collector there are three area dimensions which is usually defined on the data sheet of the system, which are gross collector area (entire area including frame), absorber area and aperture area (area through which radiation can enter) which is simply obtained from the geometry of the module and can be modified according to the area specified at the beginning of the model (Ziyadanogullari et al., 2018, Abdalla et al., 2019, Carmona and Palacio, 2019, Li et al., 2019, Sakhaei and Valipour, 2019).

In order to calculate the heat removed from the PV model, it is required to calculate the heat removal factor (FR) that depends on the geometry of the module (Tian and Zhao, 2013, Mongibello et al., 2014, Herrero López et al., 2015, Ramos et al., 2017, Aleksiejuk et al., 2018). In this case of PV/T the following equations are followed. The efficiency factors are calculated according to the geometry of the system selected, F' and F'' are iteratively calculated from equation 4-48 to 4-53.

$$F' = \frac{1}{\frac{WUL}{\pi Dhuf} + \frac{D}{W} + \frac{1}{\frac{WUL}{Cu_bond} + \frac{W}{(W-D)F}}} \quad (4-48)$$

$$F'' = \frac{mCp}{AcULF'} [1 - \exp(-\frac{mCp}{AcULF'})] \quad (4-49)$$

$$F = \frac{\text{Tanh } m(W-D)/2}{m(W-D)/2} \quad (4-50)$$

$$FR = F' F'' \quad (4-51)$$

$$(Atnload)UL = \frac{TpNOCT - TaNOCT}{GNOCT(\tau\alpha)} \quad (4-52)$$

$$Q_{heat} = AcFR[Gs - (UL(Tin - Ta))] \quad (4-53)$$

The thermal energy is removed by the HTF (heat transfer fluid) should be utilised effectively. This implies the need for the HTF system to be very closely bonded to the absorber (Faiman, 2008, Strobach et al., 2013). This parameter is defined as the heat removal factor which is dependent on the geometry, the fluid capacity of the system, mass flow rate and the heat transfer coefficients (Alam and Alouani, 2010, Nuru et al., 2012, Saleh, 2012).

The thermal efficiency is then defined in terms of the heat removal factor, T_{in} (inlet fluid temperature and heat loss coefficient as equation 4-54.

$$\eta_{th} = FR(\tau\alpha) - FR * UL \left(\frac{T_{in} - T_a}{G} \right) \quad (4-54)$$

A steady state analysis can be found if FR (heat removal factor), $\tau\alpha$ (transmittance-absorptance product), UL (overall heat loss coefficient W/m^2K) and G (radiation incident on the surface W/m^2) are considered as constant for a given flow rate. It is quite evident that efficiency is directly affected the solar radiation, fluid flow rate and ambient temperature. To find out total UL coefficient, it is known that the heat transfer happens through conduction, convection or radiation or a combination of them at different layers. Some of the main assumptions made here are as follows.

1. The heat transportation normal to the plane of the collector is assumed to be independent of heat transfer in any other direction in the collector plane.
2. The material properties are symmetrical
3. The components are of lower thickness and so the temperature differences are negligible through the layers.
4. The rear and the front of the PV/T collector have the same ambient temperature
5. All the fluid transfer is by the absorber.

There can be mismatch of output when the inlet fluid temperature is very low with low fluid rates. It should be observed that the efficiency factor should be nearly towards one while conductive and radiative losses should be very low for the system to be optimised. This type of analysis has various constraints which will be rectified using dynamic modelling.

If the outlet temperature needed according to the demand is known, mean plate temperature will generate the inlet temperature. In order to find the mean plate temperature, the heat transfer coefficient can be obtained in terms of Nusslet number (Nu) and forced convection in pipes.

$$h_{fi} = Nu * \lambda_f / D_i \quad (4-55)$$

where D_i is the inner diameter of the tube and λ_f - thermal conductivity of the fluid used.

The Nusslet number for short pipes depends on whether the Reynolds number has a laminar (when $Re < 2100$ or turbulent flow (when $Re > 2300$) and is defined by the equation . N is the number of covers on the collector, while ‘ e_p ’ and ‘ e_g ’ are the emissivity of the PV and glass layer respectively. ‘ h_f ’ is defined as the fluid heat transfer coefficient while

$$Nu = 4.4 + \frac{0.00172 * (Re * Pr * D_i / l_{tube})^{1.66}}{(1 + 0.00281 * (Re * Pr * D_i / l_{tube})^{1.29})} \quad (4-56)$$

$$UL = (N / (C / T_m * ((T_m - T_a) / (N + e_f))^{-e} + 1 / h_w))^{-1} + \left(\frac{S * (T_m + T_a) * (T_m^2 + T_a^2)}{(e_p + 0.00591 * N * h_w)^{-1}} \right) / (2 * N + e_f - 1 + 0.133 * e_p) / e_g - N \quad (4-57)$$

Where $e_f = (1 + 0.089h_f - 0.1166h_f e_p)(1 + 0.07866N)$; $C = 520(1 - 0.000051)$ when angle of tilt is less than 70° ; $e = 0.430(1 - 100/T_m)$ and ‘ h_w ’ is the wind heat transfer coefficient which can be referenced from Duffie and the Beckman(Duffie and Beckman, 2005).

The heat loss factor UL is obtained to find the mean plate temperature using at least 1000 iterations. This is further solved using IM to find the heat removal factor and thus the efficiency.

4.3 Steady State Modelling for PV/T

A steady state analysis gives an excellent comparison for finding out the performance based on specific parameters. It allows to find the relation between behavioural changes of the model according to different conditions and this defines the system in such a way that a design relation among the different components can be characterised. A preliminary steady state analysis using ScenoCalc was performed for an initial look at the thermal yield of the system at an average optimal angle of 35° for all three locations. This is the standard calculator used by the IEC (international European commission) standard for testing PV/T and solar thermal collector output with effects of wind, ambient temperature and solar radiation.

The balance equation of the PV/T is formed using the following assumptions

- 1D study is used to analyse PV/T in steady state model
- The heat capacity value is taken to be of the storage tank
- The temperature in the tank is not saturated due to forced mode of operation
- It is done in SS method

It is also noted that the number of collectors in series or parallel is mentioned to be input into the program that states, “Enter the number of collectors in series” and “Enter the number of collectors in parallel”.

The major assumptions needed to solve these equations take the smallest time period dt of 0.001 with constant parameter values in order to avoid the unstable condition. The angle of incidence taken for standard condition calculations is at noon.

The major design parameters used in this model is given below in Figure 73. The number of series collectors is 6. And parallel value collector is one.

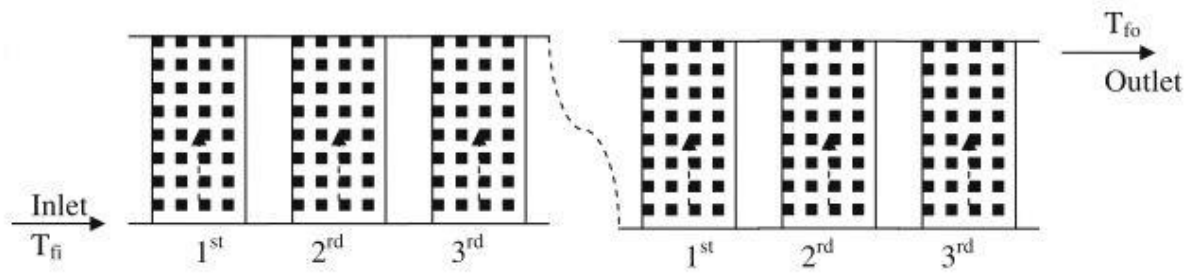


Figure 73: Series connection for modelling in steady state (Kalogirou, 2009b, Kalogirou, 2009d)

Table 8: Design Parameters of the steady state system

<i>Variable</i>	<i>Definition</i>	<i>Values</i>
A_c	<i>Area of collector</i>	$1.06m^2$
A_{PV}	<i>Area of PV</i>	$1.55 m^2$
C_f	<i>Specific heat capacity of fluid</i>	$4190 J/kg K$
D_{ext}	<i>Diameter of the external tube</i>	$0.008 m$
D_i	<i>Diameter of the internal tube</i>	$0.007m$
m	<i>Mass flow rate</i>	$0.025kg/sec$
m_f	<i>Mass of fluid used</i>	$200kg$
A_b	<i>Area of absorber</i>	$1.55 m^2$
m_g	<i>Mass density of the glass ($Kg.m^{-3}$)</i>	$2200 Kg.m^{-3}$

C_g	<i>Specific heat capacity of the glass (J/K.m)</i>	810 J/K.m
λ_g	<i>Thermal conductivity of the glass (W/K.m)</i>	1.05
m_p	<i>Mass density of the PV(Kg.m⁻³)</i>	2330 Kg.m ⁻³
C_p	<i>Specific heat capacity of the PV (J/K.m)</i>	700 J/K.m
λ_p	<i>Thermal conductivity of the PV (W/K.m)</i>	148
λ_{eva}	<i>Thermal conductivity of the eva layer (W/K.m)</i>	0.89
m_{eva}	<i>Mass density of the eva layer (Kg.m⁻³)</i>	2330 Kg.m ⁻³
C_{eva}	<i>Specific heat capacity of the eva layer (J/K.m)</i>	700 J/K.m
m_b	<i>Mass density of the absorber layer (Kg.m⁻³)</i>	2699 Kg.m ⁻³
C_b	<i>Specific heat capacity of the absorber (J/K.m)</i>	897 J/K.m
λ_b	<i>Thermal conductivity of the absorber layer (W/K.m)</i>	380

<i>mu</i>	<i>Mass density of the tubing layer (Kg.m⁻³)</i>	<i>2330 Kg.m⁻³</i>
<i>Cu</i>	<i>Specific heat capacity of the tubing and bond (J/K.m)</i>	<i>897 J/K.m</i>
<i>lu</i>	<i>Thermal conductivity of the tubing layer (W/K.m)</i>	<i>148 W/K.m</i>
<i>mf</i>	<i>Mass density of the fluid (Kg.m⁻³)</i>	<i>1000 Kg.m⁻³</i>
<i>Cf</i>	<i>Specific heat capacity of the fluid (J/Kg.K)</i>	<i>3184 J/Kg.K (with 20% ethyl glycol)</i>
<i>Ci</i>	<i>Specific heat capacity of the insulation (J/Kg.K)</i>	<i>1120 J/Kg.K</i>
<i>liso</i>	<i>Thermal conductivity of the insulation layer (W/K.m)</i>	<i>0.045 W/K.m</i>
<i>miso</i>	<i>Mass density of the insulation layer (Kg.m⁻³)</i>	<i>999.39 Kg.m⁻³</i>
<i>thickp</i>	<i>thickness of PV layer (m)</i>	<i>0.001m</i>
<i>thickeva</i>	<i>thickness of EVA layer (m)</i>	<i>0.0005m</i>
<i>thickb</i>	<i>thickness of absorber layer (m)</i>	<i>0.002m</i>

<i>thickg</i>	<i>thickness of glass layer (m)</i>	<i>0.0032m</i>
<i>thicki</i>	<i>thickness of insulation (m)</i>	<i>0.0188m</i>
<i>thickt</i>	<i>thickness of the tube (m)</i>	<i>0.001 m</i>

The heat loss for the PV/T module in steady-state condition will undergo the following effects.

1. Heat transfer from the PV surface to the inner EVA layer
2. Heat transfer from the EVA to the outer glass layer
3. Heat transfer from the glass layer to the atmosphere

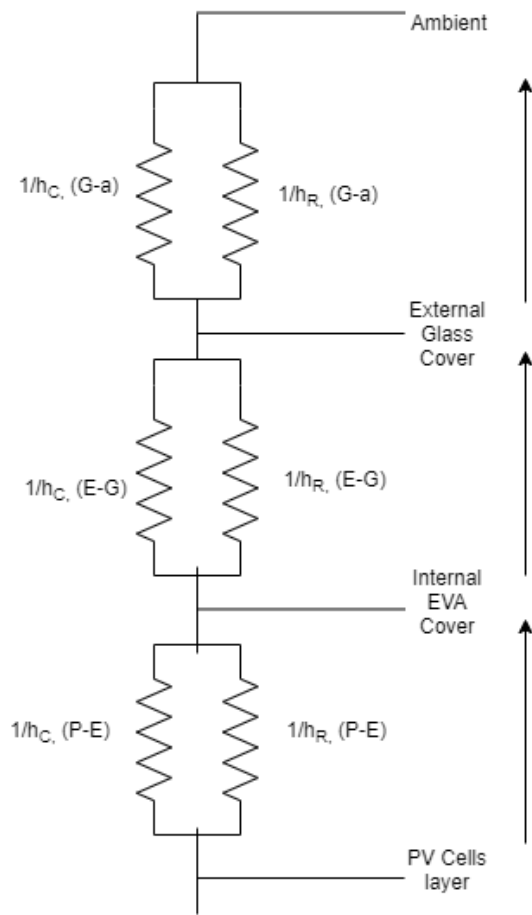


Figure 74: Analogous resistance circuit for PV/T (h_r and h_c are the heat transfer coefficients of radiation and conduction components of each layer)

The resistance circuit PV/T is shown in Figure 74 and each variation is calculated according to the equations from 4-58 to 4-62. From the Figure 74, the overall heat loss transfer coefficient (U_L) can be found by adding all heat transfer coefficients of conduction, radiation and convection of the three sections of glass, EVA and the PV layer. As this model of PV/T has no medium for convection, heat transfer coefficients are generated for conduction and radiation only. The sequence of heat transfer coefficients of conduction are $(1/h_c)$ for the glass to ambient air layer(G-a), internal glass and EVA layer(G-E) and finally the internal EVA and PV layer(P-E) and this also applies for the heat transfer coefficient of radiation $'(1/h_r)'$ for the aforementioned layers. The layer of PV unit is also considered as opaque in this modelling. It is also to be noted that in steady state conditions thermal inertia is ignored.

In order to find out the temperature of the fluid and the temperature of the absorber the following equations from 4-58 are utilised. This utilises the loss coefficient, the transmission absorption coefficient and the heat transfer coefficient to generate the temperature of the cell. The mass flow rate is kept at a constant rate of 0.025kg/s.

If there is more than one collector, say 'N' collectors, they can be either arranged in a series connection for a higher temperature output or in a parallel output for a higher electrical output. If arranged in series, the mass flow rate is same across all the collectors and if arranged in parallel, the outlet temperature is the same for all the collectors. If the collectors are arranged in a mixed array, both these conditions apply according to the number of parallel or series connections. For 'P' parallel connections the MFR is \dot{m}/P . In parallel connection, the system is also referred to as one module. In series connection of a 'S' collectors the outlet fluid of one module becomes the inlet of the next connection in series i.e. $T_{fout}=T_{fin2}$. For the purpose of a simple calculation, the steady state factor is only considered to a system of 6 series collectors.

$$K_o = \left[\frac{AFRUL}{\dot{m}fC_f} \right] \quad (4-58)$$

The useful thermal energy Q_{uth} is calculated according to the heat removal Factor FR and the initial fluid temperature T_{fin} which is also assumed at STC and IM method is used to find the result. $Q_{uth} = \text{Gain factor} - \text{Loss factor}$.

$$Q_{uth,N} = [NAFR(\tau\alpha) \left\{ \frac{1 - (1 - K_o)^N}{NK_o} \right\}] I(t) - [NAFR(UL) \left\{ \frac{1 - (1 - K_o)^N}{NK_o} \right\}] (T_{fin} - T_a) \quad (4-59)$$

$I(t)$ is assumed to be constant at $1000\text{W}/\text{m}^2$ and the average temperature value of the fluid is taken to find out the water temperature in the tank. The final output temperature of the fluid is calculated using the following equation.

$$T_{fout,N} = \left[\frac{(\tau\alpha)I(t)}{UL} + T_a \right] \left[1 - e^{-\frac{NF'AUL}{\dot{m}fC_f}} \right] + T_{fin} \left(e^{-\frac{NF'AUL}{\dot{m}fC_f}} \right) \quad (4-60)$$

The mass flow rate and the design parameters (from Table 8) is recorded at the beginning of the program. The result is the useful energy from all the collectors that are either connected in series or parallel. This can be further calculated to obtain the efficiency of the entire system by extracting the individual component of electricity generated by the PV modules, pump and the storage unit. The power consumed by the pump is manually controlled in 3 levels (36W, 43W and 49W) (A WILO Eco 3C model pump is selected as in LAB and USB) depending on the rate at which heat needs to be removed. In steady state, the value of 49W is taken, to ensure maximum heat removal. The storage capacity is taken to be at 200 litres. The PV temperature is also calculated to observe the difference in the output and the performance. It is calculated using the following formula in 4-61 where 'qb' is the heat absorbed by the PV

unit and 'Tp₀' is the PV temperature at 0°C as the layer after the glass and EVA layer here is the PV module. Thereby PV temperature is defined as

$$T_p = \left[\frac{qb}{UL} + Ta \right] \left[1 - e^{\left(-\frac{AUL}{mCe} t \right)} \right] + T_{p_0} e^{\left(-\frac{AUL}{mCe} t \right)} \quad (4-61)$$

The electrical power generated by the PV modules (Ep) can be calculated from equation 4-62 where 't' is the chosen time period.

$$E_p = \eta_{PV} A_{PV} NI(t) \quad (4-62)$$

The net useful electrical energy is obtained by removing the power consumed by the pump (P_{pump}) as in equation 4-63.

$$Q_{uele} = E_p - P_{pump} \quad (4-63)$$

As this is a type 2 PV/T, the layers between PV and glass does not have an air channel or layer and this eliminates reflective losses to a greater extent. The convective and radiative heat transfer coefficient is defined as 'hc' and 'hr' depending on the layer interaction respectively. The water temperature for the PV/T system can be calculated using the familiarity of solar collector calculation. This has been slightly modified to fit the PV/T model. There have been several models in the past that were developed and investigated. This model aims to achieve a better percentage of accuracy and a universal guide for designing or optimising PV/T systems. The power consumed by the pump is taken to be 43W for this steady state. A flowchart of the process is given in Figure 75.

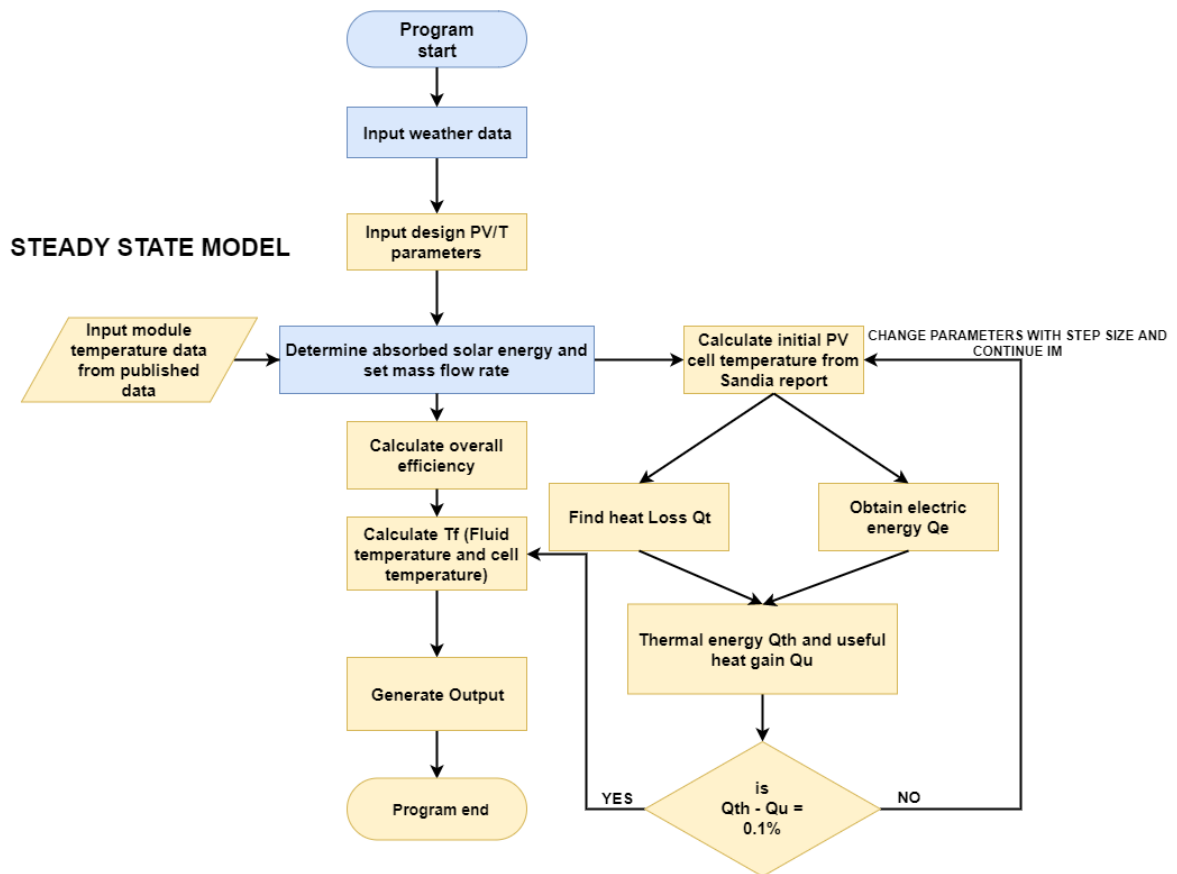


Figure 75:Flow chart of steady state model

The steady state model is developed and the major steps in this process is explained as below:

- The weather data from the weather station or even standard TMY2 data can be accepted into the model. The Global radiation, ambient temperature, cloudy or non-cloudy days depending on the rain is read. If the diffuse radiation is not given, it can be calculated using the most appropriate model decided by the program.
- The design parameters for which the steady state analysis is carried out is defined in this process and this can be manually modified to suit different types of PV/T.
- The absorbed radiation is calculated, and this can be validated using the actual weather data from the USB and published data for verification.
- The initial temperature of the PV cell can be determined from the Sandia temperature model
- The thermal energy and the useful energy are calculated to observe the difference to be at less than 0.0001 tolerance
- Once the overall efficiency can be extracted the fluid temperature can then be formulated to get the desired results.

In order to compare the effects of PV/T systems with existing models, a SCENOCalculator was simulated to obtain the steady state calculations at various locations along with the thermal yield of the systems at different temperatures of cells. Three different locations' (Lisbon, Newcastle and Cochin) resultant thermal yield is shown below in Figure 76, Figure 77 and Figure 78 respectively.

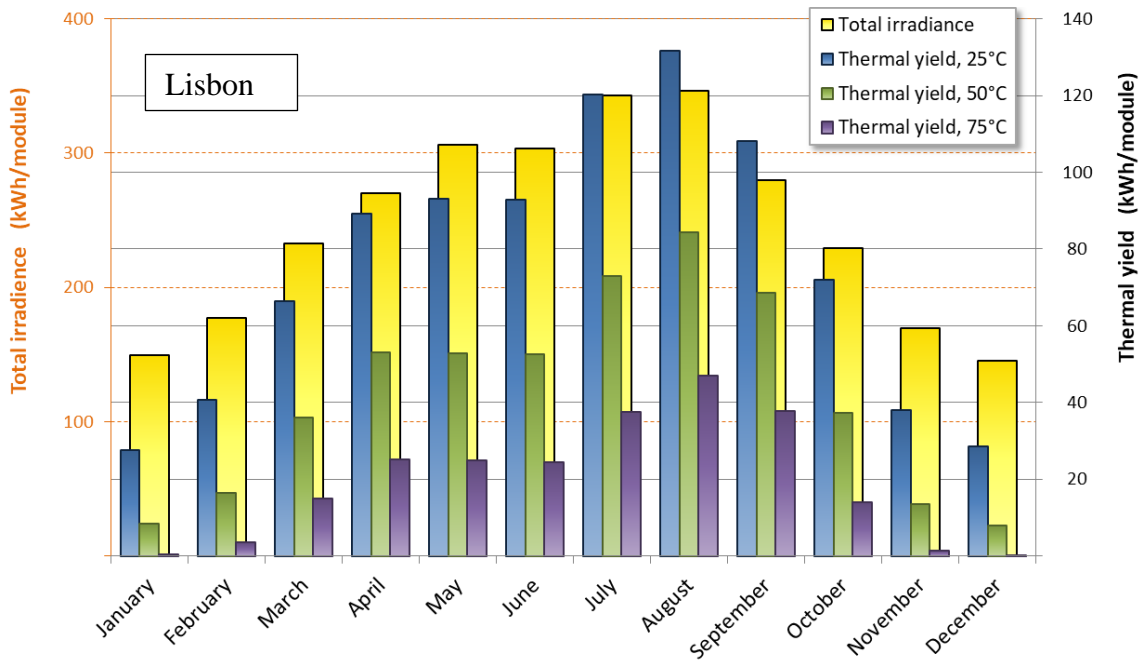


Figure 76:Lisbon thermal yield.

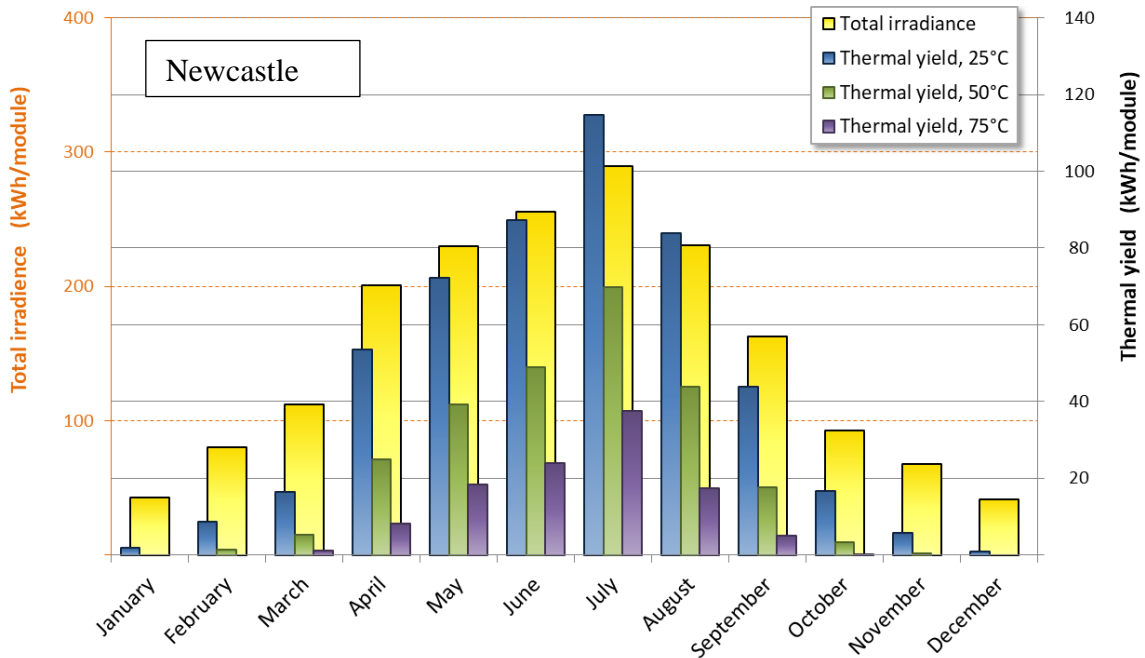


Figure 77:Newcastle annual thermal yield.

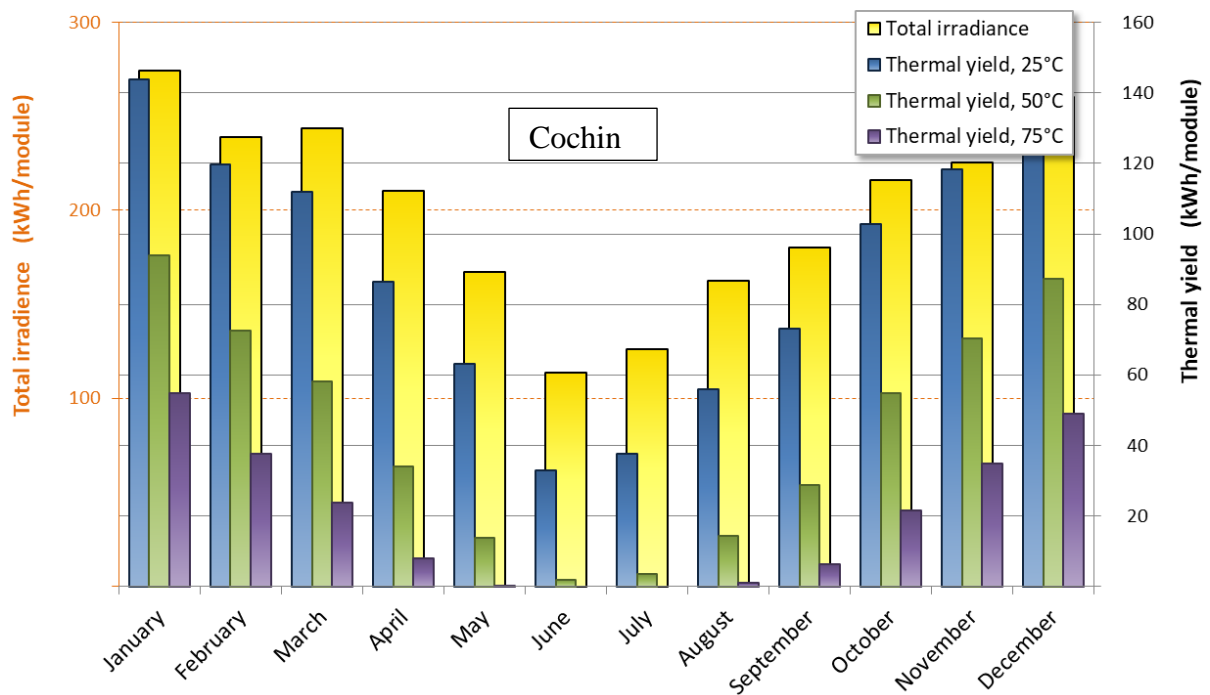


Figure 78: Cochin annual thermal yield.

The basic thermal evaluation at steady state shows the thermal yield for Cochin at 75°C is non-existent during the summer months due to extremely high ambient temperature and PV/T reaching stagnation temperature very quickly while in Newcastle and Lisbon it shows a steady increase in output at 75°C but at 25°C the collector provides the optimum output with respect to the radiation. This evaluation is done at a tilt angle of 35°.

4.4 Dynamic Modelling Method

To model the system in a dynamic method or analyse the behaviour in real time operating conditions, the ray trace method is used to differentiate the components of heat transfer coefficients for each different layer shown in

Figure 79. At each layer, the conduction, radiation and convection are determined. If there is no air layer then convection does not exist, and heat transfer occurs through conduction and radiation. Generally, PV/T system that have been extensively modelled has the air gap between the glass and the PV i.e. Type 1B is the most popular modelled PV/T. Hence using a type 2 will increase the electric output shown in Figure 80. This model can be switched between type 1 and type 2 using the program code to include or exclude the air gap. This can be done manually and can be used as a verification method for the entire model. However, type 2 model is not quite popular and needs additional layers of modelling and feedback for better accuracy. The model is also compared with real-time values to validate the output from the code. Care has been taken during the conversion of temperature from Kelvin units to Celsius and vice-versa. The conduction and radiation heat transfer coefficients are represented

by their respective layer alphabets (a, g, p, b, u, f and i that represents the ambient air, glass, PV, absorber, tube with weld bond, fluid and insulation layers respectively). The thickness of each factor is also represented by ‘thick’ followed by their represented layer letter.

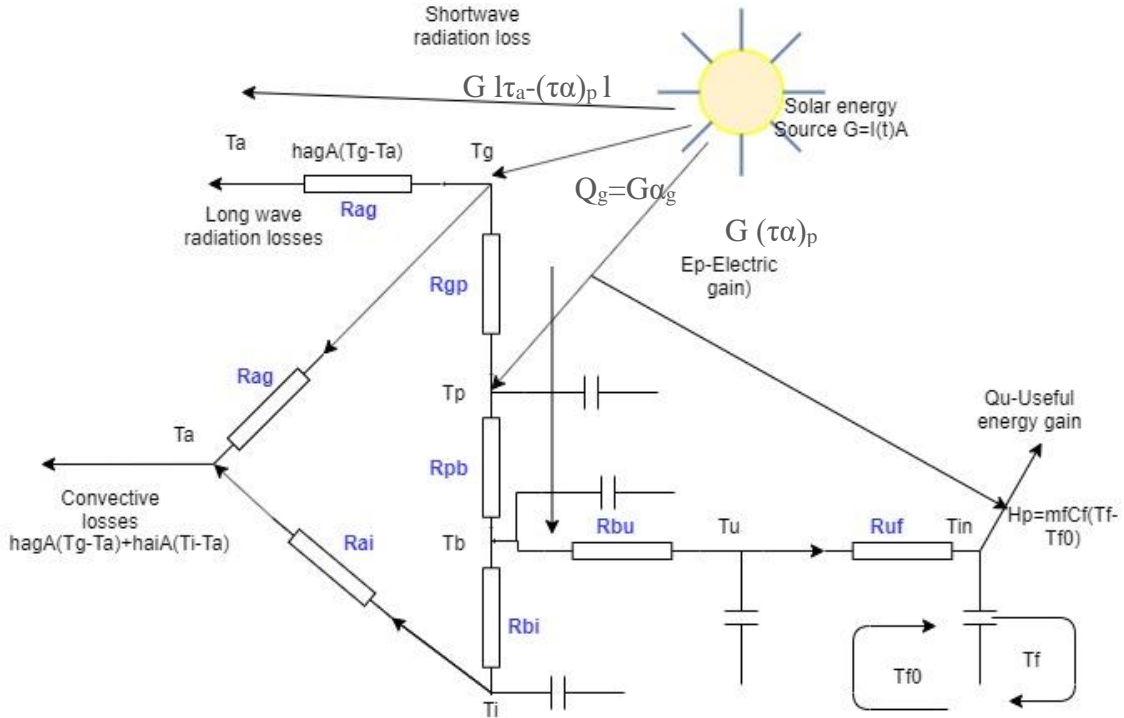


Figure 79: Ray-trace method (The resistance values changes with respect to the input conditions)

$$hac = 3 \cdot u + 2.8$$

$$har = eg \cdot \sigma \cdot (Tsky^2 + Ta^2) \cdot (Tsky + Ta) \quad (4-64)$$

Equation 4-64 represents both the individual components of radiation and convection of the total ambient layer transfer at the surface of the glass. 'ep' and 'eg' are the emissivity's of the PV and glass layers respectively.

It is also assumed that Sky temperature = ambient temperature = inlet or initial temperature.

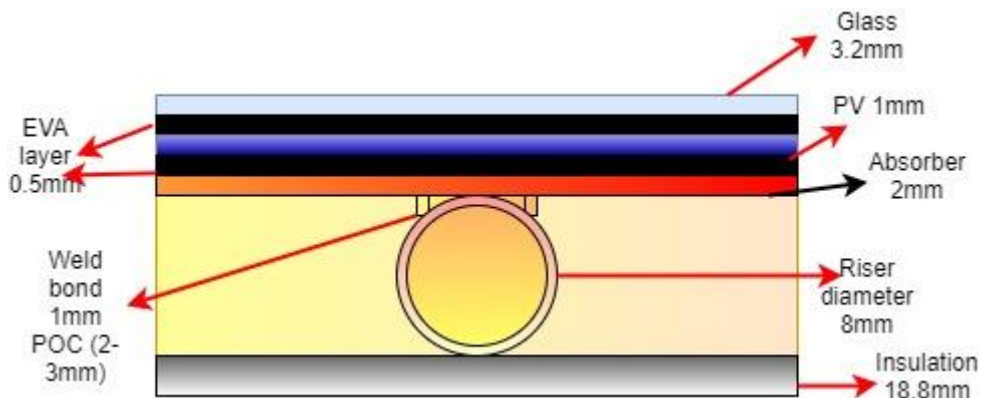


Figure 80: Side cross section of PV/T

$$hcg = \left(\frac{0.34}{thickeva} \right) + \left((\sigma * (Ta^2 + Tcell^2) * (Ta + Tcell)) / \left(\frac{1}{ep} + \frac{1}{eg} - 1 \right) \right) \quad (4-65)$$

$$hbp = \frac{0.34}{thickeva} \quad (4-66)$$

$$hpu = \left[\frac{thickp * length}{\left(\left(\frac{0.14}{130 * 8} \right) + \left(\frac{thickeva * thickp}{0.34 * Dext} \right) \right)} \right] \quad (4-67)$$

$$Qp = I(t) * A * \tau \alpha \quad (4-68)$$

$$hbi = \frac{1}{\left(\frac{1}{Cbo * length} \right) + \left(\frac{Nu * 0.0264}{Dext} \right)} \quad (4-69)$$

$$hiu = \frac{2 * 0.026}{thickins} \quad (4-70)$$

$$h(wa) = 4.364 * (0.591 / Di) \quad (4-71)$$

$$huf = (h(wa) * pi * Di * length) + 1 / (Cbo * length) \quad (4-72)$$

$$hai = \frac{1}{\left(\frac{1}{hcg} + \frac{1}{hbi} \right)} \quad (4-73)$$

Heat transfer coefficient along the tube is represented by 'h(wa)' and the weld bond specific heat capacity is 'Cbo'. The above set of equations from 4-65 to 4-73 describe the heat transfer coefficients from layer to layer about a single cross-sectional node, which can be then scaled up according to the number of nodes 'N' (if there is uniformity of variation across the entire module). But in reality, these variations are not uniform due to shadows, uneven dust formation, snow or faulty bypass diodes. This model also considers an even control volume of the six layers which is evaluated by obtaining the energy balance of each layer. Thereby this forms 6xN nodes, where 'N' is taken in the direction of the flow. Energy balances at these six nodes or six layers are constructed with respect to time. This is derived from the first law of thermodynamics where the mass transfer in the collector is influenced by the heat transfer fluid. The temperature is defined to be in the direction of the flow of the circulating fluid. Each layer node is balanced in relation to the heat transfer coefficients, which obtains six ODE's. As one-dimensional methods are quite accurate with respect to two-dimensional method, the energy balance principle follows that the change in internal energy is equivalent to the total energy generated inclusive of any heat transfer losses. They are produced as

shown in equation 4-74 to form the six equations and these are rewritten to satisfy the format of ODE23b for stiff equations to account for any unstable conditions. RK4 method is used to solve all the equations as it is more robust and has a higher accuracy rate even when solving for stiff ODE's. The partial differential equation (PDE) equation is broken down into two ODE equations using the separation of variables concept and further coded to be solved in MATLAB. A pdepe solver is also used for verification of the generated PDE solution. M_g, M_p, M_b, M_u, M_i and M_f are the mass of each respective layer.

$$\begin{aligned}
 M_g C_g \frac{dT_g}{dt} &= (h_{acA} + h_{arA})(T_a - T_g) + W_g + h_{cgA}(T_p - T_g) \\
 M_p C_p \frac{dT_p}{dt} &= h_{cgA}(T_g - T_p) + h_{bpA} b_p (T_b - T_p) + h_{puA} p_u (T_u - T_p) + W_p \\
 M_b C_b \frac{dT_b}{dt} &= h_{bpA} b_p (T_p - T_b) + h_{buA} b_u (T_u - T_b) + h_{biA} b_i (T_i - T_b) \\
 M_u C_u \frac{dT_u}{dt} &= h_{buA} b_u (T_b - T_u) + h_{iuA} i_u (T_i - T_u) + h_{ufA} u_f (T_f - T_u) + h_{puA} p_u (T_p - T_u) \\
 M_i C_i \frac{dT_i}{dt} &= h_{biA} b_i (T_b - T_i) + h_{iuA} i_u (T_u - T_i) + h_{aiA} a_i (T_a - T_i) \\
 M_f C_f \frac{dT_f}{dt} &= A_{uf} h_{uf} (T_u - T_f) - m_f C_f (T_{in} - T_{out})
 \end{aligned} \tag{4-74}$$

To solve the above equations using numerical method, the differential equations are written in format of ode23b and pdepe solvers where the implicit RK4 method and finite element methods for the PDE solver is applied with initial and boundary value boundary values. This step is completed with the ODE23b solver to solve the algebraic equations concurring to the RK4 method that is modelled into the system. The implicit RK4 method is a reasonably accurate method even for stiff equations if there is instability in any question or if the heat balance equation is stiff. RK4 method of solving these equations gives a low error and accurate enough result. The flowchart for the dynamic model is generated, shown as Figure 81 and explained below.

- 1) The weather data from the weather station or even standard TMY2 data can be accepted into the model. The global radiation, ambient temperature, cloudy or non-cloudy days depending on the rain is read. If the diffuse radiation is not given, it can be calculated using the most appropriate model decided by the program.
- 2) The design parameters for which the steady state analysis is carried out is defined in this process and this can be manually modified to suit different types of PV/T.
- 3) The heat transfer balance node is derived at each layer of the PV/T and ODE is generated according to the ode23b solver.

- 4) The fluid-tube layer has the equation expressed in PDE which is solved in pdepe solver in MATLAB, (This step is completed for further validation of the result(optional))
 - a) The initial value conditions and boundary conditions are calculated and applied to this solver
 - b) The number of mesh points is appropriately selected, and iterations are run to check for optimised values. This is solved to generate ODEs.
- 5) The ODE's from the solver is updated and solved while generating an error tolerance of 0.0001.
- 6) If the error is higher, initial conditions are adjusted to generate an optimal output
- 7) The functions to plot the results are activated once the error tolerances are closed.

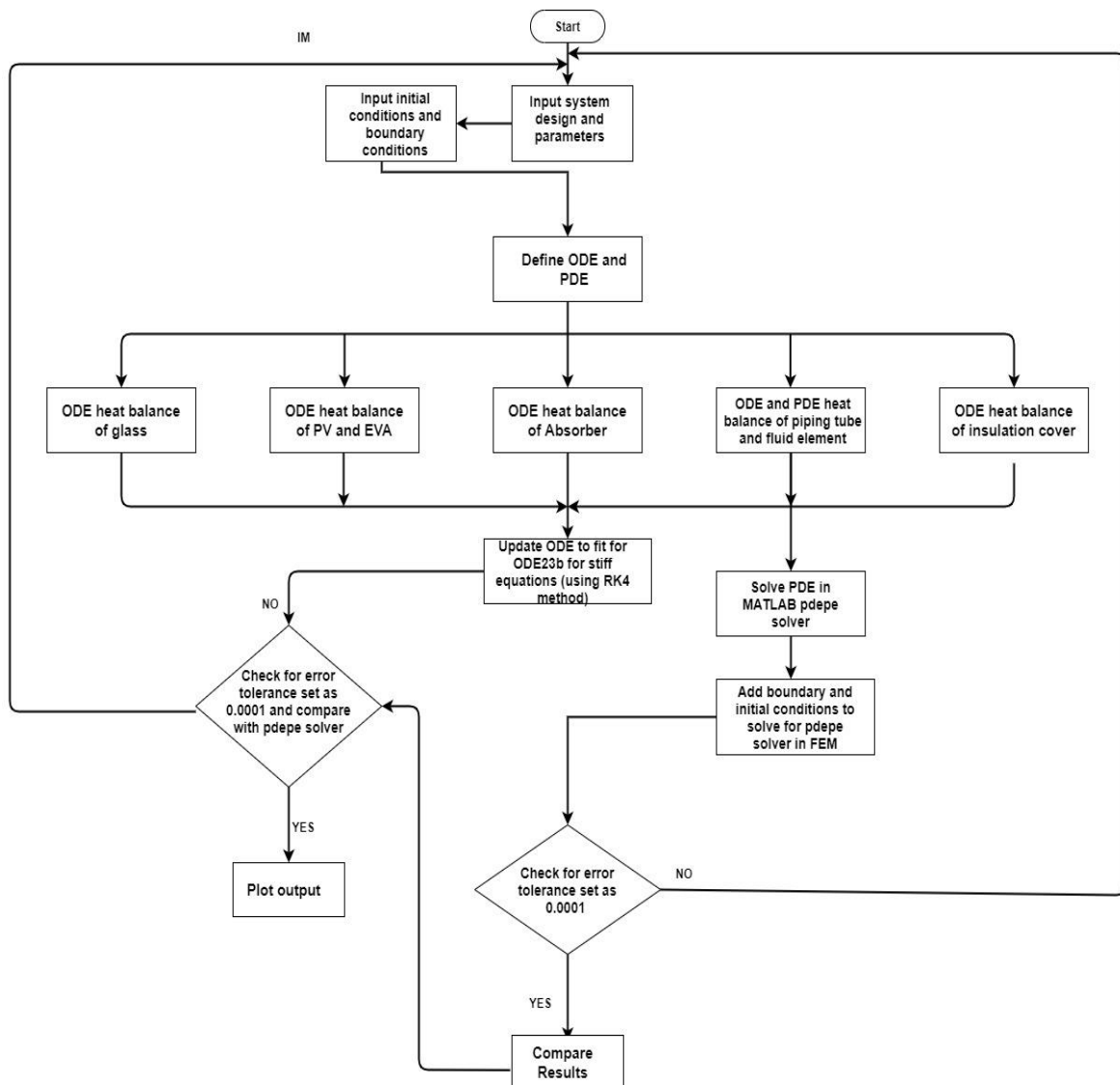


Figure 81:Flow chart of dynamic modelling

4.5 Validation Methods and Resources

Validation is obtained by comparison from similar publication case studies and highly peer-reviewed journals. This is also hoped to be achieved by the lab demonstration when the experiments start to run for the case study in Newcastle. Along with USB results, validation can be done with similar experimental values with realistic parameters. According Ouyang et al., the optimal connection for a higher thermal output is connection of collectors in series. (Ouyang et al., 2017, Vittorini et al., 2017).

Real-time performance for a period of six months was adopted to validate dynamic model. This chapter also investigates the dynamic model in detail for various weather conditions using the model that was developed. The accuracy of this model has been validated and tested the experimental results. The maximum amount of accuracy is ensured as all parameters have been considered and this model. This model can also be replicated for different kinds of PV/T and so serves as a guide for performance of PV/T

The data from the Meteorology on USB was accessed for obtaining the actual energy consumption. The dynamic analysis was formed to compare the simulated and actual energy for a month in March. A very low error was observed, and this was due to truncation error from the reading site. It was also noticed that the system had missing data, and this was rectified by obtaining another method of data collection through PQubes. The real-time system installed has had some delays in the installation and data collection process. The Solar angel is rated at 250Wp electric output and 648Wp heat output. This has been summarized into simulated energy vs measured to validate the system in Figure 82 in (a),(b) and (c).

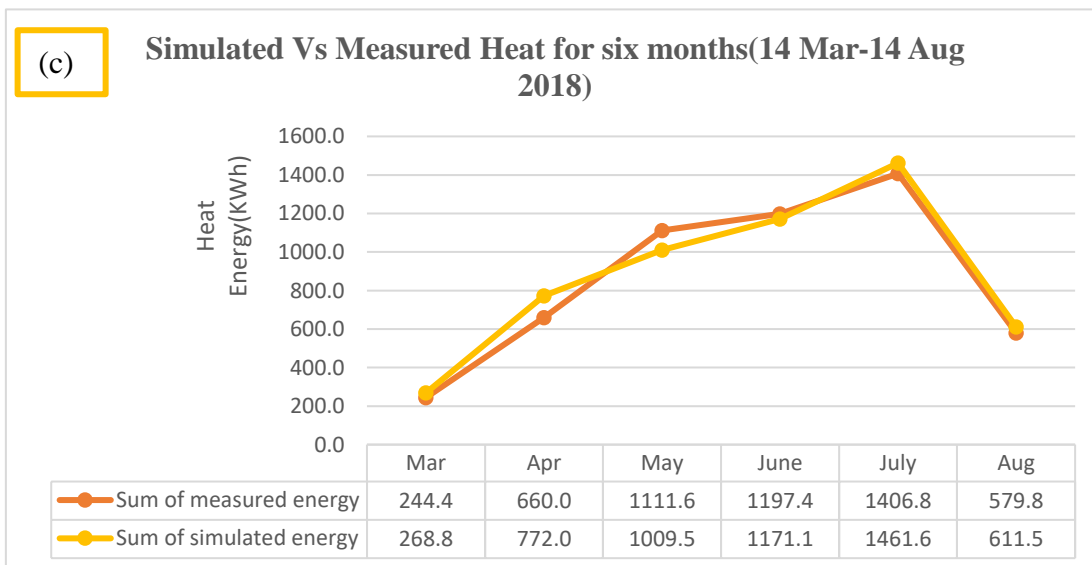
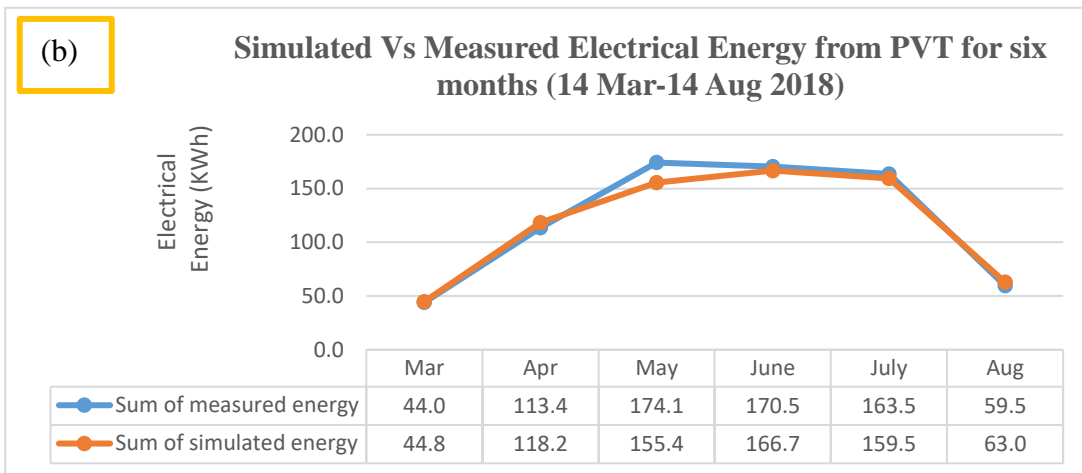
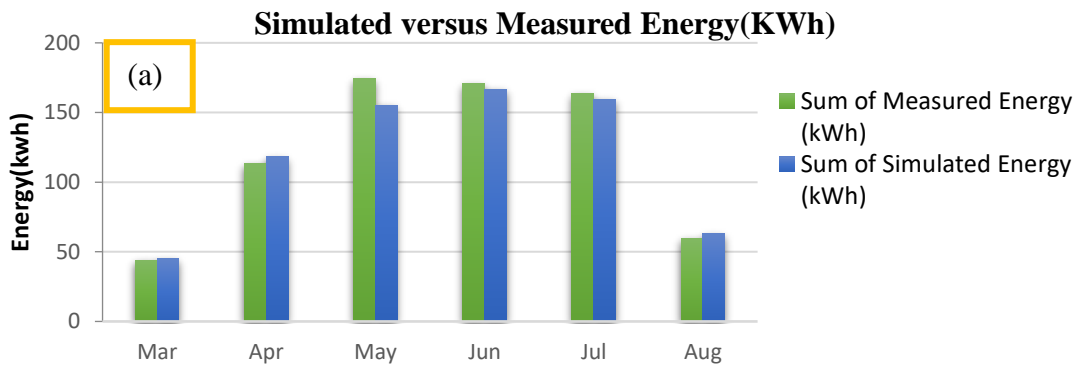


Figure 82: (a) Variability of measured and simulated total energy (b) Simulated vs actual electrical energy over a period of six months with a measured sampling rate of 30 min/interval (c) Simulated vs actual heat energy over a period of six months with a measured sampling rate of 5 min/interval

The modelling method from chapter 3 was used to model the simulation for the USB. Using the real-time parameters from the USB and modifying the simulation with respect to the model of the USB, simulated electrical and heat energy of the building for a period of 6 months from March 2018 to August 2018 was generated. This simulation is then compared

with the real time data. The useable data from the USB for both the thermal and electric energy was available from March 2018 to Aug 2018. Thereby the simulation is run for 6 months. From Figure 82 (b) and Figure 82 (c), simulated over a period of 6 months, it is evident that the simulated values and measured values has very low deviations for monthly values. This simulation was run 3-4 times to ensure for real data. Hence the error was found to be around 4.2% and this is a tolerable error value for engineering applications ($\pm 5\%$).

4.6 Impact of Factors

The major findings that corroborate with parametric studies and findings indicate that the varying dependence of the output is based on the climate, design, operation and integration. Climatic factors are completely dependent on the weather conditions like solar irradiance; ambient temperature; wind speed; dust and relative humidity. Design factors are dependent on the manufactured PV/T unit where duct length, channel depth, number of collectors, sun tracking system, internal heat transfer from PV cell to heat collection system, booster diffuse reflector, collector tilt angle (installation geometry (i.e. orientation and inclination)) and incidence angle, PV module type (the spectral characteristics of a solar PV cell and PV cell solar absorption), glazing and glass thickness (structural difference glass-glass and glass-tedlar), anti-reflection coating, the absorber plate design parameters((heat removal factor)),riser configuration, riser location, thermal conductivity of tedlar/eva,thermal insulation, effect of absorber (material conductivity absorptivity and thickness), effect of fin, effect of multi-inlet and fill factor are considered. Factors depending on the operation of the PV/T are quite significant as they can determine the overall efficiency of performance. Operational factors are mass flow rate, thermal resistance, inlet and outlet fluid temperature, heat loss coefficient, packing factor, effect of fans, effect of metal bars support, effect of other coolant types/effect of anti-freeze vs water. Additional factors can also include integrational factors like, integration into space heating/ hot water/ electrical system/heat exchanger/heat pump/battery, integration into buildings(retro/newly fitted), electricity and temperature of heat demand and shading that depends on the placement of the panel.

Chapter 3 has elaborated the effect of dust on the output current of the PV module in real-time operating conditions the PV module. It shows that the dust can reduce the performance of the PV module by increasing its losses and thereby reducing current. The amount of dust is generally calculated using a factor called the angular factor. Standard values of angular factor are 0.17 for a m-Si module and this can be modified to become 0.20 if a moderate dust

collection is observed and 0.27 is when there is a greater dust collection (Martín and Ruiz, 2002)

Photovoltaic (PV) modules in real operation present angular losses in reference to their behaviour in standard test conditions, due to the angle of incidence of the incident radiation and the surface soil. Although these losses are not always negligible, they are commonly not considered when correcting the electrical characteristics of the PV module or estimating the energy production of PV systems. The main reason of this approximation is the lack of easy-to-use mathematical expressions for the angular loss's calculation. Consequently, reflection losses can become significant when calculating the electrical PV generation. The importance of this effect strongly depends on the module orientation, as well as on local latitude and climate characteristics. Despite the interest of this question, there are few theoretical studies of the optical behaviour of PV modules applied to different technologies, and even these are merely systematic applications of Fresnel formulae. Other authors consider simplified calculations of these analyses. Therefore, a lack of easy-to-use mathematical tools for integrated reflectance effects calculations is observed. ASHRAE provides a common tool for use as IAM using only one parameter at angles lower than 90. Another study by Martin and Ruiz proposed a IAM model that is quantifiable at all incidence angles using an angular factor. The Sandia Model is also used as an effective tool to calculate IAM (Martin and Ruiz, 2001).

Jones and Underwood have studied the temperature profile of the photovoltaic (PV) module in a dynamic condition with respect to time. They conducted experiments for cloudy as well clear day conditions and observed that the PV module temperature varies in the range of 300–325K (27– 52° C) for an ambient air temperature of 297.5K (24.5° C). The main reasons for reduction of the electrical efficiency of the PV module are the packing factor (PF) of the PV module, ohmic losses between two consecutive solar cells and the temperature of the module.

Shading can occur if the solar collectors are placed in rows of several sections facing due south. The shading probability needs to be calculated as shading can occur throughout the year. If the maximum shading happens at local solar noon, this can then be calculated by obtaining the noon altitude and observe if any shadows are formed on the second and following collector row sections. Load supply can be then be re-designed to match the demand of the building.

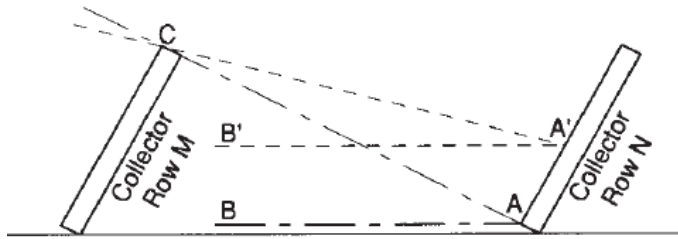


Figure 83: Shadow formation for multi-array collectors(Duffie and Beckman, 2013)

Generally, shading will not occur if the profile angle is greater than the angle CAB as shown in the figure, formed by the top corner of the front collector to the bottom end of the second row and the horizontal. If the profile angle at any time is less than this angle, then a portion of the collectors in the second and subsequent rows will be shaded from beam radiation.

It has been proven that determining the performance of a detached PV/T system is challenging. According to various studies and calculations, the PV/T system is expected to work at 80% overall efficiency for low temperature applications, but this efficiency has not yet been fulfilled for any commercial system at present in the UK.

The main performance indicators as discussed in the previous chapters in order to find performance of PV/T are narrowed down to the following

- i. Electrical yield(kWh/yr.)
- ii. Thermal yield(kWh/yr.)
- iii. System efficiency (%)
- iv. Energy savings (kWh/yr.)
- v. Cost benefit (£/yr., payback in years)

In order to comprehend why certain parameters, affect the overall performance of the PV system precedes to the fundamental behaviour of the solar cell. For example, the climatic factors determine the range of cell temperature attained by the PV. If the temperature is higher, this leads to increased vibrations of electrons and thereby reducing the interatomic spacing and thus the bandgap. A reduction in bandgap means that there will a reduction in electrons to be excited through the bandgap, which eventually reduces the current generated and thus lowering efficiency. Hence climatic factors can have a significant effect on the performance of the PV cell. The stagnation temperature is when the system does not attain

any output /the design and operational factors also affect the performance of the PV cell. The performance of the PV module is represented by the IV curve and the behaviour of the module along variation in that curve. The main indicative operators that are responsible for this change are incidence angle, tilt angle, solar radiation, ambient temperature, transmission-absorption product, NOCT, location and packing density which are investigated and analysed in the next chapter.

The performance of solar collector is usually represented as a function of the difference of mean plate temperature and ambient temperature with respect to radiation shown $(T_m - T_a)/G$. This function is shown as a variant in the efficiency curve; however, this is limited to a limited range of radiation values and second order function needs to be accounted for higher radiation values. The European standard testing which follows EN 12975 for collector states that the efficiency curve needs to be tested between 800-1000 W/m². The graph is read through the operating point which moves to left representing higher solar radiation and higher efficiency. But this also presents a higher ambient temperature and in turn increases the operating temperature and lead to lower efficiencies. The change in radiation affects the system lesser than the temperature. Hence an optimum operating efficiency can be found by an optimised temperature and radiation from the curve. This type of curve generates a comparable curve with other collectors that can potentially indicate that the actual operational efficiency is affected by the inlet temperature, mass-flow rate, heat capacity of fluid, collector area, stagnation temperature, solar radiation, ambient temperature and heat removal factor which needs further examination. The actual solar gains can only be calculated by simulation. For a PV/T all these parameters affect the system performance and the percentage weightage of these parameters is an important result used for design of a PV/T system with detail analysis. The biggest advantage of this method is that all the data is from actual external real-time data is realised instead of indoor data.

4.7 Chapter Summary

In this chapter a very detailed process of modelling has been explained and calculations have been verified with published data. The impact of factors for PV/T has been narrowed to be extracted for modelling the current unit. To summarise the results, from this chapter, it can state that the system validation paves the way to understand the impact of variable factors on the efficiency with an error rate of 4.2%. It was found that the mass flow rate and ambient temperature affects the performance according to the location. The impact factors of ambient conditions are mostly affected by the temperature and the solar radiation incident on the

surface. The optimal angle of tilt can also affect the PV output. The recommended method to generate an optimal performing unit is to have a higher heat transfer through flow rate. If the connection is in series, a higher thermal output is generated, and parallel combination substantiates a higher electrical output. In colder countries, a mixed fluid (usually with ethyl glycol) is used to avoid freezing. The inlet temperatures when maintained high can become a controlling parameter to understand the performance.

CHAPTER 5. Results and Discussion

5.1 Introduction

This chapter generates an evaluation of the PV/T system in real climatic conditions. An experimental rig was set up and assessed under real-time outdoor weather conditions by recording several parameters, e.g., solar radiation, PV power generation and temperature. The main works are listed as follows:

1. The lab demonstration output was measured over a consecutive period for about a week in real climatic conditions under two pump settings from 8th to 15th April.
2. The test results were used to validate the dynamic simulation model established in chapter 4
3. Through a congruent examination between the measured and simulated outcomes, the simulated model was approved as having an accuracy with a sensible degree of precision. The data was proven to have repeatable and reliable performance in real climatic conditions. Hence a dynamic simulation model is thus regarded as being reliable in predicting the annual system performance for the exergy and economic analysis in the next chapter. An extensive simulation is completed, and all the results are discussed in this chapter.

5.2 Dynamic Model Simulation and Evaluation

In order to study the PV/T model, the boundaries of DG-01 model from the company ‘solar angel’ are considered and the technical performance is monitored which can be further extended to a range of analysis like energy analysis and exergy analysis. In order to analyse the model in MATLAB, we consider three different locations Lisbon, Portugal (at 38.7223° N, 9.1393° W), Newcastle UK (at 54.9783° N, 1.6178° W) and Cochin, Kerala (at 9.9312° N, 76.2673° E). The regularly real changing conditions like temperature, wind and the solar irradiation (from white box weather data) at hourly intervals are subjected onto the model over the course of a year. (2013, 2017, 2018 and some data sets from 2019 are now available and used).

The technical data of the module is extracted to be used in the code for analysis of the system. As the preferred method for solving the system of ODEs is chosen as the fourth order Runge-Kutta method or the implicit (for comparison), the accuracy is predicted to be very high when compared with a previously calculated model of explicit solution which brings in lots of errors. For validation of one of the simulations, a practical run output from a solar power plant in Lisbon, Portugal is available. The solar power plant has separately run PV panels and solar collectors.

5.2.1 Simulation and Real-Time Results for Portugal

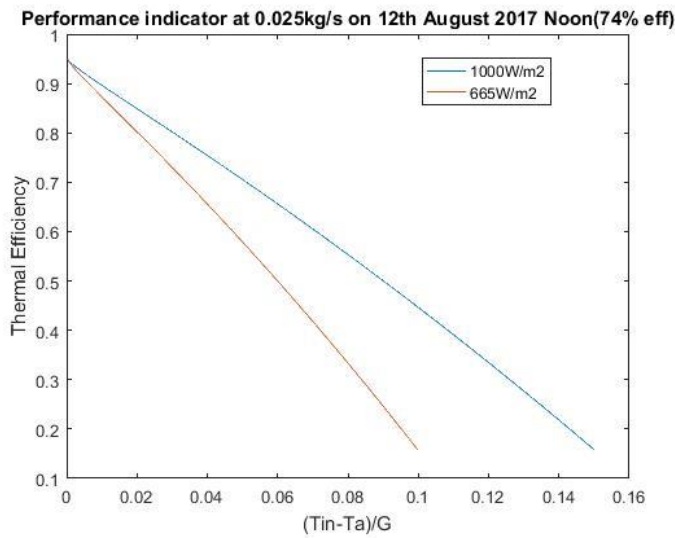


Figure 84: Performance curve for collector at different radiations at 0.025kg/s (simulated output)

For the simulated collector output shown in Figure 84, the heat removal factor was found to be 0.79 where the actual output from the solar collector for August 12th which is highly dependent on the radiation, temperature and MFR which is 0.025kg/s. A system is simulated to generate PV power from the PV/T panel at 0.04 kg/s and is shown as in Figure 85.

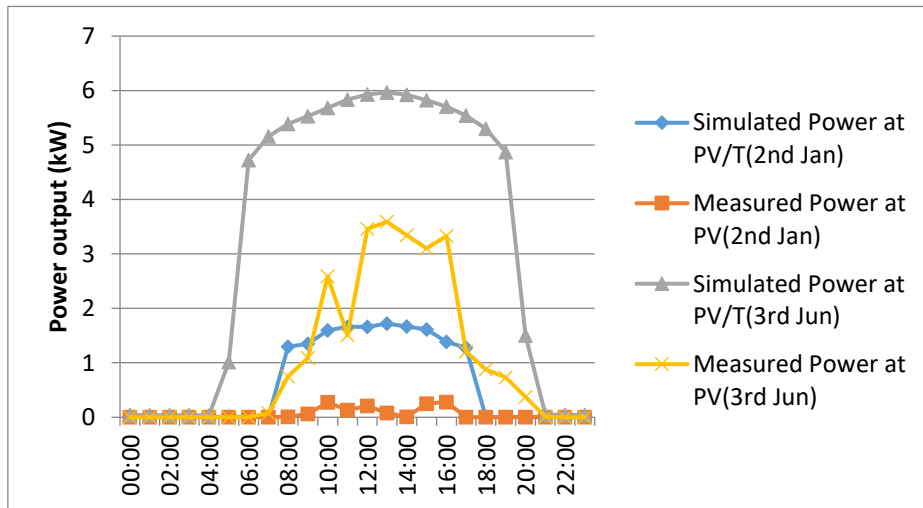


Figure 85: Simulated PV/T output vs measured PV

A simulation for two days (2nd Dec and 3rd Jun) which is the lowest and highest power generating days in Lisbon is constructed for a PV/T system. There is evident improvement in the power generated. Hence the PV/T system used here can provide a higher value output.

When this system is operated as a separate PV and two-cover thermal system, the following observation is made. The PV system without heat removal experiences a drop-in efficiency by 3% and thus it can be concluded that the PV/T system improves the efficiency by 3% which otherwise does not in a single PV which is evidently shown in Figure 85.

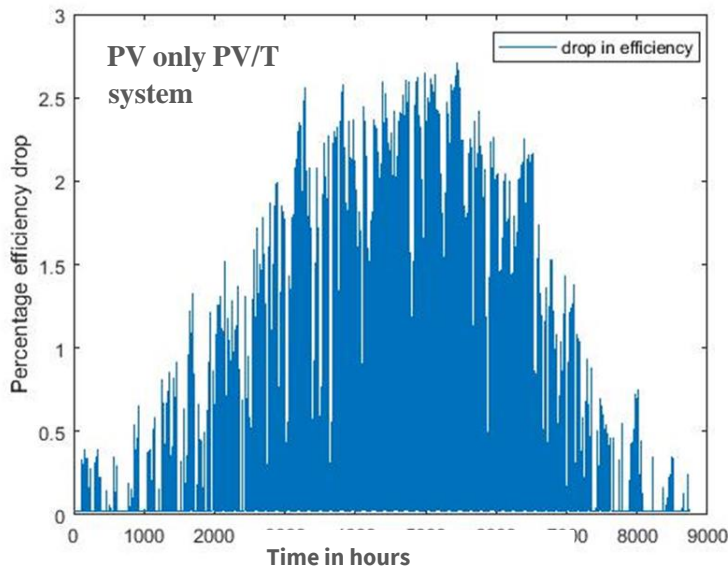


Figure 86:PV only PV/T system

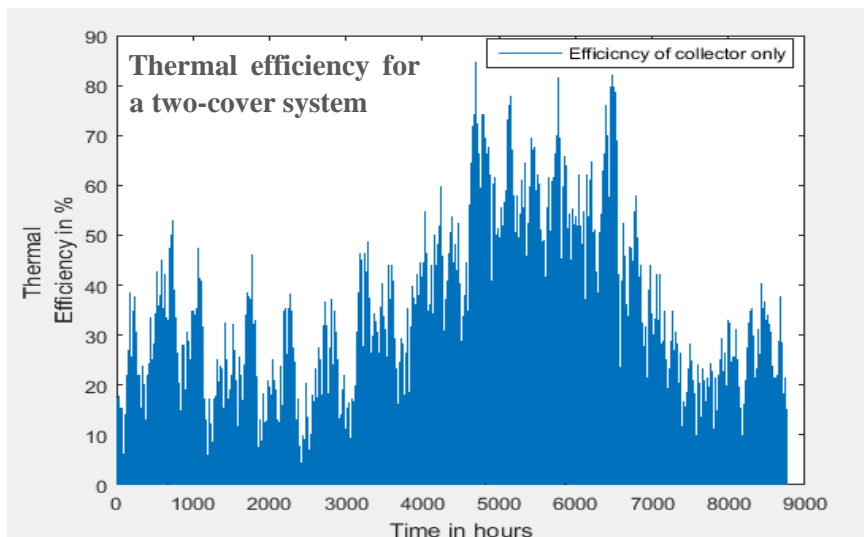


Figure 87:Two cover PV/T thermal only system

The difference in efficiency is significant. The system is validated using publication results from Tiwari et. al. 2006 and Khelifa et. al. 2015. It is quite evident that the operating curve ascends for the higher mass flow rate. Thus there is a significant improvement in the operating curve when MFR is increased(Tiwari et al., 2006, Khelifa et al., 2015).

When the system is operating as thermal collector with two covers as PV is now inactive, the efficiency is observed to increase from 75% to 80% at a flow rate of 0.025kg/sec shown in Figure 87. A complete annual analysis of three different locations revealed the maximum efficiency reached at each location and is shown in Figure 88.

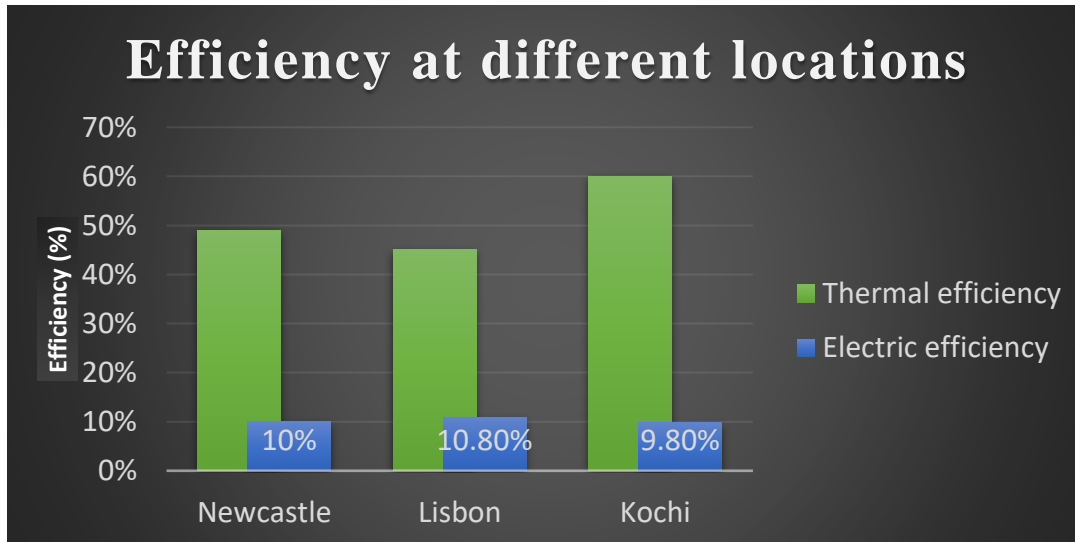


Figure 88:Efficiency at different locations

When working as a combined PV/T system, Newcastle and Lisbon can generate a thermal efficiency of 49% and 45% respectively while Cochin can generate 60% efficiency as seen in Figure 88. As from previous studies, a study in Saudi Arabia, reported a good thermal efficiency with PV/T systems, however the overall efficiency was not adaptable for the environment. Even though Cochin does not have extreme climate such as Saudi Arabia, it might not actually show the intended results due to extreme high ambient temperature during summer.

The useful thermal heat from the PV/T has a higher value in summer and it is observed to be lower than 200W during some days in the winter, which is not a high-grade energy value for usage as shown in Figure 89. A dynamic analysis proved that the maximum fluid temperature that was obtained from the system was 50°C for Newcastle and temperature for Portugal reaches around 60°C shown in Figure 90 and Figure 91 respectively. For UK, the cell temperature is maintained above 25°C only during the summer months and needs an effective heat removal source(increasing the mass flow rate) for maintaining to around 25°C.

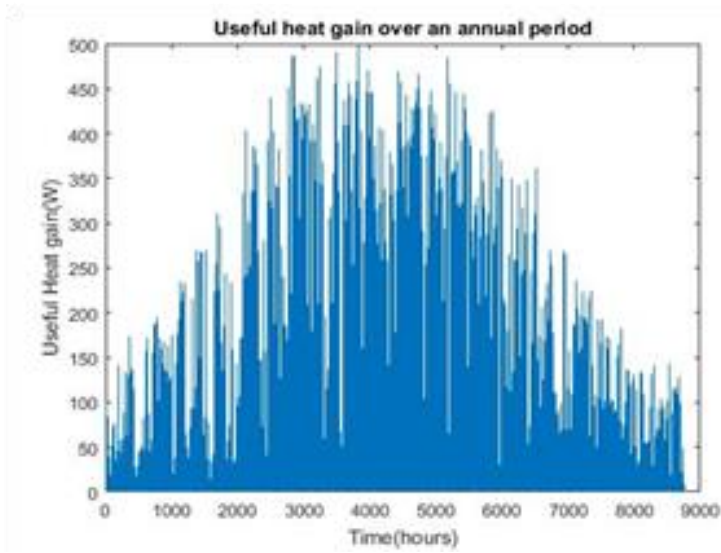


Figure 89:Thermal heat gain

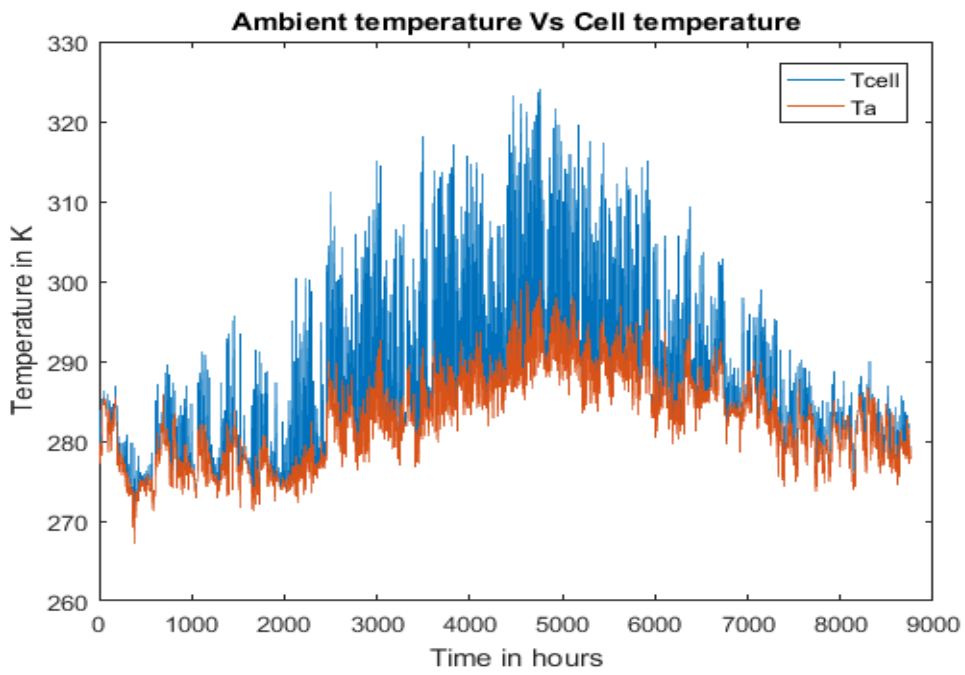


Figure 90:Cell Vs ambient temperature (UK)

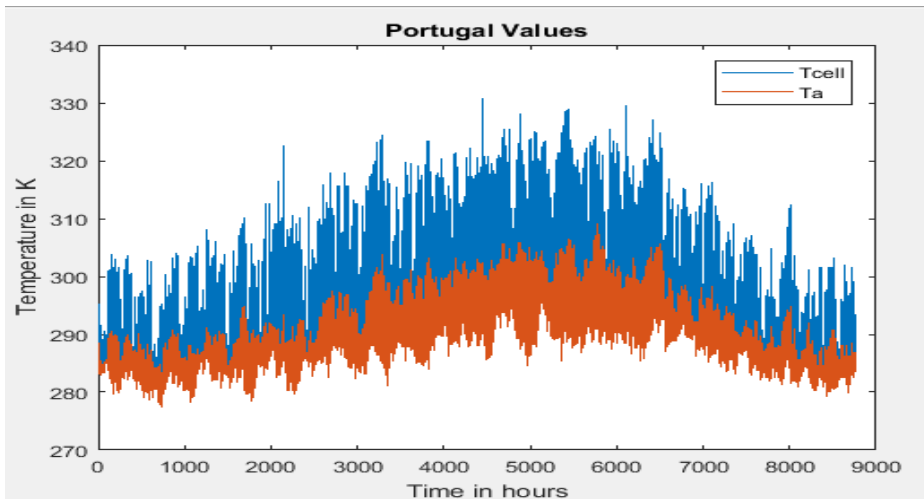


Figure 91: Cell temperature values for Portugal

In reference to Figure 91, the cell temperatures for Portugal maintains a higher value throughout most of the months and hence needs a constant heat removal system throughout the year so as to maintain the temperature of the cell below 25°C and this brings a reduction in the quality of energy.

5.2.2 Simulation and Real-Time Laboratory Results for Newcastle

The experimental rig in Newcastle was continuously operated and recorded over the short term in sunny or cloudy weather conditions over a year period. The test results indicate the system had a steady, consistent and reliable operating performance in real climate conditions. The daily average electrical and thermal efficiencies of the PV/T module were 10.13% and 49.25%, respectively for Newcastle.

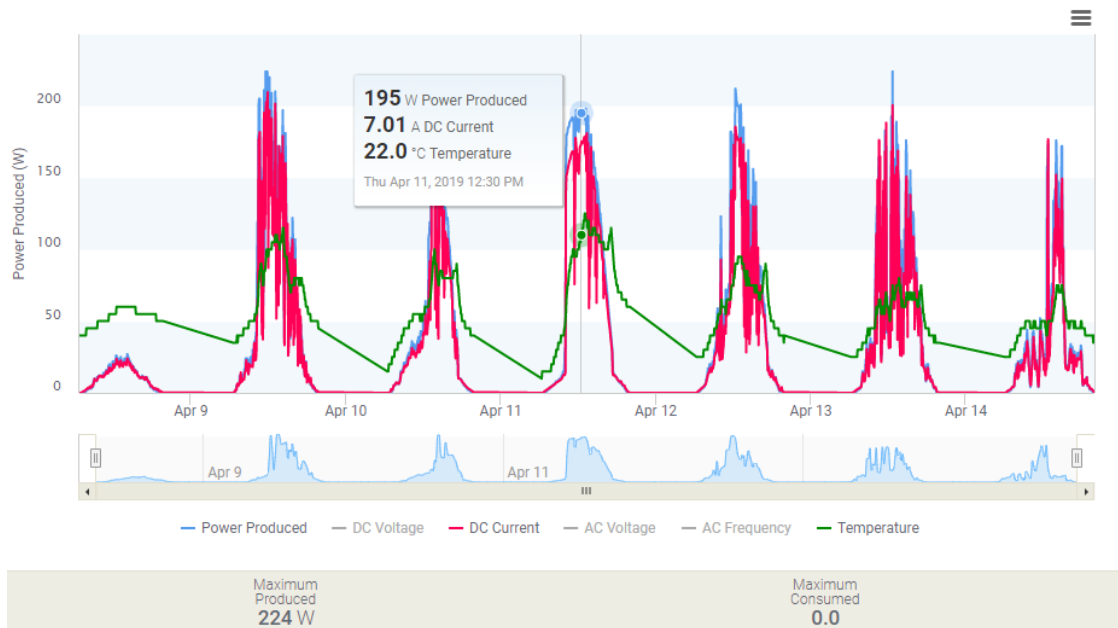


Figure 92: Power generated by the PV of PV/T (collected from one of the microinverters)

The above figure shows the energy generated at the real-time PV system. A weeklong data from 8th April to 15 April is chosen for analysis of the LAB system.

The data is obtained from an online accessible authenticated system where live data can be obtained. It is quite evident that the consumption is higher than the production. However, the system was run at optimal level during the week and a higher output is noticed (11th April) comparative to other non-optimised days as in Figure 92. The temperature values have systematically reduce when the pump speed and thus the flow rate was increased, which proves that the mass flow rate can effects the output. The generated power did not show a highly significant output. However, it must be noted that the temperature of the panel has not exceeded 25°C.

The variation in the module's electrical output was found to be like that of the solar radiation, presenting a gradually increasing trend in the morning and a decreasing trend in the afternoon, while the peak electrical output occurred at noon. The solar electrical efficiency was found to increase slowly in the morning, significantly decrease in the late afternoon, and remain at a relatively stable state for the rest of the day as the current generated is varying accordingly. This variation trend was largely affected by solar radiation and the corresponding incidence angle. It is known that greater solar radiation and a smaller incidence solar beam angle will

result in enhanced solar energy absorption and thus increase solar electrical output, which was the situation for the noontime.

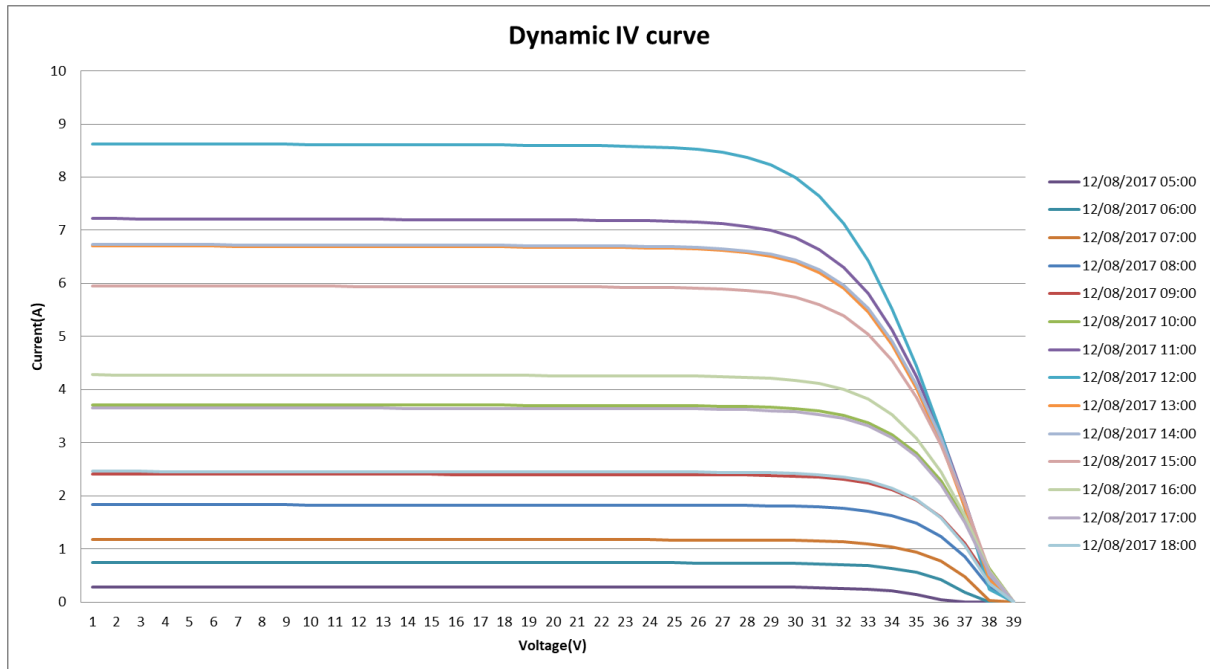


Figure 93: Real-time IV characteristics

As an example, a real-time IV curve was generated for a whole day (Figure 93). With all the parameters affecting the output, a dynamic curve was obtained to show the difference in current generated from sunrise to sun set. It is noted that the only 14 hours of sunshine is available on August 12th. For the PV/T system that was modelled, it has 39V Open-circuit Voltage and 8.6 Short-circuit current. The operation of the PV cell fluctuates according to the parameters previously mentioned. Therefore, a prediction of the generated energy is enabled for optimising the parameters and designing any system at any load. In this study it was observed there is a maximum of 3% increase in electric output when using the parameters to determine the control of output. A dynamic real-time IV curve considers all dynamic factors for PV/T.

A validation of the simulated model with a reusable accuracy was drawn when compared with the equivalent real-time system. The simulated model was generated for the USB at Newcastle where two parallel combination of 6 collectors in series at 20° tilt and azimuth at 20° from due south. The real time data was cohesive with the simulated results. Further dedicated analysis and discussions of the modelling/test results were conducted for the days where data is fully available at the lab in Newcastle for a week in April.

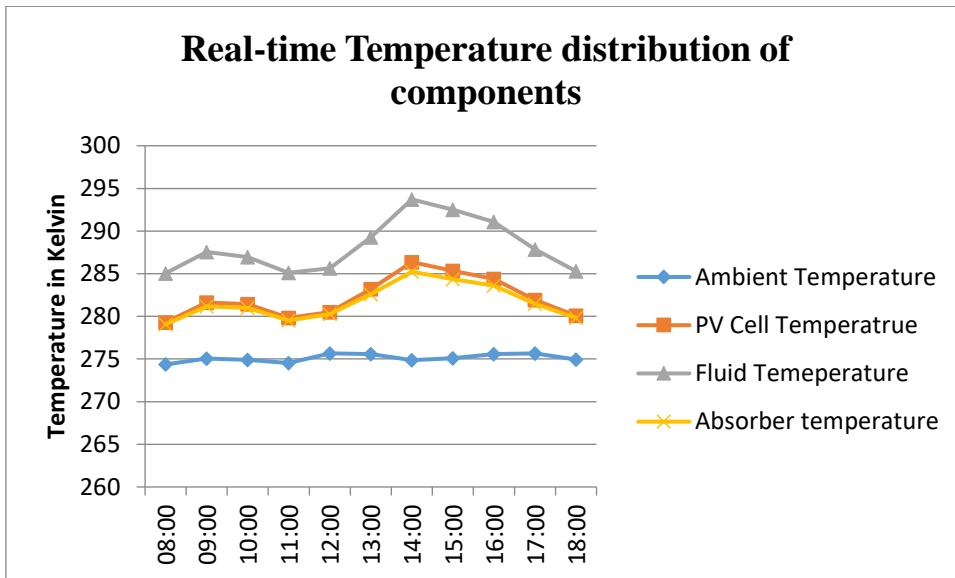


Figure 94: Temperature distribution of components

It was also found that all temperature values for the glazing cover, PV layer, absorber layer and fluid temperature has an rising trend in the morning starting at 275K and ending at 287.5K and higher rising trend in the afternoon starting at 285K and ending at 294K, as seen in Figure 94 . The temperature at the PV layer was in the range from 6 °C to 13.2° C. The temperature difference between the PV layer and the absorber was around 1°C after noon. There is also a small dip in temperature at 11:00 before a high rise in the afternoon, due to cloud cover .This final temperature occurs after 18:00 in the evening. The high rise in temperature is justified by the fact that optimising for the PV/T system through factors like solar radiation and smaller incidence angle at noon. This enabled the PV/T unit to extract a high energy during the afternoon, thus leading to a fast rise in temperature. Conversely, the higher air temperature in the afternoon resulted in a smaller heat loss from the module to the air and a lower temperature reduction speed, thus causing a reduced temperature difference between the PV layer and the fluid. A similar explanation of the temperature variation could also be related to the glazing cover.

5.2.3 Efficiency

The figures give the PV/T module electrical yield and it's relating solar electrical effectiveness. The normal electrical yield from the experiment and testing were found to be 9.6%. The variety in the module's electrical yield was observed to be like that of the sunlight-based radiation, displaying a slowly expanding pattern toward the beginning of the day and a diminishing pattern toward the evening, while the pinnacle electrical yield happened around early afternoon. The sun powered electrical productivity was found to increment gradually in

the first part of the day, essentially decline in the late evening, and stay at a generally steady state for the remainder of the day. This variety pattern was generally influenced by sun powered radiation and the relating occurrence point. It is also realized that sun oriented electrical effectiveness will change to the contrary pattern to the sun powered frequency edge and at a reliable pattern with the PV cells' temperature, and a definitive changing pattern in sunlight based electrical proficiency will rely upon the heaviness of the effect of the two elements. The thermal yield of the system was also found to be 49%. It was also found that operating the PV/T at optimal conditions can increase the efficiency by 3% more than its individual units.

5.3 Further Discussion

The three experimental cases studied above have proved to have a pattern of dependency on certain parameters. Those factors are listed as below

- i. Ambient temperature
- ii. Solar radiation
- iii. Wind speed
- iv. MFR
- v. Incident angle
- vi. Absorbed radiation
- vii. Tilt angle
- viii. Location of the system
- ix. Stagnation temperature
- x. Packing density
- xi. NOCT
- xii. HTF capacity
- xiii. Heat removal factor
- xiv. Configuration of the system

An increase in MFR as previously shown in steady state also decreases the temperature of the cell in dynamic state and improves the electric efficiency.

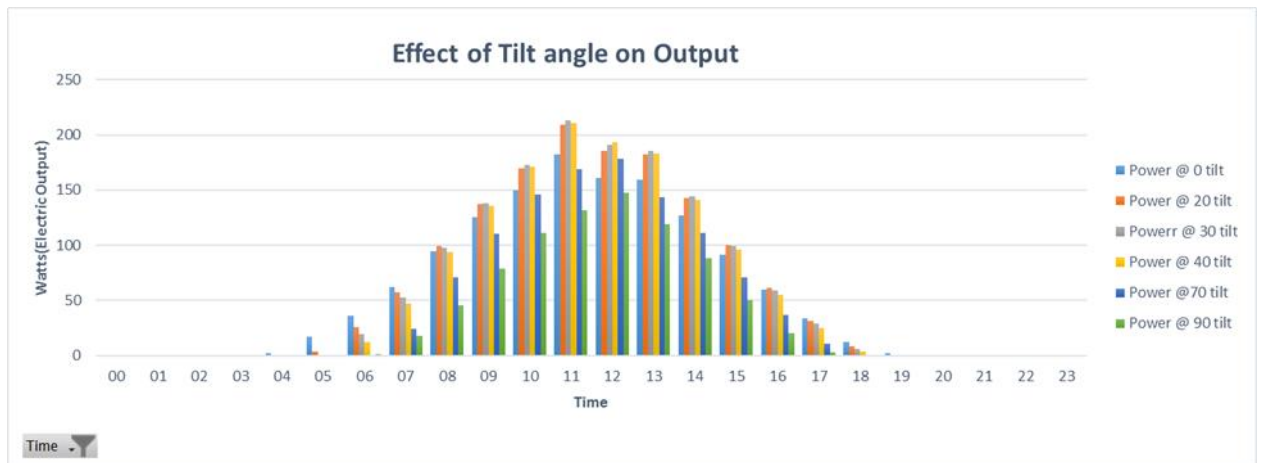


Figure 95: Effect of Tilt angles on electric output in a day

The optimum tilt angles as said by Duffie and Beckman can be varied from latitude of location $\pm 10^\circ$ depending on the whether to track output at winter or summer (Duffie and Beckman, 2013). According to Figure 95, the optimum tilt angles for UK range from 20° to 40° , with the optimum being 30° . Any angle above 70° , shows an adverse effect on the generated output.

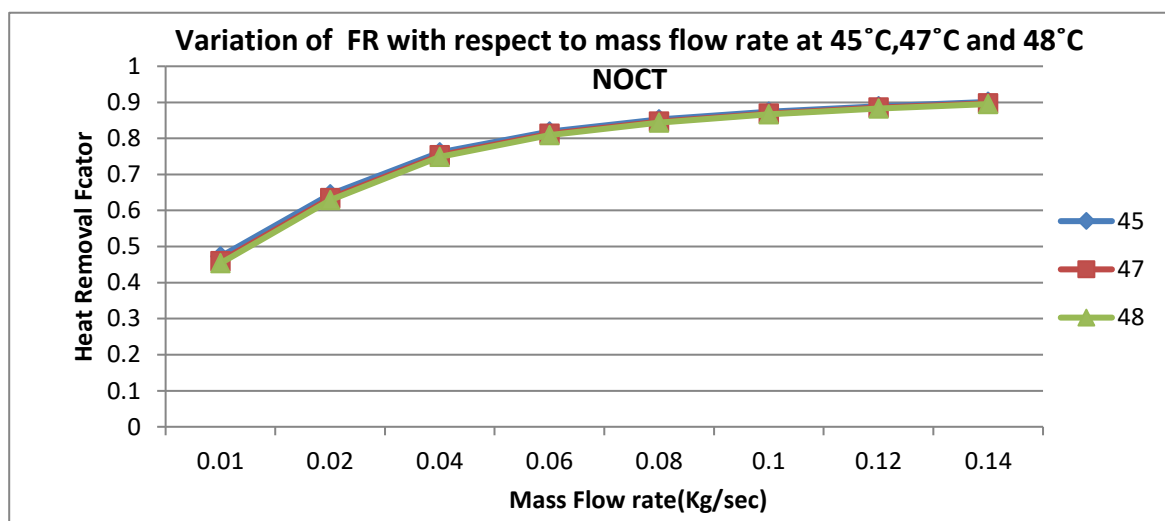


Figure 96: Variation of FR with respect to mass flow rate and NOCT at 45°C , 47°C and 48°C .

Figure 96 shows an effective variation on heat removal factor due to NOCT. It can be observed that the mass flow rate has a significant effect on the heat removal factor with respect to NOCT. This indicates that higher mass flow rate improves the heat removal factor and as the useful gain is directly proportional to the heat removal factor, output is thus affected by mass flow rate. Care must be still taken when designing the system with higher mass flow rates to avoid pump losses. The fluid heat capacity C_f depends on the location

selected (mixed with percentage of ethyl glycol) and should exponentially affect the heat output.

All the factors that were said to have a significant effect on the performance was analysed and an aggregate result was formed. The results show a significant dependence of MFR and the specific heat capacity of the fluid with respect to the heat removal factor.

5.3.1 Design and Application in Residential Systems

In order to apply the model into a residential application, two case studies at Newcastle and Cochin were considered. The system was designed for a 4-bedroom domestic house to meet the load demand and examine whether such a system will provide a feasible standalone solution.

FOR NEWCASTLE:

In order to apply the model and design a system, a 4-bed house case is selected for Newcastle based on the results obtained. The electric demand and heat demand can be supplied by an appropriate design, cost and area available.

When the actual data can be predicted along with understanding the controlling factors can give us a broader understanding of the system. Referring to Figure 61 and Figure 62, the excess electric energy can be stored and used when there is deficit energy.

Utilising the parameters and model from above, a full standalone scale system can be designed, and annual operational performance of the system can be predicted for domestic case in UK.

As mentioned previously in chapter 4, the domestic house of 4-bed system has been modelled. For the 4-bed domestic house a sum of **2399 KWh** for electricity and a sum of **20231KWh** of heat energy is consumed per year.

Here the system needs to generate at least 12KWh per day for covering the complete consumption. The heat generation should be able to meet 116KWh per day. This is chosen by the maximum generation for both.

The PV/T system installed should be able to generate this energy using a storage and heat tank for auxiliary support. The battery storage required 24V DC supply of $(12\text{KWh}/24=500\text{Ah})$ 500Ah.

The losses in the battery, regulators and cable losses are 15%, 15% and 2% respectively. The daily generation required from the storage system is corrected to be $500\text{Ah}/(0.85*0.85*0.98)=706.16\text{Ah}$

Table 9: Array current for Newcastle case study

<i>Month</i>	<i>Average Daily Irradiation (kWh/m²) for UK</i>	<i>Required Array Current (=daily Ah/irradiation)</i>
<i>January</i>	0.537959553	1312.663742
<i>February</i>	1.175629666	600.6653457
<i>March</i>	1.654629105	426.7784228
<i>April</i>	3.468319679	203.6029159
<i>May</i>	4.262557101	165.6658159
<i>June</i>	5.158956411	136.8803967
<i>July</i>	5.491236312	128.5976345
<i>August</i>	4.010445694	176.0801801
<i>September</i>	2.09842	336.5198986
<i>October</i>	1.116665	632.3830139
<i>November</i>	0.889977	793.4587087
<i>December</i>	0.497818	1418.511318

From the above table it is quite clear that the most demanding month is December that requires to generate 1418.51A. Due to losses from dirt and other variables a 10% loss is considered and the actual current needed is recalculated as **1576.12A**.

The Solar Angel PV/T parameters are re-described as in the table below

Table 10: Solar Angel parameters

<i>Number of cells</i>	60
<i>Type of cells</i>	<i>Poly crystal silicon</i>
<i>Warranted minimum power (Pmax)</i>	250 W

<i>Voltage at Pmax</i>	<i>30.4 V</i>
<i>Current at Pmax</i>	<i>8.2 A</i>
<i>Short circuit current (Isc)</i>	<i>8.6 A</i>
<i>Open circuit voltage</i>	<i>39 V</i>
<i>Temperature coefficient of Isc</i>	<i>(-0.038) %/K</i>
<i>Temperature coefficient of Voc</i>	<i>- (0.49) mV/K</i>
<i>Temperature coefficient of Pmax</i>	<i>- (0.45) %/K</i>
<i>NOCT</i>	<i>47 C</i>
<i>Maximum system voltage</i>	<i>1000 V (IEC 61215 rating)</i>
<i>Dimensions</i>	<i>1630 x 986 x 35mm</i>
<i>Weight</i>	<i>25 kg</i>
<i>Construction</i>	<i>Front: high transmission 3.2mm tempered glass Rear White tedlar Encapsulant: EVA</i>

As the maximum current at Pmax is 8.2A at STC, and the requirement to generate 1576.12A, the panels needed to be installed are 192 in order to ensure full supply.

For a storage battery bank, as the 24 V supply is enough from the PV/T panels of 30.4 V. 192 panels connected in parallel will generate enough electric energy however, heat generation will be compromised but connecting in series can increase the heat output from the panels. The optimal connection can thus be made in 192 panels in parallel for electric connections and the heat connections can be in string of four 48 series connections for a higher thermal output more than 116KWh generation.

The heat demand per day is 116KWh. The heat outlet provides a maximum fluid temperature 46° C during September when the fluid inlet temperature is high than 25 ° C , and will be improved when at least 4 panels are in series which is described in the following Figure 97.

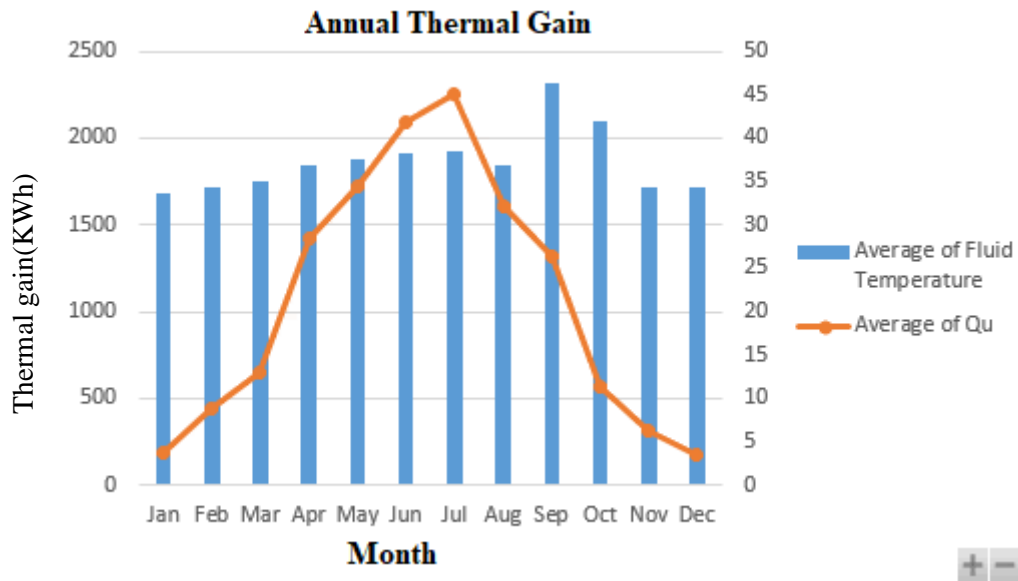


Figure 97:Thermal gain in KWh

The total weight of the solar panels and mounting components is 1256.66 kg. Assuming this is spread evenly over the area that the solar panels cover , the loading imposed by the solar PV array is 22.1 kg/m², or 0.22 kN/m².

According to the survey, the garden is 3 times the area of the house and hence all PV/T systems can be installed as obtained in the design. The space is large enough for all the panels and even extra area is available for installation of PV/T. The area required for the PV/T case in UK is 307.2 sq m. The final design schematic for the PV/T system in UK is laid out as follows in Figure 98:

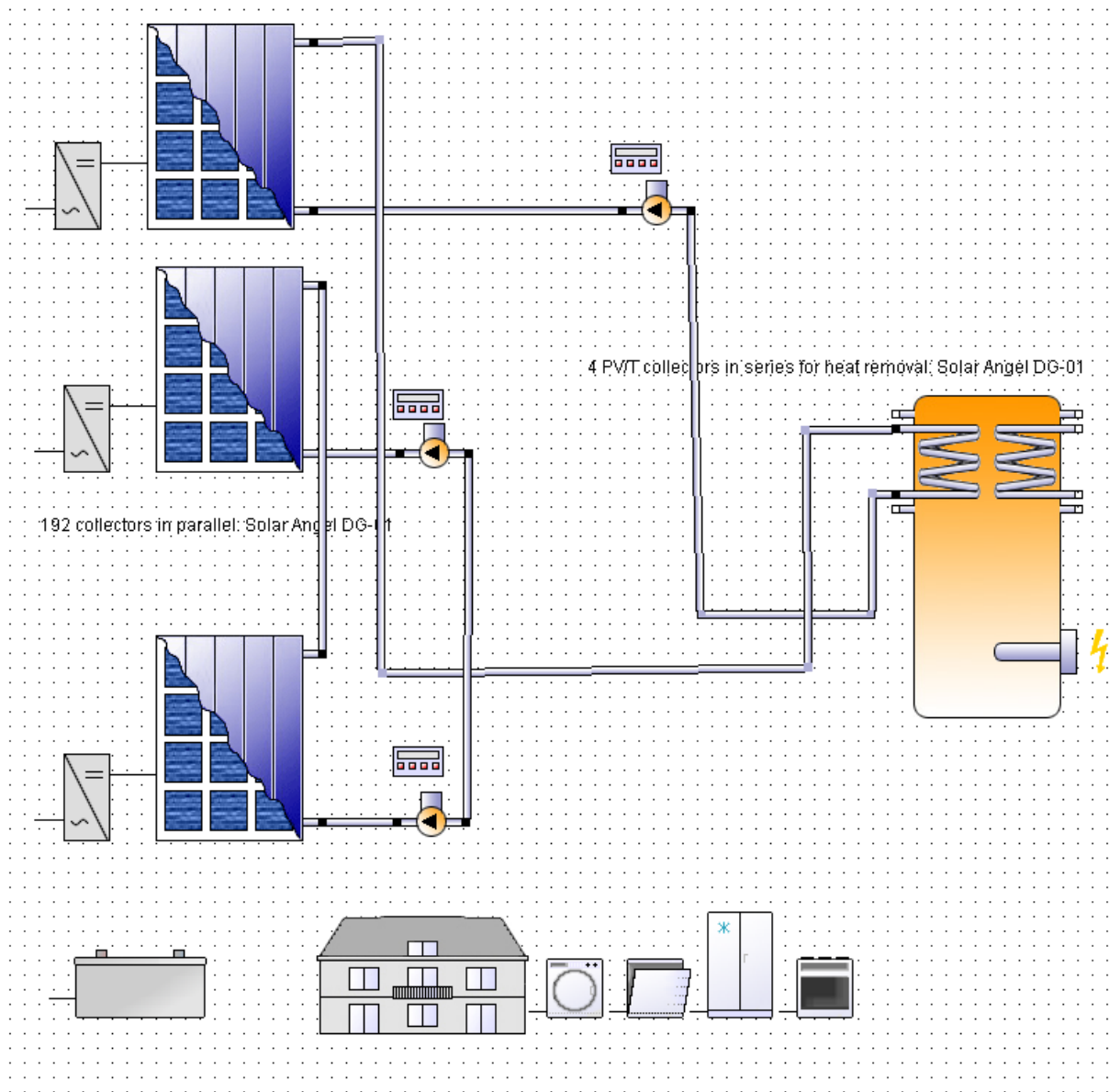


Figure 98: Schematic for PV/T in UK case study

Now the battery system can also be considered. With a 70% Depth of discharge (DOD) and 5 days of autonomy that can vary according to the battery selected, the battery capacity as previously defined was 706 Ah, the battery capacity is defined as $706 \times 5 / 0.7 = 5042.85 \text{ Ah}$. This essentially generates 5 days of output without disrupting the 70% DOD. To ensure continuous supply for 5 days, thirty-three 150 Ah batteries are required (or a different Ah battery can be selected). It is also necessary to select a charge controller that is compatible with the battery bank and the array. This can be selected at least 25% larger than the I_{sc} of the panel which also has 192 panels in parallel. Hence the current rating needs to be $1.25 \times 192 \times 8.1 = 1944 \text{ A}$

The battery voltage can be monitored by the state of charge. For a 24 V system, low level warnings would be given at about 23 V and disconnection would occur at around 22 V.

Protection devices should also be added with at least 1.25 times the current rating.

FOR COCHIN:

In order to apply the model and design a system, a 4-bed house case is selected for Cochin based on the results obtained. The electric demand and heat demand can be supplied by an appropriate design, cost and area available

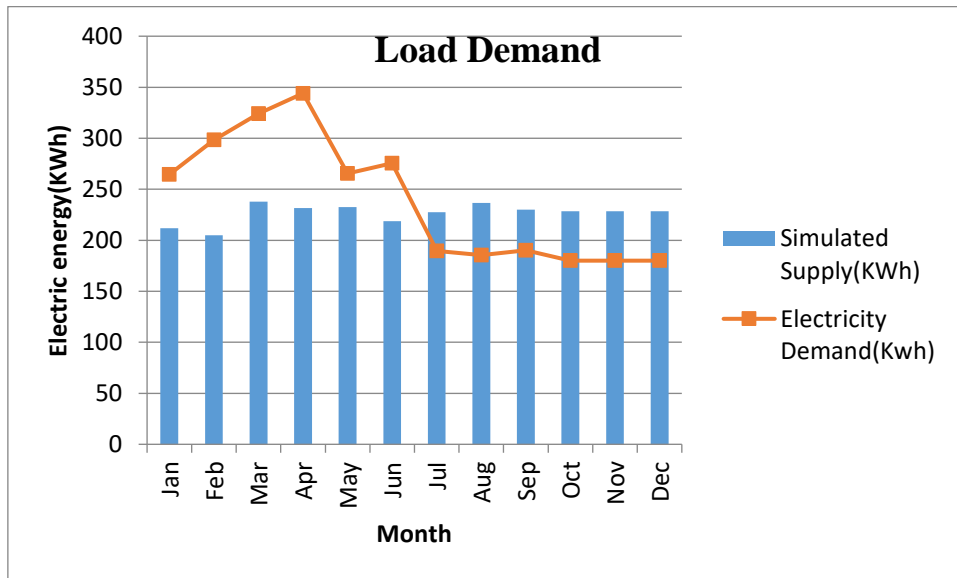


Figure 99: Predicted design for Cochin

Again, as previously followed, the demand is drawn up for the residential case. The gas consumption is not applicable here as the gas is only mainly used for cooking in LPG cylinders and all other appliances use electricity. Over the year 2877Kwh of energy is consumed. With a daily load of 11 KWh, the battery capacity is obtained at 458.33Ah and applying losses leads to a value of 648.3Ah as seen in Figure 99.

Table 11: Array current for Cochin case study

<i>Month</i>	<i>Average Daily Irradiation (kWh/m²) for Kerala</i>	<i>Required Array Current (=daily Ah/irradiation)</i>
<i>January</i>	4.704301075	137.8100571
<i>February</i>	4.903416896	132.2139263
<i>March</i>	5.105491367	126.9809218
<i>April</i>	5.275674412	122.884763
<i>May</i>	4.592056969	141.1785621

<i>June</i>	3.410823985	190.0713736
<i>July</i>	3.567902192	181.7034115
<i>August</i>	4.118912841	157.3959015
<i>September</i>	4.092114049	158.4266695
<i>October</i>	4.169122208	155.500359
<i>November</i>	4.064069177	159.5199224
<i>December</i>	4.359943652	148.6945823

The most demanding month is June as evident from above table with a requirement of 211Ah generation adding the 10% losses. Each panel generates 8.1A. Hence there is a requirement of only 26 panels. As the heat requirement is low, the panels are connected in parallel for maximum current. The heat removal system ensures that the heat stays lower than stagnation. An area of only 40sq.m is needed for all the panels. A survey conducted ensures the use of all 40Sq.m on the roof itself. Utilising a similar calculation, a battery system of 30 batteries of 150Ah is required. A current rating of 263.25A needs to be observed for all protection devices. A final schematic of Cochin is generated as below in Figure 100.

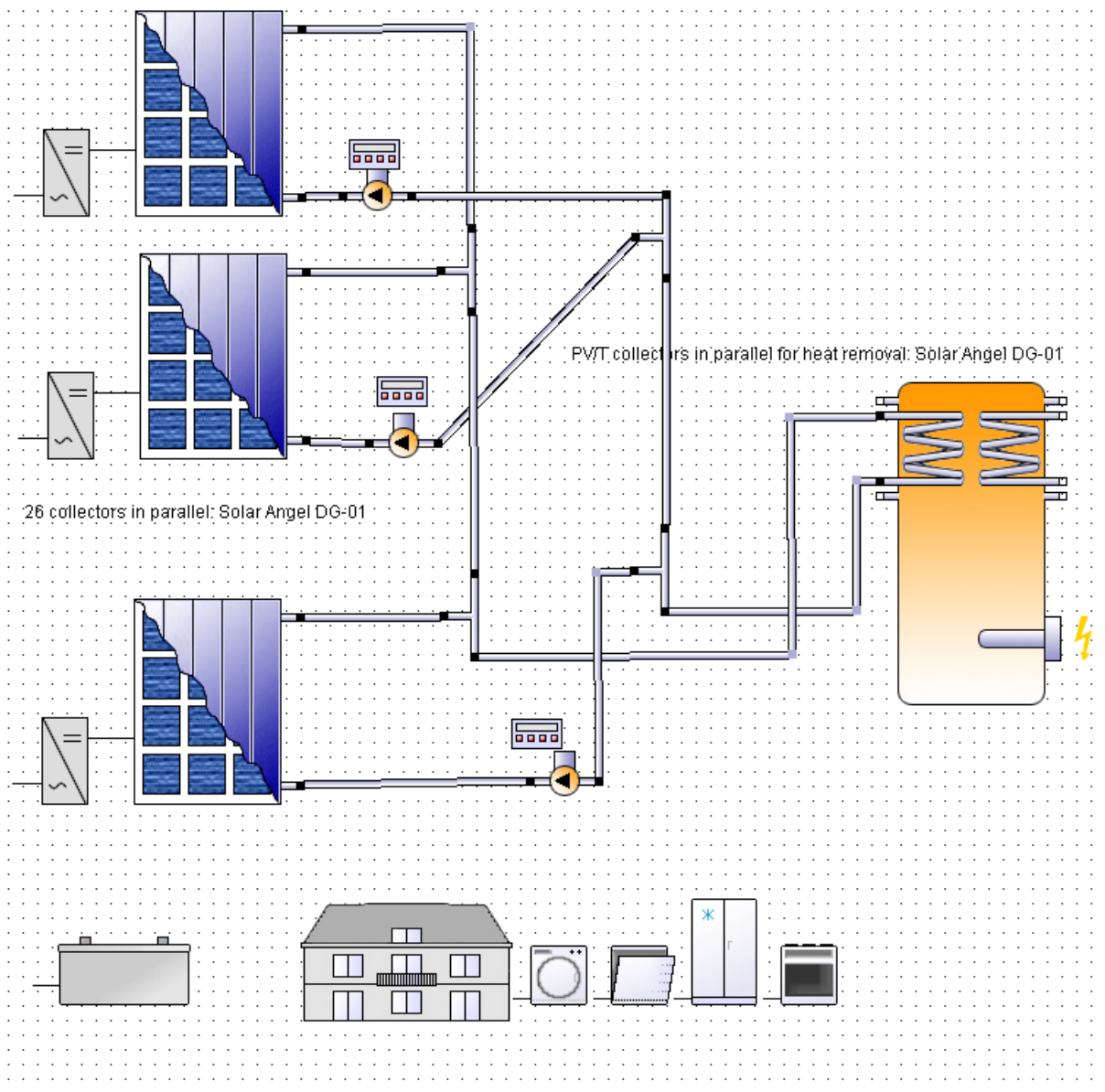


Figure 100: Schematic of Cochin

5.4 Chapter Summary

An extensive result was obtained in order to find the performance and the factors affecting the PV/T system. Major factors were recognised and analysed to find the weightage of the parametric effect on the output.

Right now, the standard system assess the performance of PV/T based on tests with respect to PV and Solar collector but this model helps to analyse all parameters as a whole all the main 8 parameters and then some, as well as to predict the performance of the whole PV/T system without the need to assess it separately.

Through the parallel examination of the displaying and test outcomes, the powerful model was approved as having a sensible degree of accuracy. It was discovered that the normal water temperature in the capacity tank (200 liters) developed step by step from 9 °C to 20°C, over the term of the test. The temperature of the PV layer was in the scope of 13 °C during daytime activity, while its highest mean worth was 20 °C. The temperature contrast between the PV layer and HTF was in the scope of 4°C to 7 °C. Analysis of the measurement data indicated that the thermal and electrical outputs corresponded to 49% and 9.6%.

This part of the research will further help to predict system performance over a long-term scheme in different climate regions and provides the basis for the following economic analysis in the next chapter. Error analysis is also briefly addressed from the theoretical and experimental sides, indicating that the discrepancies were more likely to have come from the theoretical assumptions.

The dynamic model was checked as having the option to foresee to a sensible degree of precision. The system simulations were carried out in 0.025kg/s MFR. This is also seen to improve thermal output to maximum of 0.04kg/sec.

CHAPTER 6. EXERGY AND ECONOMIC ANALYSIS

6.1 Introduction

In this chapter, a feasibility study of the prototype system for use in Newcastle, Lisbon and Cochin is carried out, involving an annual energy performance prediction, economic analysis and environmental sustainability assessment. The main focus of this chapter is to analyse the annual performance generated from the dynamic simulation model from chapter 4, understand the economic benefits of the designed with conventional water heating systems and provide an exergy analysis to understand the quality of the model and the prototype in three different locations.

A good level of agreement was realised between the simulated dynamic model and the real-time test results. The dynamic model can now be utilised for calculating the annual operational performance of any chosen system with the variation of input parameters.

6.2 Annual Operational Performance

The average monthly weather data for the three different climatic conditions is summarised in Figure 101 from data collected in chapter 4.

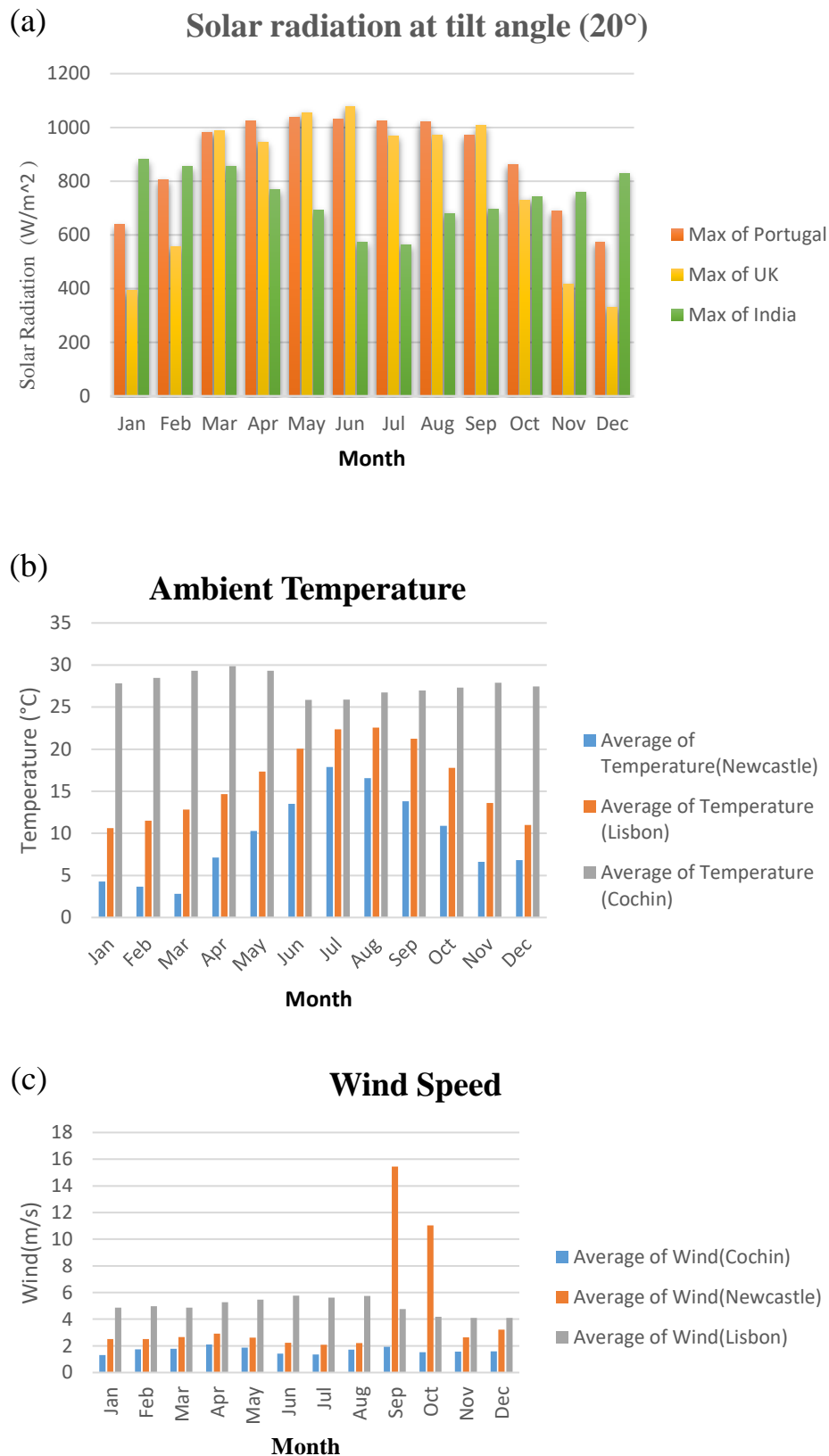


Figure 101: Location based (a) monthly radiation (b) temperature (c) wind speed for all three cases Cochin and Portugal values were purchased from Whitebox weather technologies and UK data is obtained from the USB weather data. The economic data was obtained from the Newcastle admin cost directory. Using this data, an appropriate PV/T model can be designed

by carefully selecting components that can maintain the PV temperature below 25°C. This can be done for a higher mass flow rate and more parallel connection. Like this model, any conditional design can be generated to investigate the output and design a system based on these results. This means that the PV/T design can be modified to each design requirement. During the simulation, it was assumed that the system operation is continuously monitored through the day and night. The PV/T panel installation angle was set to the same level as the local altitude in the three selected regions. The initial temperature of the water stored in the tank was the water temperature at a height of 0.5 m below ground level.

By running the established dynamic model from data in Figure 101, the hourly performance data for the prototype system, the average temperature of the PV layer on a typical day during different months at different locations was obtained. The PV temperature presents the same trend of variation (Figure 102) as for the solar radiation and air temperature. Its maximum figure reached over 38 C during March and April, and the minimum went down to less than 5 C during December and January.

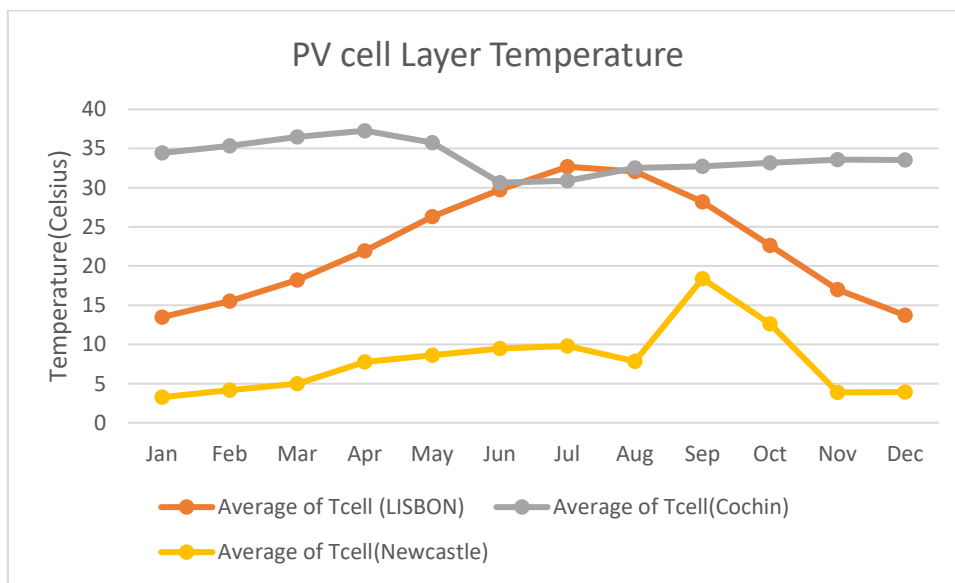


Figure 102: PV cell temperature variation in three cases

6.3 Economic Analysis of the Lab Prototype

The capital cost of the prototype PV/T heat pump system was estimated by adding together the individual prices of all the system components and considering appropriate commercial profits. Table 12 and Figure 103 provides a list of cost breakdowns and indicates that the initial cost of such a system is GBP 9,916.66 (excluding VAT). The thermal network of the PV/T was the most expensive of the system components, accounting for 19% of the total component only cost followed by PV/T solar modules (17.4%).

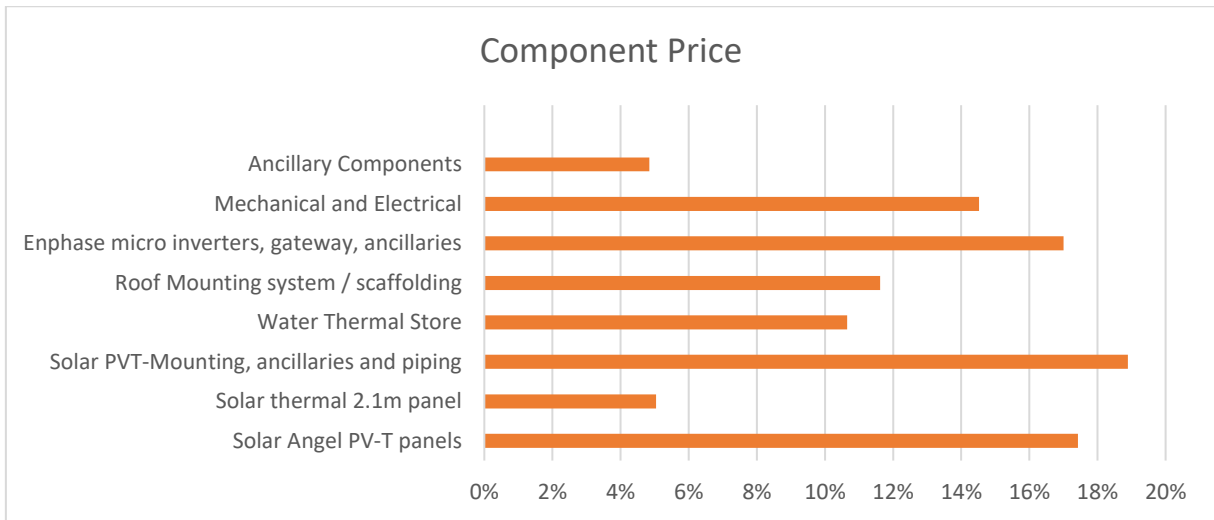


Figure 103: Component prices

Table 12: Cost breakdown of LAB system installed (from the Newcastle University cost directory)

CODE	DESCRIPTION	QTY	UNIT PRICE	TOTAL
1	Solar Angel PV-T panels	4	£450.00	£1800
2	Solar thermal 2.1m panel	1	£520.65	£520.65
3	Solar PV/T-Mounting, ancillaries and pipework	1	£1,950.49	£1,950.49
4	Roof Mounting system / scaffolding	1	£1,200.00	£1,200.00
5	Enphase micro inverters, gateway, ancillaries	1	£1,755.52	£1,755.52
6	Labour mechanical, documentation & Electrical	1	£1,800.00	£1,800.00
7	Commissioning of system	1	£200.00	£200.00
8	Ancillary Components	1	£500.00	£500.00
9	Delivery	1	£200.00	£200.00
10	DL2 RESOL data-logger optional	1	£240.00	£240.00

11	Water Thermal store	2	£550.00	£1100.00
12	Optional RHI-Heat meters	0	£700.00	£0.00
			Total Ex VAT and other Labour charges	£9,916.66

The cost breakdown is further lumped as different energy systems from the Figure 104 below.

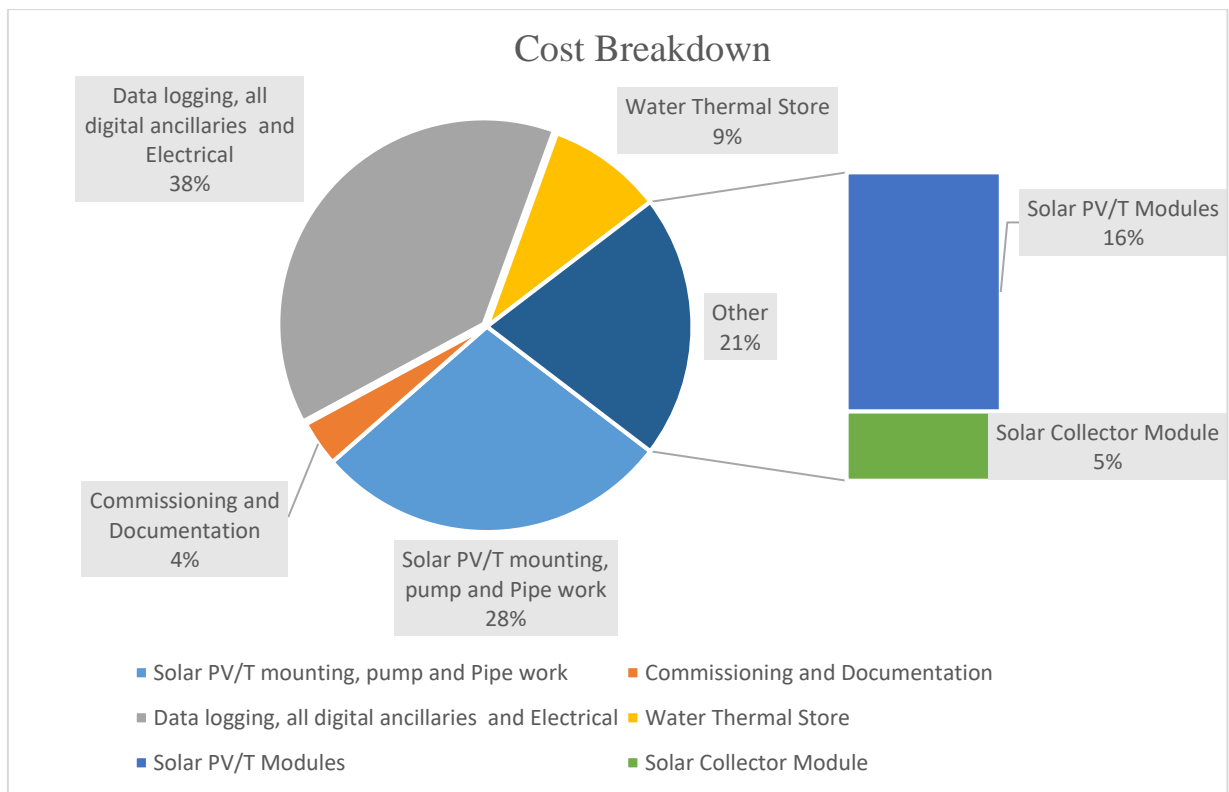


Figure 104: Cost breakdown of installation

To install a heating system, it may be conceivable to get funds through the administration's inexhaustible approach, for example, the Renewable Heat Incentive (RHI), which is proposed to energize the take-up of sustainable warming advancements inside family units, networks and organizations or through the arrangement of budgetary impetuses(Ofgem, 2017).

6.4 Exergy Analysis

The energy of PV cells is around 12 to 17% even though this is low, the top of the line exergy type of energy is changed over to profitable power. However, the solar thermal collectors

have a higher efficiency of around 80% in ambient conditions and 60 to 50% under normal operating conditions and it generates high efficiency high exergy energy.

However, if they can the two units are combined to generate PV/T collector the exergy and energetic energy can be improved to 20% and 70%, under these basic premises as this technology showcases a reasonable and promising future. Further investigation needs to be done in terms of exergy as energy analysis has a few limitations and exergy analysis provides a more practical method of understanding the energy that is generated and gives them more quantifiable way to understand and redefine the system energy(Fudholi et al., 2018). The energy efficiency is usually identified through the first law of thermodynamics while exergy analysis is conducted based on the second law of thermodynamics. Exergy analysis for PV/T (based on first and second laws of thermodynamics) by Chow was based on net exergy output rate and by Tiwari et. al., was based on exergy losses which have errors at low solar radiation(Chow et al., 2009, Tiwari et al., 2015). The limitations of energy-based analysis are summarised as follows:

- a. It does not provide a measure of how nearly the system performance approaches ideal value
- b. Energy losses do not represent the true losses that exist to generate the desired product
- c. Temperatures of supply, recoverable energy source and surroundings are not included.

The exergy analysis is done in order to obtain the quality of the output obtained calculated from energy analysis. And it can be elaborated in the following equations where Ex_{in} and Ex_{out} represents the exergy input and output. Ex_{out} is the sum of thermal exergy($Ex_{thermal}$) and electric exergy($Ex_{electrical}$). The difference of input and output exergy is called destructed exergy(Ex_f).

$$\sum Ex_{in} - \sum Ex_{out} = \sum Ex_f \quad (6-1)$$

$$\sum Ex_{out} = \sum Ex_{thermal} + \sum Ex_{electrical} \quad (6-2)$$

Where

$$Ex_{in} = A_c N_c I(t) \left[1 - \frac{4}{3} \left(\frac{T_a}{T_s} \right) + \frac{1}{3} \left(\frac{T_a}{T_s} \right)^4 \right] \quad (6-3)$$

$$Ex_{electrical} = \eta_c A_c N_c I(t)$$

(6-4)

$$Ex_{thermal} = Q_u \left[1 - \frac{T_a + 273}{T_{fo} + 273} \right] \quad (6-5)$$

T_s is the sun temperature at 6000K. Exergy analysis is important to understand the economic behaviour or life cycle cost of the PV/T. The exergy output (Ex_{out}) for the single unit PV/T under Newcastle weather conditions in an annual year was compiled to be 1307.428KWh while exergy input was summed up to be 9805.166KWh. Under Cochin weather conditions, the exergy output was 2302.846KWh and exergy input was 15049.924KWh.

The total exergy efficiency (η_{ex}) of the PV/T is defined in equation 6-6 and found be 13.33% for Newcastle and 15.3% for Cochin. Various modelling methods has established the exergy efficiency for a PV/T system and the value varied changing from ~10% to 17% with respect to mass flow rate. However, the mass flow rate effect on exergy is not as significant as on energy.

$$\eta_{ex} = 1 - \frac{\sum Ex_f}{\sum Ex_{in}} \quad (6-6)$$

The embodied energy for a PV/T is defined as the combined energy of all the collector components needed to work as a whole unit, it also includes the energy needed to manufacture the PV cells and the other component layers of the PV/T. The usual total embodied energy for one FPC collector (including components) of nearly 2m² is taken as 1715KWh and the embodied energy of the same area PV unit is around 607KWh {Tiwari, 2016 #1539}. If the pump energy can be obtained from the PV of around 12.61KWh, then the other embodied energy is the storage systems which is 150KWh and 121.4KWh for battery.

Then for a PV/T unit the total embodied energy (E_{em}) is 2048.56KWh. The embodied energy distribution of a PV/T system is shown in Figure 105.

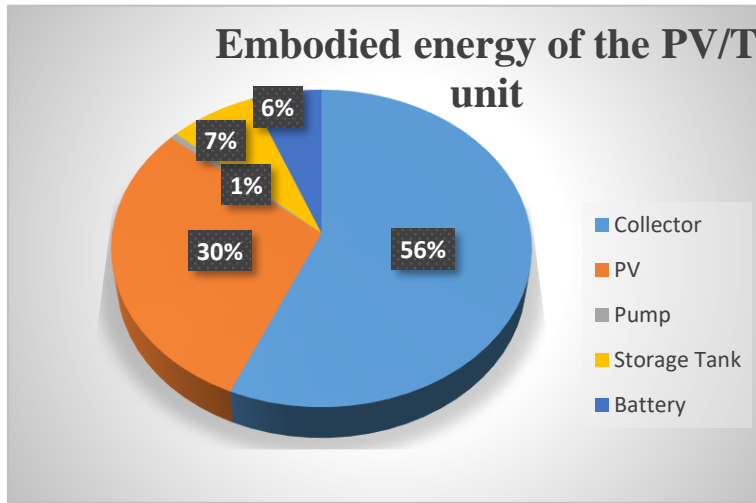


Figure 105: Embodied energy of PV/T

This energy can help to define the energy payback time (EPBT) for the system which is the ratio of embodied energy (E_{em}) and high-grade annual exergy output of the system (E_{out}).

$$EPBT = \frac{E_{em}}{E_{out}} \quad (6-7)$$

When EPBT is low, the system is effective. Annual energy high grade exergy output from the PV/T system is 1307.428KW for Newcastle. The EPBT for Newcastle is 1.56 years if the pump is sustained by the PV and thereby the EPBT is higher while for Cochin EPBT is 0.88 years which can make the system a stand-alone unit. The inverse of EPBT is called energy production factor (EPF) where the value (limits to one) determines if the PV/T system is sensible or not. The EPF here for Newcastle 0.63 determining that the PV/T system is quite not quite feasible in terms of exergy, while for Cochin it is 1.136 which leans toward a better quality of exergy. Using this information to scale up for Newcastle and Cochin residential case studies, the EPF, EPBT and life cycle cost efficiency(LCCE) as from equation 6-7 is generated.

$$LCCE = \frac{Ex_{out}T - E_{em}}{E_{sol}T}$$

(6-8)

A summary of the average values of EPBT, EPF and life cycle cost efficiency(LCCE) after scaling up are given in the Table 13 .

Table 13: Exergy analysis for Newcastle and Cochin

Location	EPBT	EPF (on a life-time basis of 25 years)	LCCE
Newcastle(4-bed house)	8.14	3.06	0.106
Cochin(4-bed house)	4.523	5.526	0.232

From Table 13, it is quite evident from an exergy standpoint, the case study at Cochin generates a more favourable output.

6.5 Mean Absolute Error

The mean absolute error is a quantity used to measure how close forecasts or predictions are to the eventual outcomes. The mean absolute error (MAE) is given by where X_i =predicted value and Y_i =true value. MAE is chosen to as the number of test samples are small.

$$MAE = \frac{1}{N} \sum_{i=1}^N |X_i - Y_i| \quad (6-9)$$

It was discovered that specific contrasts existed between the demonstrating and test aftereffects of the systems trademark parameters, i.e., the temperatures of the component segments, the electric efficiencies, and the thermal coefficients. When MAE is calculated it is found that for electric energy it was 5.94KW and MAE for heat energy was 58.54KW .

The minor disparity could have been brought about by both hypothetical and estimation mistakes. For the hypothetical examination, some disentangled suppositions and experimental recipes were made and used, for example, the wrong oversight of the thermal limits of the two EVA layers, erroneous construction for the thermal pipe by ignoring the fluid losses during its transportation, and may have been potential explanations behind unexplained losses. For the estimations, factors like erroneous instruments/sensors, off base establishment of indicators, may have caused the deviation in the testing figures concerning forecast. In any case, inferable from the devoted apparatus development, the chosen test gadgets and the cautious arrangement, the investigation results appear to be increasingly dependable and in this manner there ought to be further enhancement for the PV/T models.

6.6 Sensitivity and Uncertainty

To understand the effect of the parameters on the efficiency and overall performance a sensitivity analysis will be helpful to generate a reference standard for all parameters (Ji et al., 2007). “*Statistics is a mathematical science pertaining to the collection, analysis, interpretation or explanation and presentation of data. It also provides tools for prediction and forecasting based on data*” (Goossens and Kerschaefer, 1999, Tripanagnostopoulos et al., 2000). Statistical analysis is available to a wide variety of fields whereas Statistical methods analyse a collection or a set of data in a more comprehensive method. This is identified by understanding patterns in data that has randomness and uncertainty in the observation this pattern is then used to understand the relation of the correlation between various factors and a conclusion can be drawn from the experimental analysis. In the dynamic model studied here, the result is first validated by comparing experimental results with the system operating temperatures and gains on an actual weather data. There was a good agreement between the experimental and validated result this same dataset can be used to carry out a sensitivity analysis it was also assumed that the initial water temperature is the same as the ambient temperature and the initial boundary conditions is also said to be at ambient temperature.

For all simulation runs, the initial water-temperature in the tank was set at the mean ambient temperature of 20°C. Subsequently the working temperature and efficiency values were determined and compared along with the mean, mode, median and RMS (Sarhaddi et al., 2010). For example, $(T_m - T_a)$ can be the system reference.

The main goal of a sensitivity analysis is to understand the effect of the parameters in the model on the output. This type of analysis is used to point out the inadequate aspects in the model. Once an observation is made, the model can easily be modified to rectify these issues. In practical modelling, this analysis is rectified by changing the unstable parameters and running simulations for a stable response for a similar input. If ‘P’ is the parametric variation and ‘x’ is the dependant variable, in this scenario, it is the temperature of the PV/T unit, equation 6-10 describes the selected variable response.

$$S = [\partial x / x] / [\partial P / P] \quad (6-10)$$

Sensitivity analysis in effect estimates the effect of uncertainties in the input being affecting the output. The mathematical models are described as the forward sensitivity analysis (FSA) and adjoint sensitivity analysis (ASA). The FSA is used when small variation in the input generated small variations in the output as the derivative of the output itself. Consider that the small changes generate a response function described by ‘TF’ and the model parameters that are

changed are described by 'p'. Then FSA can be defined mathematically as normalized sensitivity indexes shown in the following equations (6-10 and 6-11). FSA generates the variation according to ∂p and provides the output variation by ∂u .

$$S_{u_p} = \lim_{\partial p \rightarrow 0} \left(\frac{\partial u}{u} \right) \left(\frac{\partial p}{p} \right)^{-1} = \left(\frac{p}{u} \right) \frac{\partial u}{\partial p} \quad (6-11)$$

$$S_{TF_p} = \lim_{\partial p \rightarrow 0} \left(\frac{\partial TF}{TF} \right) \left(\frac{\partial p}{p} \right)^{-1} = \left(\frac{TF}{p} \right) \frac{\partial u}{\partial p} \quad (6-12)$$

The model presented here is a dynamic model, this means that the sensitivity indexes depend on the time and the parametric variation on time. If the mathematical model is a dynamical system, then the sensitivity indexes can now depend on time and the relative importance of the parameters can also depend on time and thereby a dynamic factor is introduced.

Uncertainty analysis can be applied to any model that has assumptions and generates an error due to unpredictability and lack of accuracy of those conditions. This is applicable to the prediction of data through physical measurements that were done or that is instantaneously generated. Some of the factor that is responsible for this is mentioned below.

- a) The accuracy of the mathematical model representing the physical structure of the real-life PV/T unit.
- b) The number of assumptions in the numerical analysis of the method and the accuracy and stability of the method in various situations
- c) The initial and boundary conditions that were chosen.
- d) The input data and design parametric limitations
- e) Unknown or unpredictable factors.

There are certain uncertainties that cannot be controlled as mentioned in the chapter 5. The variable factors of input and design parameters can be adjusted to reduce error as this readily available.

CHAPTER 7. CONCLUSION AND FUTURE WORK

7.1 Conclusion

The research has provided a thorough examination of different methods and their accuracy to determine performance and an improved model has been redesigned, validated and applied for residential buildings at two different locations. This was tackled with the use of critical literature review, optimal modelling method through analysis of several PV/T systems, validation of simulation model, application to extend for redesigning residential buildings and laboratory testing for predicting higher performance.

It can be concluded from chapter 5 that a higher heat gain output can be extracted from the panels if the mass flow rate is increased, the output from one module can be matched with the maximum thermal output of the system. This is one of the factors used for controlling the output temperatures. The temperature band width was also controlled for generating a better temperature value. The PV/T system can achieve a 3% improvement in electric efficiency. PV/T can work at 16% electrical efficiency by regulating thermal factors appropriately otherwise; it drops by 3% in summer. Thus, case study results suggest that the electricity generated at the Portugal site reduces, due to extreme ambient temperatures; however, this can be improved if the flow rates are varied. This indicates that even at high radiation, high temperature is the most affecting factor. The model has seen an increase in heat gain during the summer months. The electric gain varies when tilt angles are varied, and a higher thermal output is produced when the mass flow rate is increased from the initial constant value of 0.025kg/s to 0.04kg/s as the thermal output is directly proportional the heat removal factor. A comparison between simulated and available actual electricity energy data suggest that there is a variation in energy generated caused due to weather data error and fixed mass flow rate (0.04kg/sec). The electric gain is also higher when the excess temperature is removed from the system and a higher output is produced when the mass flow rate is increased from the initial constant value of 0.025kg/s. However, the thermal gain while remaining high shows a consistent output and this varies with varying mass flow rate. A validation was drawn with respect to simulated and measured values and only 4.2% error was observed

It was observed that flow rates, heat removal factor, latitude and longitude as well as the fluid used to remove heat affect the system more than other factors like nominal operating cell temperature, packing density and stagnation temperature affect the performance of the system of which MFR has the highest influence. The efficiency of the output was also affected by the packing factor of the PV cells.

It has also to be noted that the exergy efficiency was found to be at 10.6% for Newcastle case study and the system was found to be worthwhile with an energy payback period of 8.14 years while exergy efficiency at Cochin was found to be at 23.2 % at EPBT of 4.5 years, when the inlet flow temperature was maintained at 30°C emphasising electric output. After scaling up to meet the design parameters of the case studies, the EPF for Newcastle was found to be 3.06 while for Cochin the EPF is found to be 5.52. This indicate that the exergy from the PV/T is feasible for Cochin more than it is for Newcastle.

7.2 Advantages

Some of the main advantages of the system is considered when the space for installation is limited and during periods of high-water demand. As this project signifies standard compliance with EN12975 and ISO 9806, it is easy to replicate the results when standardised test conditions need to perform. This is also reusable for other projects like including desiccant system as storage for low grade heat.

7.3 Errors and Challenges

Errors happen due to cloudy days, shaded parts, dust accumulation, constant thermal conductivity and errors in data measurements.

One of the main challenges was data extraction from the USB. As the system installed was extremely new and advanced, there was a need to learn and master the data analytics and jargon to understand the nature of system. The entire dataset had to be relearnt and constant communication with different parties and delays in responses was a hurdle. The PQubes made aware of the issues and trouble shooting in the later stages of data collection, hence meteorology data at no load output was taken for comparison with PQubes. The flow meter sensors had difficulty in recording the values. The MFR was used from the three pump levels that are fixed and running at 100% and varying capacity.

7.4 Future Work and Opportunities

Building integrated PV systems (BIPV) is yet another type of PV/T system that has been gaining popularity in recent years. In most instances the PV/T panels will need to be integrated into existing heating, ventilation and air conditioning (HVAC) systems in the building stock. This requires the system controls to be set up properly to optimise the operation of the thermos-electrical sides of the PV/T correctly. Some future prospective technologies that seem promising for the application of the PV/T seems to be in optimised PV-T system control. Investigating thermo-electric generators can be on the next steps in this

project. Understanding a large-scale model of converting low grade heat into electricity is an interesting perspective especially for PV/T system. However, the recordable life cycle analysis can determine if the system is usable enough to pursue for further research. The mass flow rates need to be varied for a higher range to observe canonical differences. A fully flexible control system to optimise the model according to the input conditions is also a foreseeable future for this model. The current lab unit data analyses were done for a week in April. In an ideal situation, yearly data needs to be analysed for further conclusions.

7.4.1 The Module Design

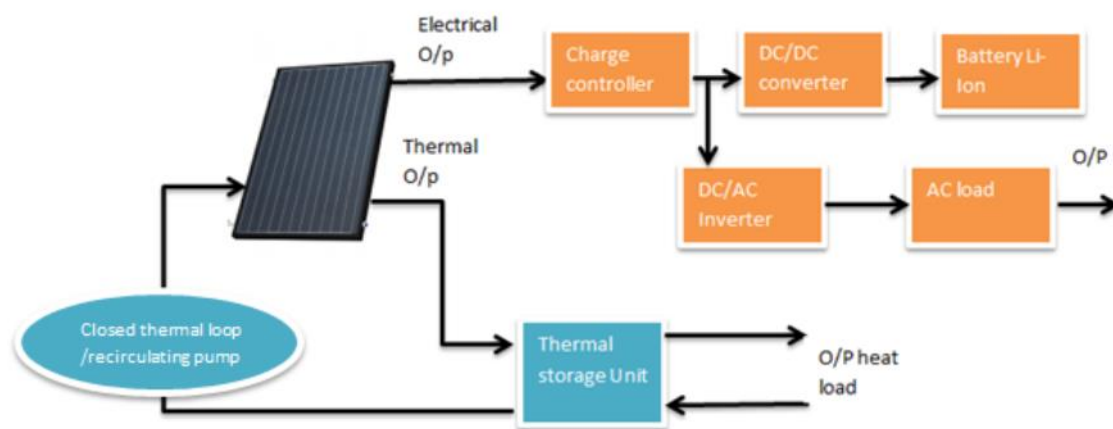


Figure 106: Block diagram of PV/T model

A domestic design using a PV/T system can easily be duplicated with knowledge of its accurate performance. The PV/T tubes used here are made of aluminium. Aluminium has seen a steady increase in market due to copper price rise. Even though the conductivity is low (200–240 W/mK), the aluminium absorber sheet is of lower thickness than the copper equivalent.

To design an optimal PV/T system the main parameters that need to be considered for the model should be

- Spectral behaviour of PV cells
- PV cell solar absorption
- Heat transfer from PV to absorber
- Orientation and inclination
- Integration into space heating/ hot water/DHW and electric system
- Load demand

Utilising the weather data, the simulated model and designing for a system, a general PV/T block diagram can be explored as shown in Figure 106.

7.4.2 Long-Term Reliability

According to the fundamental theory and experimental research studies in the field of PV/T, it has been shown that long-term operations can be achieved through storage. Evaluations can be effectively carried out in long-term but the uncertainties in long term have not been addressed yet especially in the case of building integrated PV/T's. Building integrated PV/T systems address or bring about a huge new challenge to integrate, distribute, test, maintain and assess the performance of the PV/T under uncertain operating conditions. However, since performance of the system can be achieved successfully the behaviour of the PV/T can be carefully studied and designs can be chosen accordingly to provide a better solution to the problem.

7.4.3 Replicability

Solar Keymark certification of PV/T collectors was decided as a standard for PV/T testing. They were three different types of conditions that the PV/T's was subjected to, open circuit, short circuit and maximum power point conditions to find the exact operating point in the IV curve of the system. Research has likewise discovered that PV/T systems that can be advanced for electrical age can get together to 51% of absolute power utilization for a run of the mill local house in the UK whose authority region is 15m², it additionally distinguished that they can produce a 2% greater power ordinary PV asset. The PV/T systems can be adjusted to be utilized in blend with systems with heat pumps, absorption or desiccant systems. Consequently they can be replicable when the exhibition is precisely anticipated (Herrando et al., 2014).

7.4.4 Policy Support

Appropriate policy support provides a more effective way to use renewable and achieve their targets. Policymakers have a major role in providing building energy saving and reducing environmental pollution through different market players. Local policy makers should be able to take market decisions that contribute to reduce market problems by providing subsidies and financial support to PV/T systems as well as their conventional counterparts. PV/T standards and regulations has not yet been established and hence there is a difficulty in actually providing policy regulations from the government however specific policies can be used to retrofit or integrate into conventional systems and hence deployment of such technology should be able to provide respective financial benefit for the consumers.

PV/T investors and industrial PV and solar collector partners feel that the scope of PV/T is realisable. However, for this to turn into a reality, PV/T system needs to be used as a combination with heat pumps, absorption refrigeration or with PCM storage.

7.4.5 Present and Future Market for PV/T

There have been several areas that were identified by the department of business Energy and industrial strategy to display the higher level of efficiency of PV/T needs to generate. They are

- Compatibility of PV/T product data among various factors
- The reliability of such a report
- Performance data
- Integrity of cost
- Effect other markets may have on the future of PV/T

It is expected that hundreds of PV/T system will be installed in the coming years and even though the technology would not be eligible for the FIT and the domestic RHI scheme, it will still produce a massive impact on the market of PV/T's. Yet, there is no such product specification or recommendation for PV/T that addresses factors like

- Solar irradiance
- Ambient temperature
- Heat and electricity demand
- System control like flow rates and operational temperatures
- Thermal storage capacity
- System losses

The majority of the reports and datasets only provide one or two of these factors and some of them were collected manually from metre readings, they might be providing errors in aggregated data and as such this project will be a helpful foot across to address all the factors required to assess the performance of PV/T and standardise such a system on a global level.

References

- Abdalla, O., Rezk, H. & Ahmed, E.M. (2019) 'Wind Driven Optimization Algorithm Based Global Mppt for Pv System under Non-Uniform Solar Irradiance', *Solar Energy*, 180, pp. 429-444.
- Abedi, S., Alimardani, A., Gharehpetian, G.B., Riahy, G.H. & Hosseini, S.H. (2012) 'A Comprehensive Method for Optimal Power Management and Design of Hybrid Res-Based Autonomous Energy Systems', *Renewable and Sustainable Energy Reviews*, 16(3), pp. 1577-1587.
- Akhtar, N. & Mullick, S.C. (1999) 'Approximate Method for Computation of Glass Cover Temperature and Top Heat-Loss Coefficient of Solar Collectors with Single Glazing', *Solar Energy*, 66(5), pp. 349-354.
- Al Tarabsheh, A., Ghazal, A., Asad, M., Morci, Y., Etier, I., El Haj, A. & Fath, H. (2016) 'Performance of Photovoltaic Cells in Photovoltaic Thermal (Pvt) Modules', *IET Renewable Power Generation*, 10(7), pp. 1017-1023.
- Alam, M.S. & Alouani, A.T. (2010) 'Dynamic Modeling of Photovoltaic Module for Real-Time Maximum Power Tracking', *Journal of Renewable and Sustainable Energy*, 2(4), p. 043102.
- Aleksiejuk, J., Chochowski, A. & Reshetiuk, V. (2018) 'Analog Model of Dynamics of a Flat-Plate Solar Collector', *Solar Energy*, 160, pp. 103-116.
- Ampuño, G., Roca, L., Berenguel, M., Gil, J.D., Pérez, M. & Normey-Rico, J.E. (2018) 'Modeling and Simulation of a Solar Field Based on Flat-Plate Collectors', *Solar Energy*, 170, pp. 369-378.
- Araneo, R., Grasselli, U. & Celozzi, S. (2014) 'Assessment of a Practical Model to Estimate the Cell Temperature of a Photovoltaic Module', *International Journal of Energy and Environmental Engineering*, 5(1).
- Ascher, U.M. (2011). *A First Course in Numerical Methods*, Philadelphia, Pennsylvania : Society for Industrial and Applied Mathematics SIAM, 3600 Market Street, Floor 6, Philadelphia, PA 19104.
- Aste, N., Del Pero, C. & Leonforte, F. (2012) 'Optimization of Solar Thermal Fraction in Pvt Systems', *Energy Procedia*, 30, pp. 8-18.
- Aste, N., Leonforte, F. & Del Pero, C. (2015) 'Design, Modeling and Performance Monitoring of a Photovoltaic-Thermal (Pvt) Water Collector', *Solar Energy*, 112, pp. 85-99.
- Atkin, P. & Farid, M.M. (2015) 'Improving the Efficiency of Photovoltaic Cells Using Pcm Infused Graphite and Aluminium Fins', *Solar Energy*, 114, pp. 217-228.
- Avezov, R.R., Akhatov, J.S. & Avezova, N.R. (2011) 'A Review on Photovoltaic-Thermal (Pv-T) Air and Water Collectors', *Applied Solar Energy*, 47(3), pp. 169-183.
- Ayvazoğlu, Ö. & Filik, Ü.B. (2018) 'Estimation Methods of Global Solar Radiation, Cell Temperature and Solar Power Forecasting: A Review and Case Study in Eskişehir', *Renewable and Sustainable Energy Reviews*, 91, pp. 639-653.
- Balcombe, P., Rigby, D. & Azapagic, A. (2015) 'Environmental Impacts of Microgeneration: Integrating Solar Pv, Stirling Engine Chp and Battery Storage', *Applied Energy*, 139, pp. 245-259.
- Barengi, C.F. (2012) 'Chaos with Matlab', in.
- Battersby, S. (2019) 'News Feature: The Solar Cell of the Future', *Proceedings of the National Academy of Sciences of the United States of America*, 116(1), pp. 7-10.
- Beikircher, T., Osgyan, P., Reuss, M. & Streib, G. (2014) 'Flat Plate Collector for Process Heat with Full Surface Aluminium Absorber, Vacuum Super Insulation and Front Foil', *Energy Procedia*, 48, pp. 9-17.
- Bhattacharai, S., Oh, J.H., Euh, S.H., Kafle, G.K. & Kim, D.H. (2012) 'Simulation and Model Validation of Sheet and Tube Type Photovoltaic Thermal Solar System and Conventional Solar Collecting System in Transient States', *Solar Energy Materials and Solar Cells*, 103, pp. 184-193.
- Buonomano, A., Calise, F., Palombo, A. & Vicidomini, M. (2016) 'Bipvt Systems for Residential Applications: An Energy and Economic Analysis for European Climates', *Applied Energy*, 184, pp. 1411-1431.
- Burton, P.D., Hendrickson, A., Ulibarri, S.S., Riley, D., Boyson, W.E. & Bruce H. King (2016) *Journal of Photovoltaics*.
- Calise, F., D'accadia, M.D. & Vanoli, L. (2012) 'Design and Dynamic Simulation of a Novel Solar Trigenation System Based on Hybrid Photovoltaic/Thermal Collectors (Pvt)', *Energy Conversion and Management*, 60, pp. 214-225.

- Carmona, M. & Palacio, M. (2019) 'Thermal Modelling of a Flat Plate Solar Collector with Latent Heat Storage Validated with Experimental Data in Outdoor Conditions', *Solar Energy*, 177, pp. 620-633.
- Cencertificationcommitte (2018) 'Specific Cen Keymark Scheme Rules for Solar Thermal Products'. Madrid, pp. 1-32.
- Chandel, S.S. & Aggarwal, R.K. (2011) 'Estimation of Hourly Solar Radiation on Horizontal and Inclined Surfaces in Western Himalayas', *Smart Grid and Renewable Energy*, 02(01), pp. 45-55.
- Charalambous, P.G., Maidment, G.G., Kalogirou, S.A. & Yiakoumetti, K. (2007) 'Photovoltaic Thermal (Pv/T) Collectors: A Review', *Applied Thermal Engineering*, 27(2-3), pp. 275-286.
- Cho, H.I., Yeo, S.M., Kim, C.H., Terzija, V. & Radojević, Z.M. (2009) 'A Steady-State Model of the Photovoltaic System in Emtp', *International Conference on Power Systems Transients*. Japan. pp. 1-6.
- Chow, T.T. (2003) 'Performance Analysis of Photovoltaic-Thermal Collector by Explicit Dynamic Model', *Solar Energy*, 75(2), pp. 143-152.
- Chow, T.T. (2010) 'A Review on Photovoltaic/Thermal Hybrid Solar Technology', *Applied Energy*, 87(2), pp. 365-379.
- Chow, T.T., Pei, G., Fong, K.F., Lin, Z., Chan, A.L.S. & Ji, J. (2009) 'Energy and Exergy Analysis of Photovoltaic-Thermal Collector with and without Glass Cover', *Applied Energy*, 86(3), pp. 310-316.
- Cibse (2015) 'Solar Radiation, Longwave Radiation and Daylight'. CIBSE, pp. 1-75.
- 'A Comparison of Methods to Estimate Hourly Total Irradiation on Tilted Surfaces from Hourly Global Irradiation on a Horizontal Surface', (Year).
- Cremers, J., Mitina, I., Palla, N., Klotz, F., Jobard, X. & Eicker, U. (2015) 'Experimental Analyses of Different Pvt Collector Designs for Heating and Cooling Applications in Buildings', *Energy Procedia*, 78, pp. 1889-1894.
- Daghighi, R., Ruslan, M.H. & Sopian, K. (2011) 'Advances in Liquid Based Photovoltaic/Thermal (Pv/T) Collectors', *Renewable and Sustainable Energy Reviews*, 15(8), pp. 4156-4170.
- Dal Pai, A., Escobedo, J.F., Dal Pai, E. & Dos Santos, C.M. (2014) 'Estimation of Hourly, Daily and Monthly Mean Diffuse Radiation Based on Meo Shadowing Correction', *Energy Procedia*, 57, pp. 1150-1159.
- Danilo Yu, R.G., Cateau, R., Kamel, R., Fung, A., Mohammadi, F. & Raahemifar, K. Validating a Simplified Pv Model against Trnsys Model. Ryerson University.
- De Keizer, C., De Jong, M., Mendes, T., Katiyar, M., Folkerts, W., Rindt, C. & Zondag, H. (2016) 'Evaluating the Thermal and Electrical Performance of Several Uncovered Pvt Collectors with a Field Test', *Energy Procedia*, 91, pp. 20-26.
- De Soto, W., Klein, S.A. & Beckman, W.A. (2006) 'Improvement and Validation of a Model for Photovoltaic Array Performance', *Solar Energy*, 80(1), pp. 78-88.
- Department of Buisness, E.a.I.S.D. (2016) *Evidence Gathering – Low Carbon Heating Technologies*. London: Crown Publishing.
- Department of Business, E.a.I.S. (2016) *Evidence Gathering – Low Carbon Heating Technologies*. UK: Crown.
- Diab, Y., Auger, F., Schaeffer, E. & Wahbeh, M. (2017) 'Estimating Lithium-Ion Battery State of Charge and Parameters Using a Continuous-Discrete Extended Kalman Filter', *Energies*, 10(8), p. 1075.
- Dubey, G.N.T.a.S. (2010) 'Chapter 5. Role of Batteries and Their Uses', in *Fundamentals of Photovoltaic Modules and Their Applications*. Royal Society of Chemistry, pp. 130-156.
- Dubey, S., Sandhu, G.S. & Tiwari, G.N. (2009) 'Analytical Expression for Electrical Efficiency of Pv/T Hybrid Air Collector', *Applied Energy*, 86(5), pp. 697-705.
- Duffie, J.A. & Beckman, W.A. (2005). *Solar Engineering of Thermal Processes (2005)*, USA, John Wiley & Sons Inc.
- Duffie, J.A. & Beckman, W.A. (2013). *Solar Engineering of Thermal Processes*, John Wiley and Sons, Inc.
- Dupeyrat, P., Ménéz, C. & Fortuin, S. (2014) 'Study of the Thermal and Electrical Performances of Pvt Solar Hot Water System', *Energy and Buildings*, 68, pp. 751-755.
- Dutil, Y., Rousse, D.R., Salah, N.B., Lassue, S. & Zalewski, L. (2011) 'A Review on Phase-Change Materials: Mathematical Modeling and Simulations', *Renewable and Sustainable Energy Reviews*, 15(1), pp. 112-130.

- El-Shatter, T.F., Eskander, M.N. & El-Hagry, M.T. (2006) 'Energy Flow and Management of a Hybrid Wind/Pv/Fuel Cell Generation System', *Energy Conversion and Management*, 47(9-10), pp. 1264-1280.
- 'Energy and Exergy Analysis', in.
- Europeancommission (2017a) 'Eu Energy in Figures'. Luxembourg: European Commission, pp. 2-265.
- Europeancommission (2017b) 'Eu Energy in Figures Statistical Pocketbook 2017' Europeancommission. Brussels, pp. 1-265.
- Europeancommission (2017c) 'Report from the Commission to the European Parliament, the Council, the European Economic and Social Committee and the Committee of the Regions'. Brussels: European Commission, pp. 1-18.
- Europeancommission (2019) 2030 Climate & Energy Framework. Available at: https://ec.europa.eu/clima/policies/strategies/2030_en (Accessed: 15/10/2019).
- Faiman, D. (2008) 'Assessing the Outdoor Operating Temperature of Photovoltaic Modules', *Progress in Photovoltaics: Research and Applications*, 16(4), pp. 307-315.
- Feldman, D. & Margolis, R. (2018) 'Q1/Q2 2018 Solar Industry Update'. NREL.
- Felix Regin, A., Solanki, S.C. & Saini, J.S. (2009) 'An Analysis of a Packed Bed Latent Heat Thermal Energy Storage System Using Pcm Capsules: Numerical Investigation', *Renewable Energy*, 34(7), pp. 1765-1773.
- Fudholi, A., Zohri, M., Jin, G.L., Ibrahim, A., Yen, C.H., Othman, M.Y., Ruslan, M.H. & Sopian, K. (2018) 'Energy and Exergy Analyses of Photovoltaic Thermal Collector with V-Groove', *Solar Energy*, 159, pp. 742-750.
- Gaur, A., Ménézo, C. & Giroux--Julien, S. (2017) 'Numerical Studies on Thermal and Electrical Performance of a Fully Wetted Absorber Pvt Collector with Pcm as a Storage Medium', *Renewable Energy*, 109, pp. 168-187.
- Goossens, D. & Kerschaever, E.V. (1999) 'Aeolian Dust Deposition on Photovoltaic Solar Cells: The Effects of Wind Velocity and Airborne Dust Concentration on Cell Performance', *Solar Energy*, 66(4), pp. 277-289.
- Guarracino, I., Mellor, A., Ekins-Daukes, N.J. & Markides, C.N. (2016) 'Dynamic Coupled Thermal-and-Electrical Modelling of Sheet-and-Tube Hybrid Photovoltaic/Thermal (Pvt) Collectors', *Applied Thermal Engineering*, 101(1), pp. 778-795.
- Gueymard, C. (2000) 'Prediction and Performance Assessment of Mean Hourly Global Radiation', *Solar Energy*, 68(3), pp. 285-303.
- Günter Gartler, D.J., Gottfried Purkarthofer, Waldemar Wagner (2004) 'Development of a High Energy Density Sorption Storage System'.
- H. A. Zondag , D.W.D.V., Helden, W.G.J.V., Zolingen, R.J.C.V. & Steenhoven, A.a.V. (2002) 'The Thermal and Electrical Yield of a Pv-Thermal Collector', *Solar Energy*, 72(2), pp. 113-128.
- H. Schranzhofer, P.P., A. Heinz, and W. Streicher (2005) 'Validation of a Trnsys Simulation Model for Pcm Energy Storages and Pcm Wall Construction Elements', *Institute of Thermal Engineering, University of Technology Graz*.
- Haro Velastegui, A., Sanchez Moscoso, R.U., Zavala, G., Llosas Albuérne, Y. & Haber Guerra, R. (2015) 'Modelado De Un Colector Solar De Placas Planas En El Altiplano Ecuatoriano', *Dyna Energia Y Sostenibilidad*, 4(3), pp. [16 p.]-[16 p.].
- Hashim, H., Bomphrey, J.J. & Min, G. (2016) 'Model for Geometry Optimisation of Thermoelectric Devices in a Hybrid Pv/Te System', *Renewable Energy*, 87, pp. 458-463.
- Herrando, M., Markides, C.N. & Hellgardt, K. (2014) 'A Uk-Based Assessment of Hybrid Pv and Solar-Thermal Systems for Domestic Heating and Power: System Performance', *Applied Energy*, 122, pp. 288-309.
- Herrero López, S., López Perez, S., Del Hoyo Arce, I. & Mesonero Dávila, I. (2015) 'Dynamic Modelling of a Flat-Plate Solar Collector for Control Purposes', 118, pp. 419-426.
- Huld, T. (2011) 'Estimating Solar Radiation and Photovoltaic System Performance, the Pvgis Approach' European Commission, J. R. C. I., Italy AFRETEP 1ST Regional Workshop Kampala. Uganda: European Commission, pp. 1-84.
- Huld, T., Friesen, G., Skoczek, A., Kenny, R.P., Sample, T., Field, M. & Dunlop, E.D. (2011) 'A Power-Rating Model for Crystalline Silicon Pv Modules', *Solar Energy Materials and Solar Cells*, 95(12), pp. 3359-3369.
- Hussein, T.a.T. (2012) 'Estimation of Hourly Global Solar Radiation in Egypt Using Mathematical Model', *International Journal of Latest Trends in Agriculture & Food Sciences*, 2(2), pp. 74-82.

- Ibrahim, A., Othman, M., Ruslan, M.H., Alghoul, M., Yahya, M., Zaharim, A. & Sopian, K. (2009) 'Performance of Photovoltaic Thermal Collector (Pvt) with Different Absorbers Design', WSEAS Transactions on Environment and Development, 5.
- Ibrahim, A., Othman, M.Y., Ruslan, M.H., Mat, S. & Sopian, K. (2011) 'Recent Advances in Flat Plate Photovoltaic/Thermal (Pv/T) Solar Collectors', Renewable and Sustainable Energy Reviews, 15(1), pp. 352-365.
- IRENA (2017) 'Turning to Renewables: Climate-Safe Energy Solutions'. Abu Dhabi: International Renewable Energy Agency.
- Iso9806 (2018) Skn_N0106annexj_R2.
- J.K.Tonui & Y.Tripanagnostopoulos (2007) 'Air-Cooled Pv/T Solar Collectors with Low Cost Performance Improvements', Solar Energy, 81(4), pp. 498-511.
- Ji, J., Lu, J.-P., Chow, T.-T., He, W. & Pei, G. (2007) 'A Sensitivity Study of a Hybrid Photovoltaic/Thermal Water-Heating System with Natural Circulation', Applied Energy, 84(2), pp. 222-237.
- Joshi, A.S., Dincer, I. & Reddy, B.V. (2009) 'Thermodynamic Assessment of Photovoltaic Systems', Solar Energy, 83(8), pp. 1139-1149.
- Kader, F.H.a.-E., Said, G., Attia, G. & Fadl, A.M.a.-E. (2006) 'Study of Structural and Optical Properties of Ethylene Vinyl Acetate Copolymer Films Irradiated with Γ -Rays', Egyptian Journal of Physics, 37(2), pp. 111-126.
- Kalogirou, S.A. (2000) 'Use of Trnsys for Modelling and Simulation of a Hybrid Pv–Thermal Solar System for Cyprus', Renewable Energy, 23(2001), pp. 247–260.
- Kalogirou, S.A. (2001) 'Use of Trnsys for Modelling and Simulation of a Hybrid Pv–Thermal Solar System for Cyprus', Renewable Energy, 23, pp. 247–260.
- Kalogirou, S.A. (2009a) 'Environmental Characteristics ', in 2009 (ed.) Solar Energy Engineering: Processes and Systems. USA: Elsevier's Science & Technology Rights pp. 50-122.
- Kalogirou, S.A. (2009b) 'Performance of Solar Collectors', in Solar Energy Engineering: Processes and Systems. USA: Elsevier's Science & Technology Rights pp. 221-256.
- Kalogirou, S.A. (2009c) 'Solar Space Heating and Cooling', in Solar Energy Engineering: Processes and Systems. USA: Elsevier's Science & Technology Rights pp. 323-394.
- Kalogirou, S.A. (2009d) 'Solar Thermal Power System', in Solar Energy Engineering: Processes and Systems. USA: Elsevier's Science & Technology Rights pp. 541-580.
- Kalogirou, S.A. (2009e) 'Solar Water-Heating Systems', in Solar Energy Engineering: Processes and Systems. USA: Elsevier's Science & Technology Rights pp. 257-320.
- Kamali, G.A., Moradi, I. & Khalili, A. (2005) 'Estimating Solar Radiation on Tilted Surfaces with Various Orientations: A Study Case in Karaj (Iran)', Theoretical and Applied Climatology, 84(4), pp. 235-241.
- Kambezidis, H.D. & Psiloglou, B.E. (1997) 'Comparison between Measurements and Models for Daily Solar Irradiation on Tilted Surfaces in Athens, Greece', Renewable Energy, 10(4), pp. 505-518.
- Kanyarusoke, K., Gryzagoridis, J. & Oliver, G. (2016) 'Validation of Trnsys Modelling for a Fixed Slope Photovoltaic Panel', Turkish Journal of Electrical Engineering & Computer Sciences, 24, pp. 4763-4772.
- Katiyar, A.K. & Pandey, C.K. (2010) 'Simple Correlation for Estimating the Global Solar Radiation on Horizontal Surfaces in India', Energy, 35(12), pp. 5043-5048.
- Kharseh, M. 'Solar Radiation Calculation'.
- Khelifa, A., Touafek, K. & Moussa, H.B. (2015) 'Approach for the Modelling of Hybrid Photovoltaic–Thermal Solar Collector', IET Renewable Power Generation, 9(3), pp. 207-217.
- Kim, J.-H. & Kim, J.-T. (2012) 'Comparison of Electrical and Thermal Performances of Glazed and Unglazed Pvt Collectors', International Journal of Photoenergy, 2012, p. 7.
- King, D.L., Boyson, W.E. & Kratochvill, J.A. (2004) 'Photovoltaic Array Performance Model' Sandia Report. US: Sandia National Laboratories, pp. 1-43.
- Kirn, B., Brecl, K. & Topic, M. (2015) 'A New Pv Module Performance Model Based on Separation of Diffuse and Direct Light', Solar Energy, 113, pp. 212-220.
- Koch-Ciobotaru, C., Mihet-Popa, L., Isleifsson, F. & Bindner, H. (2012) 'Simulation Model Developed for a Small-Scale Pv System in Distribution Networks', The 8th International Symposium on Applied Computational Intelligence and Informatics-SACI 2012. Timisoara, Romania. pp. 341-346.

- Koronaki, I.P. & Nitsas, M.T. (2018) 'Experimental and Theoretical Performance Investigation of Asymmetric Photovoltaic/Thermal Hybrid Solar Collectors Connected in Series', *Renewable Energy*, 118, pp. 654-672.
- Kumar, S. & Mullick, S.C. (2010) 'Wind Heat Transfer Coefficient in Solar Collectors in Outdoor Conditions', *Solar Energy*, 84(6), pp. 956-963.
- Kumar, S. & Mullick, S.C. (2012) 'Glass Cover Temperature and Top Heat Loss Coefficient of a Single Glazed Flat Plate Collector with Nearly Vertical Configuration', *Ain Shams Engineering Journal*, 3(3), pp. 299-304.
- Laiti, L., Giovannini, L., Zardi, D., Belluardo, G. & Moser, D. (2018) 'Estimating Hourly Beam and Diffuse Solar Radiation in an Alpine Valley: A Critical Assessment of Decomposition Models', *Atmosphere*, 9(4), p. 117.
- Lämmle, M., Thoma, C. & Hermann, M. (2016) 'A Pvt Collector Concept with Variable Film Insulation and Low-Emissivity Coating', *Energy Procedia*, 91, pp. 72-77.
- Lamnatou, C. & Chemisana, D. (2017) 'Photovoltaic/Thermal (Pvt) Systems: A Review with Emphasis on Environmental Issues', *Renewable Energy*, 105, pp. 270-287.
- Lave, M. (2016) 'Pv Spectral Mismatch: Modeling Options' 5th PV Performance Modeling Workshop [Workshop Material]. 03/09/2017. Sandia National Laboratories 13.
- Lee, H.-J., Kim, S.-Y. & Yun, C.-Y. (2017) 'Comparison of Solar Radiation Models to Estimate Direct Normal Irradiance for Korea', *Energies*, 10(5), p. 594.
- Li, D.H.W., Lou, S.W. & Lam, J.C. (2015) 'An Analysis of Global, Direct and Diffuse Solar Radiation', *Energy Procedia*, 75, pp. 388-393.
- Li, G., Huang, H., Zhang, J. & Zhang, H. (2019) 'Study on the Performance of a Solar Collector with Heat Collection and Storage', *Applied Thermal Engineering*, 147, pp. 380-389.
- Lopez, C.P. (2014a). *Matlab Integral and Differential Calculus*, New York, Springer Science and Business Media.
- Lopez, C.P. (2014b). *Matlab Programming for Numerical Analysis*, New York, Springer Science and Business Media.
- Lu, L., Wang, X., Wang, S. & Liu, X. (2017) 'Analysis of Three Different Sheet-and-Tube Water-Based Flat-Plate Pvt Collectors', *Journal of Energy Engineering*, 143(5), p. 04017022.
- Madani, S., Schaltz, E. & Knudsen Kær, S. (2019) 'An Electrical Equivalent Circuit Model of a Lithium Titanate Oxide Battery', *Batteries*, 5(1), p. 31.
- Martin, N. & Ruiz, J.M. (2001) 'Calculation of the Pv Modules Angular Losses under Field Conditions by Means of an Analytical Model', *Solar Energy Materials & Solar Cells*, 70, pp. 25-38.
- Martín, N. & Ruiz, J.M. (2002) 'A New Model for Pv Modules Angular Losses under Field Conditions', *International Journal of Solar Energy*, 22(1), pp. 19-31.
- Masson, G. & Kaizuka, I. (2018) 'Trends 2018 in Photovoltaic Applications' 23. IEA, pp. 1-88.
- Matuska, T. (2014) 'Performance and Economic Analysis of Hybrid Pvt Collectors in Solar Dhw System', *Energy Procedia*, 48, pp. 150-156.
- Mcintosh, K.R., Cotsell, J.N., Cumpston, J.S., Norris, A.W., Powell, N.E. & Ketola, B.M. (2009a) 'An Optical Comparison of Silicone and Eva Encapsulants for Conventional Silicon Pv Modules: A Ray-Tracing Study', Centre for Sustainable Energy Systems, Australian National University, [Online].
- Mcintosh, K.R., Cotsell, J.N., Cumpston, J.S., Norris, A.W., Powell, N.E. & Ketola, B.M. (Year) 'An Optical Comparison of Silicone and Eva Encapsulants for Conventional Silicon Pv Modules: A Ray-Tracing Study', 2009 34th IEEE Photovoltaic Specialists Conference (PVSC). 7-12 June 2009. pp. 000544-000549.
- Mishra, G.N.T.a.R.K. (2012) 'Solar Energy Is a Direct Source of Energy for Renewable Sources and an Indirect Source of Energy for Nonrenewable Sources Too', in *Advanced Renewable Energy Sources*. Royal Society of Chemistry, pp. 45-109.
- Mongibello, L., Bianco, N., Di Somma, M., Graditi, G. & Naso, V. (2014) 'Numerical Simulation of a Solar Domestic Hot Water System', *Journal of Physics: Conference Series*, 547, p. 012015.
- Mousavi Maleki, S., Hizam, H. & Gomes, C. (2017) 'Estimation of Hourly, Daily and Monthly Global Solar Radiation on Inclined Surfaces: Models Re-Visited', *Energies*, 10(1), p. 134.
- Mubarak, R., Hofmann, M., Riechelmann, S. & Seckmeyer, G. (2017) 'Comparison of Modelled and Measured Tilted Solar Irradiance for Photovoltaic Applications', *Energies*, 10(11), p. 1688.
- Nakedenergy (2018) 'Naked Energy Product', Virtuo. Available at: <https://www.nakedenergy.co.uk/the-product> (Accessed: 01/01/2019).

- Network, S.K. (2018) 'List of Decisions: Solar Keymark Network Meeting in Madrid, March 2018' Network, S. K. Spain: Solar Keymark Network, pp. 1-66.
- Nordmann, T. & Clavadetscher, L. (Year) 'Understanding Temperature Effects on Pv System Performance', Proceedings of 3rd World Conference on Photovoltaic Energy Conversion. pp. 2243–2246.
- Nualboonrueng, T., Tuenpusa, P., Ueda, Y. & Akisawa, A. (2012) 'The Performance of Pv-T Systems for Residential Application in Bangkok', Progress in Photovoltaics: Research and Applications, pp. n/a-n/a.
- Nualboonrueng, T., Ueda, Y., Hirayama, K. & Akisawa, A. (2011) 'A Simulation of the Performance of Pv-Thermal (Pvt) Systems for Residential Application in Tokyo', 38(2).
- Nuru, Z.Y., Arendse, C.J., Khamlich, S. & Maaza, M. (2012) 'Optimization of Alxoy/Pt/Alxoy Multilayer Spectrally Selective Coatings for Solar–Thermal Applications', Vacuum, 86(12), pp. 2129-2135.
- Ofgem (2017) 'An Introduction to the Domestic Renewable Heat Incentive Scheme (New Regulation Changes to Be Read)' Rhi. ofgem.
- Ossenbrink, H., Müllejans, H., Kenny, R. & Dunlop, E. (2012) 'Standards in Photovoltaic Technology', in Comprehensive Renewable Energy. pp. 787-803.
- Ouyang, L., Sun, L., Yuan, Y., Cao, X. & Xiang, B. (2017) 'Optimum Connection Modes for Photovoltaic Thermal Collectors in Different Radiation Zones of China', Applied Thermal Engineering, 122, pp. 661-672.
- Pal, S., Hajj, M.R., Wong, W.P. & Puri, I.K. (2014) 'Thermal Energy Storage in Porous Materials with Adsorption and Desorption of Moisture', International Journal of Heat and Mass Transfer, 69, pp. 285-292.
- Pearsall, N. & Gottschalg, R. (2012) 'Performance Monitoring', in Comprehensive Renewable Energy. pp. 775-786.
- 'Progress on Flat-Plate Water Based of Photovoltaic Thermal (Pv/T) System: A Review', (2014) Iranica Journal of Energy & Environment.
- Qu, M., Abdelaziz, O. & Yin, H. (2014) 'New Configurations of a Heat Recovery Absorption Heat Pump Integrated with a Natural Gas Boiler for Boiler Efficiency Improvement', Energy Conversion and Management, 87, pp. 175-184.
- Raj, P. & Subudhi, S. (2018) 'A Review of Studies Using Nanofluids in Flat-Plate and Direct Absorption Solar Collectors', Renewable and Sustainable Energy Reviews, 84, pp. 54-74.
- Rajput, P., Shyam, Tomar, V., Tiwari, G.N., Sastry, O.S. & Bhatti, T.S. (2018) 'A Thermal Model for N Series Connected Glass/Cell/Polymer Sheet and Glass/Cell/Glass Crystalline Silicon Photovoltaic Modules with Hot Solar Cells Connected in Series and Its Thermal Losses in Real Outdoor Condition', Renewable Energy, 126, pp. 370-386.
- Ramos, A., Guarracino, I., Mellor, A., Alonso-Álvarez, D., Childs, P.P., Ekins-Daukes, N.J. & Markides, C.N. (2017) 'Solar-Thermal and Hybrid Photovoltaic-Thermal Systems for Renewable Heating'. London: Imperial College, pp. 1-20.
- Reifsnyder, W.E. (1966) 'Radiation Geometry in the Measurement and Interpretation of Radiation Balance', Agricultural Meteorology, 4, pp. 255-265.
- Rekstad, B.S.a.J. (2002) 'A Photovoltaic/Thermal (Pv/T) Collector with a Polymer Absorber Plate, Experimental Study and Analytical Model', Solar Energy, 72(1), pp. 63–73.
- REN21 (2018) 'Renewables 2018 Global Status Report'. Paris: REN21, pp. 1-325.
- Riffat, S.B. & Cuce, E. (2011) 'A Review on Hybrid Photovoltaic/Thermal Collectors and Systems', International Journal of Low-Carbon Technologies, 6(3), pp. 212-241.
- Saini, V., Tripathi, R., Tiwari, G.N. & Al-Helal, I.M. (2018) 'Electrical and Thermal Energy Assessment of Series Connected N Partially Covered Photovoltaic Thermal (Pvt)-Compound Parabolic Concentrator (Cpc) Collector for Different Solar Cell Materials', Applied Thermal Engineering, 128, pp. 1611-1623.
- Sakhaei, S.A. & Valipour, M.S. (2019) 'Performance Enhancement Analysis of the Flat Plate Collectors: A Comprehensive Review', Renewable and Sustainable Energy Reviews, 102, pp. 186-204.
- Saleh, A.M. (2012) Modeling of Flat-Plate Solar Collector Operation in Transient States. Masters thesis. Purdue University.
- Sarhaddi, F., Farahat, S., Ajam, H., Behzadmehr, A. & Mahdavi Adeli, M. (2010) 'An Improved Thermal and Electrical Model for a Solar Photovoltaic Thermal (Pv/T) Air Collector', Applied Energy, 87(7), pp. 2328-2339.

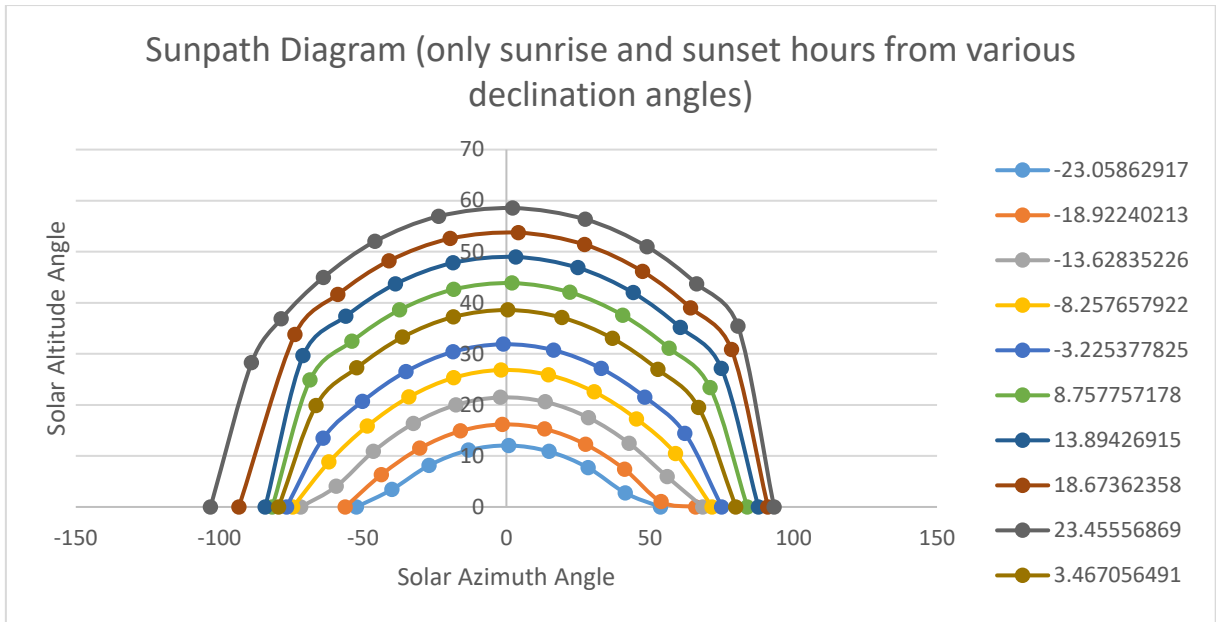
- Sawin, J.L., Rutovitz, J. & Sverrisson, F. (2018) 'Renewables 2018 Global Status Report'. Paris: REN21 Secretariat: REN21, pp. 1-325 ISBN 978-3-9818911-3-3.
- Sawin, J.L., Seyboth, K. & Sverrisson, F. (2016) 'Renewables 2016 Global Status Report' Sawin, J. L. Paris: REN21 Secretariat: REN21, pp. 1-272 ISBN 978-3-9818107-0-7.
- Sawin, J.L., Seyboth, K. & Sverrisson, F. (2017) 'Renewables 2017 Global Status Report'. Paris: REN21 Secretariat: REN21, pp. 1-302 ISBN 978-3-9818107-6-9.
- Sawin, J.L., Sverrisson, F. & Rickerson, W. (2015) 'Renewables 2015 Global Status Report' Sawin, J. L. Paris: REN21 Secretariat: REN21, pp. 1-251 ISBN 978-3-9815934-6-4.
- Schweiger, H.G., Obeidi, O., Komesker, O., Raschke, A., Schiemann, M., Zehner, C., Gehnen, M., Keller, M. & Birke, P. (2010) 'Comparison of Several Methods for Determining the Internal Resistance of Lithium Ion Cells', *Sensors*, 10(6), pp. 5604-25.
- Schwingshackl, C., Petitta, M., Wagner, J.E., Belluardo, G., Moser, D., Castelli, M., Zebisch, M. & Tetzlaff, A. (2013) 'Wind Effect on Pv Module Temperature: Analysis of Different Techniques for an Accurate Estimation', *Energy Procedia*, 40, pp. 77-86.
- Shukla, K.N., Rangnekar, S. & Sudhakar, K. (2015) 'Comparative Study of Isotropic and Anisotropic Sky Models to Estimate Solar Radiation Incident on Tilted Surface: A Case Study for Bhopal, India', *Energy Reports*, 1, pp. 96-103.
- Shyam, Tiwari, G.N., Fischer, O., Mishra, R.K. & Al-Helal, I.M. (2016) 'Performance Evaluation of N-Photovoltaic Thermal (Pvt) Water Collectors Partially Covered by Photovoltaic Module Connected in Series: An Experimental Study', *Solar Energy*, 134, pp. 302-313.
- Simón-Martín, M., Montserrat, D.-M. & Alonso-Tristán, C. (2016) 'Shadow-Band Radiometer Measurement of Diffuse Solar Irradiance: Calculation of Geometrical and Total Correction Factors', *Solar Energy*, 139, pp. 85-99.
- Skoplaki, E. & Palyvos, J.A. (2009) 'Operating Temperature of Photovoltaic Modules: A Survey of Pertinent Correlations', *Renewable Energy*, 34(1), pp. 23-29.
- Soga, K., Akasaka, H. & Nimiya, H. (Year) 'A Comparison of Methods to Estimate Hourly Total Irradiation on Tilted Surfaces from Hourly Global Irradiation on a Horizontal Surface', *Kyoto, Japan. Building Simulation*, pp. 635-642.
- Sohel, M.I., Ma, Z., Cooper, P., Adams, J. & Scott, R. (2014) 'A Dynamic Model for Air-Based Photovoltaic Thermal Systems Working under Real Operating Conditions', *Applied Energy*, 132, pp. 216-225.
- Solarangel (2016) 'Data Sheet', Solar Angel Dg-01 Available at: <https://www.epcbuildings.co.uk/wp-content/uploads/2018/10/Solar-Angel.pdf> (Accessed: 10/04/2016).
- Solarus (2018) How It Works. Available at: <https://solarus.com/powercollector/> (Accessed: 08/09/2019).
- Solarventi-International (2019) 'Vacation Homes', Solar Heating Dehumidifies and Ventilates Vacation Homes. Available at: <https://www.solarventi.com/why-solar-air-collectors/vacation-homes/> (Accessed: 03/08/2019).
- Sopian, K., Liu, H.T., Kakaç, S. & Veziroglu, T.N. (2000) 'Performance of Double Pass Photovoltaic Thermal Solar Collector Suitable for Solar Drying Systems', *Energy Conversion and Management*, 41, pp. 353-365.
- Spirkl, J.M.a.W. (1993) 'Dynamic Solar Collector Performance Testing', *Solar Energy Materials and Solar Cells*, 30, pp. 95-105.
- 'Standard Test Methods for Photovoltaic Modules in Cyclic Temperature and Humidity Environments'.
- Strobach, E., Faiman, D., Bader, S.J. & Hile, S.J. (2013) 'Effective Incidence Angles of Sky-Diffuse and Ground-Reflected Irradiance for Various Incidence Angle Modifier Types', *Solar Energy*, 89, pp. 81-88.
- Strutt, J.V.a.D. (2002) 'Basic Heat Transfer and Some Applications in Polymer Processing', in *Plastics Technician's Toolbox*. pp. 21-33.
- Sun, L.L., Li, M., Yuan, Y.P., Cao, X.L., Lei, B. & Yu, N.Y. (2016) 'Effect of Tilt Angle and Connection Mode of Pvt Modules on the Energy Efficiency of a Hot Water System for High-Rise Residential Buildings', *Renewable Energy*, 93, pp. 291-301.
- Tian, Y. & Zhao, C.Y. (2013) 'A Review of Solar Collectors and Thermal Energy Storage in Solar Thermal Applications', *Applied Energy*, 104, pp. 538-553.
- Tiwari, A., Sodha, M.S., Chandra, A. & Joshi, J.C. (2006) 'Performance Evaluation of Photovoltaic Thermal Solar Air Collector for Composite Climate of India', *Solar Energy Materials and Solar Cells*, 90(2), pp. 175-189.

- Tiwari, G.N. & Mishra, R.K. (2012) 'Solar Energy', in *Advanced Renewable Energy Sources*. Royal Society of Chemistry, pp. 1-66.
- Tiwari, G.N., Tiwari, A. & Shyam (2016). *Handbook of Solar Energy*, Singapore, Springer Science and Business Media.
- Tiwari, G.N., Yadav, J.K., Singh, D.B., Al-Helal, I.M. & Abdel-Ghany, A.M. (2015) 'Exergoeconomic and Enviroeconomic Analyses of Partially Covered Photovoltaic Flat Plate Collector Active Solar Distillation System', *Desalination*, 367, pp. 186-196.
- Tiwari, S. & Tiwari, G.N. (2016) 'Thermal Analysis of Photovoltaic-Thermal (Pvt) Single Slope Roof Integrated Greenhouse Solar Dryer', *Solar Energy*, 138, pp. 128-136.
- Tripanagnostopoulos, Y., Th.Nousia & Souliotis, M. (2000) 'Low Cost Improvement to Building Integrated Air Cooled Hybrid Pv- Thermal Systems', 16th European Photovoltaic Solar Energy Conference. Glasgow, Scotland. pp. 1-5.
- Tsai, H.-L. (2010) 'Insolation-Oriented Model of Photovoltaic Module Using Matlab/Simulink', *Solar Energy*, 84(7), pp. 1318-1326.
- Tsirakoglou, T. (2011) Numerical Simulation of a Flat Plate Collector. International Hellenic University.
- Tyagi, V.V., Kaushik, S.C. & Tyagi, S.K. (2012) 'Advancement in Solar Photovoltaic/Thermal (Pv/T) Hybrid Collector Technology', *Renewable and Sustainable Energy Reviews*, 16(3), pp. 1383-1398.
- Usama Siddiqui, M., Arif, A.F.M., Kelley, L. & Dubowsky, S. (2012) 'Three-Dimensional Thermal Modeling of a Photovoltaic Module under Varying Conditions', *Solar Energy*, 86(9), pp. 2620-2631.
- V.Badescu (1991) 'The Lambertian Geometric Factor of the Radiation Flux Emitted by a Spherical Source of Black-Body Radiation.', *Europhysics Letters*, 14(4), pp. 309-311.
- Vittorini, D., Castellucci, N. & Cipollone, R. (2017) 'Heat Recovery Potential and Electrical Performances in-Field Investigation on a Hybrid Pvt Module', *Applied Energy*, 205, pp. 44-56.
- Vokas, G.A., Theodoropoulos, N.G. & Georgiou, D.P. (2014) 'Simulation of Hybrid Photovoltaic/Thermal Air Systems on Building Facades', *Energy Procedia*, 50, pp. 917-930.
- Wang, S.-Y., Qiu, J. & Li, F.-F. (2018) 'Hybrid Decomposition-Reconfiguration Models for Long-Term Solar Radiation Prediction Only Using Historical Radiation Records', *Energies*, 11(6), p. 1376.
- Wojcicki, D.J. (2015) 'The Application of the Typical Day Concept in Flat Plate Solar Collector Models', *Renewable and Sustainable Energy Reviews*, 49, pp. 968-974.
- Wu, J., Zhang, X., Shen, J., Wu, Y., Connelly, K., Yang, T., Tang, L., Xiao, M., Wei, Y., Jiang, K., Chen, C., Xu, P. & Wang, H. (2017) 'A Review of Thermal Absorbers and Their Integration Methods for the Combined Solar Photovoltaic/Thermal (Pv/T) Modules', *Renewable and Sustainable Energy Reviews*, 75, pp. 839-854.
- Y. Tripanagnostopoulos, S.T. 'Hybrid Solar/Wind (Pvt/Wt) Building Integrated Systems', 2nd European PV-Hybrid and Mini-Grid Conference.
- Yandri, E. (2017) 'The Effect of Joule Heating to Thermal Performance of Hybrid Pvt Collector During Electricity Generation', *Renewable Energy*, 111, pp. 344-352.
- Yao, W., Li, Z., Xiu, T., Lu, Y. & Li, X. (2015) 'New Decomposition Models to Estimate Hourly Global Solar Radiation from the Daily Value', *Solar Energy*, 120, pp. 87-99.
- Yousef Nezhad, M.E. & Hoseinzadeh, S. (2017) 'Mathematical Modelling and Simulation of a Solar Water Heater for an Aviculture Unit Using Matlab/Simulink', *Journal of Renewable and Sustainable Energy*, 9(6), p. 063702.
- Zakharchenko, R., Licea-Jiménez, L., Pérez-García, S.A., Vorobiev, P., Dehesa-Carrasco, U., Pérez-Robles, J.F., González-Hernández, J. & Vorobiev, Y. (2004) 'Photovoltaic Solar Panel for a Hybrid Pv/Thermal System', *Solar Energy Materials and Solar Cells*, 82(1), pp. 253-261.
- Ziapour, B.M., Palideh, V. & Mokhtari, F. (2016) 'Performance Improvement of the Finned Passive Pvt System Using Reflectors Like Removable Insulation Covers', *Applied Thermal Engineering*, 94, pp. 341-349.
- Ziyadanogullari, N.B., Yucel, H.L. & Yildiz, C. (2018) 'Thermal Performance Enhancement of Flat-Plate Solar Collectors by Means of Three Different Nanofluids', *Thermal Science and Engineering Progress*, 8, pp. 55-65.
- Zohri, M., Fudholi, A., Ruslan, M.H. & Sopian, K. (2017) 'Mathematical Modeling of Photovoltaic Thermal Pv/T System with V-Groove Collector', 1862, p. 030063.

Zondag, H. (2008) 'Flat-Plate Pv-Thermal Collectors and Systems: A Review', *Renewable and Sustainable Energy Reviews*, 12(4), pp. 891-959.

Appendices

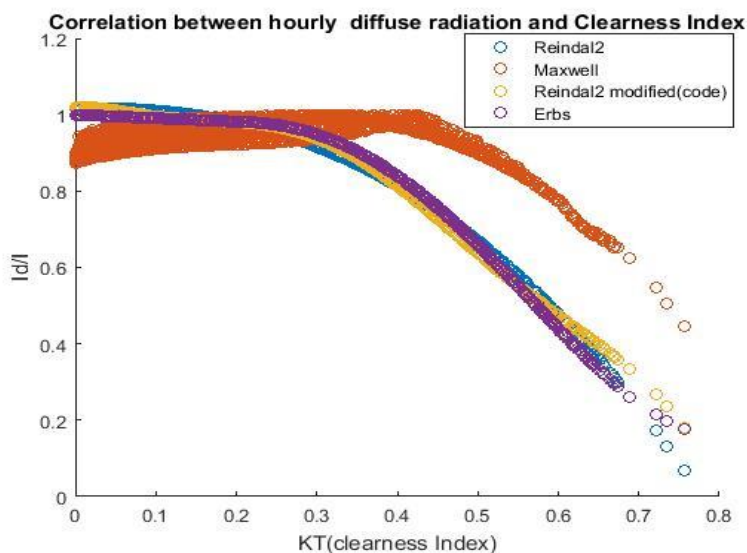
I. Sunpath Diagram



A 1: Sunpath diagram for a day in UK.

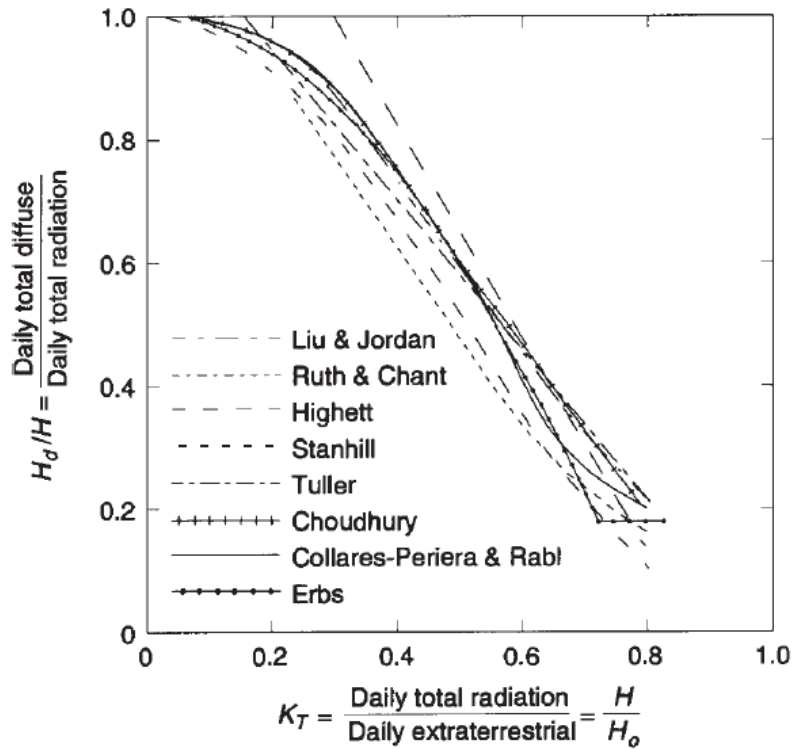
The sunpath diagram shows the path of incidence angles in a day and can indicate the impact the design site should there be any obstacles like trees and buildings and their corresponding shadow.

II. Diffuse Hourly Diffuse Radiation vs Clearness Index



A 2: Relation between diffuse hourly diffuse radiation and clearness index with respect to standard models.

III. Hourly Diffuse Radiation Models



A 3: Hourly diffuse radiation models vs total radiation (Duffie and Beckman, 2013)

IV. Correcting Factor Equations

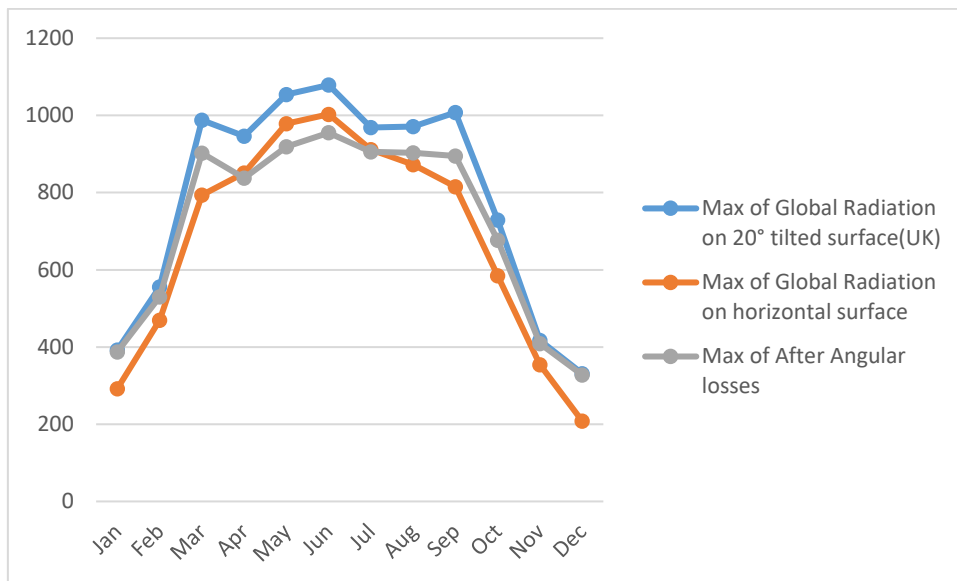
The correcting factors for finding the diffuse, beam and the ground reflected radiation are given as

$$F_b = \frac{\text{Angularlosses}(IA) - \text{Angularlosses}(0^\circ)}{1 - \text{Angularlosses}(0^\circ)} \quad \text{A- 1}$$

$$F_d = e^{-\frac{1}{0.173} \left[\frac{1}{3\pi} \left(\sin(\beta) + \frac{\beta - \sin(\beta)}{1 - \cos(\beta)} \right) + (-0.069) \left(\sin(\beta) + \frac{\beta - \sin(\beta)}{1 - \cos(\beta)} \right)^2 \right]} \quad \text{A- 2}$$

$$F_b = e^{-\left(\frac{1}{0.173} \left[\frac{4}{3\pi} \left(\sin(\text{arra}) + \frac{\pi - \text{arra} - \sin(\text{arra})}{1 + \cos(\text{arra})} \right) + (-0.069) \left(\sin(\text{arra}) + \frac{\pi - \text{arra} - \sin(\text{arra})}{1 + \cos(\text{arra})} \right)^2 \right]} \quad \text{A- 3}$$

V. Radiation generated for Newcastle

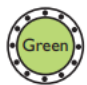
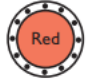




A 4: Radiation values generated from code for Newcastle

V. Pump Controls for Manual Operation

3.3 Control lamp

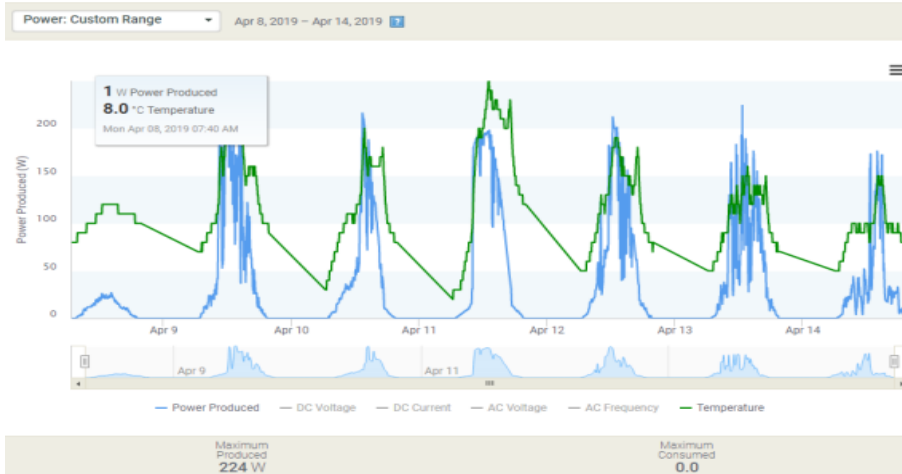
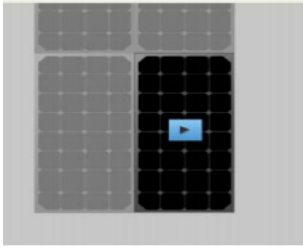
The controller is equipped with a multicolour LED in the centre of the Lightwheel®, indicating the following states:

Colour	Permanently shown	Flashing
	Everything OK	Manual mode: at least one relay HAND ON / minimum speed / maximum speed
		Sensor line break, sensor short circuit, flow rate monitoring, overpressure, low pressure
	Holiday function active	ΔT too high, night circulation, FL/RE interchanged, store maximum temperature exceeded
		Manual mode: at least one relay HAND OFF

A 5: Pump controls

VI. Data From All Microinverters 8th to 15th April

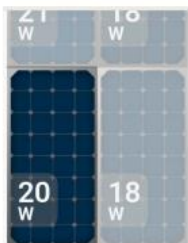
On observation of the data, it is to be noted that a slight decrease in temperature of all panels is noted when the pump 3 at 49W is switched from 43W on 11th April.



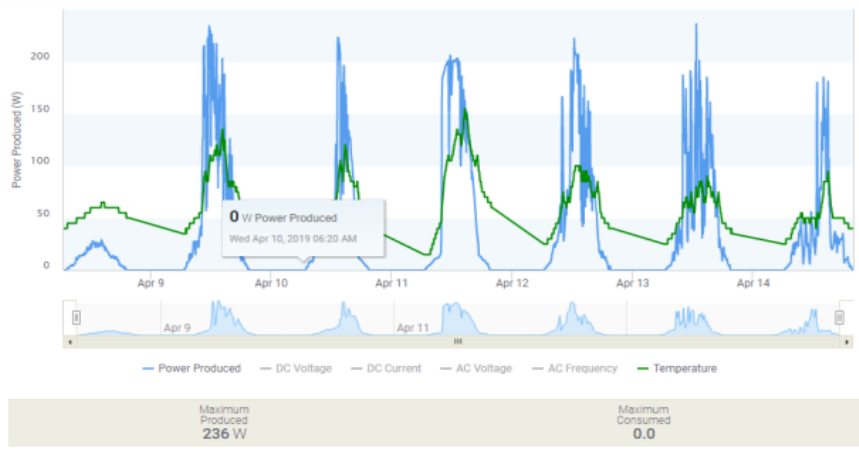
A 6:Microinverter-1 output



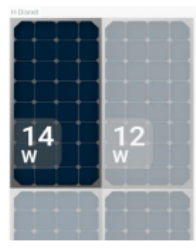
Microinverter: 121748030134



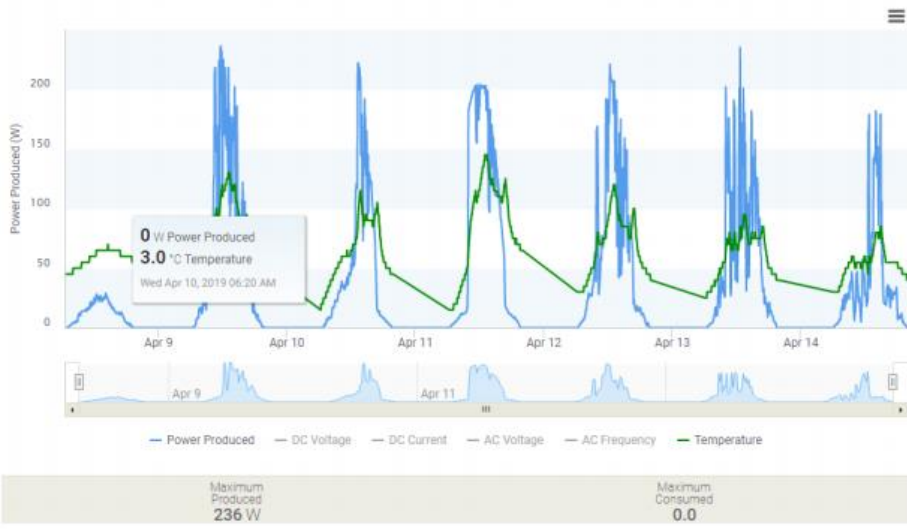
A 7:Microinverter-2 output



Microinverter: [121748029525](#)



A 8:Microinverter 3 output



A 9:Microinverter 4 output

VII. Solar Angel Data Sheet and Manufacturer Parameters From Polysun

Technical Data

PV Output (Wp) (Polycrystalline)	250	Frame material	Aluminium
Thermal Output (Wp)	648	Insulation material	Polymer foam
Gross collector area (m ²)	1.607	Connections	22mm Compression
Aperture area (m ²)	1.552	Max. operating pressure (KPa)	600
Absorber area (m ²)	1.501	Pressure tested to (KPa)	1500
Dimensions (mm)	1630 x 986 x 35	Pressure drop (mBar) @ 2.5 l/min	50
Weight – empty (kg)	25	Max System Voltage (V)	1000
Liquid content (l)	0.82	Voltage at max power (V)	30.4
Glass (low iron)	3.2 mm	Current at max power (A)	8.1
Stagnation temperature (°C)	78.9	Over current Protection Rating (A)	12
Absorber material	Aluminium	Snow and Wind Loading (max Pa)	6600

A 10:Solar angel data sheet

Polysun 9.1 - Simulation Software - DESIGNER

PVT collector - Catalog

Name	Manufacturer
Solar Angel DG012015	Natural Technology Developments Ltd

Module type	Temperature coefficient [%/K]	Efficiency STC	Nominal power STC [W]	Output voltage MPP-STC [V]	Output current MPP-STC [A]
polycrystalline	-0.45	0.153	250	30.8	8.2

Open circuit voltage [V]	Short circuit current [A]	Temperature coefficient voltage [%/K]	Temperature coefficient current [%/K]	Maximum system voltage [V]
39	8.8	-0.49	0.038	1,000

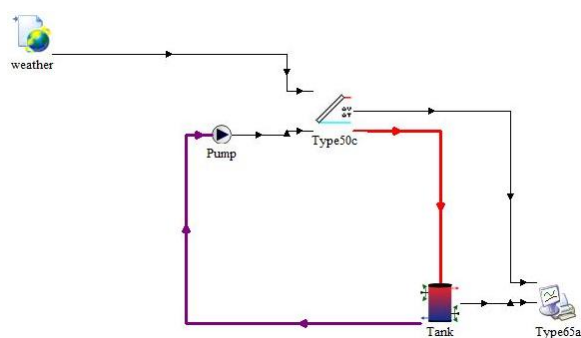
Collector type	Test date	Quality test	Keymark	Absorber area [m ²]	Aperture area [m ²]	PVT gross area [m ²]	Eta0 (laminar) ; bu [-] ; [s/m]	Eta0 (turbulent) [-] ; [-]	A1 (without wind) ; b1 [W/m ² K] ; [W/m ² K]	A1 (with wind) ; b2 [W/m ² K] ; [W/m ² K]
Flat-plate coll...	2014	no	yes	1.501	1.55	1.61	0.534	0.534	10.1	12.488

A2 ; Epsilon/Alpha [W/m ² K] ; [-]	Dyn. heat capacity [J/K]	North-South axis	IHM model	Angle factors	Diffuse irradiation fraction	Volume [l]	Internal pipe diameter [m...]	Single pipe length [m]	Parallel piping	Pipe roughness [m...]
0.062	6,248.5	North-South	Table	Table	0	0.82	7	1.536	8	0.1

Linear form factor	Friction factor	Fluid for test	Mixture concentration during test [%]	Test flow rate [l/h]	Max. flow rate [l/h]	Max. pressure [bar]	Maximum temperature [°C]
1	0	Water	0	180	300	6	79

A 11:Polysun solar angel catalog

VIII. TRNSYS Model of PV/T



A 12:Simulation model for TRNSYS PV/T

IX. Main Code of PV/T (without functions)

```
%SI units ALL TEMPERATURE IS IN CALCULATED IN KELVIN Select a clear day for
%validation along with a cloudy day to show difference
tic%
clear all % TURN DATA AS TMY DATA FORMAT- EASY TO INTEGRATE
close all
%% %READ TMY2/3 FILES-time
PA=input('Enter the number of Parallel modules?');
SE=input('Enter the number of Series modules?');
FO=(PA*SE);
display(FO)
portfile = 'UK(NOTinput).xlsx';%INPUTED USB PUBLIC DATA WHICH IS AVAILABLE
wind = xlsread(portfile,'A1:A8760');%B UK 1:0
rad = xlsread(portfile,'B1:B8760');%C UK
temp = xlsread(portfile,'C1:C8760');
portfile ='DEW.xlsx';
Dew= xlsread(portfile,'A1:A52577');
Dew= Dew(~isnan(Dew));
rain=xlsread(portfile,'B1:B52577');
rain= rain(~isnan(rain));
portfile = 'RESOLRAD.xlsx';
LEG = xlsread(portfile,'B12:B1355');%6th OCT 00:00
%% %READ VALUES, CALCULATION OF OTHER VALUES FROM GIVEN AND STANDARD VALUES
AreaofSolarMod=1.552;%APERATURE AREA OF GLAZING RECIEVING RADIATION
Absorberarea=1.501; %ABSORBER AREA
Grossarea=1.607; %AREA INCLUDING CASING
count1=0;
count2=0;
count3=0;
%NUMBER OF SOLAR CELLS IN SERIES /if completely in series
Ncp=6; %NUMBER OF CELLS IN PARALLEL
Ncs=10; %NUMBER OF CELLS IN SERIES
Ns=Ncp*Ncs;
%if cells are in series-parallel
Np=Ncp;
Nsc=Ncs;
AreaoftotalSolarCell=0.024336*60; %THERE ARE 60 CELLS(156*156mm)
Beta=AreaoftotalSolarCell/AreaofSolarMod;%PACKING FACTOR
rc=Beta;
gap=AreaofSolarMod/Grossarea;
Moduleeff=15.3; %AT STC MODULE EFFICIENCY
q =1.6022E-19; %ELCTRON CHARGE
kb=1.381E-23; %FOR ELECRICAL ANALYSIS BOLTZMAN CONSTANT
%KG/SEC STANDARD MASS FLOW RATE FOR FLATE PLATE COLLECTORS IS 0.02KG/SEC
FOR OUR CASE ITS 153L/HR WHICH IS 0.04KG/SEC
m=0.04;%0.035 PER TUBE SEEMS VERY OPTIMUM AT 300 AND 0.013 AT 310 (0.05-
0.03)
Isc=8.6;
Voc=39;
Vm=30.8;
Im=8.2;
Pm=250;
Egref=1.121; %FOR SILICON EV
Tref=298.16; %STC REF TEMPERATURE
fvolt=0.49*Voc; % TEMPERATURE COEFFICIENT OF VOLTAGE(-) %/K
fisc=0.038*Isc ; %(+) % TEMPERATURE COEFFICIENT OF CURRENT(+)figure
fpower=0.45;%(-) % TEMPERATURE COEFFICIENT (-)
%AT NOCT has 800W/m^2 44-48 C)
Celleff=Moduleeff/(Beta); %not percentage-Celleff=Moduleeff/(Beta*100)
FillFactorSTC=Moduleeff*(AreaofSolarMod*1000)/(100*Isc*Voc);
TcNOCT=318.16; %NOCT temp 47 C (RANGE 45-48 C))
```

```

TaNOCT=293.16;      %NOCT AMBIENT 25 C
GNOCT=800;         %IRRADIATION AT NOCT 800W/m2
sig=5.67037E-08;  %BOLTZMAN'S CONSTANT FOR THERMAL ANALYSIS
eg=0.92;          %EMISSIVITY OF GLASS
ep=0.96;          %EMISSIVITY OF PV PANEL
A=1.552;          %AREA OF GLASS AND PV PANEL ON WHICH IRRADIATION OCCURS
length=1.552;     %LENGTH OF TUBE
Refg=1.526;       %REFRACTIVE INDEX OF GLASS SOLAR ENGINEERING PROCESS CH 2
refeva=1.496710526;%https://www2.pvlighthouse.com.au/resources/photovoltaic%20materials/refractive%20index/refractive%20index.aspx avg over 360-750nm
Refeva= 1.4760;   %ETHYLENE/VINYL ACETATE COPOLYMER-40% VINYL ACETATE
1.4760 RI INVERSELY PROPORTIONAL TO TEMPERATURE
RefPV=4.346666667;%[PAL85D] E.IN PALIK, HANDBOOK OF OPTICAL CONSTANTS OF
SOLIDS VOL I, ACADEMIC PRESS, ORLANDO, PP. 577-580, 1985.
thickg=0.0032;    %THICKNESS OF GLASS LAYER
thickp= 0.001;    %THICKNESS OF PV LAYER
thickeva=0.0005; %THICKNESS OF EVA LAYER
thickab= 0.002;   %THICKNESS OF ABSORBER LAYER
thickweld= 0.001; %THICKNESS OF WELD BOND
thickins=0.0188; %THICKNESS OF INSULATION LAYER
dia=0.008;        %OUTER DIAMETER OF TUBE
poc=0.003;        %POINT OF CONTACT OF WELD BOND AND LENGTH SHOULD BE ALONG
LENGTH OF TUBE
Alum=230 ;        %THERMAL CONDUCTIVITY OF ALUMINIUM(W/m-K)
lat=54.9;         %38.7223 54.9 9.9312 LATITUDE OF LOCATION
arra=20;          %TILT ANGLE OF PV/T PANEL
g=20;             %SURFACE AZIMUTH ANGLE TOWARDS WEST POSIIVE-(NORTHERN
HEMI ONLY OR BOTH)
%% MISCELLANEOUS
hour1=zeros(8760,1);
inci=zeros(24,1);
ri=1;
fi=1;
kpop=1;
npop=1;
for i=1:8760
eClear(i,1)= 0.711 + 0.56*(Dew(i,1)/100) + 0.73 *(Dew(i,1)/100)^2; %CLEAR
DAY COEFFICIENT
G(i,1)=rad(i,1); %HOURLY IRRADIATION OF LOCATION IN W/m2 OR WH/m2
if G(i,1)==0
G(i,1)=0.1;
end
end
for da=1:365
ti=0;
for j=1:24
valti(npop,1)=ti;
npop=npop+1;
ti=ti+1;
end
end
% for npop =1:8760
% if valti(npop,1)==0
% valti(npop,1)=24;
% end
% end
Lloc=1.6178;      %LONGITUDE OF LOCATION IN DEGREES WRT WEST 0<Lloc<360
103.7327 1.6178 9.1393
kpop=1;
npop=1;
%collectoreff trnsys
% Efficiency:
eta = qUseful / (Gt A) = mdot Cp (To - Ti) / (Gt A) = eta0 - eta1 * Gt /
(To-Tamb);

```

```

%% can be rewritten as:
To = (eta0*Gt+mdot*Cp/A*Ti+etal*Tamb) / (mdot*Cp/Aa+etal);
%% Collector area [m^2]
A = 1.607;
%% Intercept efficiency [-]
eta0 = 0.8;
%% Negative First order loss coefficient [kJ/h-m^2-K]
etal = 15;
%% Specific heat [kJ/kg-K]
Cp = 4.19;
%% %FIND ANGLES
u=1;
syms V U
for dayy=1:365
B=(dayy-1)*360/(365); %ANGLE B
dec=(180/pi)*(0.006918-0.399912*cosd(B) +0.070257*sind(B) -
0.006758*cosd(2*B)+0.000907*sind(2*B) -
0.002697*cosd(3*B)+0.00148*sind(3*B)); %DECLINATION ANGLE
sunriseset(dayy,1)=acosd(tand(lat)*tand(dec))/15;%SUNRISE FROM NOON NOT
HOURLY! AND THIS IS ON LOCATION
sunriseset(dayy,2)=acosd(-tand(lat)*tand(dec))/15;%SUNSET FROM NOON
Sunshinehours(dayy,1)=2*acosd(-tand(lat)*tand(dec))/(15);%TOTAL SUNSHINE
HOURS EACH DAY
E=229.2*(0.000075+0.001868*cosd(B)-0.032077*sind(B)-0.014615*cosd(2*B) -
0.04089*sind(2*B)); %EQUATION OF TIME
DayAngle(dayy,1)=dayy*(360/365.25)
corec(dayy,1)=1+(0.03344*cosd(DayAngle(dayy,1)-2.80));
%DAYLIGHT SAVINGS NEED TO BE CONSIDERED DEPENDING ON LOCATION
if dayy>90 & dayy<300 %UK AND PORTUGAL (BOTH HAVE DST)
LSTM=(1)*15;
Dy=1;%CONVERTED TO DECIMAL FORMAT
else
LSTM=0;
Dy=0;
end
LC=(Lloc)*4;%CONVERTED DEGREES TO MINUTES
% LSTM=15*(5.5) %KOCHI DEGREES
% vallLSTM(dayy,1)=LSTM;
% ki2(5185:5210,1)
Gc=1367;
for j=1:24
Go(kpop,1)=Gc*(1.000110+0.034221*cosd(B)
+0.001280*sind(B)+0.000719*cosd(2*B)+0.000077*sind(2*B)); %EXTRATERRESTRIAL
RADIATION
if j==12
E111(dayy,1)=B;
GD(kpop,1)=24*corec(dayy,1)*Gc*( )/pi( );
end
E2(kpop,1)=E;
appsolartime=(4*(Lloc-LSTM)+E)/60; %SOLAR TIME (PER HOUR) IN MINUTES
LST=valti(kpop,1)+((appsolartime));%IN DECIMAL HOURS FROM MINUTES %SOLAR
TIME IN MINUTES
ki2(kpop,1)=LST;
if LST>24
LST= 24-LST;
elseif LST<0
LST=24+LST;
else
LST=LST;
end
ki3(kpop,1)=LST;
DECL(kpop,1)=dec;

```

```

hour1(kpop,1)=15*(LST-12); %HOUR ANGLE IN DEGREES IS BETWEEN SUNRISE AND
SUNSET NOW CALCULATE HOUR ANGLES AT SURFACE SUNRISE AND SUNSET-CUTOFF IF
>ACTUAL SUNRISE/SUNSET ANGLES
zeinth(j,1)=acosd((cosd(lat)*cosd(dec)*cosd(hour1(kpop,1)))+(sind(lat)*sind
(dec))); %SOLAR ZENITH ANGLE
inci(j,1)=acosd(sind(dec)*sind(lat)*cosd(arr)-
sind(dec)*cosd(lat)*sind(arr)*cosd(g)+cosd(dec)*cosd(lat)*cosd(arr)*cosd(
hour1(kpop,1))+cosd(dec)*sind(lat)*sind(arr)*cosd(g)*cosd(hour1(kpop,1))+c
osd(dec)*sind(arr)*sind(g)*sind(hour1(kpop,1))); %ANGLE OF INCIDENCE
kpop=kpop+1;
%{
SIDE NOTE- THE CALCULATION GIVES ONLY HOURLY VALUES IN A DAY- TO FIND
MINUTE ANALYSIS IN AN HOUR- OR EVEN EVERY 4min- then 1 degree change
INCIDENCE ANGLES need to be modified, SOME MODIFICATION IS NEEDED IN THE
CODE-END APPEND THIS CODE AS WELL FOR ADDITIONAL -APPENDIX BUT NOTE THAT
THE MOST COMMON DATA AVAILABLE IS ONLY FOR HOURLY VALUES!!%}
incilfin(npop,1)=inci(j,1);%PG 29 OF SOLAR ENG BIBLE -TILT INFLUENCES GAIN
zeinthincil(npop,1)=zeinth(j,1);
sunriseh(npop,1)=sunriseset(dayy,1);
sunseth(npop,1)=sunriseset(dayy,2);
sunrisehA(npop,1)=sunriseh(npop,1)*15;
sunsethA(npop,1)=sunseth(npop,1)*15;
out23(npop,1)=~rem(j,13)*j/13;

if out23(npop,1)~=0
    hournoon(npop,1)=zeinthincil(npop,1);
    incinoon(npop,1)=(incilfin(npop,1));
else
    hournoon(npop,1)=NaN;
    incinoon(npop,1)=NaN;
end
npop=npop+1;
end
j=1;
end
npop=1;
incinoon=incinoon(~isnan(incinoon));
hournoon=hournoon(~isnan(hournoon));
% if aRa(1,1)>0 & bRb(1,1)>0 | aRa(1,1)<0 & bRb(1,1)<0
% else
opo=1;
for dayy=1:365
    for j=1:24
        tmm(j,1)=temp(opo,1);
        opo=opo+1;
    end
    tmax(dayy,1)=max(tmm);
    tmin(dayy,1)=min(tmm);
end
count=1;
aRa=zeros(8760,1);

for dayy=1:365
    for j=1:24
        tn_2=circshift(temp,2);
    maxt(npop,1)=tmax(dayy,1);
    mint(npop,1)=tmin(dayy,1);
    incinoon1(npop,1)=incinoon(dayy,1);
    aly(dayy,1)=hournoon(dayy,1)-(arra);%IF THERE WAS NO DST

if incilfin(npop,1)<89.73
incilfin1(npop,1)=(incilfin(npop,1));
else
incilfin1(npop,1)=89.73;

```



```

end
if zeinthincil(npop,1)<89.73
zeinthincill(npop,1)=zeinthincil(npop,1);
else
zeinthincill(npop,1)=89.73;
end
%Rb not greater than Solar constant/(max G radiation) SO HERE G NOT
GREATER THAN 1.3659;
%CLEARNESS INDEX FOR INSTANTANEOUS RADIATION -IEX CAN BE USED FOR HOULY
VALUES
KT(npop,1)=G(npop,1)/Go(npop,1);
% if KT(npop,1)<0.08064516129
%     KT1(npop,1)=G(npop,1);
% else
%     KT1(npop,1)=NaN;%ISSUES WITH IRRADIATION BELOW 120w/M2
% end
% if G(npop,1) < 120
% G(npop,1)=120;
% else
%     G(npop,1)=G(npop,1);
% end
% KT(npop,1)=G(npop,1)/Go(npop,1);
%ERBS CORRELATION (NEED TO MAKE IT MAXWELL HAS KT AND M CORREALTION(1987)
ktr(npop,1)=G(npop,1)*cosd(zeinthincill(npop,1))/Go(npop,1);%EFFECTIVE
GLOBAL HORIZONTAL TRANSMITTANCE
%ERBS can be unreasonable sometimes
if KT(npop,1)<=0.22
kde(npop,1)=(1-0.09* KT(npop,1));
elseif KT(npop,1)>0.22 & KT(npop,1)<=0.8
kde(npop,1)=(0.9511-0.1604*KT(npop,1)+(4.388*KT(npop,1)^2)-
(16.638*KT(npop,1)^3)+(12.336*KT(npop,1)^4));
else
kde(npop,1)=0.165;
end
angle(npop,1)=asind(sind(incilfinl(npop,1))/Refg);
anglel(npop,1)=real(asind((sind(angle(npop,1))*Refg)/Refeva));
AM(npop,1)=1/cosd(anglel(npop,1));%DESOTO 2006 BIBLE PAG 234 THIS FORMULA
BETTER AND STABLE
% AM(1,1)=1/(cosd(zeinthincill(1,1))+0.05057*(96.08-zeinthincill(1,1))^-
1.034);
knc(npop,1)=0.866-0.122*(AM(npop,1)^2)-
0.000653*(AM(npop,1))^3+0.000014*(AM(npop,1))^4;
AMmax(npop,1)=real((cosd(zeinthincill(npop,1))+0.50572*(96.07995-
zeinthincill(npop,1))^-1.6364)^-1);% if AMmax(npop,1)>=18 | AMmax(npop,1)<0
%     AMmax(npop,1)=AM(npop,1);
%;end
%%%%%%%%%%%%%%%%%%%%%%%%%%%%%%%%%%%%%%%%%%%%%%%%%%%%%%%%%%%%%%%%%%%%%%%% Maxwell MODEL/DISC
if KT(npop,1)<=0.6
an(npop,1)=0.512-1.56*KT(npop,1)+2.286*KT(npop,1)^2-
2.222*KT(npop,1)^3;
bn(npop,1)=0.37+0.962*KT(npop,1);
cn(npop,1)=-0.28+0.932*KT(npop,1)-2.048*KT(npop,1)^2;

elseif KT(npop,1)>0.6
an(npop,1)=-5.743+21.77*KT(npop,1)-
27.49*KT(npop,1)^2+11.56*KT(npop,1)^3;
bn(npop,1)=41.4-
118.5*KT(npop,1)+66.05*KT(npop,1)^2+31.9*KT(npop,1)^3;
cn(npop,1)=-47.01+184.2*KT(npop,1)-
222.0*KT(npop,1)^2+73.81*KT(npop,1)^3;
else
end
delKn(npop,1)=real(an(npop,1)+bn(npop,1)*exp(cn(npop,1)*AM(npop,1)));
km(npop,1)=knc(npop,1)-delKn(npop,1);

```

```

%rendall 2 model we use input as G so its a decomposition model
if KT(npop,1)>0 & KT(npop,1)<=0.3
    kdr(npop,1)= 1.020 - 0.254* KT(npop,1) +
0.0123*cosd(zeinthincil1(npop,1));

elseif KT(npop,1)>0.3 & KT(npop,1)<=0.78
    kdr(npop,1)=1.400 - 1.749* KT(npop,1) +
0.177*cosd(zeinthincil1(npop,1));

elseif KT(npop,1)>0.78 & KT(npop,1)<=1
    kdr(npop,1)=0.486*KT(npop,1)-0.182*cosd(zeinthincil1(npop,1));
else
end

%NEW DGSRD model4 Yao, W., Li, Z., Xiu, T., Lu, Y. and Li, X. (2015)
'New decomposition models to estimate hourly global solar radiation from
the daily value', Solar Energy, 120, pp. 87-99.
if KT(npop,1)>=0 & KT(npop,1)<=0.3 %CHANGE HOURLY AND DAILY RATIO!FOR
KT
    kdsrg(npop,1)=-0.0142+0.0734*cosd(zeinthincil1(npop,1))-
0.0087*cosd(zeinthincil1(npop,1))^2-0.0807*cosd(zeinthincil1(npop,1))^3-
0.0203*cosd(g)-0.0218*cosd(g)^2+0.0327*cosd(g)^3-
0.0044*cosd(hour1(npop,1))+0.1313*cosd(hour1(npop,1))^2+0.0135*cosd(hour1(n
pop,1))^3-0.0129*(KT(npop,1))+0.0414*((tn_2(npop,1)-
mint(npop,1))/(maxt(npop,1)-mint(npop,1)));
    count1=count1+1;
elseif KT(npop,1)>0.3 & KT(npop,1)<=0.6
    kdsrg(npop,1)=-
0.0133+0.0672*cosd(zeinthincil1(npop,1))+0.0024*cosd(zeinthincil1(npop,1))^
2-0.0867*cosd(zeinthincil1(npop,1))^3-0.0210*cosd(g)-
0.0204*cosd(g)^2+0.0319*cosd(g)^3-
0.0013*cosd(hour1(npop,1))+0.1284*cosd(hour1(npop,1))^2+0.0149*cosd(hour1(n
pop,1))^3-0.0133*(KT(npop,1))+0.0401*((tn_2(npop,1)-
mint(npop,1))/(maxt(npop,1)-mint(npop,1)));
    count2=count2+1;
elseif KT(npop,1)>0.6
    kdsrg(npop,1)=0.0128-
0.0243*cosd(zeinthincil1(npop,1))+0.1187*cosd(zeinthincil1(npop,1))^2-
0.1358*cosd(zeinthincil1(npop,1))^3-0.0282*cosd(g)-
0.0346*cosd(g)^2+0.0347*cosd(g)^3-
0.0078*cosd(hour1(npop,1))+0.2399*cosd(hour1(npop,1))^2-
0.0398*cosd(hour1(npop,1))^3+0.0085*(KT(npop,1))-0.0148*((tn_2(npop,1)-
mint(npop,1))/(maxt(npop,1)-mint(npop,1)));
    count3=count3+1;
else
end
end
%reindallfit
arf = -1.859 ;
brf = 2.411 ;
crf = 1.018 ;
krf(npop,1)= arf*KT(npop,1)^brf+crf ;
npop=npop+1;
end

end
for l=1:8760
count=count+1;
hou1 = circshift(hour1,1);
if zeinthincil(l,1)>sunriseA(l,1) & zeinthincil(l,1)<sunsethA(l,1)
    aRa(l,1)=(sind(dec)*sind(lat)*cosd(arrA)-
sind(dec)*cosd(lat)*sind(arrA)*cosd(g))*((hou1(l,1)-
hour1(l,1))*pi)/180+(cosd(dec)*cosd(lat)*cosd(arrA)+cosd(dec)*sind(lat)*sin

```

```

d(arr)*cosd(g))*(sind(houl(1,1))-sind(hour1(1,1)))-
(cosd(dec)*sind(arr)*sind(g))*(cosd(houl(1,1))-cosd(hour1(1,1)));
bRb(1,1)=(cosd(lat)*cosd(dec))*(sind(houl(1,1))-
sind(hour1(1,1)))+(sind(lat)*sind(dec))*((houl(1,1)-hour1(1,1))*pi)/180;
else
    aRa(1,1)=1;
    bRb(1,1)=1;
end

end

end

    npop=1;
    for dayy=1:365
        for j=1:24
% Rb(npop,1)=(cosd(incilfin1(npop,1))/cosd(zeinthincil1(npop,1)));
% if npop<8760 & j>sunriseh(npop,1) & j< sunseth(npop,1)
% Iex(npop,1)=1350*(1.000110+0.034221*cosd(B)
+0.001280*sind(B)+0.000719*cosd(2*B)+0.000077*sind(2*B))*cosd(lat)*cosd(dec)
*cosd(hour1(npop+1,1)-hour1(npop,1))+((pi/180)*hour1(npop+1,1)-
hour1(npop,1))*(sind(lat)*sind(dec));
% else
%     Iex(npop,1)=1;
%     end
% if     Iex(npop,1)<0
%     Iex(npop,1)=1;
% end
%FOUR CLIMATE TYPES(TROPICAL,MIDLATITUDE WINTER,MIDLATITUDE SUMMER,SUBARTIC
SUMMER)
Altitudeofobserver=0.021; %ALTITUDE OF OBSERVATION ONLY IN KM
a01=0.4237-0.00821*(6-Altitudeofobserver)^2;
a11=0.5055+0.00595*(6.5-Altitudeofobserver)^2;
k1=0.2711+0.01858*(2.5+Altitudeofobserver)^2;
%CORRECTION FACTOR
%MIDLATITUDE WINTER
r0=1.03;
r1=1.01;
rk=1;
%%TROPICAL
r0=0.95;
r1=0.98;
rk=1.02
%MIDLATITUDE SUMMER
r0=0.97;
r1=0.99;
rk=1.02;
%SUBARTIC SUMMER
r0=0.99;
r1=0.99;
rk=1.01;
a0=r0*a01;
a1=r1*a11;
k12=rk*k1;
if j>sunriseh(npop,1) & j< sunseth(npop,1)
tb(npop,1)=a0+a1*exp(-k12/cosd(zeinthincil1(npop,1)));
else
tb(npop,1)=a0;
end

    %HDKR METHOD IS USED FOR FINDING DIFFUSE- EVEN THOUGH PEREZ MODEL IS THE
BEST
    %TYPE OF MODEL, PEREZ MODEL ISNT VERY ACCURATE AS IT CAN PREDICT HIGHER
%IRRADIATION AND IT IS THE LEAST CONSERVATIVE. WHEN SURFACE AZIMUTH IS
VERY
    %FAR FROM 0 IN NORTHERN HEMISPHERE OR 180 IN SOUTHERN HEMISPHERE- PEREZ
%MODEL IS SUGGESTED BY DUFFIE AND BECKMAN(MODIFY CODE TO CHOSE PEREZ OR

```

```

%HDKR BASED ON AZIMUTH-APPEND CODE)

%KT WAS HERE
% Ax=[1 0
%     0 1];
% bx=[0.3 1]
% Aeq=[0.248 1];
% beq=1.02;
% lb=[0,0];
% ub=[0.3,1];
% f=[0 0];
% options = optimoptions('linprog','Algorithm','interior-point');
% xfin = linprog(f,Ax,bx,Aeq,beq,lb,ub,options)
%%%%%%%%%%%%%%%%%%%%%%%%%%%%%%%%%%%%%%%%%%%%%%%%%%%%%%%%%%%%%%%%%%%%%%%%

ID(npop,1)= kde(npop,1)*G(npop,1);%ON HORIZONTAL
    if temp(npop,1) <0
        gr(npop,1)=0.8;
    else
        gr(npop,1)=0.25;
    end
    if ID(npop,1)<0
        ID(npop,1)=0;
    end
%Diffuse horz tansmittance
    Ktd=ID(npop,1)*cosd(zeinthincil1(npop,1))/Go(npop,1);
IB(npop,1)=G(npop,1)*(1- kde(npop,1)); %ON HORIZONTAL
    npop=npop+1;
    end
    j=1;
end
npop=1;
SROMEGA= 6.835E-05;%STERADIAN
DROMEGA= SROMEGA*(180/pi)^2;%SQUAREDEGREE
dell=2*sqrt(asind(DROMEGA/4*pi));
for dayy=1:365
    for j=1:24
%%%%%%%%%%%%%%%%%%%%%%%%%%%%%%%%%%%%%%%%%%%%%%%%%%%%%%%%%%%%%%%%%%%%%%%%
%USING LAMBARTIAN GEOMETRIC FACTOR OF RADIATION FLUX.(FOR ALL ANGLES
%FROM 0-90)

thetadash(npop,1)=90-(dell+incilfin1(npop,1));
thetanot(npop,1)=incilfin1(npop,1)-thetadash(npop,1);
Rb1(npop,1)=2*pi*((DROMEGA/(2*pi))*(1-
DROMEGA/(4*pi)))*cosd(thetanot(npop,1))-(asind(sqrt(DROMEGA/(4*pi))-
sqrt(DROMEGA/(4*pi)*(1-DROMEGA/(4*pi))) )*(1-
DROMEGA/(2*pi))))*sind(thetanot(npop,1)));
Rb2(npop,1)=2*pi*((DROMEGA/(2*pi))*(1-
DROMEGA/(4*pi)))*cosd(thetadash(npop,1))-(asind(sqrt(DROMEGA/(4*pi))-
sqrt(DROMEGA/(4*pi)*(1-DROMEGA/(4*pi))) )*(1-
DROMEGA/(2*pi))))*sind(thetadash(npop,1)));
Rb3(npop,1)=(Rb1(npop,1)/Rb2(npop,1));
%
Rb(npop,1)=aRa(npop,1)/bRb(npop,1);

%
Gcb(npop,1)=Gc/max(IB(npop,1));
Rb4(npop,1)=cosd(incilfin(npop,1))/cosd(zeinthincil(npop,1));

if j>-1*sunriseh(npop,1) & j<12+ sunseth(npop,1) &
zeinthincil(npop,1)<=87.9 & incilfin(npop,1)<=87.9 %IGNORE SUNSET AND
SUNRISE HOUR AND ANYTHING OUTSIDE THIER RANGE
Rb(npop,1)=cosd(incilfin(npop,1))/cosd(zeinthincil(npop,1));
else
Rb(npop,1)=1;
end
end

```

```

%%%%%%%%%%%%%%%%%%%%%%%%%%%%%%%%%%%%%%%%%%%%%%%%%%%%%%%%%%%%%%%%%%%%%%%%
ICB(npop,1)=Go(npop,1)*tb(npop,1)*Rb(npop,1); %INSTANTANEOUS BEAM
RADIATION
IBCLSKY(npop,1)=Go(npop,1)*tb(npop,1)*cosd(zeinthincil1(npop,1));

    td(npop,1)= ID(npop,1)/Go(npop,1);
    if IB(npop,1)<0
        IB(npop,1)=0;
    end
    Ai(npop,1)=IB(npop,1)/Go(npop,1);
    fk(npop,1)=sqrt(IB(npop,1)/G(npop,1));

% HDKR MODEL
if g<20
    IBT(npop,1)=(IB(npop,1))*Rb(npop,1);
    IDT(npop,1)=(ID(npop,1)*Ai(npop,1)*Rb(npop,1))+ID(npop,1)*(1-
Ai(npop,1))*((1+cosd(arr))/2)*(1+(fk(npop,1)*(sind(arr)/2)^3));
    IT(npop,1)=real((IB(npop,1)+(ID(npop,1)*Ai(npop,1)))*Rb(npop,1)+ID(npop,1)
)* (1-
Ai(npop,1))*((1+cosd(arr))/2)*(1+(fk(npop,1)*(sind(arr)/2)^3))+G(npop,1)*
gr(npop,1)*((1-cosd(arr))/2));
%PEREZ MODEL WHEN AZIMUTH IS FAR FROM 0 IN NORTHERN HEMISPHERE OR 180 IN
%SOUTHERN.
else
emmp(npop,1)=((ID(npop,1)+IB(npop,1))/ID(npop,1))+zeinthincil1(npop,1)^3*5.
535E-6;
bpdel(npop,1)=1.5*td(npop,1);
if emmp(npop,1)>=1 & emmp(npop,1)<=1.065
    p11=-0.008;
    p12=0.588;
    p13=-0.062;
    p21=-0.06;
    p22=0.072;
    p23=-0.022;
elseif emmp(npop,1)>1.065 & emmp(npop,1)<=1.23
    p11=0.13;
    p12=0.683;
    p13=-0.151;
    p21=-0.019;
    p22=0.066;
    p23=-0.029;
elseif emmp(npop,1)>1.23 & emmp(npop,1)<=1.5
    p11=0.330;
    p12=0.487;
    p13=-0.221;
    p21=0.055;
    p22=-0.064;
    p23=-0.026;
elseif emmp(npop,1)>1.5 & emmp(npop,1)<=1.95
    p11=0.568;
    p12=0.187;
    p13=-0.295;
    p21=0.109;
    p22=-0.152;
    p23=0.014;
elseif emmp(npop,1)>1.95 & emmp(npop,1)<=2.8
    p11=0.873;
    p12=-0.392;
    p13=-0.362;
    p21=0.226;
    p22=-0.462;
    p23=0.001;
elseif emmp(npop,1)>2.8 & emmp(npop,1)<=4.5
    p11=1.132;

```

```

    p12=-1.237;
    p13=-0.412;
    p21=0.288;
    p22=-0.823;
    p23=0.056;
elseif emmp(npop,1)>4.5 & emmp(npop,1)<=6.2
    p11=1.06;
    p12=-1.6;
    p13=-0.359;
    p21=0.264;
    p22=-1.127;
    p23=0.131;
else
    p11=0.678;
    p12=-0.327;
    p13=-0.25;
    p21=0.156;
    p22=-1.377;
    p23=0.251;

end
end
f1=max(0,(p11+p12*bpdel(npop,1)+p13*pi*zeinthinci11(npop,1)/180));
f2=p21+p22*bpdel(npop,1)+p23*pi*zeinthinci11(npop,1)/180;
a2=max(0,cosd(incilfin1(npop,1)));
b2=max(cosd(85),cosd(zeinthinci11(npop,1)));
F1(npop,1)=(1-f1)*(0.5*(1+cosd(arra)));
F2(npop,1)=f1*a2/b2;
F3(npop,1)=f2*sin(arra);
IBT(npop,1)=IB(npop,1)*Rb(npop,1);
IDT(npop,1)=(F1(npop,1)+F2(npop,1)+F3(npop,1))*ID(npop,1);
IGT(npop,1)=G(npop,1)*gr(npop,1)*((1-cosd(arra))/2);
IT(npop,1)=G(npop,1)*gr(npop,1)*((1-
cosd(arra))/2)+IB(npop,1)*Rb(npop,1)+(F1(npop,1)+F2(npop,1)+F3(npop,1))*ID(
npop,1);
    npop=npop+1;
end
j=1;
end
%PV SECTION
%FINDING SHUNT AND SERIES RESISTANCE OF THE CELL (ITERATIVE METHOD)
I0ref1=Isc/(exp((Voc/1))-1);%Rse=0 and Rsh=Inf (IDEAL CONDITION)
Iphref1=(Isc);
Egref=1.12;%SILICON
asoem=(Ns*298.18*kb*1.1)/q;%STC %IDEALITY FACTOR FOR POLY 1.1 SUGGESTED FOR
ONE JUNCTION CELLS- (1-1.5)
x0 =[0.3,600];
Is=8.6;
Vo=39;
Vm=30.8;
Im=8.2;
% ASSIGN PARAMETER VALUES
%NOVEL EQUATION AND EXPRESSION FOR PV/T MODULES-WITH CONDITIONS CAN BE
%APPLIED TO PV AND COLLECTOR
Fun = @(x1)PVelectrical(x1,Is,Vo,Vm,Im,asoem)
options = optimoptions('fsolve','Display','iter','TolFun',1e-3,'TolX',1e-
3);
[x,fval]= fsolve(Fun,x0,options)
Rshref=x(2);
Rs=x(1);

Ioref=(-Voc+Isc*Rs+Isc*Rshref)/(Rshref*(exp(Voc/asoem)-
exp((Isc*Rs)/asoem)));
Iphref2=Ioref*(exp(Voc/asoem)-1)+(Voc/Rshref);

```

```

Iphotheref=Isc+Ioref*(exp(Isc*Rs/asoem)-1)+(Isc*Rs/Rshref);
errorI0=100*abs(Ioref-I0ref1/(Ioref));

Tin=303.16; %INITIAL INLET TEMPERATURE OF HTF
% c=6246.5;
% eff0=0.70;
% alloss=12.488;
% a2loss=0.062;
% extinc=AreaoftotalSolarCell*0.4343;
% Pra=0.707;
Cbo=(Alum*poc)/thickweld;

%TRANSMITTANCE-ABSORBTANCE
%STC CONDITIONS (1000W/M2 AND 25 DEGREES AND 1M/S AT A REFERENCE IN GRAPHS)

for l=1:8760
Kthetad= 59.7-0.1388*arra+0.001497*arra^2;%5.4.1
Kthetag=90-0.5788*arra+0.00293*arra^2;
FUN1 = @IAM;
APV1(l,1) = FUN1(incilfin1(l,1),Refg,thickg,Refeva);
FUN1 = @IAM;
APV2(l,1) = FUN1(Kthetad,Refg,thickg,Refeva);
FUN1 = @IAM;
APV3(l,1) = FUN1(Kthetag,Refg,thickg,Refeva);
angle(l,1)=asind(sind(incilfin1(l,1))/Refg);
angled(l,1)=asind(sind(Kthetad)/Refg);
angleg(l,1)=asind(sind(Kthetag)/Refg);
tuoa(l,1)=real(exp((-4*thickg)/(cosd(angle(l,1)))));%convection by wind%K
is 4m-1 for good white glass and called extinction coefficient
Ta(l,1)=temp(l,1)+273.16;
Tini(l,1)=Ta(l,1)+(0.045*IT(l,1));
Tclear_sky(l,1) = Ta(l,1)*(eClear(l,1)^0.25);
if rain(l,1)>2
CC=1;
else
CC=0;
end
if CC==1
Ca(l,1) =1.00 +0.0224*CC+ 0.0035*CC^2 + 0.00028*CC^3; %1 for full cloud
Tsky(l,1) =Tclear_sky(l,1) *((Ca(l,1))^0.25);
else
Tsky(l,1)= Tclear_sky(l,1);
end
Qg(l,1)=IT(l,1)*A*(1-tuoa(l,1));%HEAT FLUX(G SHOULD BE IN WATT) (BUT WATT-
HOURL/M2 SO Q IS HEAT TRANSFER)
%AIR TO GLASS

rper(l,1)=(sind(angle(l,1)-
incilfin1(l,1))/sind(angle(l,1)+incilfin1(l,1)))^2;
rpar(l,1)=(tand(angle(l,1)-
incilfin1(l,1))/tand(angle(l,1)+incilfin1(l,1)))^2;

%b
rperd(l,1)=(sind(angled(l,1)-Kthetad)/sind(angled(l,1)+Kthetad))^2;
rpard(l,1)=(tand(angled(l,1)-Kthetad)/tand(angled(l,1)+Kthetad))^2;
%g
rperg(l,1)=(sind(angleg(l,1)-Kthetag)/sind(angleg(l,1)+Kthetag))^2;
rparg(l,1)=(tand(angleg(l,1)-Kthetag)/tand(angleg(l,1)+Kthetag))^2;

tpar(l,1)=(tuoa(l,1)*(1-rpar(l,1))^2)/(1-(rpar(l,1)*tuoa(l,1))^2);
tper(l,1)=(tuoa(l,1)*(1-rper(l,1))^2)/(1-(rper(l,1)*tuoa(l,1))^2);
rhopar(l,1)=rpar(l,1)*(1+tpar(l,1)*tuoa(l,1));
rhopar(l,1)=rper(l,1)*(1+tper(l,1)*tuoa(l,1));
TUA1(l,1)=0.5*(tpar(l,1)+tper(l,1));

```

```

RHO1(1,1)=1-TUA1(1,1);

AP1(1,1)=0.9;%ABSORBER PLATE

tuaofin14(1,1)=TUA1(1,1)*AP1(1,1)/(1-((1-AP1(1,1))*RHO1(1,1)));
% aper(1,1)=(1-tua(1,1))*((1-rper(1,1)))/((1-(rper(1,1)*tua(1,1))));
% apar(1,1)=(1-tua(1,1))*((1-rpar(1,1)))/((1-(rpar(1,1)*tua(1,1))));
%GLASS TO EVA
angle1(1,1)=real(asind((sind(angle(1,1))*Refg)/Refeva));
tuoal(1,1)=real(exp((4.3E-10*0.0005)/(cosd(angle1(1,1)))));
%convection by wind%K is 4m-1 for good white glass and called extinction
coefficient
rper1(1,1)=(sind(angle1(1,1)-angle(1,1))/sind(angle1(1,1)+angle(1,1)))^2;
rpar1(1,1)=(tand(angle1(1,1)-angle(1,1))/tand(angle1(1,1)+angle(1,1)))^2;

tpar1(1,1)=(tuoal(1,1)*(1-rpar1(1,1))^2)/(1-(rpar1(1,1)*tuoal(1,1))^2);
tper1(1,1)=(tuoal(1,1)*(1-rper1(1,1))^2)/(1-(rper1(1,1)*tuoal(1,1))^2);

rhopar1(1,1)=rpar1(1,1)*(1+tpar1(1,1)*tuoal(1,1));
rhoper1(1,1)=rper1(1,1)*(1+tper1(1,1)*tuoal(1,1));
% aper1(1,1)=(1-tuoal(1,1))*((1-rper1(1,1)))/((1-(rper1(1,1)*tuoal(1,1))));
% apar1(1,1)=(1-tuoal(1,1))*((1-rpar1(1,1)))/((1-(rpar1(1,1)*tuoal(1,1))));

tact(1,1)=0.5*(((tper(1,1)*tper1(1,1)))/(1-(rhoper(1,1)*rhoper1(1,1))))+(((tpar(1,1)*tpar1(1,1)))/(1-(rhopar(1,1)*rhopar1(1,1))));
tact1(1,1)=tuoal(1,1)*tact(1,1);
tr(1,1)=0.5*(((1-rper(1,1))/(1+rper(1,1)))+(1-rpar(1,1))/(1+rpar(1,1))));
rhoact1(1,1)=0.5*(((rhoper1(1,1)+(tact(1,1)*rhoper1(1,1)*tper(1,1))/tper1(1,1)))+(rhopar1(1,1)+(tact(1,1)*rhopar1(1,1)*tpar(1,1))/tpar1(1,1));
aact1(1,1)=1-tact(1,1)-rhoact1(1,1);
aact(1,1)=1-tuoal(1,1);
rhoact(1,1)=tuoal(1,1)-tact1(1,1);%EQNS ARE RIGHT BUT VALUES ARE?
% absco(1,1)=(log((1-rhoact(1,1))^2/(2*tact(1,1)))+(rhoact(1,1))^2+(1-rhoact(1,1))^2/(4*tact(1,1)^2))^(1/2))/0.0037;
tuaofin(1,1)=tact1(1,1)*0.9/(1-((1-0.9)*rhoact(1,1)));%EVA TRANSMITS ALL
(90% ABSORBTANCE)
TAPV(1,1)=tr(1,1)*tua(1,1)+(1-tuoal(1,1))*aact1(1,1);
%IAM IS DIFFERENT FOR PV AND COLLECTOR-IN PV GLAZING IS ATTACHED TO
%BOND SURFACE SO IAM IS DIFFERENT TO COLLECTIR TUOA( FOR OUR PV/T ITS LIKE
IAM OF
%THE COLLECTOR WITH AIR GAP IN GENERAL BUT OUR PV/T HAS NO AIR GAP)-CAUSE
OF THE CONFIGURATION)
%IAMSC has ANGLE instead of incidence angle.
%SOLAR COLLECTOR with AIR GAP AN LESS THAN 60
% if incilfin1(1,1)<=60
    IAMSC(1,1)=1-(0.2*((1/cosd(incilfin1(1,1)))-1));
% else
%     IAMSC(1,1)=0;
% end
if    IAMSC(1,1)<0
    IAMSC(1,1)=0;
end
    TUAPVn(1,1)=exp(-4*0.0032)*(1-((Refg-1)/(Refg+1))^2);
%FOR PV-ANGLES UPTO 90
    ini=[0.136,1];
    F=@(x2) IAM(x2,incilfin1,1)
    options = optimoptions('fsolve','Display','iter','TolFun',1e-3,'TolX',1e-3);
    [x2,fval]= fsolve(F,ini,options)
    ALT =0 :5;
    Bo=[0.998515,-0.012122, 1.440E-03,-5.576E-05,8.779E-07,-4.919E-09];

```



```

IAMPVALT(1,1)=sum(Bo(ALT+1).*(incilfin1(1,1)).^ALT);%PV AND PV/T WITH AIR
GAP.
%SAME AS TUAPV TAPV1(1,1)=exp(-4*0.0032/(cosd(angle(1,1))))*(1-
(0.5*(rper(1,1)+rpar(1,1))));
TUAPV(1,1)=exp(-4*0.0032/cosd(angle(1,1)))*(1-
0.5*(rper(1,1)+rpar(1,1)));%no eva/air gap
TUAPVd(1,1)=exp(-4*0.0032/cosd(angled(1,1)))*(1-
0.5*(rperd(1,1)+rpard(1,1)));%no eva/air gap
TUAPVg(1,1)=exp(-4*0.0032/cosd(angleg(1,1)))*(1-
0.5*(rperg(1,1)+rparg(1,1)));%no eva/air gap
% PAGE 390 LAST PARA-data scatter ARE TO BE EXPECTED
% AM(1,1)=1/cosd(angle1(1,1));%DESOTO 2006 PAGE 234 THIS FORMULA BETTER AND
STABLE
% % AM(1,1)=1/(cosd(zeinthincil1(1,1))+0.05057*(96.08-zeinthincil1(1,1))^
1.034);
% knc(1,1)=0.866-0.122*(AM(1,1)^2)-
0.000653*(AM(1,1))^3+0.000014*(AM(1,1))^4;

%TO INCLUDE ANGLES OVER 90
ALT =0 :3;
Bo=[1.0028,-1.7207E-03, 2.1539E-04,-1.0375E-05,2.0293E-07,-1.413E-09];
MIAMPV(1,1)=sum(Bo(ALT+1).*(incilfin1(1,1)).^ALT)+2.0293E-
07*incilfin1(1,1)^2+-1.413E-09*incilfin1(1,1)^5;

ALT1 =0 :5;
Bo1=[0.99979,9.2774E-05, -3.7165E-03,4.7927E-09,5.3784E-09,-1.7892E-10];
MIAMSC(1,1)=sum(Bo1(ALT1+1).*(incilfin1(1,1)).^ALT1);

K =0 : 4;
so=[0.918093,0.086257,-0.024459,0.002816,-0.000126];%POLY
M(1,1)=sum(so(K+1).*AM(1,1).^K);%ONLY PV with no airgap double checked-yay
POLY,MONO,SINGLE-FILM,THIN FILM.
MPV/T(1,1)=MIAMSC(1,1)+MIAMPV(1,1);
MPV/T(1,1)=max(MPV/T(1,1),M(1,1));

tuab(1,1)=TUAPV(1,1)/TUAPVn(1,1);
tuab1(1,1)=APV1(1,1)/TUAPVn(1,1);
tuad(1,1)=TUAPVd(1,1)/TUAPVn(1,1);
tuad1(1,1)=APV2(1,1)/TUAPVn(1,1);
tuag(1,1)=TUAPVg(1,1)/TUAPVn(1,1);
tuag1(1,1)=APV3(1,1)/TUAPVn(1,1);
SPV(1,1)=M(1,1)*TUAPVn(1,1)*((IB(1,1)*Rb(1,1))*tuab(1,1)+ID(1,1)*tuad(1,1)*
(1-
Ai(1,1))*((1+cosd(arras))/2)*(1+(fk(1,1)*(sind(arras/2))^3)))+(Rb(1,1)*Ai(1,1)
)+G(1,1)*tuag(1,1)*gr(1,1)*((1-cosd(arras))/2));%DUE TO AN AIRGAP
SPV/T(1,1)=M(1,1)*TUAPVn(1,1)*((IB(1,1)*Rb(1,1))*tuab1(1,1)+ID(1,1)*tuad1(1
,1)*(1-
Ai(1,1))*((1+cosd(arras))/2)*(1+(fk(1,1)*(sind(arras/2))^3)))+(Rb(1,1)*Ai(1,1)
)+G(1,1)*tuag1(1,1)*gr(1,1)*((1-cosd(arras))/2));%DUE TO AN AIRGAP
%FIND IAM THEN FIND DIFFUSE AND GOUND
Qp1(1,1)=IT(1,1)*A*TAPV(1,1);%FLUX WITHOUT ELECTRIC POWER REDUCTION

% HEAT TRANSFER COEFFICIENTS
Gvalue(1,1)=(IT(1,1)/GNOCT);
% //////////////////////////////////iteration after the assumed value of Tcell)
Tcellh(1,1)=(Ta(1,1)+(27*Gvalue(1,1)*(1-(0.153354*(1-(-
fpower*298.16)))/TAPV(1,1))))/(1+(27*Gvalue(1,1)*((-
fpower*0.153354)/TAPV(1,1))));
Tbm(1,1)=IT(1,1)*(exp(-3.56-0.0756*wind(1,1)))+Ta(1,1);
Tcell(1,1)=Tbm(1,1)+(IT(1,1)*3/1000);
%TCel(1,1)=Ta(1,1)+(rad(1,1)*(27)/800);
TCel(1,1)=Ta(1,1)+(rad(1,1)*(27)/800);

%FROM HERE ITERATION NEEDS TO BE DONE

```

```

Effofcelltemp(1,1)=(15.3*(1--fpower*(Tcell(1,1)-293.16)))/100;
Modeff(1,1)=(Moduleeff-(fpower*abs(Tcell(1,1)-298.16)))/100;% CELL TEMP
WITHOUT TUOA EFFECT

%MODULE ONLY OUTPUT

a(1,1)=asoem*Tcell(1,1)/Tref;

Rsh(1,1)=Rshref*1000/IT(1,1);%BAD AT LOW IRRADIANCE
Iph(1,1)=M(1,1)*(Iphref2+fisc*(Tcell(1,1)-Tref))*SPV(1,1);%AT REF
IPHREF=ISCREF %AIRMASS=1.5
Eg(1,1)=Egref*(1-0.00026778*(Tcell(1,1)-Tref));
Io(1,1)=Ioref*(Tcell(1,1)/Tref)^3*exp(((q*Eg(1,1))/(a(1,1)*kb))*(1/(Tref)-1/Tcell(1,1))));

Effofconversion=Pm/(1000*A);
PMother=Effofconversion*870*A;%FOR 885 W
Vocother(1,1)=Voc-(fvolt*(Tcell(1,1)-298.16));
if Tcell(1,1)>=298.16
Iscother(1,1)=Isc+(Isc*fisc*(Tcell(1,1)-298.16));%optimise
Ptemp(1,1)=Pm*(1-(fpower*(Tcell(1,1)-293.16)));
else
Iscother(1,1)=Isc;
% Vocother(1,1)=Voc;
Ptemp(1,1)=Pm;
end

fvol(1,1)=(Vocother(1,1)-Voc)/(Tcell(1,1)-Tref);
if Tcell(1,1)>293.16
Modeff(1,1)=Moduleeff-(fpower*Moduleeff*(Tcell(1,1)-293.16));
else
Modeff(1,1)=Moduleeff;
end% CELL TEMP WITHOUT TUOA EFFECT
%KWH
EP(1,1)=(Modeff(1,1)*IT(1,1)*1.603*rc)/100;%WATT (COULD ALSO BE JUST TWO
LAYER PV SYSTEM)AS ACTUAL CURRENT AND VOLATGE ARE NOT CALCULATED YET?*rc
reduces op
%KILOWATT-HOUR(IF THIS CAN ACUALLY BE JUST PV THEN THIS IS FIXED (EXCEPT
FOR EFF,AREA AND TILT-ON NON TRACK SYSTEM-ITS FIXED) NO MATTER WHAT WHILE
PV/T O/P CAN BE ALTERED ON PARAMETRIC CHANGES
Eleceff(1,1)=Modeff(1,1)-(EP(1,1)/(IT(1,1)*A));
Qp(1,1)=Qp1(1,1)-EP(1,1);
qu1(1,1)=Qp(1,1)+Qg(1,1);
hag1(1,1)=3*wind(1,1)+2.8;
hag2(1,1)=eg*sig*(Ta(1,1)^2+Ta(1,1)^2)*(Ta(1,1)+Ta(1,1));
hag(1,1)=hag1(1,1)+hag2(1,1);%OUTER
hgp(1,1)=(0.34/thickeva)+((sig*(Ta(1,1)^2+Tcell(1,1)^2)*(Ta(1,1)+Tcell(1,1)))/(1/ep+1/eg-1));%0.34 CONDUCTIVITY OF EVA~INNER
hw(1,1)=4.364*(0.591/dia);%LAMINAR AND THERMAL CONDUCTIVITY OF WATER
inhtw(1,1)=1/(hw(1,1)*pi*dia*length)+1/(Cbo*length);
htw(1,1)=1/inhtw(1,1);
hbp=0.34/thickeva;
hpt1A=(thickp*length)/(((0.14-dia)/130+(thickeva*thickp)/(0.34*dia)));
hpt=(thickp*length)/(((0.14)/130*8)+(thickeva*thickp)/(0.34*dia));
hbt=8*Alum/((0.14-dia));
Ra(1,1)=(9.8*(Tcell(1,1)-Ta(1,1))*(dia)^3*0.7)/(330*1.568E-10);
Snd(1,1)=1-1708/(Ra(1,1)*cosd(arr));
if Snd(1,1)<0
Snd(1,1)=0;
end
Trd(1,1)=((Ra(1,1)*cosd(arr))/5830)^0.33-1;
if Trd(1,1)<0

```

```

Trd(1,1)=0;
end
Nua(1,1)=1+1.44*(1-(1708*(sind(1.8*arra))^1.6)/(Ra(1,1)*cosd(arra)))*Snd(1,1)+(Trd(1,1));
hbi(1,1)=1/((1/(Cbo*length))+(Nua(1,1)*0.0264/dia));
hbi1=2*0.026/thickins;%HIT ALL LAMINAR FLOW RE<2300
hai(1,1)=1/(1/hag1(1,1)+1/hbi(1,1));
end
V=24;
Ioo=Isc;
% for b=1:Voc
for k=4479
options = optimoptions('fsolve','Display','final','TolFun',1e-6,'TolX',1e-6);
I(k,1)=fsolve(@(x2)Iph(k,1)-Io(k,1)*(exp((V+x2*Rs))/(a(k,1)))-1)-((V+x2*Rs)/Rsh(k,1))-x2,Ioo,options);
if I(k,1)<0
I(k,1)=0;
end % cftool(Pmtemp,EP);
Pmiv(k,1)=I(k,1)*V;
end
% V=V+1;
% end

Di=0.007;alfa=1.9E-05;N=2;
if (B<70)
C=520*(1-0.000051*(B)^2); %C
else
C=520*(1-0.000051*70^2);
end
Cb=690;
W=0.014;D=0.008;
Ap=1.552;

%NOTE THAT PRESSURE LOSS IS INCREASING EXPONENTIALLY WHEN MASS FLOW RATE IS
%INCREASED ESPECIALLY WHEN SYSTEM IS CONNECTED AS PARALLEL AND SERIES-SO AN
%OPTIMUM SHOULD BE CHOSEN.PRESSURE LOSS IN PIPES IN MBAR WHEN MFR IS IN
%L/MIN to find cell value c{2,2}->displays values

for l=1:8760
ef(1,1)=(1+0.089*wind(1,1)-0.1166*wind(1,1)*ep)*(1+0.07866*N); %f
for j=1

Cp=-0.0000854235*Tcell(1,1)^3+0.09488036*Tcell(1,1)^2-34.2228*Tcell(1,1)+8212.82;
CP1(1,1)=Cp;
visc=(0.0000001406*Tcell(1,1)^2-0.0001024062*Tcell(1,1)+0.01895682)/(-0.003284948*Tcell(1,1)^2+1.687644*Tcell(1,1)+785.6677);
Re=2*m*Di/(1000*pi*Di^2*visc); %REYNOLDS NUMBER
Pr=visc/alfa; %PRANDTL NUMBER

if (Re>2300)
friction=(0.79*log(Re)-1.64)^-2; %DARCY FRICTION FACTOR
Nulong=(friction/8)*(Re-1000)*Pr/(1+12.7*sqrt(friction/8)*(Pr^(2/3)-1));
Nu=Nulong*(1+(Di/1.6)^0.7); %NUSSELT NUMBER
else
Nu=4.4+0.00172*(Re*Pr*Di/1.6)^1.66/(1+0.00281*(Re*Pr*Di/1.6)^1.29);
end
thcond=-0.00000981358*Tcell(1,1)^2+0.007536807*Tcell(1,1)-0.7674181; %THERMAL CONDUCTIVITY OF WATER
hfi=Nu*thcond/Di; %FORCED-CONVECTION HEAT TRANSFER COEFFICIENT INSIDE OF TUBES
e(1,1)=0.43*(1-100/Tcell(1,1)); %e

```

```

Ut(1,1)=(N/(C/Tcell(1,1) * ((Tcell(1,1)-Ta(1,1))/(N+7
))^e(1,1))+1/hw(1,1))^(-
1)+(sig*(Tcell(1,1)+Ta(1,1))*(Tcell(1,1)^2+Ta(1,1)^2
))/(ep+0.00591*N*hw(1,1))^(-1)+(2*N+eg-1+0.133*ep)/eg-N);
VISS(1,1)=Nu;%
% OVERALL HEAT LOSS COEFFICIENT
UL2(1,1)=Ut(1,1)*A/1.552; %MODIFIED OVERALL HEAT LOSS COEFFICIENT
mi=1.55*0.001*0.002*2700*7; %PARAMETER OF THE FIN-AIR ARRANGEMENT
F=tanh(mi*(W-D)/2)/(mi*(W-D)/2); %STANDARD FIN EFFICIENCY
F1=(1/UL2(1,1))/(W*(1/(UL2(1,1)*(D+(W-
D)*F))+1/Cb+1/(pi*Di*hfi))); %COLLECTOREFFICIENCY FACTOR F'
FR=m*Cp/(Ap*UL2(1,1))*(1-exp(-Ap*UL2(1,1)*F1/(m*Cp))); %COLLECTOR HEAT
REMOVAL FACTOR
Qu(1,1)=Ap*(SPV(1,1)-(UL2(1,1)*(Tcell(1,1)-Ta(1,1)))); %USEFUL GAIN FROM
THE COLLECTOR
Tpm2(1,1)=Ta(1,1)+Qu(1,1)/(Ap*FR*UL2(1,1))*(1-FR); %MEAN PLATE TEMPERATURE
Quse(1,1)=Ap*FR*(SPV(1,1)-UL2(1,1)*(Tpm2(1,1)-Ta(1,1)));
F2=FR/F1;
Tfm(1,1)=Tpm2(1,1)+Quse(1,1)/(Ap*FR*UL2(1,1))*(1-F2);
HP(1,1)=m*3184*(Tfm(1,1)-(Ta(1,1)-10));
Eleeff(1,1)=Qu(1,1)/(A*IT(1,1));
Thereff(1,1)=HP(1,1)/(IT(1,1));
Sincident(1,1)=G(1,1)*sind(90-lat+DECL(1,1)+arra)/sind(90-lat+DECL(1,1));
PR(1,1)=EP(1,1)/(IT(1,1)*250);
%////////////////////////////////////h=0.0001-1
h=0.0001;t= 0:h:60;
options = odeset('AbsTol',1e-6,'RelTol',1e-6);
[t,y4]
=ode23tb(@implRK,[t],[Tpm2(1,1),Tpm2(1,1),Tpm2(1,1),Tpm2(1,1),Ta(1,1),Ta(1,
1)+20],options);%13th
% %HOUR
% %NOW NEW VALUE OF TG TP ETC IS KNOWN(13TH HOUR)-USE FEM TO FIND ALL
TEMPERAURE ACTUAL VALUES.
To(:,j)=2*y4(:,end)-Ta(5391,1)-20; %329.16
ke=y4(:,4);
le=y4(:,end);
nther(1,j)=(m*6246*100*(To(end,j)-y4(end,end)))/(1.552*IT(5391,1));
if nther(1,j)>100|| nther(1,j)<0
nther(1,j)=0.1;
end
nele(1,j)=EP(5391,1)*100/(1.552*IT(5391,1));
Ij=((Ta(j,1)+30-y4(end,end))/(IT(5391,1)));

KO=To(11,:);
end
end
%IAM = pvl_ashraeam(b, theta);
% plot(IT,'DisplayName','IT');hold on;plot(G,'DisplayName','G');hold off;

LEPETITE=Sincident(5954:7297,1);
% plot(Tfm(1:72,1),'DisplayName','Tfm');
% hold on;
% plot(Tpm2(1:72,1),'DisplayName','Tpm');
% plot(TCel(1:72,1),'DisplayName','TCel');
% plot(Tcell(1:72,1),'DisplayName','Tcell');
% plot(Ta(1:72,1),'DisplayName','Ta');
% hold off;

LAP=G(5953:7296,1);
% createFit1(LEG, LEPETITE);
LAWP=ID(5953:7296,1);

% [myfit,gof,out] = fit(LEG,LEPETITE,'poly1');
% LECorrected = myfit(LEPETITE);

```

```

% LENEW=IT*0.35+35.64;
% scatter(KT,krf)
% hold on
% scatter(KT,kdr)
% scatter(KT,kde)
% scatter(KT,km)
% scatter(KT,kdsrg)
% hold off
l=1;
for dayy=1:365

    for k=1:24
    % Y,M,D,H,MI,S
    % (Y,M,D)

Time(l,1) = datetime(2017,1,dayy,k-1,0,0);
l=l+1;

        end
    end
% ALLRAD=[IDT,IBT,IT];
% out = @pivottable;
% VA= out(ALLRAD, 1, 2, 3, @max);
% bar(Time,ALLRAD,'stacked');
% hold on
plot(LEPETITE,'DisplayName','LEPETITE');plot(LEG,'DisplayName','LEG');hold
off;
% plot(Time,IDT,'DisplayName','Diffuse');hold
on;plot(Time,IBT,'DisplayName','Beam');plot(Time,IT,'DisplayName','TotalRad
');hold off;
% plot(Time,LEPETITE,'DisplayName','LEPETITE');hold
on;plot(Time,LAP,'DisplayName','LAP');plot(Time,LEG,'DisplayName','LEG');ho
ld off;
% for l=1:1354
%     if LEG(l,1)==0
%         LEG(l,1)=1;
%     end
% RMSE(l,1)=sqrt((sum(LEPETITE(l,1)-LEG(l,1))^2)/312);
% perRMSE(l,1)=RMSE(l,1)*100/mean(LEG);
% end
toc

```